

Development of a Liquid Inerted Microwave Pyrolysis Process

Benjamin John Shepherd, MEng

Thesis submitted to the University of Nottingham

for the degree of Doctor of Philosophy

January 2020

Abstract

The research presented in this thesis evaluates the potential of a new approach to carrying out pyrolysis. A pyrolysis process was demonstrated that combined microwave heating with an external liquid medium at atmospheric pressure. Generally, gases such as nitrogen are used to inert pyrolysis, however in this research liquids were used which had the benefit of acting as a heat-sink to maintain the external temperature at the atmospheric boiling point of the liquid.

An advantage of the presented pyrolysis technology was the ability of the liquid surround to control the external temperature, as this was only possible due to the selective and volumetric heating that occurs with microwaves. The new concept produced a pyrolysis oil that naturally partitioned into a sugar-rich aqueous phase and a phenol-rich organic phase when using solvents that were only miscible with one of the phases, such as *n*-hexane. The liquid medium overcame many of the challenges encountered in traditional and gas-based microwave pyrolysis processes, acting to eliminate arcing, slow the onset of plasma formation, and prevent carbonaceous residues from forming from the pyrolysis oil produced, phenomena which have so far proved challenging for the scale-up of microwave pyrolysis processes. Energy requirements were as low as 2 kJ/g for 50 % volatilisation, comparable to microwave pyrolysis using inert gases. It was also shown that the liquid inerted concept had the potential to utilise both microwave-transparent and microwave-absorbent solvents effectively.

Two methods were investigated to perform microwave pyrolysis process within a liquid medium. The first process was a feasibility study, which was successful, however due to the scale of the process, oil volumes produced were low and the volatilisation of the

sycamore coupled with boiling solvent resulted in challenges in maintaining the surface temperature of the block during pyrolysis.

The second process configuration involved the investigation on controlling the boiling regime and bubble disengagement, along with allowing for sycamore geometries that would allow for larger volumes of pyrolysis oil to be produced. This presented advantages and challenges when compared to the first process. It was found that due to the size of the sycamore blocks used, internal temperature control was reduced in the second process, however there was greater surface cooling potential due to the larger volume of liquid surrounding the block.

It was discovered throughout the work in the thesis that in addition to providing an alternative way of heating the sycamore, microwave pyrolysis offered processing characteristics that were not present in conventionally heated processes. It was known that due to volumetric heating, larger particles could be heated faster than conventional heating. It became apparent, however, that due to the large volume of volatiles being produced within the sycamore block, the pressures achieved would allow for internal temperature control of the sycamore. The volatiles production would potentially result in variations of the dielectric properties of the sycamore that would not be expected when using conventional analysis methods.

Acknowledgements

I would firstly like to thank the EPSRC CDT in Sustainable Chemistry for giving me the opportunity to undertake this PhD, and for allowing for me to grow and develop both my professional and personal skills beyond that of pure research.

I am extremely grateful to my main supervisor, Dr. John Robinson for his unwavering support, guidance and encouragement throughout my PhD. Thank you to my examiners for their insightful comments. A big thank you to my colleagues, friends and technicians who offered their ears, ideas, help and support.

Finally, I would like to thank my Mum, Dad, Sister, Grandparents and Emily for their unconditional support and for keeping me sane throughout this PhD journey.

List of publications

Shepherd, B.J., Ryan, J., Adam, M., Vallejo, D.B., Castaño, P., Kostas, E.T. and Robinson, J.P., 2018. Microwave pyrolysis of biomass within a liquid medium. *Journal of analytical and applied pyrolysis*, *134*, pp.381-388.

Kostas, E.T., Cooper, M., **Shepherd, B.J.** and Robinson, J.P., 2019. Identification of Bio-oil Compound Utilizing Yeasts Through Phenotypic Microarray Screening. *Waste and Biomass Valorization*, pp.1-13.

Kostas, E.T., Durán-Jiménez, G., **Shepherd, B.J.**, Meredith, W., Stevens, L.A., Williams, O.S., Lye, G.J. and Robinson, J.P., 2019. Microwave pyrolysis of olive pomace for bio-oil and bio-char production. *Chemical Engineering Journal*, p.123404.

Table of contents

Abstract 1

Acknowledgements 3

List of publications 4

Table of contents 5

List of Tables 12

List of Figures 17

List of abbreviations and nomenclature 33

1. Introduction 36

1.1 Composition of biomass 38

1.1.1 Cellulose 38

1.1.2 Hemicellulose 39

1.1.3 Lignin 40

1.1.4 Extractives and inorganics 41

1.2 Biomass conversion technologies 41

1.2.1 Thermochemical biomass conversion 42

1.3 Pyrolysis principles 47

1.3.1 Pyrolysis reactions of lignocellulosic constituents 47

1.3.2 Pyrolysis products 48

1.3.3 Pyrolysis temperature and pyrolysis oil yield 54

1.3.4 Processing factors affecting pyrolysis 56

1.3.5 Types of pyrolysis reactor....58
1.4 Microwave fundamentals....62
1.4.1 Microwave reactor cavity configurations....63
1.4.2 Dielectric properties as a function of temperature....65
1.4.3 Microwave pyrolysis principles....66
1.4.4 Microwave pyrolysis studies....68
1.5 Aims and Objectives....71
2. Experimental materials and methods....73
2.1 Reagents....73
2.2 Source and preparation of Sycamore....73
2.3 Sycamore analysis techniques....73
2.3.1 Dielectric properties....73
2.3.2 Thermogravimetric analysis (TGA)....74
2.3.3 Simultaneous Differential Scanning Calorimetry-TGA (SDT)....74
2.3.4 Determination of moisture content....75
2.3.5 Density of the sycamore block....75
2.3.6 Determination of lignin....75
2.3.7 Determination of cellulose and hemicellulose....76
2.4 Microwave pyrolysis....77
2.4.1 Cold matching of the system....77
2.4.2 Single-mode and multi-mode pyrolysis systems....77

2.4.3 Specific absorbed energy 78
2.4.4 Determination of solid mass loss 78
2.4.5 Solvent/solid ratio required to maintain the liquid environment 78
2.5 Oil categorisation 80
2.5.1 Pyrolysis oil analysis using gas chromatography-mass spectroscopy (GC-MS) 80
2.6 Mathematical modelling and computational simulations 82
2.6.1 Heat transfer models 82
3. Effect of solvents on a pyrolysis process 86
3.1 Introduction 86
3.2 Materials and methods 90
3.2.1 Liquid-inerted microwave pyrolysis equipment configuration 90
3.2.2 Gas-inerted microwave pyrolysis equipment configuration 91
3.2.3 Pyrolysis oil collection 92
3.2.4 Impedance matching 94
3.2.5 Single-mode microwave cavity characteristics 95
3.3 Liquid-solvent characterisation 96
3.3.1 Microwave transparency – Dielectric properties and dipole moment 96
3.3.2 Physical properties 99
3.3.3 Favourable solvent properties 103
3.4 Results and discussion 104
3.4.1 Solvent screening and process repeatability 104

3.4.2 Effect of solvent on solid mass loss 115
3.4.3 Pyrolysis oil yields 125
3.4.4 Pyrolysis oil composition 132
3.4.5 Processing implications – solvent recycling 137
3.4.6 Estimating internal sycamore temperature 141
3.4.7 Observations of gas bubble behaviour 148
3.5 Conclusions 154
4. Controlling the boiling regime 157
4.1 Introduction 157
4.1.1 Limitations of the single-mode microwave pyrolysis system and benefits of the multi-mode scaled-up system 158
4.2 Aims and objectives 163
4.3 Materials and methods 163
4.3.1 Microwave experimental system 163
4.3.2 Pyrolysis oil collection 165
4.4 Results and discussion 167
4.4.1 Power absorption for the multi-mode system 167
4.4.2 Block geometry testing in the multi-mode system 172
4.4.3 Effect of heating conditions 176
4.4.4 Pyrolysis oil yield 181
4.4.5 Pyrolysis oil composition 185
4.4.6 Solid analysis pre and post pyrolysis 189

4.5 Conclusions 198

5. New insights into microwave pyrolysis mechanisms 201

5.1 Introduction 201

5.2 Materials and methods 202

5.2.1 Microwave pyrolysis 202

5.2.2 Microwave cavity modelling 202

5.3 Results and discussion 205

5.3.1 Effect of power density on pyrolysis performance 205

5.3.2 Factors affecting temperature predictions of the sycamore block 209

5.3.3 Dielectric properties from the pyrolysis process 216

5.3.4 Pressure generation within the sycamore during pyrolysis 224

5.4 Conclusions 240

6. Conclusions and recommendations for future work 243

6.1 Overview 243

6.2 Overall discussion and final conclusions 244

6.3 Recommendations for future work 248

6.3.1 Processing considerations – continuous processing 248

6.3.2 Maximum and minimum geometry possible for liquid inerted microwave pyrolysis 251

6.3.3 Kinetic studies on a microwave pyrolysis process 253

6.3.4 Comprehensive pyrolysis oil product analysis and categorisation 254

6.3.5 Dielectrics during the microwave process 254

6.3.6 Alternative feedstock investigation....255
6.3.7 Solvent recycle....255
6.3.8 Selective decomposition analysis....256
References....257
Appendix A – Sycamore specific heat capacity from differential scanning calorimetry (DSC)....269
Appendix B – Chapter 3 supplementary information....270
B.1 Additional absorbance curves....270
B.2 Pyrolysis oil composition....273
Appendix C – Chapter 4 supplementary information....285
C.1 Supplementary absorbance curves....285
C.2 Total pyrolysis oil yield, and oil and gas yields as a percentage of total volatiles produced.....286
C.3 Pyrolysis oil composition....289
C.4 Lignin concentration from thermogravimetric analysis correlations....300
Appendix D – Chapter 5 supplementary information....303
D.1 Material parameters for the microwave simulations....303
D.2 Levoglucosan dielectric properties....304
D.3 Parameters for volatiles generation model....304
D.4 Kinetic equations and material parameters for the pressure generation models....305
D.5 Preliminary investigations on processing considerations....306

Soaking sycamore in liquid solvent pre-pyrolysis.....306

Multiple sample pyrolysis – multi-mode.....312

Compositional changes predicted by the models 313

List of Tables

Table 1-1 – An overview of the main types of pyrolysis, with typical product yields, adapted from Jahirul et al. (2012). 44

Table 1-2 – Physical properties of pyrolysis oil, taken from (Jahirul et al., 2012)..... 49

Table 1-3 – Optimal temperatures for liquid pyrolysis products. 55

Table 2-1 – Energy required to boil the solvents used in the thesis. 79

Table 2-2 – Minimum solvent volume required per gram of biomass. 80

Table 2-3 – The parameters for the computational models for sycamore, all values at 25°C unless otherwise specified. 85

Table 3-1 – Physical and system properties of gaseous and liquid inert media for microwave pyrolysis. Comparative heat transfer coefficients calculated based on Nu = 2 and a spherical biomass particle with 10 mm diameter (Green and Perry, 2007). All properties quoted at 20 °C, unless otherwise stated. [a] (Meredith, 1998, Hermiz et al., 1982), [b] (Haynes, 2014). 87

Table 3-2 – The physical state of the pyrolysis oil after pyrolysis in the inerting media investigated. 93

Table 3-3 - Dielectric constants, loss tangents, and dipole moments of solvents. *Not available. 97

Table 3-4 – Penetration depths of the solvents investigated in this study 98

Table 3-5 – Physical properties of the solvents investigated in this study, all values given at 20 °C (Haynes, 2014). 101

Table 3-6 – GSK solvent selection guide parameters for the solvents investigated in the thesis, higher values are better (EHS = Environmental, Health, and Safety) (Henderson et al., 2011). 102

Table 3-7 – Favourable properties for a liquid used as an inerting medium. 103

Table 3-8 - The inerting media investigated, with highest mass losses presented, and energy requirements for the sycamore block reach 20 % and 40 % mass loss during the pyrolysis process 121

Table 3-9 – Estimated losses during the collection and subsequent separation of the aqueous pyrolysis oil phase for approximately 2.5±0.04 kJ/g, 21±3 % aqueous pyrolysis oil yield (3 repeats). 125

Table 3-10 – Vapour composition of the organic phase-solvent mix based on 5 % organic pyrolysis oil phase by mass 127

Table 3-11 – Prominent major compounds of the pyrolysis oil products for varying inerting media, with analysis carried out by each collaborator denoted. 134

Table 3-12 - Average values for the liquid solvent lost post-pyrolysis averaged out over every successive run. 140

Table 3-13 – The composition (dry basis) of the centre of the sycamore and centre of the pyrolysed samples for approximately 0.6 – 1.5 kW applied power to the system. 147

Table 4-1 - Average absorbed power and standard deviation over the entire pyrolysis process for the solvents investigated 172

Table 4-2 – Highest mass loss achieved and energy requirements for pyrolysis and 50 % mass loss to occur for the solvents investigated in the multi-mode system, with comparisons for the single-mode system presented 178

Table 4-3 – Summary of the oil yields obtained in the multi-mode system, with the single-mode results as a comparison 183

Table 4-4 – Prominent major compounds for the multi-mode liquid inerted microwave pyrolysis process in various inerting media, with the single-mode oils presented for comparison, and analysis carried out by each collaborator denoted. 187

Table 4-5 -The composition of the sycamore used in this study. 190
Table 4-6 - Proximate analysis for chars (dry basis) at the point of pyrolysis at specific energies of 0 – 4 kJ/g. 197
Table 5-1 – The four models presented and their respective kinetic parameters.....231
Table 5-2 – The modified composition of the sycamore block for models 2 and 3. .232
Table 5-3 – Governing equations for models 1 – 4 (Park et al., 2010, Chan and Krieger, 1981, Capart et al., 2004, Varhegyi et al., 1989, Kilzer and Broido, 1965, Mok and Antal, 1983). 233
Table 5-4 – Variable properties of the wood for models 1 – 4 (Park et al., 2010). ...234
Table B-1 - Group abundance in the inerting media used, based on peak area. 273
Table B-2 – Aqueous phase oil composition, *n*-hexane solvent, analysed by collaborators in Spain (hydrocarbons not considered in the final peak area calculations, considered impurities).....274
Table B-3 – Organic phase oil composition, *n*-hexane solvent, analysed by collaborators in Spain (hydrocarbons not considered in the final peak area calculations, considered impurities).....276
Table B-4 – Pyrolysis oil composition, nitrogen inerted, 1.08 kJ/g, analysed by a collaborator in the University of Nottingham. 278
Table B-5 – Pyrolysis oil composition, nitrogen inerted, 1.89 kJ/g, analysed by a collaborator in the University of Nottingham. 280
Table B-6 – Pyrolysis oil composition, 2-propanol inerted, analysed by a collaborator in the University of Nottingham. 282
Table B-7 – Pyrolysis oil composition, water inerted, analysed by a collaborator in the University of Nottingham. 283

Table C-1 – Compound groups for the multi-mode liquid inerted microwave pyrolysis process in various inerting media, with the single-mode oils presented for comparison. 289
Table C-2 – Aqueous phase oil composition, cyclohexane solvent, 1.33 kJ/g, analysed by a collaborator in the University of Nottingham. 290
Table C-3 – Aqueous phase oil composition, cyclohexane solvent, 1.87 kJ/g, analysed by a collaborator in the University of Nottingham. 293
Table C-4 –Organic phase oil composition, cyclohexane solvent, 1.33 kJ/g, analysed by a collaborator in the University of Nottingham. 295
Table C-5 –Organic phase oil composition, cyclohexane solvent, 1.87 kJ/g, analysed by a collaborator in the University of Nottingham. 298
Table D-1 – The material parameters for the microwave field simulations. 303
Table D-2 – The dielectric properties of levoglucosan from 20 - 350 °C. 304
Table D-3 – The parameters of the wood and volatiles for the volatiles generation model.....304
Table D-4 – The parameters of the wood and volatiles for the volatiles generation model, with variable porosity and permeability (ML = mass loss). 304
Table D-5 -Vaporisation kinetics of water within the sycamore structure (Ding et al., 2018). 305
Table D-6 – The parameters for model 1 (Park et al., 2010). 305
Table D-7 – The parameters for model 2 (Chan and Krieger, 1981, Capart et al., 2004, Varhegyi et al., 1989). [a]Initial proportion of cellulose A and B. 305
Table D-8 – The parameters for model 3 (Ding et al., 2018). [a]The heats of pyrolysis are taken from (Park et al., 2010). 305

Table D-9 – The parameters for model 4 (Kilzer and Broido, 1965, Park et al., 2010, Mok and Antal, 1983). 306
Table D-10 – The material properties of the wood and volatiles produced during the pyrolysis process. 306
Table D-11 - Densities of the liquids and samples at 25 °C 307

List of Figures

Figure 1-1 – (A) World, (B) EU, (C) UK total primary energy supply by sector as of 2017. *Others include geothermal, solar, wind, tide/wave/ocean and heat. (IEA, 2019a) 37

Figure 1-2 – (a) D-glucopyranose, (b) cellobiose unit. 39

Figure 1-3 – The monomers that comprise hemicellulose. 40

Figure 1-4 – The alcohol constituents of lignin. 41

Figure 1-5 – The pathway of biomass to pyrolysis products, adapted from Venderbosch and Prins (2010). 44

Figure 1-6 - Prominent compounds produced from conventional and microwave pyrolysis of European Larch, adapted from Robinson et al. (2015). 50

Figure 1-7 – Applications for pyrolysis oil, adapted from Bridgwater (2012). 52

Figure 1-8 – An illustration of the random wave propagation within a multi-mode cavity, and formation of cold and hot spots within the cavity. 63

Figure 1-9 - The loss tangent of European Larch over the temperature range 20 - 600 °C, determined by the cavity perturbation method (Section 2.3.1) (Robinson et al., 2015). 65

Figure 1-10 – The temperature gradient of a microwave pyrolysis process and conventionally heated pyrolysis process, with the arrows representing mass transfer of the volatiles produced during the pyrolysis process. 67

Figure 2-1 – The absorbance over the microwave generator frequency range. 77

Figure 3-1 – Heating profiles of a solvothermal process (left), and in a liquid inerted microwave pyrolysis process (right), with arrows showcasing the direction of heat transfer. 86

Figure 3-2 – A cross-sectional temperature profile of a 45×15×15 mm sycamore block pyrolysed at 0.5 kW, 18 seconds, in *n*-hexane and nitrogen, showcasing increased temperature control on the surface of the block when processed within a liquid medium. 88

Figure 3-3 - The schematic of the single-mode liquid-inerted microwave pyrolysis system 91

Figure 3-4 - The schematic of the single-mode gas-inerted microwave pyrolysis system 92

Figure 3-5 - The fractionated pyrolysis oil product, showing the aqueous and organic fractions when cyclohexane was used as an inerting liquid. 92

Figure 3-6 – A representative example of a dynamic and fixed impedance matching process with cyclohexane as an inerting medium, with the absorbance shown for approximately 1.5±0.1 kW applied to the system.....94

Figure 3-7 – (Left) Absorbed power for *n*-hexane based on approximately (A) 1.0 kW, (B) 1.5 kW, (C) 1.8 kW applied power over 5 runs per applied power with fixed impedance matching, and a treated block (1.0 kW applied, 15 seconds), showcasing heating within the centre of the sycamore block. (Right) Sycamore blocks after pyrolysis at the respective powers, 15 second processing time. 105

Figure 3-8 – (Left) Absorbed powers for cyclohexane as an inerting liquid, with real-time impedance matching to increase absorbance of the solid sample, and fixed impedance matching for equivalent applied powers (approximately 1.5±0.1 kW) over 10 runs. (Right) A cross section of a sycamore block treated at 1.5 kW applied power, 4 second processing time, dynamic impedance matching. 106

Figure 3-9 – (Left) Absorbed power for water as a solvent based on approximately (A) 1.25 kW, (B) 1.50 kW, (C) 1.80 kW applied powers with fixed impedance matching

over 3 runs per applied power. (Right) A cross section of a sycamore block treated at 1.8 kW applied, 120 second processing time.....107
Figure 3-10 – (Left) Absorbed power for 2-propanol as an inerting liquid, with fixed impedance matching, and dynamic impedance matching to increase absorbance of the solid sample, at approximately 1.5 kW applied power over 5 runs. (Right) A cross section of a sycamore block after treating at 1.5 kW applied power, 45 second processing time, dynamic impedance matching. 108
Figure 3-11 – (Left) Absorbed power for acetic acid as a solvent based on approximately (A) 1.00 kW, (B) 1.25 kW, (C) 1.50 kW applied powers with fixed impedance matching over 3 runs per applied power. (Right) A sycamore block sample post pyrolysis in acetic acid (1.5 kW applied, 12 seconds). 110
Figure 3-12 – (Left) Power absorbed for sycamore with glycerol as an inerting liquid, with dynamic impedance matching to increase absorbance of the solid sample at 1.0 kW over 4 runs. (Right) The sycamore block post pyrolysis within glycerol, (1 kW applied, 100 seconds).....111
Figure 3-13 – (Left) Power absorbed for sycamore with nitrogen as an inerting medium, with dynamic impedance matching to increase absorbance of the solid sample at approximately 0.5, 1.0 and 1.5 kW applied power over 5 runs per applied power. (Right) The sycamore block after nitrogen inerted pyrolysis, 0.5 kW applied, 10 second processing time. 112
Figure 3-14 – The sycamore block pre pyrolysis (left) and post-pyrolysis within acetic acid (middle) and glycerol (right), showing charring on the surface of the block.....115
Figure 3-15 - Bulk mass loss of the sycamore blocks against specific energy absorbed by the sycamore using n-hexane as an inerting liquid for applied powers ranging from approximately 1.0 – 1.8 kW.....116

Figure 3-16 - Bulk mass loss of the sycamore blocks against specific energy absorbed by the sycamore for cyclohexane as an inerting liquid with applied powers from approximately 0.6 – 1.7 kW.....116
Figure 3-17 – Bulk mass loss of the sycamore blocks against specific energy absorbed by the sycamore for isooctane as an inerting liquid, with applied powers ranging from approximately 1.0 - 1.8 kW. 117
Figure 3-18 - Bulk mass loss of the sycamore blocks against specific energy absorbed by the sycamore for kerosene as an inerting liquid, with applied powers ranging from approximately 1 - 1.8 kW. 117
Figure 3-19 - Bulk mass loss of the sycamore blocks against specific energy absorbed by the sycamore for pentane as an inerting liquid, with applied powers ranging from approximately 1 - 1.8 kW. 117
Figure 3-20 - Bulk mass loss of the sycamore blocks against specific energy absorbed by the sycamore for acetic acid as an inerting liquid, with applied powers ranging from approximately 1.0 - 1.5 kW. 118
Figure 3-21 - Bulk mass loss of the sycamore blocks against specific energy absorbed by the sycamore for water as an inerting liquid, with applied powers ranging from approximately 1.25 - 1.8 kW with fixed impedance matching.....118
Figure 3-22 - Bulk mass loss of the sycamore blocks against specific energy absorbed by the sycamore for 2-propanol as an inerting liquid, with an applied power of 1.5 kW. 118
Figure 3-23 – Bulk mass loss for sycamore against specific energy absorbed by the sycamore inerted by nitrogen with applied powers ranging from approximately 0.6 – 1.5 kW.....119

Figure 3-24 – The maximum mass loss achieved for the inerting media investigated, and specific energy requirements to achieve 20 % and 40 % mass loss during the pyrolysis process. 121
Figure 3-25 – Bulk mass loss for sycamore (cyclohexane inerted, nitrogen inerted) and a 5 g larch fixed bed of particle size <4mm (Robinson et al., 2015) inerted by nitrogen 124
Figure 3-26 –Pyrolysis oil yields from the liquid-inerted microwave pyrolysis process in cyclohexane at applied powers of approximately 0.6 – 1.5 kW, with mass loss included for reference, error bars represent potential variation due to the separation process..... 128
Figure 3-27 – Total pyrolysis oil yields from the liquid-inerted microwave pyrolysis process in 2-propanol, with mass loss included for reference. 128
Figure 3-28 – Total pyrolysis oil yields from the nitrogen-inerted microwave pyrolysis process with approximately 0.5 – 1.5 kW applied power, with mass loss included for reference..... 129
Figure 3-29 – Pyrolysis oil yields in relation to the mass loss, and in relation to the total oil yields for the cyclohexane inerted microwave pyrolysis process..... 130
Figure 3-30 – Pyrolysis oil yield in relation to the mass loss for the 2-propanol inerted microwave pyrolysis process. 131
Figure 3-31 – Pyrolysis oil yield in relation to the mass loss for the nitrogen inerted microwave pyrolysis process. 131
Figure 3-32 - Group abundance in the inerting media used, based on peak area, with analysis carried out by each collaborator denoted. 135

Figure 3-33 – Bulk mass loss for sycamore with cyclohexane as an inerting medium, five successive runs at 1.5 ±0.06 kJ/g, 1.5 kW applied power (three repeats) with dynamic impedance matching to maximise the absorbed power.....138
Figure 3-34 – Liquid solvent mass as a percentage of the starting liquid mass when pyrolysing sycamore with cyclohexane as an inerting medium, five successive runs at 1.5 ±0.06 kJ/g, starting volume 100 mL (77.9g), 1.5 kW applied power.....139
Figure 3-35 - Predicted internal temperature in the centre of the block over time, and a cross sectional temperature profile at 10 seconds based on 0.6 kW absorbed power with *n*-hexane as an inerting liquid.....141
Figure 3-36 - Cross sections of the pyrolysed sycamore at approximately A) 0.5 kJ/g, B) 1.0 kJ/g, C) 1.5 kJ/g, D) 2.0 kJ/g, E) 2.5 kJ/g, 1.5 kW applied power within cyclohexane and dynamic impedance matching.....142
Figure 3-37 - Cross-sectional images of sycamore blocks after pyrolysis (1.5 kW applied, approximately 0.6 kW absorbed, 12 seconds) within n-hexane (45 x 15 x 15 mm).....143
Figure 3-38 – Computed temperature cross section of the sycamore block 1.5 kW applied power (0.6 kW absorbed power), 12 seconds, within n-hexane (top), and nitrogen (bottom).....143
Figure 3-39 - Weight and derivative weight changes for three subsections of the pyrolysed sycamore, and non-pyrolysed sycamore with a heating rate of 10 °C/min. 145
Figure 3-40 – Composition (dry basis) of the non-pyrolysed sycamore and centre of the pyrolysed samples.....147
Figure 3-41 – Predicted temperatures reached within the centre of the pyrolysed samples, with non-pyrolysed sycamore for reference.....147

Figure 3-42 - Behaviour of the nitrogen and liquid inerted (cyclohexane and kerosene) single-mode microwave pyrolysis system at approximately 0.6 kW and 1.5 kW absorbed, over specific energies of 0.0 – 2.5 kJ/g. 149

Figure 3-43 – Condensate formation in the gas-inerted microwave pyrolysis system, approximately 0.6 kW absorbed, representative of 0.79 – 0.85 kJ/g specific energy. 150

Figure 3-44 – Pool boiling curve for water, adapted from Serth (2007). 151

Figure 3-45 – Behaviour of the cyclohexane inerted microwave pyrolysis process at approximately 0.6 kW absorbed power. 153

Figure 4-1 - A schematic representation of how bubble regime leads to limited volumes of liquid surrounding the biomass, tube diameter 30mm, biomass block 45×15×15 mm 158

Figure 4-2 – Flowrate of *n*-hexane vaporised based on heat transfer from the 45×15×15mm sycamore block to the solvent in the single-mode liquid-inerted microwave system at 0.5 – 1.5 kW absorbed power..... 160

Figure 4-3 - A schematic showing how the liquid replenishes the biomass surface in the scaled-up system 162

Figure 4-4 - Liquid-inerted multi-mode microwave pyrolysis system 165

Figure 4-5 - (Left) Aqueous phase pyrolysis oil with kerosene separated out after 24h of air drying. (Right) the organic kerosene fraction after washing with methanol.... 166

Figure 4-6 – Power absorbed by the system for approximately 0.5 and 3.0 kW applied power in the multi-mode microwave pyrolysis system, sycamore block of dimensions 50×50×25 mm and using cyclohexane as an inerting liquid for 10 runs per applied power..... 168

Figure 4-7 - Power absorbed by the system for approximately 0.5 and 3.0 kW applied power in the multi-mode microwave pyrolysis system, sycamore block of dimensions 50×50×25 mm and using kerosene as an inerting liquid for 8 runs per applied power. 169
Figure 4-8 - Power absorbed by the system for approximately 3.0 kW applied power in the multi-mode microwave pyrolysis system, sycamore block of dimensions 50×50×25 mm and using 2-propanol as an inerting liquid over 5 runs. 170
Figure 4-9 – Power absorbed by the system for 3.0 kW applied power, in the multi-mode microwave pyrolysis system, sycamore block of dimensions 50×50×25 mm and using water as an inerting liquid, averaged over 5 runs.....171
Figure 4-10 – Overall block mass loss against specific energy for 1.5 kW applied power, 10 - 82 seconds for the sycamore block geometries investigated in cyclohexane.....173
Figure 4-11 – Pyrolysis oil yield against Specific Energy at an applied power level of 1.5 kW, 10 - 82 seconds for the sycamore block geometries investigated. 174
Figure 4-12 - Solid mass of sycamore blocks against absorbed specific energy at applied power levels of 0.5 – 5.5 kW using cyclohexane as an inerting liquid.....176
Figure 4-13 - Solid mass loss of sycamore blocks against absorbed specific energy at applied power levels of 0.5 – 5.0 kW using kerosene as an inerting liquid.....177
Figure 4-14 – The sycamore blocks after processing within 2-propanol (left), water (middle), cyclohexane (right), with the water and 2-propanol blocks exhibiting no mass loss, cyclohexane 44 % mass loss.....178
Figure 4-15 - A cross section of a sample pyrolysed at approximately 0.5 kW applied, 60 seconds in cyclohexane, showcasing uneven heating of the sycamore block 179
Figure 4-16 –Aqueous and organic pyrolysis oil yields for cyclohexane as an inerting liquid, with non-condensable gas yields shown (by difference).....181

Figure 4-17 – Aqueous and organic pyrolysis oil yields for kerosene as an inerting liquid, with non-condensable gas yields shown (by difference). 181
Figure 4-18 – The total oil yield as a percentage of volatiles for the single-mode system and the multi-mode system, with cyclohexane as an inerting medium. 184
Figure 4-19 - Internal temperature plot of a 50 × 50 × 25 mm sycamore block, heated under the conditions 3 kW absorbed, 40 seconds. 184
Figure 4-20 - Compound groups for the multi-mode liquid inerted microwave pyrolysis process in various inerting media, with the single-mode oils presented for comparison, with collaborators denoted. 188
Figure 4-21 – Hemicellulose, cellulose and lignin content against mass loss for the pyrolysed sycamore char. 190
Figure 4-22 – Lignin composition of the single-mode and multi-mode system, 0 – 4 kJ/g. 191
Figure 4-23 – The composition of the blocks as a whole for the specific energies investigated, with the composition of the chars for reference. 193
Figure 4-24 - Temperature estimates based on simulations for various processing conditions on 50×50×25 mm sycamore blocks within cyclohexane, and cross-sections of the empirical counterparts within cyclohexane, showcasing heating from a certain point in the biomass. 195
Figure 4-25 – Derivative mass loss curves for the pyrolysed sections of the sycamore block, heating rate 10 °C/min. 196
Figure 4-26 – Proximate composition (dry basis) of the non-pyrolysed sycamore and centre of the pyrolysed samples. 197

Figure 4-27 – Temperatures estimated by TGA within the centre of the pyrolysed samples within cyclohexane, with non-pyrolysed sycamore and the single-mode results for reference. 197

Figure 5-1 – (Left) The single-mode and (right) the multi-mode liquid inerted microwave pyrolysis systems, with the microwave inlet port highlighted in blue. ... 203

Figure 5-2 – The measured dielectric constant and loss factor of the sycamore. 204

Figure 5-3 - Bulk mass loss of the sycamore blocks against absorbed specific energy for cyclohexane as an inerting liquid for approximately 0.6 and 1.5 kW absorbed power in the single-mode system. 205

Figure 5-4 – Total pyrolysis oil yields of the sycamore blocks against absorbed specific energy for cyclohexane as an inerting liquid for approximately 0.6 and 1.5 kW absorbed power in the single-mode system. 206

Figure 5-5 - Solid mass loss and pyrolysis oil yield (based on the non-pyrolysed sycamore mass) of sycamore blocks against absorbed specific energy at applied power levels of 0.5 and 3 kW using cyclohexane as an inerting liquid, dynamic impedance matching. 206

Figure 5-6 - Solid mass loss and pyrolysis oil yield (based on the non-pyrolysed sycamore mass) of sycamore blocks against absorbed specific energy at applied power levels of 0.5 and 3 kW using kerosene as an inerting liquid, dynamic impedance matching. 206

Figure 5-7 – (Left) The power density (W/m^3) distribution within the sycamore block in the single-mode liquid inerted microwave pyrolysis process at 1.5 kW applied power. (Right). A cross section of a sycamore block pyrolysed at 1.5 kW applied power, 0.5 kJ/g. 210

Figure 5-8 - (Left) The power density (W/m^3) distribution within the sycamore block in the multi-mode liquid inerted microwave pyrolysis process at 0.5 kW applied power. (Right). A cross section of a sycamore block pyrolysed at 0.5 kW applied power, 0.92 kJ/g. 210

Figure 5-9 – Sampling points within the sycamore block for the single-mode and multi-mode computational simulations. 211

Figure 5-10 – Internal temperatures at the sampling point for a block heated by 1.5 kW power absorbed, and heated in the theoretical microwave field with 1.5 kW applied power, with temperatures predicted by TGA for comparison for the single-mode system. 212

Figure 5-11 – The power absorbed of the microwave field model, power absorbed model, and empirical data for approximately 1.5 kW applied power (cyclohexane inerted), for the single-mode system. 213

Figure 5-12 – The internal temperature at the sampling point for a block heated by 3.0 kW power absorbed, and heated in the theoretical microwave field with 3.0 kW applied power, with temperatures predicted by TGA for comparison for the multi-mode system. 214

Figure 5-13 – The temperature at the centre of the 4.5 × 1.5 × 1.5 cm sycamore block, 1.5 kW absorbed power, with modified thermal conductivity (k×41), and modified specific heat capacity (C_p×3.5), with internal temperature predicted by TGA for reference. 215

Figure 5-14 – The relationship between applied power and the peak electric field strength within the single-mode microwave pyrolysis system without the sample present, and with the sample present at 20 °C. 217

Figure 5-15 – Theoretical power absorbed by the sycamore block, based on applied powers of 0.5 – 1.5 kW, over the temperature range of 0 - 550°C. 218
Figure 5-16 – The dielectric loss factor for sycamore within the single-mode liquid inerted pyrolysis process over 22 runs, 0.6 – 1.8 kW applied power. 219
Figure 5-17 – The dielectric constant of the sycamore over the temperature range 0 – 600 °C for the microwave method and the cavity perturbation method. 221
Figure 5-18 - The dielectric loss factor of the sycamore over the temperature range 0 – 600 °C for the microwave method and the cavity perturbation method. 222
Figure 5-19 – The internal temperature at the sampling point for a sycamore block heated in the theoretical microwave field with 1.5 kW applied power, with the cavity dielectrics and modified dielectrics, with temperatures predicted by TGA for comparison for the single-mode system. 223
Figure 5-20 – The mass loss data for approximately 1.5 kW absorbed power, 6 ±0.25 g sycamore block mass. 225
Figure 5-21 – The simple schematic for determining peak pressure within the sycamore block during microwave pyrolysis. 227
Figure 5-22 – Pressure generation within the 4.5 × 1.5 × 1.5 cm sycamore block during the pyrolysis process, with no physical changes to the sycamore block. 227
Figure 5-23 – The schematic for determining peak pressure within the sycamore block during microwave pyrolysis, with permeability and porosity changes applied. 228
Figure 5-24 – Pressure generation within the 4.5 × 1.5 × 1.5 cm sycamore block during the pyrolysis process, permeability and porosity increases considered. 228
Figure 5-25 – The peak pressure within the 4.5 × 1.5 × 1.5 cm, and 5.0 × 5.0 × 2.5 cm sycamore block against the processing permeability range. 229

Figure 5-26 – The drying process of all four models, $kH2O = AH2Oe - EH2ORT$, (Ding et al., 2018). 232
Figure 5-27 – Internal temperature prediction (modelled) over time for a 4.5×1.5×1.5 cm block in a furnace at 1000 °C, and heated by microwave with 1.5 kW absorbance. 235
Figure 5-28 - Pressure generation within the sycamore block, models 1 - 4 for (left) a microwave pyrolysis process, sycamore block 1.5 kW applied, 4.5×1.5×1.5 cm, 10 second processing time and (right) a 1mm diameter spherical sycamore particle placed in a 1000 °C furnace, 20 second processing time. 236
Figure 5-29 – The boiling temperature of levoglucosan at elevated pressures..... 239
Figure 6-1 – Process flow diagram for a continuous pyrolysis process with (A) organic phase solvent, (B) aqueous phase solvent and (C) oil-miscible solvent. 250
Figure A-1 – The specific heat capacity of the sycamore used within the thesis, and line of best fit equation. 269
Figure B-1 - Absorbance data for isooctane based on (A) 1.00 kW, (B) 1.25 kW, (C) 1.50 kW, (D) 1.80 kW applied powers with fixed cold-matching..... 270
Figure B-2 - Absorbance data for kerosene based on (A) 1.00 kW, (B) 1.25 kW, (C) 1.50 kW, (D) 1.80 kW forwarded powers with fixed cold-matching 271
Figure B-3 - Absorbance data for pentane based on (A) 0.70 kW, (B) 1.00 kW, (C) 1.25 kW, (D) 1.50 kW forwarded powers with fixed cold-matching 271
Figure B-4 - Applied power, absorbed power and percentage power absorbed for the cavity only containing the quartz tube with cyclohexane, no sycamore present 272
Figure C-1 – Absorbance curves for powers 0.5 – 5.5 kW applied powers in the multi-mode system, cyclohexane inerted, error bars represent the standard deviation from the mean. 285

Figure C-2 – Absorbance curves for powers 0.5 – 5.0 kW applied powers in the multi-mode system, kerosene inerted, error bars represent the standard deviation from the mean. 285
Figure C-3 – Total pyrolysis oil yields of the multimode system, using cyclohexane as an inerting liquid. 286
Figure C-4 – Total pyrolysis oil yields of the multimode system, using kerosene as an inerting liquid. 286
Figure C-5 – Aqueous and organic phase pyrolysis oil, and gas yields in relation to mass loss. 287
Figure C-6 – Aqueous and organic phase pyrolysis oil yields in relation to the total yield as a percentage against specific energy for the multi-mode process using cyclohexane as an inerting medium. 287
Figure C-7 – Total pyrolysis oil yield in relation to total volatiles produced as a percentage against specific energy for the multi-mode process using cyclohexane as an inerting medium. 287
Figure C-8 – Aqueous and organic phase pyrolysis oil, and gas yields as a percentage of total volatiles produced for kerosene as an inerting liquid. 288
Figure C-9 – Aqueous and organic phase pyrolysis oil yields in relation to the total yield as a percentage against specific energy for the multi-mode process using kerosene as an inerting medium. 288
Figure C-10 – Total pyrolysis oil yield as a percentage of total volatiles produced against Specific Energy for the multi-mode process using kerosene as an inerting medium. 288

Figure C-11 – Lignin concentration of the sycamore blocks, pre and post pyrolysis, samples taken from char and homogenised blocks, against the volatile matter/fixed carbon ratio (dry, ash free basis) obtained from TGA. 301
Figure D-1 - Bulk mass loss against specific energy for soaked sycamore blocks in the multimode system with 1 kW absorbed power within cyclohexane.....308
Figure D-2 – Pyrolysis oil yields against specific energy for soaked sycamore blocks in the multimode system with 1.0 kW absorbed power within cyclohexane.....309
Figure D-3 – Pyrolysis oil yields compared to bulk mass loss of the sycamore blocks against specific energy for soaked biomass in the multimode system with 1 kW absorbed power 310
Figure D-4 - Five samples simultaneously pyrolysed at specific energies of 1.0, 2.0 and 3.0 kJ/g, and the mass losses obtained for each sample.....313
Figure D-5 – Lignocellulosic composition of the sycamore block (single-mode) for 1.5 kW applied power for model 2. 315
Figure D-6 – Lignocellulosic composition of the sycamore block (single-mode) for 1.5 kW applied power for model 3. 315
Figure D-7 - Lignocellulosic composition of the sycamore block (single-mode) for 1.5 kW applied power for model 2, with empirical mass fractions for comparison.....316
Figure D-8 - Lignocellulosic composition of the sycamore block (single-mode) for 1.5 kW applied power for model 3, with empirical mass fractions for comparison.....317
Figure D-9 - Lignocellulosic mass fraction of the sycamore block (single-mode) for 0.6 and 1.5 kW applied power for model 2, with the internal temperature limited to 450°C. 318

Figure D-10 - Lignocellulosic mass fraction of the sycamore block (single-mode) for 0.6 and 1.5 kW applied power for model 3, with the internal temperature limited to 450°C. 319

List of abbreviations and nomenclature

Abbreviations

BFB	-	Bubbling fluidised bed
CFB	-	Circulating fluidised bed
DSC	-	Differential scanning calorimetry
FC	-	Fixed carbon
GC-MS-		Gas chromatography-mass spectroscopy
ML	-	Mass loss
SDT	-	Simultaneous DSC-TGA
TGA	-	Thermogravimetric analysis

Nomenclature

ΔH_{vap}	-	Enthalpy of vaporisation, kJ/mol
∇	-	Gradient vector, $\left(\frac{\delta}{\delta x}, \frac{\delta}{\delta y}, \frac{\delta}{\delta z}\right)$
A	-	Area, m^2
c_0	-	Speed of light in a vacuum, m/s
C_p	-	Specific heat capacity, J/kg·K
D_p	-	Penetration depth, m
E	-	Electric field strength, V/m
E_s	-	Specific absorbed energy, kJ/g
f	-	Frequency, Hz
f_0	-	Resonant frequency of the empty cavity
f_s	-	Resonant frequency of the cavity with the sample present
h	-	Heat transfer coefficient, $W/m^2 \cdot K$
H(T)	-	Specific heat flow at temperature T, W/g
i	-	$\sqrt{-1}$
$J_1^2(x_{1,m})$	-	Second order of the first kind root of the Bessel function
k	-	Thermal conductivity, W/m·K
k_0	-	Wave number ($k_0 = \omega/c_o$)
L	-	Characteristic length, m

M	-	Initial mass of the sample, g
Nu	-	Nusselt number
P	-	Power, W
p_x^*	-	Partial vapour pressure
p	-	Pressure, Pa
P_D	-	Power density of the sample, W/m^3
q	-	Heat flux, W/m^2
$\dot{Q}$	-	Power absorbed by the biomass, W/s
Q_0	-	Quality factor of the empty cavity
Q_m	-	Volatiles mass concentration generation rate, kg/m^3·s
Q_s	-	Quality factor of the cavity with the sample present
R	-	Constant, 8.3145 J/mol·K
T	-	Temperature, K (°C)
t	-	Time, s
tan δ	-	Loss tangent
u	-	Velocity, m/s
$\dot{V}$	-	Flowrate of gas, m^3/s
V	-	Volume, m^3
V_c	-	Volume of the cavity
V_s	-	Volume of the sample
x_x	-	Liquid composition of component x, mole basis
y_x	-	Vapour composition of component x, mole basis
ε_r	-	Relative permittivity
ε’	-	Dielectric constant
ε”	-	Dielectric loss factor
ε_p	-	Porosity
γ	-	Char yield fraction
κ	-	Intrinsic permeability, m^2
λ^0	-	Wavelength, m
μ	-	Dynamic viscosity, Pa·s
μ	-	Relative permeability

ρ	-	Density, kg/m^3
σ	-	Electrical conductivity, S/m
ω	-	Wave angular frequency, rad/s

Subscripts

a	-	Virgin wood
A, B	-	Cellulose fractions, model 2
C	-	Cellulose, model 3
c	-	Char, primary char generation
c2	-	Char, secondary char generation
cl	-	Cellulose, model 2
g	-	Gas, primary reaction pathway
g2	-	Gas, secondary reaction pathway
H	-	Hemicellulose, model 3
H_2O	-	Water
H_2OL	-	Liquid water
H_2OV	-	Water vapour
hcl	-	Hemicellulose, model 2
is	-	Intermediate solid
l	-	Lignin, model 2
L	-	Lignin, model 3
v	-	Total volatiles

1. Introduction

Currently, the world is reliant on fossil fuels for energy, chemicals and pharmaceuticals (Hess et al., 2011) in the forms of crude oil, coal and natural gas (IEA, 2019b, BP, 2019). The world is undergoing a rapid outgrowth of population and urbanisation, with the world's population predicted to grow from 7.7 billion in 2019 to 8.5 billion in 2030 (United Nations, 2019). The demand for energy, food, natural resources and fossil fuel derived chemicals will increase alongside this. It is therefore possible that the current sources of energy and pharmaceuticals will be insufficient to meet the increasing demands (Goyal et al., 2008). Along with the increasing demand for fossil fuel derived energy and chemicals, legislation and treaties are increasingly being introduced to regulate emissions, for example the United Nations (UN) Paris Agreement, which places limits on greenhouse gas emissions (United Nations, 2015). Bioenergy policies set by the European Union (EU) also have their own mandatory renewable energy target, with the ultimate goal that 20 % of the total energy produced by the EU is replaced by renewable energy sources, and all EU countries require to use 10 % biofuel in transport fuels (European Union, 2009).

Sustainable sources of energy, chemicals and pharmaceuticals are gaining more attention due to their feasibility to meet the increasing energy and chemical demands whilst managing environmental concerns due to the carbon neutrality of biomass (Fernando et al., 2006, Field et al., 2008, Proskurina et al., 2019, Romashov and Ananikov, 2017, Zhang et al., 2015). Renewable energy is considered essential for reducing the consumption of fossil fuels and mitigating the atmospheric greenhouse effect (Ayalur Chattanathan et al., 2012). There are many ways to produce electricity through sustainable sources which include hydroelectricity, solar, and biofuels (BP, 2019). Figure 1-1 presents the world's total primary energy supply by sector as of 2017.

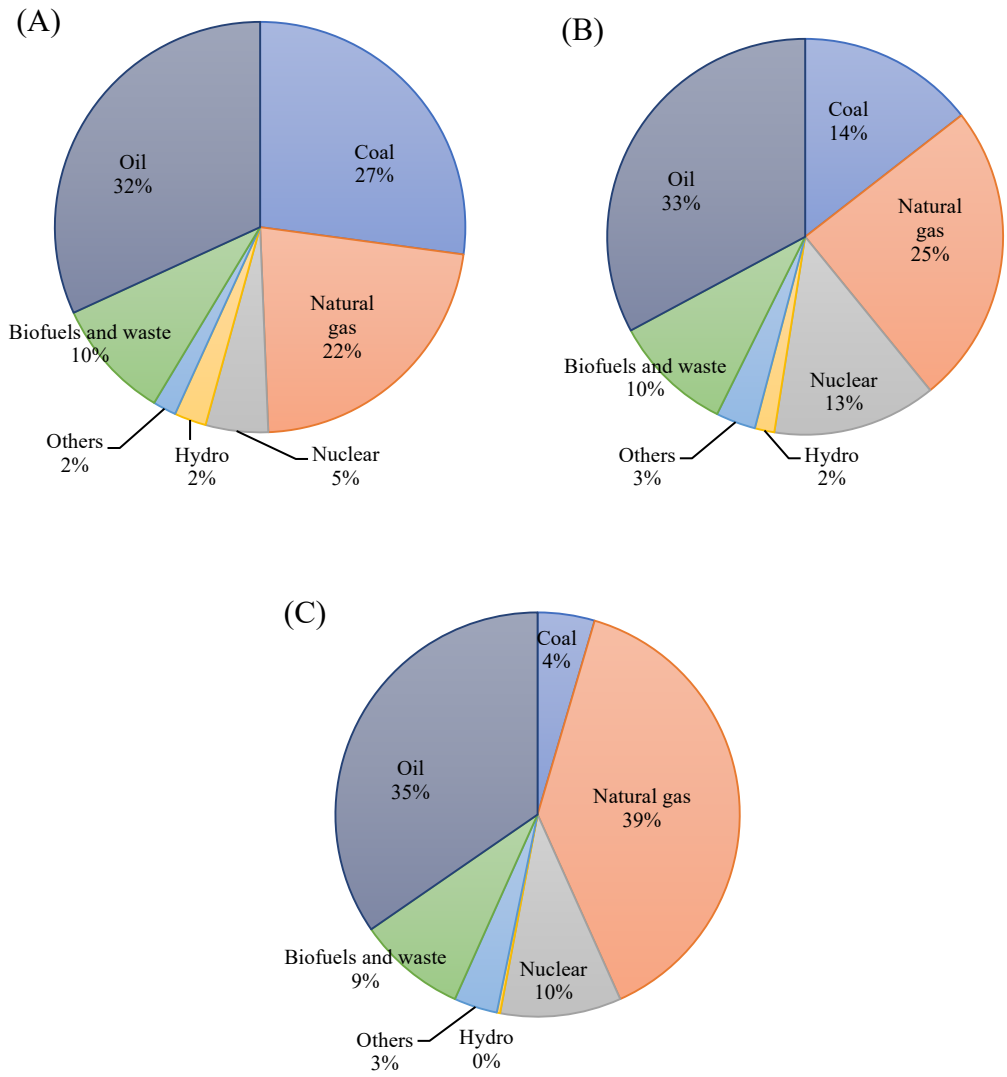


Figure 1-1 – (A) World, (B) EU, (C) UK total primary energy supply by sector as of 2017. *Others include geothermal, solar, wind, tide/wave/ocean and heat. (IEA, 2019a)

The consumption of worldwide energy in 2017 was 13,970 million tonnes of oil equivalent (Mtoe). Globally, more than 80 % of this energy was provided by fossil fuels alone, with renewables (nuclear, hydro, biofuels and waste and others) comprising only approximately 20 %. In the UK and the EU, renewables accounted for approximately 22% and 29% of the total energy supply, respectively. Biofuels and waste comprised over 50 % of the renewables globally, approximately 40% in the UK, and 30% in the EU. Most biomass and wastes have lower mass and energy densities compared to coal

(Kandiyoti et al., 2017). Conventional energy generation equipment is built for high energy density fuels which are not compatible with biomass and so more attention is being diverted into converting biomass into fuels that have both a higher energy density and are able to compete with and eventually replace conventional fuels (Macquarrie et al., 2012).

Sustainable process development would include replacing current sources of fossil fuel derived energy and chemicals with sustainable sources, such as waste-stream biomass sources. Renewable energy sources such as hydroelectricity and solar are useful for energy production, however they cannot deliver on the societal needs of transportation fuels, organic chemicals and polymers. Valorising biomass into useful bio-based products and biofuels therefore has the potential to meet these demands.

1.1 Composition of biomass

Lignocellulosic biomass such as wood, straws and grasses are primarily composed of cellulose, hemicellulose, lignin and small amounts of other biochemical constituents such as lipids, proteins, starches, ash and water (Jenkins et al., 1998, Balat et al., 2009).

1.1.1 Cellulose

Cellulose $(C_6H_{10}O_5)_n$, is a homopolysaccharide consisting of repeating (5000 - 10000) linearly chained β (1-4) linked D-glucopyranose (glucose) units. Cellulose provides strength to the structure of wood and typically makes up approximately 40 – 50 % of dry wood composition (Finch, 1986, Mohan et al., 2006). The basic repeating unit of the cellulose polymer consists of two D-glucopyranose units, otherwise known as a cellobiose unit. Figure 1-2 shows the structure of the D-glucopyranose, and cellobiose units present in cellulose.

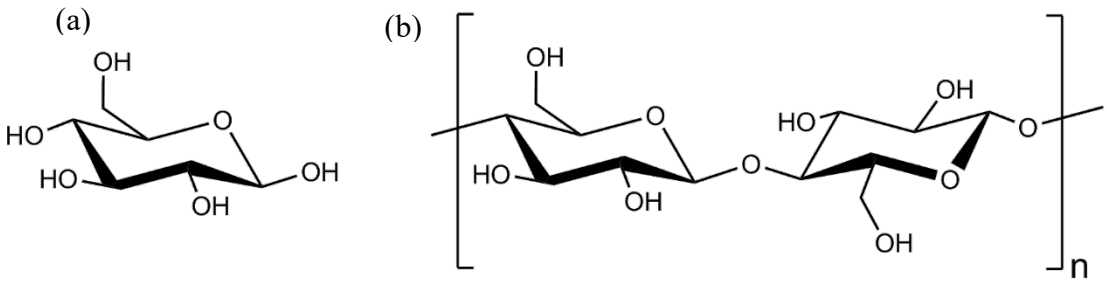


Figure 1-2 – (a) D-glucopyranose, (b) cellobiose unit.

Cellulose chains bond in parallel to each other via inter- and intra-molecular hydrogen bonds to form a crystalline structure. The groups of cellulose chains twist inwards to form microfibril sheets, which are the basic construction units for a variety of complex fibres. These microfibrils form composite tubular structures that run along a longitudinal tree axis and provide the structural backbone for lignocellulosic biomass (Mohan et al., 2006, Balat et al., 2009).

1.1.2 Hemicellulose

Hemicellulose is a heteropolysaccharide comprising of C_5 and C_6 monosaccharides, such as glucose, mannose, galactose, xylose, arabinose, glucuronic acid and galacturonic acid residues (Mohan et al., 2006). Hemicellulose typically makes up 20 – 30 % dry wood weight, and each chain of hemicellulose has fewer monomers than cellulose, with a degree of polymerisation around 200. Hemicellulose chains can also branch out, rather than consisting of only straight chains (Pecha and Garcia-Perez, 2015). Figure 1-3 presents the monomers that comprise hemicellulose.

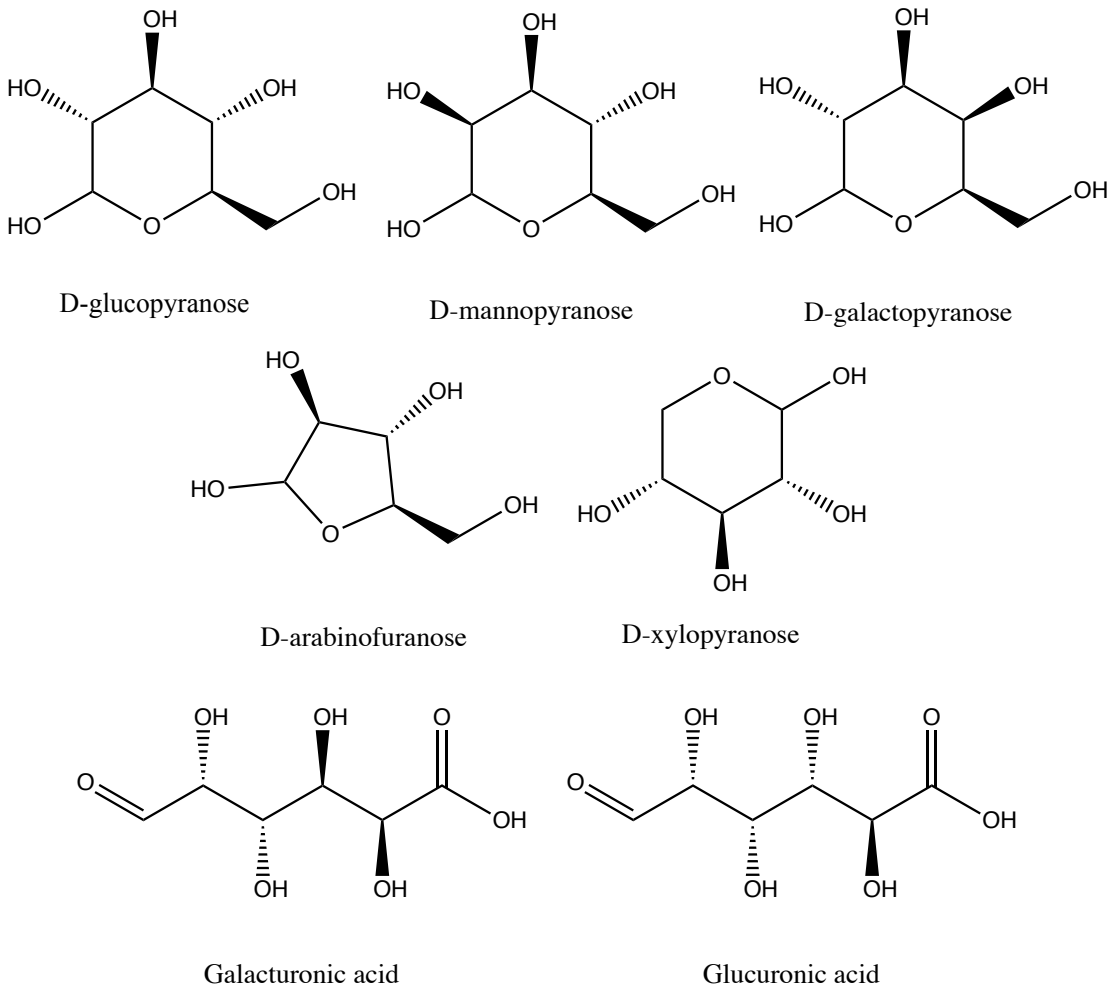
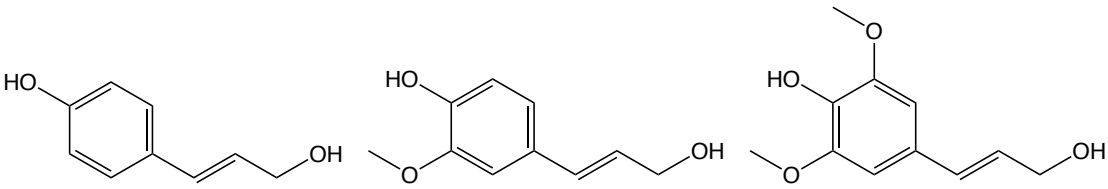


Figure 1-3 – The monomers that comprise hemicellulose.

1.1.3 Lignin

Lignin typically comprises 15 – 36 % of a dry wood weight and it is a network of phenylpropanoid units. The alcohol base units for lignin are p-hydroxyphenyl, guaiacyl, and syringyl lignins, forming three alcohols, p-coumaryl alcohol, coniferyl alcohol and sinapyl alcohol, respectively (Pecha and Garcia-Perez, 2015). These monomers form polymers in many different ways to form the lignin structure. Lignin itself binds the cellulose and hemicellulose matrices and adds flexibility and crystallinity to the

structure (Montazeri and Eckelman, 2015). Figure 1-4 presents the monomers that comprise lignin.



p-Coumaryl alcohol Coniferyl alcohol Sinapyl alcohol

Figure 1-4 – The alcohol constituents of lignin.

1.1.4 Extractives and inorganics

Extractives generally comprise 2 – 10 % of wood mass (Pecha and Garcia-Perez, 2015). Extractives in biomass are the components that can be extracted using solvents such as water, hexane, ethanol and dichloromethane. The components do not contribute to the structure of the biomass and can be categorised as fats, proteins, terpenes, gums, waxes, starches, phenolics, pectins, fatty acids, lipids, saponins, sterols, and essential oils (Kallioinen et al., 2003, Roy et al., 1990). In wood, the heartwood and bark contain phenolic extractives which protect the lignocellulosic structure from fungal and microbial attack (Pecha and Garcia-Perez, 2015).

Mineral or inorganic matter present in biomass becomes ash after combustion (Pattiya, 2018). The ash content present within the biomass can have an effect on the pyrolysis process, and can catalyse char formation reactions, reducing pyrolysis oil yields, and increasing char and pyrolysis-gas yields (Nik-Azar et al., 1997, Raveendran et al., 1995).

1.2 Biomass conversion technologies

Biomass can be converted to valuable products through different conversion routes, which include chemical, biochemical, fermentation and thermochemical processes

(Fernando et al., 2006). The work presented in this thesis focusses on pyrolysis, which is a high temperature thermochemical decomposition process.

1.2.1 Thermochemical biomass conversion

1.2.1.1 Thermochemical pre-treatment

Thermochemical biomass pre-treatments generally occur at temperatures ranging from 50 - 250°C. Biomass feedstocks are typically treated at such temperatures in order to reduce the lignin content and its crystallinity, whilst simultaneously disrupting the cell wall architecture to allow for easier hydrolysis of cellulose into its monomeric constituents (glucose) (Daza Serna et al., 2016, Zhang et al., 2016a).

Low temperatures and high pressures can be utilised to pre-treat biomass and remove a lignocellulosic constituent, such as lignin. One such example involved the pre-treatment of rice husk biomass at a low temperature (80°C), high pressure (270 bar) supercritical CO_2 environment for 10 minutes. This resulted in a lignin reduction of 90.6 %, allowing for an increase in enzymatic saccharification (hydrolysis of polysaccharides into monosaccharides) (Daza Serna et al., 2016).

Thermal pre-treatment in the absence of high pressures is also feasible. Zhang et al (2016a) pre-treated mature sweet gum biomass by conventionally heating it to 200 - 240°C for 4 - 12 minutes in the presence of glycerol and shear stresses via agitation (to disrupt the cell wall architecture). The biomass was then treated with solvents (dioxane, acetone) and alkalis (NaOH) to remove the lignin and xylan content. The removal of xylan significantly increased the hydrolysis rate, resulting in an increased conversion of cellulose into glucose of 70 % over 24 hours.

Microwaves can also be used for thermal biomass pre-treatment. Ganesapillai et al. (2016) initially microwave pre-treated olive kernels and then subsequently

conventionally pyrolysed the pre-treated olive kernels. This resulted in an increased pyrolysis oil yield of 59.9 % at 500°C, and an increased syngas yield (84.9 v/v % as opposed to 79 % untreated) at 720°C.

1.2.1.2 Thermochemical decomposition processes

When biomass is heated in an inert atmosphere, four main stages of the structural breakdown of the biomass occurs (Pecha and Garcia-Perez, 2015):

1. Evaporation of moisture (<200 °C).
2. Slow pyrolysis (torrefaction) (225 - 300 °C)
3. Pyrolysis (300 - 650 °C)
4. Gasification (>700 °C)

In slow pyrolysis and torrefaction (<10 °C/s), these reactions happen successively, however in fast pyrolysis (~200 °C/s), the events are thought to happen simultaneously (Pecha and Garcia-Perez, 2015).

1.2.1.3 Pyrolysis

Pyrolysis derives from the Greek words πυρ (*pýr*), meaning "fire," and λύσις (*lýsis*), meaning "splitting" or "cracking." Pyrolysis is used to thermochemically convert a solid material into carbonaceous char, pyrolysis oil and gas between temperatures of approximately 300 - 650 °C, in the absence of oxygen. The constituents of biomass; cellulose, hemicellulose and lignin break down into liquid and gas fractions containing numerous compounds for use in fuel blends or for speciality chemicals, and the remaining solid residue is char. (Bridgwater et al., 1999, Vispute et al., 2010).

Pyrolysis of organic matter involves simultaneous successive and competitive reactions in an inert atmosphere, as shown for a fast pyrolysis process in Figure 1-5.

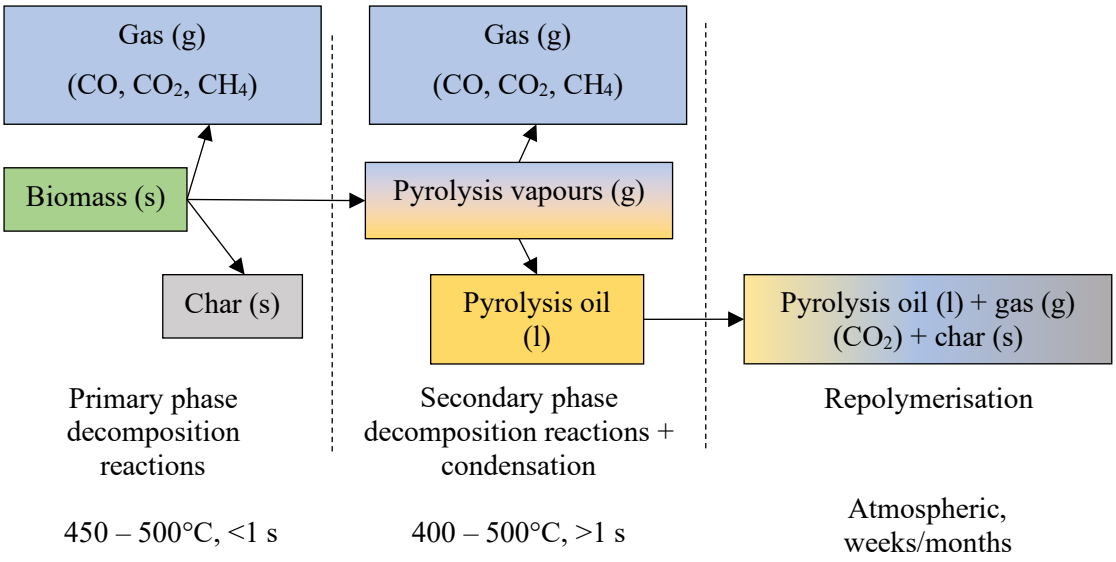


Figure 1-5 – The pathway of biomass to pyrolysis products, adapted from Venderbosch and Prins (2010).

There are three main types of pyrolysis: slow (torrefaction), fast and flash pyrolysis. A summary of the types of pyrolysis are presented in Table 1-1.

Table 1-1 – An overview of the main types of pyrolysis, with typical product yields, adapted from Jahirul et al. (2012).

Pyrolysis process	**Solid residence time (s)**	**Heating rate (°C/s)**	**Particle size (mm)**	**Temperature (°C)**	**Product yield (%)**		
					Oil	**Char**	**Gas**
Slow	450 – 550	0.1 – 1	5 – 50	280 - 680	30	35	35
Fast	0.5 – 1.0	10 – 200	<1	580 – 980	50	20	30
Flash	<0.5	>1000	<0.2	780 - 1020	75	12	13

Slow pyrolysis is the process of using a slow heating rate (<1 °C/s), and high residence times (~10 minutes). Torrefaction produces a large amount of char, and as the residence time is high, vapour phase products react with each other and undergo secondary degradation, reducing the pyrolysis oil yield and quality (Balat et al., 2009, Jahirul et al., 2012). It is possible to use torrefaction as a pre-treatment for biomass, as the mechanical disruption of the biomass fibres by thermal degradation could lead to

smaller particle sizes, reduced amounts of hemicellulose, extractives, inorganic ash and metals (Das and Sarmah, 2015).

Fast pyrolysis involves heating the biomass rapidly in an inert atmosphere. It requires a short vapour residence time (0.5 – 10 seconds), fine particles (<1 mm) and high operating temperatures (>500 °C). The vapours and aerosols cool rapidly to produce pyrolysis oil, and as such, the process produces mainly liquid and gaseous products (Demirbas et al., 2009).

Flash pyrolysis involves incredibly short gas residence times (< 1s) with a very high heating rate of the particles. Very small particles are typically used (< 0.2 mm) and up to 75 % of the biomass can be converted into oil (Demirbas and Arin, 2002, Demirbas, 2000, Aguado et al., 2002).

1.2.1.4 Gasification

Gasification involves high temperatures (>700°C) and long heating times, ranging from 10 minutes up to one hour (Ge et al., 2016, Lundberg et al., 2016, Sharma and Sheth, 2016). Gasification, unlike pyrolysis, does not necessarily require an inert atmosphere, and instead requires the presence of a gasifying agent. Gasifying agents can include controlled amounts of air or oxygen, steam, CO_2, or a mixture of the aforementioned agents (Situmorang et al., 2020). In gasification processes, the production of gas, known as syngas, is favoured over oil formation. The syngas fraction consists of mainly H_2 and CO, with smaller amounts of CO_2 and N_2 present. Syngas is largely used as a fuel gas in internal combustion engines (Hagos et al., 2015). The products produced during the gasification process can be tuned based on the ratio of gasification agents chosen (Speight, 2014).

Steam can be used as a gasification agent, which promotes hydrogen production and allows for a larger H_2/CO ratio in the gas (Sharma and Sheth, 2016), however the oil quality may be limited by the biomass water content (Parthasarathy and Narayanan, 2014). For steam gasification of biomass, many factors must be controlled in order to obtain maximum yields, such as the steam to biomass ratio, reactor type, reactor temperature, catalyst, biomass particle size and type of oxygen carrier (Parthasarathy and Narayanan, 2014, Ge et al., 2016).

Studies have been carried out on co-gasification of biomass with coal (Song et al., 2019, Thengane et al., 2019, Sattar et al., 2014) which has proved to be advantageous as greater conversion syngas yields could be obtained. This is due to the fact that mineral rich (particularly high in potassium) biomass are often used, which when heated forms ash. The ash can then act as a catalyst for gasification of both the coal and biomass (Zhang et al., 2016b, Song et al., 2019, Sattar et al., 2014).

Gasification can also be performed in a microwave-based process, using microwaves to heat biomass directly. It was found by Xie et al. (2014) that gasifying corn stover in the presence of a Ni/Al_2O_3 catalyst, using a 750 W, 2.45 GHz microwave reactor, a yield of 80 wt % gas and a tar content of less than 7 wt % was achievable. In the absence of the catalyst, however, a gas yield of around 65 wt % was acquired. Gasification can be carried out not only on biomass, but also on biomass-derived chars, such as char produced from pyrolysis processes (Mafu et al., 2018, Li et al., 2017, Slezak et al., 2019).

1.3 Pyrolysis principles

1.3.1 Pyrolysis reactions of lignocellulosic constituents

During the pyrolysis process, the lignocellulosic content of the biomass is thermochemically broken down. Each lignocellulosic constituent breaks down over different temperature ranges, and results in the formation of a range of different compounds within the pyrolysis oil product.

1.3.1.1 Cellulose

The depolymerisation of cellulose occurs between 240 - 350°C and produces anhydrocellulose, levoglucosan, cellobiosan and cellotriosan (Mohan et al., 2006, Pecha and Garcia-Perez, 2015). Levoglucosan, cellobiosan and cellotriosan boil at approximately 290°C, 581°C, and 792°C respectively. Due to the boiling points, sugars that are larger than levoglucosan are generally not observed under typical atmospheric pyrolysis conditions, and likely remain within the liquid phase within the biomass structure, undergoing secondary degradation into smaller molecular weight compounds (Pecha and Garcia-Perez, 2015, Stankovikj et al., 2017).

Secondary degradation reactions occur from the products of initial cellulose pyrolysis, and occur in the liquid intermediate phase, solid phase or vapour phase. The secondary degradation reactions produce smaller molecular weight compounds such as furfural, acetol, hydroxymethylfurfural (Antal and Varhegyi, 1995).

1.3.1.2 Hemicellulose

Hemicellulose thermochemically decomposes readily in the temperature range similar to cellulose, approximately 220 - 315°C. Pyrolysis of hemicellulose produces acetic acid, formic acid, acetol, xylosefurfural, glycolaldehyde and furfural (Patwardhan et al., 2011, Zhou et al., 2018).

1.3.1.3 Lignin

Thermochemical decomposition of lignin can be categorised into low temperature and high temperature reactions. The low temperature reactions occur around 180 - 300°C and form lignin oligomers that can further decompose to form lignin monomers. The ether bonds present in lignin break first, forming a liquid intermediate containing larger molecules that do not evaporate under the low temperature conditions. At high temperatures, if the liquid intermediate remains heated, the oligomers can cross link to form char with side products of the char formation being methanol and formaldehyde. If the lignin oligomers are thermally ejected from the biomass, the liquid intermediate can thermally decompose to form the lignin monomers (Pecha and Garcia-Perez, 2015, Zhou et al., 2013).

1.3.2 Pyrolysis products

As stated in Section 1.2.1.3, the three primary products of pyrolysis are char, gas and pyrolysis oil. Generally, fast/flash pyrolysis is focused on obtaining maximum-oil yield, which occurs at temperatures between 350 - 500 °C (Primaz et al., 2018, Demirbas, 2007).

1.3.2.1 Pyrolysis oil

Pyrolysis oil consists of hundreds of compounds, including alcohols, ketones, esters, carboxylic acids, aldehydes, phenols, alkenes, aromatics, sugars, among others (Evans and Milne, 1987). These compounds can generally be grouped into classes: polycyclic aromatic hydrocarbons (PAH), benzene, toluene, xylene and their derivatives (BTX), aliphatics (alkane/enes) and oxygenates (alcohols, ketones, esters and their derivatives), nitrogenates (N-heterocyclic compounds, amides and nitriles) and fatty acids (Beneroso et al., 2015a). Pyrolysis oil is typically composed of a mixture of water (19 – 30 %),

organic compounds (20 – 30 %), water soluble oligomers (28 – 36 %) and water-insoluble lignin-oligomers (15 – 23 %) (Stankovikj et al., 2017, Stankovikj et al., 2016, Stankovikj and Garcia-Perez, 2017, Garcia-Perez et al., 2008a, Han et al., 2019).

Typically only 30 % of the compounds present within pyrolysis oil are detectable by gas-chromatography/mass spectroscopy (GC-MS) analysis, known as GC-MS detectable organics (Han et al., 2019). The GC-MS detectable organic compounds consist of 10 – 22 % C_2 – C_4 oxygenated compounds such as hydroxyl-acetaldehyde, acetol and acetic acid, derived from cellulose and hemicellulose, and 1 – 5 % mono-phenols, from lignin decomposition (Stankovikj et al., 2017). The water soluble oligomers comprise of levoglucosan, cellobiosan and cellotriosan (Pecha and Garcia-Perez, 2015).

A summary of the physical properties of pyrolysis oil produced from pyrolysis processes are presented in Table 1-2.

Table 1-2 – Physical properties of pyrolysis oil, taken from (Jahirul et al., 2012).

Properties	Oil characteristics	Reasons
Appearance	Dark red-brown to dark green	Chemical composition and carbon contamination
Odour	Acrid smoky smell	Low molecular weight aldehydes and acids
Density	~1.2 kg/L	High moisture content and molecule contamination
Viscosity	Can vary from ~25 - 1000 centistokes	Feedstock, water and light compound collection variability
Heating value	Lower than fossil oil	High oxygen content
Aging	Viscosity increase, volatility decrease, phase separation and deposition of gum	Low pH value and complex structure
Miscibility	Miscible with polar solvents but not with petroleum fuels	Polar in nature

The composition of the compounds in the pyrolysis oil are dependent on the biomass that has been pyrolysed, as well as the type of pyrolysis conducted (slow, fast or flash). Conventional and microwave pyrolysis was investigated by Robinson et al. (2015), and the effect of the two processes on the oil product composition is presented in Figure 1-6.

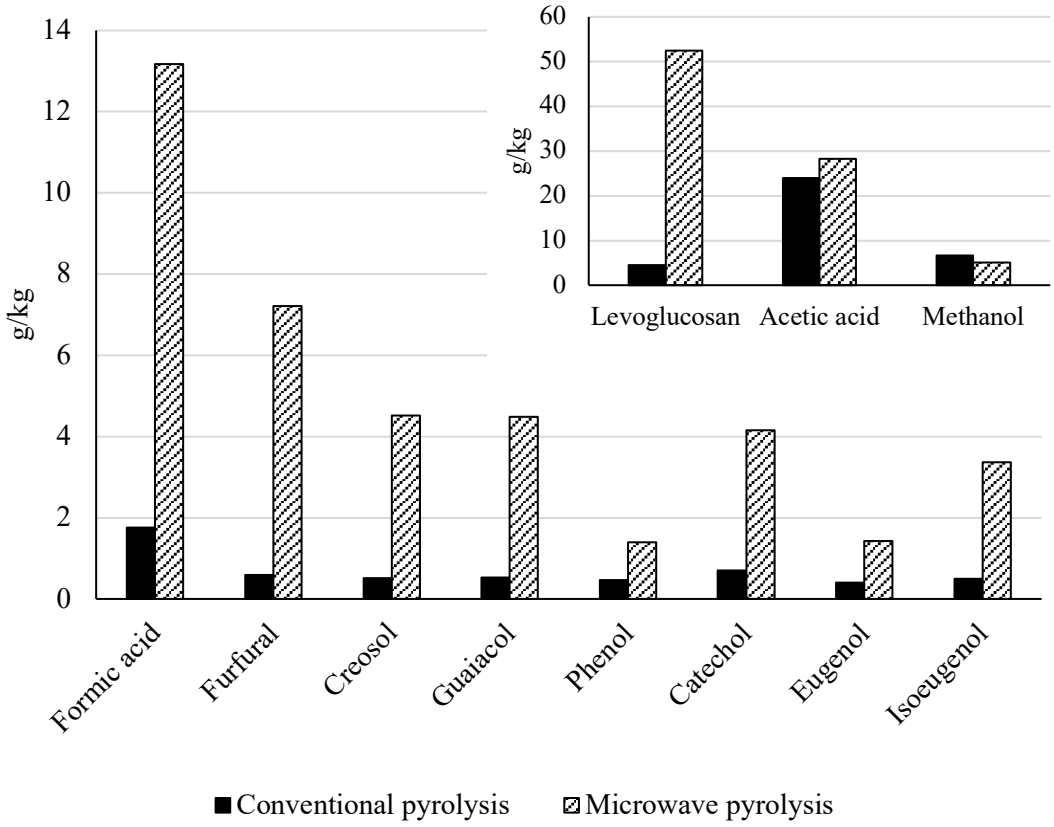


Figure 1-6 - Prominent compounds produced from conventional and microwave pyrolysis of European Larch, adapted from Robinson et al. (2015).

The conventionally heated process was carried out in a 500 g/h fluidised bed process at 500°C, whereas the microwave process was carried out in a batch reactor. It is suggested that due to the presence of the cold sweep gas and low thermal inertia resulting from the fast cooling of the products, secondary degradation was much less likely to occur in microwave pyrolysis as evidenced by the larger prominence of

levoglucosan in the microwave process. In the conventionally heated process, the atmosphere of the reactor was at 500°C, and the secondary degradation of volatiles was, therefore, more likely. The presence of semi-volatile compounds in the liquid product was therefore much more likely in microwave pyrolysis. However, as the organic composition (methanol and acetic acid) were in similar quantities, it was implied that the primary pyrolysis mechanism was the same for both conventional and microwave pyrolysis (Robinson et al., 2015).

Pyrolysis oil is generally immiscible in petroleum fuels due to its high water content, with petroleum fuels generally being hydrophobic. Pyrolysis oil also has a very low pH in the range of 2-4, due to its high concentration of acetic and formic acid (Robinson et al., 2015, Zhang et al., 2016b, Mortensen et al., 2011). This ultimately creates transport, processing and storage issues as corrosion will occur in common plant materials such as aluminium and carbon steel.

Pyrolysis oil can be utilised in multiple ways, which include its raw form, fractionated form, or it could have its biochemical constituents extracted and either directly utilised or used as precursors to generate other compounds of interest. Pyrolysis oil can be used in diesel engines (Yuan et al., 2018, Chiaramonti et al., 2003, Solantausta et al., 1993, Asokan et al., 2018), for heat production in boilers, furnaces or combustors (Gust, 1997, Bridgwater, 2012, Sippula et al., 2019, Hou et al., 2017), and in gas-turbines (Buffi et al., 2018, Chiong et al., 2018). Pyrolysis oil can also be upgraded to hydrocarbon products for use as a fuel (Elliott et al., 2009, Jones et al., 2009). Due to the large number of compounds present within pyrolysis oil, specialty chemicals can be produced via chemical extraction or reactions. These include preservatives, liquid smoke, additives, pharmaceutical precursors, flavouring agents, additives for fertilisers and

resin precursors (Goyal et al., 2008, Czernik and Bridgwater, 2004, Balat, 2011). Figure 1-7 presents an overview of the potential uses of pyrolysis oil.

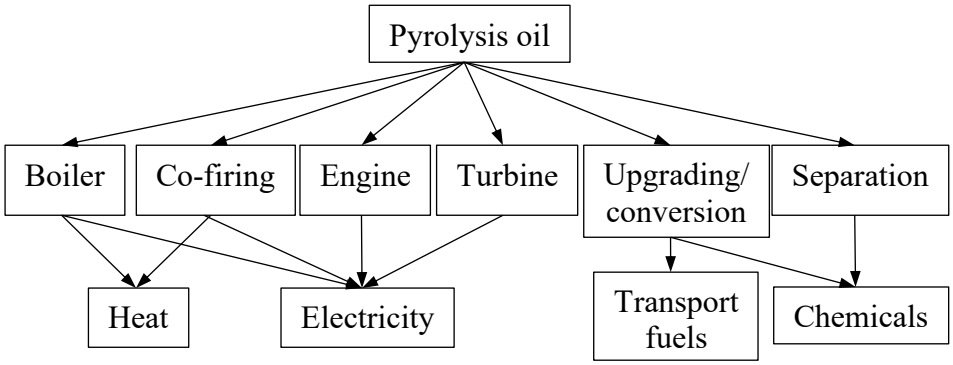


Figure 1-7 – Applications for pyrolysis oil, adapted from Bridgwater (2012).

1.3.2.2 Potential pyrolysis oil analysis methods

Potential pyrolysis oil analysis methods to determine physical properties involve determining density, moisture content, ash content, pH, refractive index, cetane index, elemental composition, viscosity, and heating values (Chukwuneke et al., 2019, Jahirul et al., 2012, Czernik and Bridgwater, 2004, Bridgwater, 2012). The aforementioned properties are generally analysed to determine the suitability of pyrolysis oil for storage and fuel usage (Bridgwater, 2012).

Further analysis methods involve compositional analysis of the pyrolysis oil to determine compounds present. Such analysis methods include gas chromatography-mass spectroscopy (GC-MS) (Guo et al., 2011, Kostas et al., 2019a), gas chromatography-flame ionization detection (GC-FID) (Choi et al., 2014), high-performance liquid chromatography (HPLC) (Choi et al., 2014), ion-exchange chromatography, Fourier-transform infrared (FTIR) spectroscopy (Castellví Barnés et al., 2015), and nuclear magnetic resonance (NMR) spectroscopy (Kim, 2015, Chandran et al., 2019, Hao et al., 2016). As the scope of the thesis was involved in determining

compounds that were present in abundance, GC-MS was chosen to identify the aforementioned abundant compounds, further discussion is carried out in Section 2.5.1.

1.3.2.3 Pyrolysis-gas

The gas produced has a varied composition, consisting of light hydrocarbons (such as methane and ethane/ene), tar, ash, nitrogen, carbon monoxide, carbon dioxide, hydrogen, and water (Goyal et al., 2008, Jahirul et al., 2012, Robinson et al., 2015, Huang et al., 2015b). Much like pyrolysis oil, the composition of the gas is dependent on the biomass used, and the type of pyrolysis that had been performed. The presence and the amount of CO and CO_2 in the gas is an indication of the oxygen content of the biomass and is determined largely by the amount of cellulose and hemicellulose in the biomass, as they are highly oxygenated. It was found by (Huang et al., 2015a) that by enriching the cellulose and hemicellulose content within the biomass, the CO and CO_2 yields in pyrolysis syngas also increased. As pyrolysis gas has a large composition of CO_2 and combustible gases, it can be used for combustion purposes (Goyal et al., 2008), or as a fluidising gas for fluidised bed reactors (Bridgwater, 1994).

1.3.2.4 Bio-char

During pyrolysis the biomass will volatilise and produce a biochar high in carbon, along with hydrogen, graphene and amorphous aromatic structures (Iason et al., 2009). The amount of biochar produced is largely dependent on the temperature and time of pyrolysis; slow pyrolysis results in much greater yields of char than a flash or fast pyrolysis process (Vamvuka, 2011, Pecha and Garcia-Perez, 2015, Safdari et al., 2019). Bio-char can be utilised in soil amendment and as a char absorber (Antal and Grønli, 2003, Khare and Goyal, 2013, Sato et al., 2019), and for combustion applications (Bridgwater, 2012).

1.3.3 Pyrolysis temperature and pyrolysis oil yield

As the main desired product of fast pyrolysis is pyrolysis oil, various studies have been undertaken to determine the optimal pyrolysis temperature to maximise pyrolysis oil yield. A summary of the optimal temperatures for liquid pyrolysis products from multiple studies are presented in Table 1-3, and suggests that the optimal temperature for pyrolysis oil yield for lignocellulosic biomass range from approximately 400 - 550 °C for fast pyrolysis processes.

Table 1-3 – Optimal temperatures for liquid pyrolysis products.

Feedstock	Product	Peak yield temperature (°C)	Source
Wood chips	Pyrolysis oil	500	(Di Blasi et al., 1999)
Lignin	Pyrolysis oil compounds (acetic acid, guaiacol, syringol)	500 - 540	(Trinh et al., 2013)
Spent coffee grounds	Pyrolysis oil	500	(Primaz et al., 2018)
Mallee wood	Pyrolysis oil	450 - 475	(Garcia-Perez et al., 2008b)
Poplar wood	Organic fraction pyrolysis oil	500	(International Energy Agency, 2007)
Various biomasses	Pyrolysis oil	450 - 550	(Demirbas, 2007)
Rice straw and water hyacinth	Pyrolysis oil	400	(Jin et al., 2019)
Orange bagasse	Pyrolysis oil	525	(Bhattacharjee and Biswas, 2019)
Nut shells	Pyrolysis oil	400 – 550	(Demirbas, 2006)
Pine wood	Pyrolysis oil	450 – 530	(Westerhof et al., 2010)
Rapeseed cake	Pyrolysis oil	550	(Smets et al., 2011)
Napier grass	Pyrolysis oil	480	(Suntivarakorn et al., 2018)
Pine wood	Resin acids	500	(Kim et al., 2019)
Douglas fir wood	Pyrolysis oil	500	(Liaw et al., 2012)
Saw dust	Pyrolysis oil	450	(Kumar et al., 2017)
Walnut shell	Pyrolysis oil	500	(Açıkalın and Karaca, 2017)
Rice husk	Pyrolysis oil	550	(Ma et al., 2018)

1.3.4 Processing factors affecting pyrolysis

In order for pyrolysis to occur and be feasible as a process, efficient reactor configurations must be determined, alongside the type and size of the feedstock that is used.

1.3.4.1 Biomass preparation for pyrolysis

For biomass to be pyrolysed properly, the biomass sample must be milled to a small particle size (<4 mm) and then dried as a high water content could have an adverse effect on the pyrolysis process, especially during microwave based pyrolysis (Robinson et al., 2015). If the biomass moisture content is not reduced, then the pyrolysis oil produced could have a large moisture content, reducing its calorific value and therefore energy density, ultimately resulting in a lower value product. The particles must also be a small size for conventional pyrolysis, as too large a particle size will reduce the heat transfer via conduction (Jahirul et al., 2012).

1.3.4.2 Biomass water content

The water content of the biomass affects the pyrolysis products, as a high water content would result in large amounts of water condensate within the pyrolysis oil (Demirbaş, 2000). This higher water content could result in extraction of the water-soluble compounds within the gas and liquid-intermediate fractions, reducing gas and solid yield (Al-Arni et al., 2010). A higher water content could also increase the energy requirements for pyrolysis, as the biomass would dry before pyrolysing, and the condensing energy for the volatiles would be increased due to the increased vapour produced during the pyrolysis process (Pattiya, 2018).

1.3.4.3 Reactor configuration

The reactor configuration can have an effect on the pyrolysis oil yield from the pyrolysis process. Although each configuration could have its own associated advantages and challenges, no configuration could be considered the most efficient with most configurations giving 65 – 75 % oil yield (Bridgwater, 2012). Generally, the essential features of a fast-pyrolysis reactor involve a very high heating rate, efficient heat transfer to the feedstock, with rapid cooling or quenching of the pyrolysis vapours produced (Bridgwater, 2012, Bridgwater and Peacocke, 1994, Diebold and Bridgwater, 1997). Pyrolysis reactor configurations are further discussed in Section 1.3.5.

1.3.4.4 Char and ash separation

As the biomass must be reduced to smaller sizes (<6 mm) for the pyrolysis process, it is possible that fine char will become entrained within the fluidising gas (in the case of fluidised bed processes). Any char that is entrained within the vapour would be required to be separated with cartridge or rotary filters (Bridgwater, 2012), ultimately increasing downstream processing costs.

1.3.4.5 Vapour residence time

Vapour residence time is important in maintaining high quality pyrolysis oil produced from fast pyrolysis processes. If the vapour is kept at a high temperature due to the high reactor temperatures (>500 °C), then the vapours will undergo secondary degradation and cracking, reducing oil quality (Bridgwater and Peacocke, 2000, Bridgwater et al., 1999).

1.3.4.6 Liquid collection

In fast pyrolysis, the gaseous products consist of aerosols, vapours and non-condensable gases, which makes collection and capture inefficient. The products

require rapid cooling to condense the vapours and minimise secondary degradation, and the aerosols require coalescence or agglomeration. Typically, electrostatic precipitation is the preferred method for liquid collection, over conventional units such as demisters (Bridgwater et al., 1999, Bridgwater, 2012).

1.3.5 Types of pyrolysis reactor

1.3.5.1 Fixed bed

In a fixed bed pyrolysis configuration, gas moves through a fixed, or slow downward moving, bed of fine biomass particles (<3 mm) (Daouk et al., 2017). The gas velocity will generally be low, and the solids will have a long residence time. Heat transfer to the particles in the fixed bed would be provided by either a hot gas (Garba et al., 2018) or by hot sand (Ábrego et al., 2019, Suntivarakorn et al., 2018). Currently available industrial scale fixed beds can process approximately 600 kg/h biomass (Bridgwater, 2012).

1.3.5.2 Bubbling fluidised bed reactor

In a bubbling fluidised bed (BFB) reactor, fluidising gas is provided to a bed of fine biomass particulates, typically around 2 – 3 mm in size, to give the solids fluid-like properties (Isahak et al., 2012). Heat transfer to the biomass is provided by convection, conduction, and radiation from a hot medium. Thermal transport in this reactor is more efficient than a fixed bed reactor, however efficient heat transfer via conduction could require an additional solid phase such as heated sand to transfer heat to the biomass (Jahirul et al., 2012). This would create extra processing steps to separate the char from the sand after the pyrolysis process. The particle size distribution is narrow for a fluidised bed process, as particle sizes that are too large would not be entrained within the inerting gas and would not leave the fluidised bed reactor (Isahak et al., 2012). The

BFB promotes several advantageous characteristics; the movement of the particles due to the gas flow results in adequate mixing of the particles, resulting in increased heat transfer efficiency and increased temperature control. The residence time of the vapours produced can be controlled using the gas flow to the reactor (Resende, 2014). Currently available industrial-scale bubbling fluidised bed reactors can process tonne-scale processes (approximately 8 t/h) (Bridgwater, 2012).

1.3.5.3 Circulating fluidised bed reactor

Circulating fluidised beds (CFB) behave similarly to bubbling fluidised beds, however the gas velocity to the reactor is much greater than the BFB, meaning that the residence times of the char and vapours are approximately equivalent for the pyrolysis vapours and gas (Resende, 2014). The char produced from the pyrolysis process are also generally entrained more than bubbling fluidised bed reactors due to the higher gas velocities, resulting in higher char contents in the oil unless processing units are added to remove the char (Bridgwater, 2012). An alternative to char removal would be to separate it from the vapours using a cyclone, and then combust the char within the sand to provide heat energy to the sand, essentially controlling the reactor temperature (Resende, 2014). Currently available industrial scale circulating fluidised bed reactors can generally process tonne-scale processes (approximately 4 t/h) (Bridgwater, 2012).

1.3.5.4 Ablative reactor

Ablative reactors use the principle of pressing biomass against a hot surface in the absence of inert fluidising gas, which produces an oil film that evaporates and leaves the system as vapour. The heating rate of ablative reactors are typically limited by the heat supply rate to the reactor. Ablative reactors are surface area based and therefore scale up would require exponentially larger reactors to keep a large surface area to

volume ratio. (Bridgwater et al., 1999). There have been attempts, however, to create a more efficient surface area to volume ratio with the development of vortex or rotating cone reactors (Jones et al., 2009). The scale of an ablative reactor design would largely be limited by surface area, processing time, and solid throughput. Therefore, high throughput processes would require very high temperatures, or very high surface areas, increasing processing cost. Currently available industrial/large pilot scale reactors can process approximately 250 kg/h biomass (Bridgwater, 2012).

1.3.5.5 Rotating cone reactor

In a rotating cone reactor, the biomass inside the reactor is agitated mechanically by a rotating cone and either heated with hot sand and/or a hot surface. The vapours exit near the bottom of the reactor, while the solid biochar leave out of the bottom. This reactor could be used as an alternative to fluidised bed reactors as it aims to achieve the same outcome but without carrier gas (Bridgwater, 2012). Commercially available rotating cone reactors can pyrolyse approximately 2 t/h biomass (Bridgwater, 2012).

1.3.5.6 Vortex reactor

In a vortex (cyclone) reactor, the carrier gas carries the biomass particles to the reactor, at which point, due to the velocity of the carrier gas, the particles are forced against the internal walls. The biomass particles are therefore heated by solid-solid contact, much like an ablative reactor. The high velocity of the incoming particles also results in char adhered to the reactor wall to be abraded off. Much like an ablative reactor, the heat transfer rate is surface area controlled and the particle size is limited by what can be entrained within the carrier gas (Resende, 2014). Commercially available vortex reactors can process approximately 250 kg/h biomass (Bridgwater, 2012).

1.3.5.7 Auger reactor

Auger reactors use a screw to move a feedstock through a tube. The screw rotates to move biomass along the reactor until the end of the heating zone. Heat to the biomass is provide though hot sand or by the reactor wall (Bridgwater, 2012). The residence time within the reactor can be controlled by the screw rotation speed or the pitch of the tube. The vapour residence time of reactors is typically longer than fluidised bed reactors and as such, the pyrolysis oil yield is generally lower, increasing the yield of char via secondary reactions (Resende, 2014, Brassard et al., 2017). Auger reactors can also be configured to use two intermeshing screws, which promote feedstock mixing along with conveying the feedstock through the tube (Campuzano et al., 2019). Commercially available auger reactors can generally process up to 2 t/h biomass (Bridgwater, 2012).

1.3.5.8 Microwave reactor

Microwave reactors involve energy transfer through the interaction of molecules or atoms in a material with microwaves. Microwave pyrolysis can involve very large heating rates, very low residence times, and relatively high temperatures in an inert atmosphere. Microwave heating attempts to overcome the issues present in conventional pyrolysis processes by utilising the ability of microwaves to provide selective and volumetric heating, and so the biomass can be heated directly without having to rely on convection and conduction. Due to the volumetric heating effect, no heating elements such as heating sand would need to be us such as in conventional flash pyrolysis, reducing separation demand later in the process (Robinson et al., 2015). Microwave reactors, when compared to conventionally heated process, are not yet fully commercially realised, and as such are not available on a commercial scale (Bridgwater, 2012). Microwave reactor types are discussed in more detail in Section 1.4.1.

1.4 Microwave fundamentals

Microwaves are a form of electromagnetic radiation in the 1 mm to 1 m wavelength range with corresponding frequencies in the range of 300 MHz to 300 GHz, with the two most common frequencies used being 0.915 and 2.45 GHz, corresponding to wavelengths of approximately 33 cm and 12 cm respectively (Thostenson and Chou, 1999).

In conventionally heated processes, energy transfer occurs through convection, conduction and radiation from a hot medium (sand, gas, reactor wall) through the material. During microwave heating, microwave energy interacts with the material directly through molecular interaction with the electromagnetic field. Heat transfer could therefore be considered energy conversion, as heat transfer does not occur due to thermal gradients but instead due to the conversion of electromagnetic energy to thermal energy (Thostenson and Chou, 1999).

The microwave's ability to interact with a material and transfer energy is largely affected by the material's dielectric properties, and the higher the loss tangent, the more likely the microwave is to interact with the material. Microwaves themselves can alter the dielectric properties of the material, changing the amount of heating and thus the heating properties of a material will be non-uniform (Thostenson and Chou, 1999). The dielectric constant (ε') is the material's ability to store electromagnetic energy through polarisation, and the dielectric loss factor (ε") is the material's ability to convert the energy to heat (Robinson et al., 2010a). The loss tangent (tan δ) is a function of the dielectric constant and the dielectric loss factor, and represents a material's ability to heat in an electromagnetic field. A material with a high loss tangent would therefore undergo rapid absorption of microwave energy and therefore rapid heating (Kappe,

2004). The relationship between the loss tangent and the dielectric constant and dielectric loss factor are shown in Equation 1-1.

$$\tan \delta = \frac{\varepsilon''}{\varepsilon'} \qquad 1\text{-}1$$

1.4.1 Microwave reactor cavity configurations

There are two main types of microwave applicator (also known as cavities) that can be applied to processes: multi-mode (also known as multi-mode resonant), and single-mode. Multi-mode cavities are used on a daily basis in the form of domestic kitchen microwaves. In a multi-mode cavity, the cavity is generally large to accept a broad range of microwave frequencies. The microwaves that enter the cavity are reflected by the walls and through the material inside (Kappe, 2004). The microwaves reflecting off the walls creates areas of constructive and destructive interference, known as hot spots and cold spots respectively (Barham et al., 2019). Constructive interference results in localised spots of a high energy density, whereas the cold spots are localised spots of low energy density (Stuerga and Delmotte, 2002).

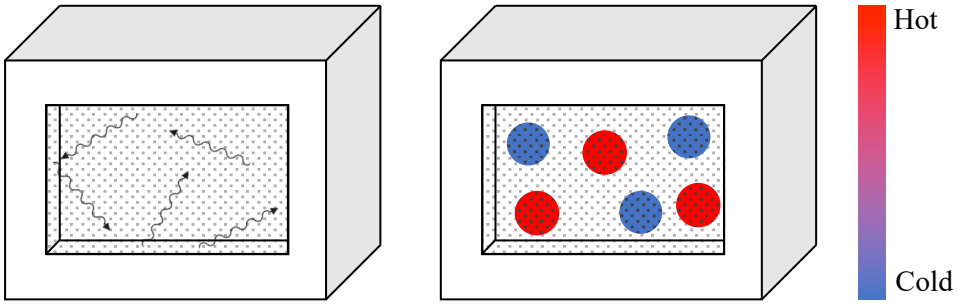


Figure 1-8 – An illustration of the random wave propagation within a multi-mode cavity, and formation of cold and hot spots within the cavity.

Typically, in multi-mode cavities, to mitigate the uneven heating caused by the reflected waves and homogenise the electromagnetic field, a rotating element would be utilised such as a turn table (as in domestic kitchen microwaves) or a rotating metal

plate known as a mode stirrer (Stuerga and Delmotte, 2002, Kappe, 2004). Due to the size of multi-mode cavities being large enough for microwaves to travel freely within and accommodate various modes, large samples can be heated, or multiple samples can be heated simultaneously. Due to the microwave distribution, however, homogeneous heating would not be guaranteed (Barham et al., 2019, Kappe, 2012, Kappe, 2004).

Single-mode cavities work by generating a definable microwave waveform (Cintas et al., 2017, Kappe, 2004). There are two main single-mode cavity subtypes: the first is a travelling wave single-mode cavity, and the second is a resonant single-mode cavity. In single-mode travelling wave cavities, the microwaves travel through the sample once. They are then are either reflected back by the cavity walls and pass through the sample a second time (Barham et al., 2019) or are absorbed by a terminating load at the end of the waveguide that would absorb any microwave energy not absorbed by the sample (Metaxas and Meredith, 1983). Resonant cavities exist as both single- and multi-mode, and can be rectangular or cylindrical (Reader, 2006). In single-mode resonant cavities, the microwave source is separate from the cavity by a fixed iris and standing waves are propagated, allowing for a localised high energy electric field. The electric field, power density and therefore heating rate of the sample is greater in a resonant cavity than a travelling wave cavity (Metaxas and Meredith, 1983, Barham et al., 2019). When comparing single- and multi-mode cavities, single mode cavities have a better defined electric field, higher energy efficiency, with the effective cavity power potentially being three orders of magnitude higher (Stuerga and Delmotte, 2002, Barham et al., 2019). The challenge with single-mode cavities, when compared to multi-mode cavities, is that the sample size is limited to a half-wavelength of the microwave field, often limiting the number of samples to one (Reader, 2006, Kappe, 2004).

1.4.2 Dielectric properties as a function of temperature

Various studies have been undertaken to determine how the dielectric properties of biomass varies with temperature during microwave pyrolysis (Sait and Salema, 2015, Motasemi et al., 2014, Robinson et al., 2015, Tripathi et al., 2015, Salema et al., 2017, Motasemi et al., 2015). Determining the loss tangent behaviour over the temperature range of pyrolysis would allow for determination of the feedstock behaviour during the microwave process; a high dielectric constant and loss tangent would result in more power absorbed by the sample. An overview of the loss tangent of European Larch (*Larix decidua*), determined by the cavity perturbation method (explained further in Section 2.3.1) over the pyrolysis temperature range is presented in Figure 1-9.

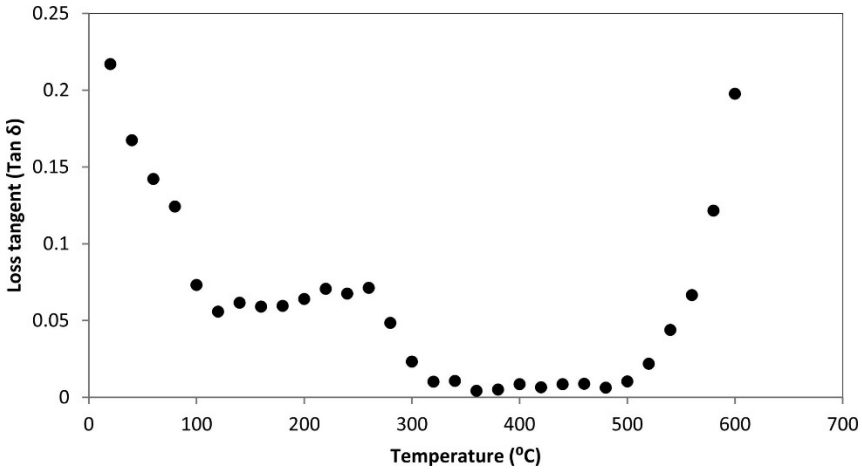


Figure 1-9 - The loss tangent of European Larch over the temperature range 20 - 600 °C, determined by the cavity perturbation method (Section 2.3.1) (Robinson et al., 2015).

In general, lignocellulosic biomass undergoes three stages as it is heated; 1) drying (room temperature - 200 °C), 2) pyrolysis (200 - 500 °C), 3) char/carbonisation (500 – 700 °C) (Sait and Salema, 2015). During the drying stage, the dielectric constant and loss factor are largely independent of temperature for relatively dry biomass (Motasemi et al., 2014), or decrease slightly due to losing the moisture content for wetter biomass (Robinson et al., 2015). During the early pyrolysis stage (200 - 300 °C) there is a further

drop in the dielectric properties, possibly due to the breaking of chemical bonds and release of volatile matter (Naik et al., 2010). Throughout the pyrolysis stage, the dielectric properties remain relatively consistent as the feedstock transforms into carbonaceous char (Motasemi et al., 2014). In the char region (>500 °C), the dielectric properties increase significantly, due to char being microwave absorbent (Robinson et al., 2010b, Meredith, 1998). The microwave absorbance of the char is due to the displacement of π-electrons within the structure, increasing conductivity and decreasing the resistance of the material (Lester et al., 2006, Sait and Salema, 2015). The cavity perturbation method is just one method to determine the dielectric properties, and has limitations. Sample preparation, for example, could have an effect on the dielectric property measurements. As explained in Section 2.3.1, the sample must be either milled into a powder or shaped into a cylinder, which may not represent a solid sample of different geometries. A powdered sample would have different solid properties to a solid sample, for example density, porosity, permeability, and as such would likely not provide equivalent dielectric property measurements. The heating rate is also slow (approximately 5 °C/min), and so any heating rate effects on the dielectric properties of the material would be lost. The cavity perturbation method, however, remains a useful method for determining dielectric properties of materials over a range of temperatures.

1.4.3 Microwave pyrolysis principles

In conventional pyrolysis, the poor thermal conductivity of biomass provides a limitation in the size of process-able biomass and as such, the surface area to volume ratio of the biomass must be kept high. Therefore, to keep processing times short, the biomass must be milled to sizes of around <200 μm for rotating cone reactors, <2 mm for fluidised beds, and <6 mm for transported or circulating fluidised beds increasing

processing units, capital and processing cost (Bridgwater and Peacocke, 2000). The small particle size also results in solids being entrained with the both the inerting gas and pyrolysis liquid, as such separation units are required downstream of the pyrolysis process (Isahak et al., 2012). With conventionally heated gas-inerted pyrolysis, the biomass is heated from the outside-in, and therefore once the internal core of the biomass begins to pyrolyse, the pyrolysis products must pass through the outer layer of pyrolysed biomass. The long processing times and hot temperatures lead to secondary decomposition of the pyrolysis products and the outer layer, rich in char, catalyses secondary decomposition of the primary pyrolysis products (Ruiz et al., 2017). Figure 1-10 shows the heating profiles of a conventionally heated and microwave heated particle, with the direction of mass transfer of the volatiles produced during the pyrolysis process.

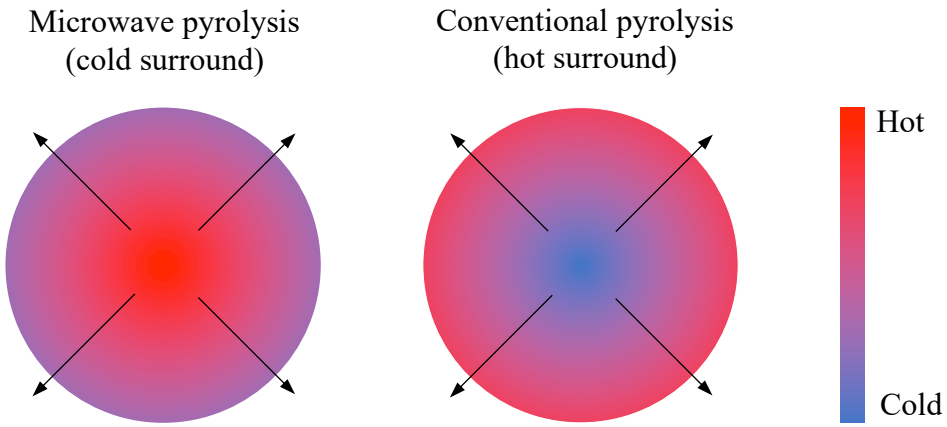


Figure 1-10 – The temperature gradient of a microwave pyrolysis process and conventionally heated pyrolysis process, with the arrows representing mass transfer of the volatiles produced during the pyrolysis process.

Microwave pyrolysis overcomes the heat transfer limitations of conventionally heated pyrolysis, as the heating rate (based on power, W) is a function of dielectric loss factor and electric field intensity, as shown in Equation 1-2 (Meredith, 1998).

$$P = 2\pi f \varepsilon_0 \varepsilon'' E^2 V \quad \text{1-2}$$

P	-	Power, W
ε_0	-	Permittivity of free space
ε''	-	Dielectric loss factor
E	-	Electric field strength, V/m
f	-	Frequency of the applied field, Hz
V	-	Volume of the material, m^3

Microwave heating allows for instantaneous volumetric heating, leading to very low processing times for larger particles than is possible in conventional pyrolysis. This can reduce process units due to the lack of need for a milling stage or solids separation stage (Robinson et al., 2015). The microwaves heat the biomass directly, resulting in no need for a hot medium; this further reduces processing cost. During volumetric heating, the internal temperature of the biomass becomes hotter than the surrounding environment. The cooler surrounding and high internal temperature means that the primary decomposition products travel through a cooler layer of biomass and therefore are much less likely to undergo secondary decomposition as the products exit the biomass. Due to the heating of the biomass being caused by the microwaves themselves, the thermal inertia of the process is low as the biomass would only heat when the microwaves are being applied to the system.

1.4.4 Microwave pyrolysis studies

The benefits of using microwaves for pyrolysis on a processing basis were outlined in Section 1.4.3, and the benefits of the oil composition were presented in Section 1.3.2.1. Studies have been undertaken to explore the use of microwaves as the sole heat source for pyrolysis (Robinson et al., 2015, Lo et al., 2017, Kostas et al., 2019b). Due to the microwave transparency of biomasses, however, microwave absorbent materials are often mixed in with the biomass to increase power absorbance. The dopants used

include activated carbon, silicon carbide or potassium carbonate (Borges et al., 2014, Lam et al., 2019, Chen et al., 2019, Namazi et al., 2015, Haeldermans et al., 2019, Beneroso et al., 2015a). The addition of microwave absorbent dopants would reduce to benefits of using microwaves in the pyrolysis process. The use of microwave absorbent dopants to heat surrounding biomass would result in heat transfer via conduction (particle to particle) and convection (internally within the biomass particle), discounting the benefit of the volumetric heating effect provided by microwaves. Due to the fact that the heat transfer would occur via convection and conduction, the particle size would have to be milled into a size similar to conventional pyrolysis, adding capital and processing cost to the process. With the addition of microwave absorbent dopants, the advantages presented by microwave pyrolysis are then overlooked, as downstream solid separation from the pyrolysis process would therefore need to be factored in. The presence of microwave absorbent solvents would also produce hot-spots within the microwave pyrolysis process, leading to thermal runaway and temperatures sufficient for gasification, rather than pyrolysis, of the biomass. Often, studies involving microwaves do not quantify power absorbed, therefore not allowing an energy balance to be made (Undri et al., 2015, Budarin et al., 2010, Huang et al., 2015b, Beneroso et al., 2015b). Studies also use modified domestic microwaves with poorly defined electric fields (Shukla et al., 2019, Dai et al., 2019, Du et al., 2010) resulting in insufficient power densities for pyrolysis, hence the requirement for the addition of dopants (Robinson et al., 2015).

When carrying out microwave pyrolysis in the absence of dopants, however, the process itself presents challenges. Heterogeneous heating and hot-spots were identified during fixed bed pyrolysis of European Larch by Robinson et al. (2015), with a 50 mm diameter fixed bed undergoing approximately 69 % volatilisation in the centre of the

bed, and 14.1 % at the circumference. This was likely due to the heating heterogeneity challenges presented by the use of a multi-mode microwave cavity, as presented in Section 1.4.1. Localised heating and increased carbonisation would promote higher absorbance of the microwaves and therefore heat the sample more (Beneroso et al., 2016). Hot spots, allowing for thermal runaway (localised temperatures >1000°C), could also be partly due to the poor heat transfer to the surroundings due to the thermal heat transfer properties of gas (further explained in Section 3.1), and so temperature control of the biomass during the process would be desirable. A method of temperature control could be utilised to exploit microwave behaviour; using a microwave transparent liquid to inert the process as opposed to a gas, essentially providing contact condensation to the biomass sample for increased temperature control. The use of liquids in pyrolysis is limited, especially in conventional pyrolysis where the hot atmosphere would lead to vaporisation of many liquids and increase energy requirements for the process. In conventionally heated processes, liquids are generally used in pre-treatment processes, such as in organosolv processes. Organosolv pre-treatments utilise ionic liquids to selectively fractionate and remove biomass constituents such as lignin, cellulose or hemicellulose (Sun and Othman, 2019, Choi et al., 2019, Romaní et al., 2019). For microwave pyrolysis, studies are largely limited to ionic liquids for performing catalytic microwave pyrolysis (Du et al., 2010), or for pre-treating biomass prior to pyrolysis (Muhammad et al., 2012, Lei et al., 2015). The use of liquids in the aforementioned pre-treatment and pyrolysis processed are used to serve a reactive purpose, such as removing biomass constituents. The use of inerting liquids as a heat sink in microwave pyrolysis has not been previously attempted. The purpose of this thesis was to therefore explore the use of inerting liquid media in a microwave pyrolysis system.

1.5 Aims and Objectives

The aim of this research is to study and develop a novel method to produce pyrolysis oil from a liquid inerted microwave-based process, and to determine the advantages and processing challenges associated with this technology. In order to reach these aims, the following objectives must be met:

1. Determine the extent to which pyrolysis occurs and the energy needed for a liquid-inerted microwave pyrolysis process using a range of solvents.
2. Understand the effects of electric field intensity and convective heat transfer on the liquid-inerted pyrolysis process.
3. Assess the composition of the liquid and solid pyrolysis products obtained from the process, and how product properties vary with processing conditions.
4. Develop a more comprehensive understanding of the physical mechanisms that govern pyrolysis when using microwave heating.

This thesis presents a novel process for carrying out microwave pyrolysis by exploiting microwave behaviour and using liquids as inerting media, as opposed to gas that is commonly utilised for conventionally heated pyrolysis and within microwave pyrolysis studies. The overarching aim of the thesis is to determine the feasibility of carrying out microwave pyrolysis within a liquid inerting medium, whilst carrying out analysis to determine an understanding of the process itself.

Chapter 2 outlines the materials used in this thesis, and the methods used.

Chapter 3 details the investigation into the feasibility of a liquid inerted microwave pyrolysis process. The screening of potential solvents to use an inerting media during the pyrolysis process were assessed, analysing their potential to allow for liquid-inerted microwave pyrolysis, and analysing the solid and liquid products.

Chapter 4 further investigates a scaled-up process in order to attempt to mitigate the challenges associated with the liquid inerted microwave pyrolysis determined from Chapter 3. The investigation involved further solvent screening in the new process, along with solid biochar and pyrolysis oil product analysis, identifying advantages and challenges associated with the direct scale-up of the liquid-inerted microwave pyrolysis process.

Chapter 5 involves further investigation into the processing parameters that could affect the liquid-inerted microwave pyrolysis process, along with presenting theoretical estimations of potential temperatures and pressures obtained within the biomass during the pyrolysis process and their potential effect on the process itself. The chapter also investigates the potential challenges when using conventional analysis techniques to determine both the material's physical and dielectric properties to predict a material's behaviour during the microwave pyrolysis process.

The conclusions and recommended future work resultant from this thesis are presented in Chapter 6.

2. Experimental materials and methods

2.1 Reagents

All reagents were of AnalaR grade and obtained from Sigma-Aldrich (UK) and Fisher Scientific (UK) unless otherwise specified.

2.2 Source and preparation of Sycamore

Sycamore (*Acer pseudoplatanus*) was used in the research for this thesis as a model feedstock and was supplied by Nottinghamshire eco-fuels (UK). It was cut into different sized blocks for microwave pyrolysis trials; 45 × 15 × 15 mm, 30 × 30 × 30 mm and 50 × 50 × (15, 25, 40, 50) mm.

2.3 Sycamore analysis techniques

2.3.1 Dielectric properties

The dielectric constant (ε′) and dielectric loss factor (ε") of sycamore was determined using the cavity perturbation technique. The measurements were performed at 2470 MHz, from 20 to 600 °C, ramping at 5°C/min. The resonant cavity consists of a cylindrical copper cavity connected to a vector network analyser, which measures the frequency shift and change in quality factor relative to the empty resonating cavity when a sample is introduced. The sample was loaded into a quartz tube and held in a conventionally heated furnace above the cavity until the temperature set-point was reached. The tube was then moved into the cavity to take the measurement at the required temperature. A detailed description of the equipment is given by Adam (2017). The dielectric constant and loss factor were calculated using the following equations (Smith et al., 2010):

$$\varepsilon' = 1 + J_1^2(x_{1,m}) + \left(\frac{f_0 - f_s}{f_s}\right)\frac{V_c}{V_s} \quad 2\text{-}1$$

$$\varepsilon'' = J_1^2(x_{1,m})\left(\frac{1}{Q_s} - \frac{1}{Q_0}\right)\frac{V_c}{V_s} \quad 2\text{-}2$$

Where:

f_s - Resonant frequency of the cavity with the sample present

f_0 - Resonant frequency of the empty cavity

Q_0 - Quality factor of the empty cavity

Q_s - Quality factor of the cavity with the sample present

V_c - Volume of the cavity

V_s - Volume of the sample

$J_1^2(x_{1,m})$ - Second order of the first kind root of the Bessel function

2.3.2 Thermogravimetric analysis (TGA)

Samples (10 – 15 mg) were analysed by TGA using a TA instruments QA-5000IR applying the method outlined by Lester et al. (2007). The samples were purged with 100 mL/min nitrogen and heated at a rate of 10 °C/min up to 900 °C to determine volatiles content, where it was held for 15 minutes to determine fixed carbon content. The gas was then switched to oxygen to allow for combustion to occur, allowing for determination of ash content.

2.3.3 Simultaneous Differential Scanning Calorimetry-TGA (SDT)

Samples (8 – 12 mg) were analysed using a TA instruments SDT-Q600, using the method outline by Lester et al. (2007) with the addition of measuring heat flow. The sycamore sample was heated from room temperature to 900 °C at a constant heating rate of 10 °C/min and was purged with nitrogen at 100 mL/min. 10 mg of sample was used, and runs were done in triplicate. The main outputs from the DSC measurements were the heat flow as a function of temperature. The heat flow values were used to

calculate the temperature dependent specific heat capacity, C_p, of the sycamore, as shown in Equation 2-3. A line of best fit was then used to define a temperature dependent specific heat capacity equation (Appendix A).

$$C_p(T) = \frac{-H(T)}{\frac{dT}{dt}} \qquad 2\text{-}3$$

Where:

H(T) - Specific heat flow to the sycamore at temperature T, W/g

dT/dt - The heating rate, 10 °C/min (0.16 °C/s)

2.3.4 Determination of moisture content

The moisture content was measured by drying a block of sycamore (approximately 5.67 g) in a convection oven at 105 °C for 2 h (ASTM D4442). The mass of the block was weighed, and the sample was further dried for 1 h and the mass measured to confirm the mass had plateaued. Results were then used to calculate the compositional data on a percentage dry weight basis.

2.3.5 Density of the sycamore block

The overall density of the sycamore blocks used during the study were determined by measuring the exact of dimensions and masses of 35 blocks ranging from sizes 3×3×3 cm to 5×5×5 cm, and using Equation 2-4 resulting in an average density of 563 ±30 kg/m^3.

$$\text{Density, } \rho = \frac{\text{Mass of block, kg}}{\text{Volume of block, m}^3} \qquad 2\text{-}4$$

2.3.6 Determination of lignin

Acetyl bromide (AcBr) soluble lignin was used for the quantification of lignin in non-pyrolysed and pyrolysed sycamore by following a modification of the method outlined

by Fukushima and Hatfield (2001). Samples (100 mg) were incubated with 4.0 mL of 25 % AcBr solution (in glacial acetic acid) at 50 °C for 2 h. After cooling to room temperature, the samples were made up to 16 mL with glacial acetic acid and left to stand for 30 min so that the biomass could settle. A sample (0.5 mL) of this solution was further diluted with glacial acetic acid (2.5 mL) and 0.3 M NaOH (1.5 mL) and gently agitated. Finally, 0.5 mL of 0.5 M hydroxylamine hydrochloride solution and a further 5.0 mL of glacial acetic acid were added, and the absorbance was measured at 280 nm using a Jenway 7315 spectrophotometer. Lignin concentrations were calculated using extinction coefficient generated from corresponding measurements using lignin standards provided by Sigma Aldrich. Experiments were carried out in triplicate.

2.3.7 Determination of cellulose and hemicellulose

A modified version of the Dubois et al. (1956) assay was followed. 1 mL of 12 M H_2SO_4 was added to 30 mg of sample and incubated at 37 °C for 1 h in a heat resistant screw cap glass tube. 11 mL water was then added to the sample to dilute the acid strength to 1 M. Samples were then incubated at 100 °C for 2 h. Liberated monosaccharides (glucose, galactose, arabinose and xylose) were analysed via Ion Chromatography using a Dionex ICS-3000, utilising the method outlined by Kostas et al. (2016). A CarboPacTM PA 20 column (3 x 150 mm) was used and the mobile phase was 10 mM NaOH with a flow rate of 0.5 mL/min. The injection volume was 10 μL and the column temperature was 30 °C. Standards of monosaccharides (glucose, galactose and xylose) of concentrations of 1 to 0.0625 g/L were used for monosaccharide quantification. The final monosaccharide concentrations were adjusted to an anhydrous correction factor to determine the percentage of polysaccharides cellulose (glucose) and hemicellulose (summation of arabinose, galactose and xylose) on a dry weight basis. Experiments were conducted in triplicate.

2.4 Microwave pyrolysis

2.4.1 Cold matching of the system

Optimal tuner settings were determined before performing any pyrolysis experiments. Cold matching at room temperature was carried out by using a vector network analyser (Rohde & Schwarz ZVL) and adjusting the stub and sliding-short positions to minimise reflected power. The vector network analyser sends signals through the waveguide and measures the magnitude and phase of the reflected signal. For the preliminary pyrolysis tests, the frequency of the generator for 0.5 – 1.8 kW applied power ranged from 2.453 – 2.457 GHz, and so reflected power over that range was minimised, as shown in Figure 2-1.

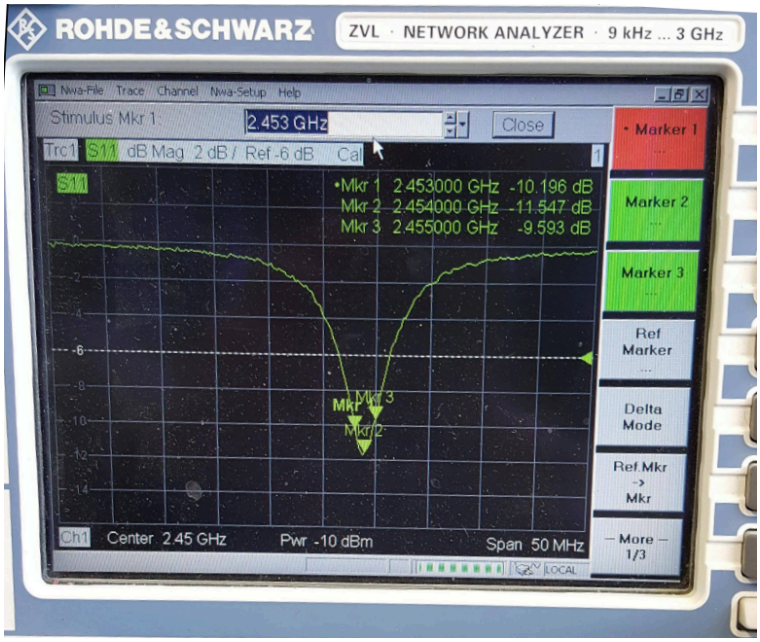


Figure 2-1 – The absorbance over the microwave generator frequency range.

2.4.2 Single-mode and multi-mode pyrolysis systems

The methods and equipment configurations are discussed in detail in Chapters 3 and 4, for the single-mode and multi-mode systems respectively.

2.4.3 Specific absorbed energy

The absorbed power could be quantified using the applied power and reflected power during pyrolysis (explained further in Sections 3.2.1 and 4.3.1) The specific absorbed energy was determined by numerical integration of the absorbed power:

$$E_s = \frac{\int P\mathrm{d}t}{M} \qquad 2\text{-}5$$

Where:

P	-	Power, W
E_s	-	Specific absorbed energy, kJ/g
t	-	Time, s
M	-	Initial mass of the sample, g

2.4.4 Determination of solid mass loss

After pyrolysis, the sample was washed with acetone to remove any residual pyrolysis oil, and oven dried using the method outlined in section 2.3.4. The mass remaining of the sycamore after pyrolysis was calculated using the following equation:

$$\text{Mass remaining (\%)} = \frac{\text{Mass of pyrolysed block}}{\text{Mass of non-pyrolysed block}} \times 100 \qquad 2\text{-}6$$

2.4.5 Solvent/solid ratio required to maintain the liquid environment

To maintain an effective liquid surround around the sycamore during the pyrolysis process, a head (height) of liquid would be required.

Pyrolysis of woody biomass in a fluidised bed column showed that the energy required to achieve 60 -70% pyrolysis is 3.5 to 4.0 kJ/g (Adam et al., 2017). Therefore, an increased value of 5.0 kJ/g (for safety) was taken as the basis for the head calculation.

As the various solvents have boiling points in the range of 56 – 250 °C, it was important to have enough liquid in the reactor to ensure the inert atmosphere during the pyrolysis

process. To calculate the minimum amount of liquid required, it was assumed that all the energy absorbed by the biomass material was transferred to the liquid, which was initially at room temperature (20 °C) at the start of the experiment.

The energy required to evaporate the liquid molecules is the sum of the sensible heat and its latent heat of vaporisation:

$$C_p \left(T_{boiling}\text{-}T_{room}\right) + \Delta H_{vap} = E_{sp} \quad \text{2-7}$$

Where:

C_p - Specific heat capacity of the liquid, kJ/g·K

T - Temperature, K

ΔH_{vap} - Latent heat of vaporisation of the liquid, kJ/g

E_{sp} - Specific energy, kJ/g

Table 2-1 – Energy required to boil the solvents used in the thesis.

Solvent	Boiling Point (°C)	Specific Heat Capacity (kJ/g·K)	Sensible Heat (kJ/g)	Latent heat of vaporisation (kJ/g)	Energy Required to boil the liquid (kJ/g)
n-Hexane	69	0.00226	0.1107	0.365	0.476
Water	100	0.00419	0.3352	2.257	2.592
Acetic Acid	118	0.00204	0.2002	0.402	0.602
Iso-Octane	126	0.00215	0.2279	0.298	0.526
2-propanol	83	0.00260	0.1638	0.732	0.896
Kerosene	250	0.00201	0.5126	0.251	0.764
Cyclohexane	81	0.00185	0.1124	0.380	0.492
Pentane	36	0.00232	0.0371	0.360	0.397

The minimum liquid to biomass ratio was therefore calculated using the following equation:

$$E_{biomass} = m_{solvent} \cdot E_{boil} \quad \text{2-8}$$

Where:

$E_{biomass}$ - Energy limit for pyrolysis, 4 kJ/g

E_{boil} - Energy required for liquid to boil, kJ/g

m - mass of solvent, g

This was then converted to a liquid volume per gram of the biomass material.

Table 2-2 – Minimum solvent volume required per gram of biomass.

Solvent	Density (g/cm^3)	Mass solvent required per gram biomass (g)	Volume required per gram biomass (ml)
Hexane	0.655	10.5	16.0
Water	1.000	1.9	1.9
Acetic Acid	1.050	8.3	7.9
Iso-Octane	0.703	9.5	13.5
2-propanol	0.786	5.6	7.1
Kerosene	0.780	6.5	8.4
Cyclohexane	0.779	10.2	13.0
Pentane	0.626	12.6	20.0

For added safety, approximately 20 ml solvent per gram of biomass was used, regardless of the solvent chosen.

2.5 Oil categorisation

2.5.1 Pyrolysis oil analysis using gas chromatography-mass spectroscopy (GC-MS)

As discussed in Section 1.3.2.2, the scope of the thesis involved determining prevalent compounds in the pyrolysis oil produced from the pyrolysis process. Therefore, GC/MS methods with injection and column temperatures up to 200 °C and 300 °C, respectively, were used to determine the semi-volatile organic compounds within the pyrolysis oil. The methods were chosen due to the fact that pyrolysis oil generally has a upper boiling limit of 280 °C (Czernik and Bridgwater, 2004), and to keep analysis temperature ranges consistent with literature (column temperature ramped to a maximum of 240 – 300 °C) (Guo et al., 2011, Robinson et al., 2015, Kostas et al., 2019a, Kostas et al., 2019b, Farag et al., 2016, Wang et al., 2013, Djokic et al., 2012, Marsman et al., 2008, Moraes et al., 2012). Therefore, any prevalent products in the oil would be volatilised and potentially determined using compositional library software, without the use of

analytical standards. Analysis of the pyrolysis oil was carried out within three weeks of being produced.

Preliminary characterisation of the *n*-hexane inerted organic and aqueous product phases was carried out by collaborators at the University of Basque country, using a Shimadzu GC-2010 coupled to a TRB-1- MS column (50 m and 0.15 mm i.d.) and a Shimadzu QP2010S mass spectrometer detector. The operating conditions involved a split ratio of 50:1 (0.02 μL of oil sample in 1 μL of dichloromethane) and an injector temperature of 180 °C; a column temperature of 45 °C for 2 min, which was then heated up to 300 °C at 8 °C/min, holding this temperature for 10 min. The carrier gas was helium, and a flowrate of 1.15 mL/min was used. The mass spectra and retention data were used to identify the compounds with greater than 80% probability by comparing them with those of the standard in the NIST 140 Mass Spectral Database (National Institute of Standards and Technology, Maryland, USA).

For further characterisation of organic and aqueous phase oils (cyclohexane, 2-propanol, kerosene, water), analysis was carried out by a collaborator at the University of Nottingham using liquid product characterisation methods published from the same research group (Kostas et al., 2019b). Pyrolysis liquid samples were analysed using a JEOL GCX 215 time-of-flight GC-MS (JEOL Ltd., Tokyo, Japan). The injection port temperature of the GC was set at 200 °C and was operated in splitless mode. The GC column used was a ThermoFisher Scientfic TG-POLAR (ThermoFisher Scientific, Massachusetts, USA) capillary column (30 m x 0.25 mm, 0.25 μm stationary phase thickness). Helium was used as the carrier gas, at a flow rate of 1.5 mL/min. The GC oven was heated from 40 °C (held for 3 min) to 260 °C at a rate of 5 °C/min. The GC interface was held at 240 °C, while the mass spectrometer ion source was heated to 280 °C. Identification of individual compounds with greater than 80% probability was

performed by comparing experimental mass spectra with those in the NIST Mass Spectral library (NIST140 Mass Spectral database; National Institute of Standards and Technology, Maryland, USA).

2.6 Mathematical modelling and computational simulations

2.6.1 Heat transfer models

It was not possible to directly measure temperature within the sycamore block during microwave heating. As the penetration depth of wood biomass is approximately 30 cm at 2.45 GHz, for the purposes of the simulations, power density was considered to be uniform throughout the sycamore block. Other assumptions were required to be made in order to allow for the simulations to be carried out:

- The particle size remained consistent throughout the heating.
- The reactor was a closed system, and no heat entered or escaped through the reactor walls.
- The liquid surrounding the sample was assumed to be equivalent to the surface biomass temperature, and would heat to boiling temperature, at which point the temperature would not increase further and any further heat transfer lead to vaporisation of the liquid.
- The microwave power was absorbed by the biomass and not by the inerting liquid.

Heat transfer to the block was modelled using 3-dimensional Fourier's law equations for conduction through the particle, along with heat transfer via convection at the surface of the particle:

$$P_D = \rho\, C_p \frac{\delta T}{\delta t} + \nabla \cdot (-k\, \nabla T) + \frac{1}{V} \left(h\, A\, (T_{ext} - T_s)\right) \qquad 2\text{-}9$$

Where:

P_D	-	Power density of the sample, W/m^3
T	-	Temperature, K
ρ	-	Material density, kg/m^3
C_p	-	Specific heat capacity, J/kg·K
k	-	Thermal conductivity, W/m·K
h	-	Heat transfer coefficient, W/m^2·K
A	-	Surface area, m^2
V	-	Material volume, m^3
T_{ext}	-	External temperature, K
T_s	-	Surface temperature, K
∇	-	Gradient vector, $\left(\frac{\delta}{\delta x}, \frac{\delta}{\delta y}, \frac{\delta}{\delta z}\right)$

For the rectangular (2D) and cuboid (3D) particles, a finite element method was used to solve the 2/3-dimensional partial differential equations and establish the temperature distribution over time. For the single-mode particle, the 2D rectangular model was meshed into 112,640 triangles and 32,513 nodes, and the 3D cuboid model was meshed into 42,394 tetrahedrons, 3,116 boundary elements and 120 edge elements. For the 3D multi-mode cuboid, the particle was meshed into 50,180 tetrahedrons, 3,196 boundary elements, and 180 edge elements.

For the purpose of calculating the heat transfer coefficient, h, the particle was assumed to be fully submerged within liquid, with heat transfer occurring via natural convection with an assumed Nusselt value of 2 (Green and Perry, 2007).

$$\mathrm{Nu} = \frac{\text{Convective heat transfer}}{\text{Conductive heat transfer}} = \frac{h\,L}{k} = 2 \qquad 2\text{-}10$$

Where:

Nu	-	Nusselt number
L	-	Characteristic length (area/perimeter), m

The particle to liquid heat transfer coefficient does not remain constant across the range of temperatures recorded, however, and so estimation of the heat transfer coefficient across a range of temperatures, calculated from data collected by Fardad and Ladommatos (1999) was used. A typical boiling curve for a liquid is presented, and its effect on the heat transfer coefficient, along with explaining the significance of the boiling point, critical point and Leidenfrost point is explained in detail in Section 3.4.7. For *n*-hexane, up to the critical heat flux at 120 °C (724 kW/m^2), the value calculated from equation 2-10 was used. Between the boiling point and the critical heat flux, and between the critical heat flux and the Leidenfrost point at 180 °C (32 kW/m^2), interpolation of the heat transfer coefficient values were used, past this point, the minimum heat transfer coefficient was be used, represented by the relationships below:

$$IF\begin{cases} T_s \leq T_{boiling}, & h = h_{Nusselt} \\ T_{boiling} < T_s \leq T_{critical}, & h = h_{Nusselt} + \dfrac{h_{max} - h_{Nusselt}}{T_{critical} - T_{boiling}} \times \left(T_s - T_{boiling}\right) \\ T_{critical} < T_s \leq T_{Leidenfrost}, & h = h_{max} + \dfrac{h_{min} - h_{max}}{T_{Leidenfrost} - T_{Critical}} \times \left(T_s - T_{critical}\right) \\ T_{Leidenfrost} < T_s & h = h_{min} \end{cases} \quad 2\text{-}11$$

Where:

h_{max} - Heat transfer coefficient (critical point), $h_{max} = \dfrac{q_{max}}{T_{critical} - T_{boiling}}$, W/m^2·K

h_{min} - Heat transfer coefficient (Leidenfrost point), $h_{min} = \dfrac{q_{min}}{T_{Leidenfrost} - T_{boiling}}$, W/m^2·K

q - Heat flux, W/m^2

Heat flux data for cyclohexane was unavailable, for the hydrocarbons tested by Fardad and Ladommatos (1999), however, the critical and Leidenfrost points were approximately 50 - 60 °C and 100 °C above the boiling point of the respective liquids, with similar values for heat fluxes. The boiling, critical and Leidenfrost points for

cyclohexane were therefore considered to be 131 °C and 181 °C respectively, with equivalent heat fluxes to *n*-hexane.

The boundary parameters and sycamore properties used in the computational simulations are presented in Table 2-3.

Table 2-3 – The parameters for the computational models for sycamore, all values at 25°C unless otherwise specified.

Parameter	Value	Source
Power absorbed	Variable, 0.6 – 1.8 (kW)	Independent variable
Thermal conductivity, k	0.155 (W/m·K)	(Guo et al., 2013)
Density, ρ	563 (kg/m^3)	Calculated
Specific heat capacity, C_p	$0.0567T^2 - 59.89T + 16772$ (J/kg·K)	Calculated
Heat transfer coefficient, h	Variable (Equation 2-11)	Estimated, (Fardad and Ladommatos, 1999, Green and Perry, 2007)

3. Effect of solvents on a pyrolysis process

3.1 Introduction

Microwave pyrolysis and its advantages, compared to conventional pyrolysis methods, have been discussed in Chapter 1. In this chapter, a novel processing concept is presented which substitutes the inert gas for a liquid. Previous literature exploring the use of liquids in conjunction with a pyrolysis process exist, however the application of the liquid differs and is used in processes such as hydrothermal gasification (Garlapalli et al., 2016) and/or solvothermal processes utilising ionic liquids (Xu et al., 2015, Du et al., 2010). In the aforementioned processes, the liquids are used to transfer heat to the biomass (by the liquids heating via microwaves and reaching temperatures around 400 °C). In this research, the liquid acts as a 'heat-sink' at atmospheric pressure, by transferring heat away from the biomass, as opposed to providing heat directly to the biomass.

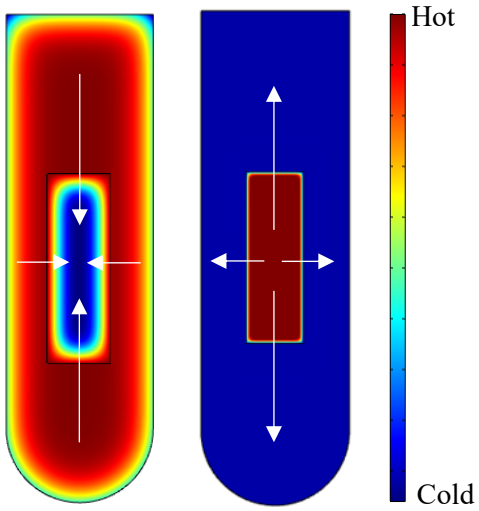


Figure 3-1 – Heating profiles of a solvothermal process (left), and in a liquid inerted microwave pyrolysis process (right), with arrows showcasing the direction of heat transfer.

Pyrolysis requires heating of the biomass within an inert atmosphere to avoid oxidation of the species evolved during primary decomposition. As the requirement for inerting an atmosphere is solely based on the removal of oxygen, a suitable liquid environment can be used as opposed to a gas-inerted atmosphere. A consideration of using a liquid rather than a gas as an inerting agent is that the gas is microwave transparent and only the biomass absorbs electromagnetic energy. If a liquid is used as the inert media then the biomass can still be heated selectively provided that the dielectric constant and loss factor are low, and this is the case for most non-polar hydrocarbons and liquid fuels.

A comparison between gas and n-hexane, a microwave-transparent liquid, are presented in Table 3-1.

Table 3-1 – Physical and system properties of gaseous and liquid inert media for microwave pyrolysis. Comparative heat transfer coefficients calculated based on Nu = 2 and a spherical biomass particle with 10 mm diameter (Green and Perry, 2007). All properties quoted at 20 °C, unless otherwise stated. [a] (Meredith, 1998, Hermiz et al., 1982), [b] (Haynes, 2014).

	Inert medium	
	Gas (nitrogen)	Liquid (n-hexane)
Loss factor at 2.45 GHz [a]	<0.001	<0.001
Breakdown voltage at 1 atm (kV/mm) [b]	3	42
Maximum temperature at 1 atm (°C)	>500	68
Thermal conductivity (W/m·K) [b]	0.026	0.126
Convective heat transfer coefficient ($W/m^2 \cdot K$)	5.2	25.2

Heat transfer from the biomass to the surrounding environment occurs via convection. The temperature attained by the gas depends on the flowrate, inlet temperature and contact surface area. It is feasible that the gas temperature could approach the surface temperature of the biomass, as gas is largely more insulating than a liquid due to the

much lower thermal conductivity and heat transfer coefficient. The convective heat transfer coefficient for the liquid is around five times higher than that of the gas, suggesting that there will be greater heat loss from biomass to a liquid rather than to a gas. This implies that the cooling of the biomass will be more efficient when using a liquid. Another benefit in terms of processing and efficient temperature control is that the maximum temperature which can be reached within the liquid, under atmospheric conditions, is its normal boiling point. In the case of n-hexane this would be 68 °C, which is much lower than the gas-inerted environment. A simulation of the cross-sectional temperature profiles of a microwave pyrolysis process inerted by nitrogen and n-hexane, highlighting temperature control at the surface of the sycamore block in a liquid inerted environment is shown in Figure 3-2.

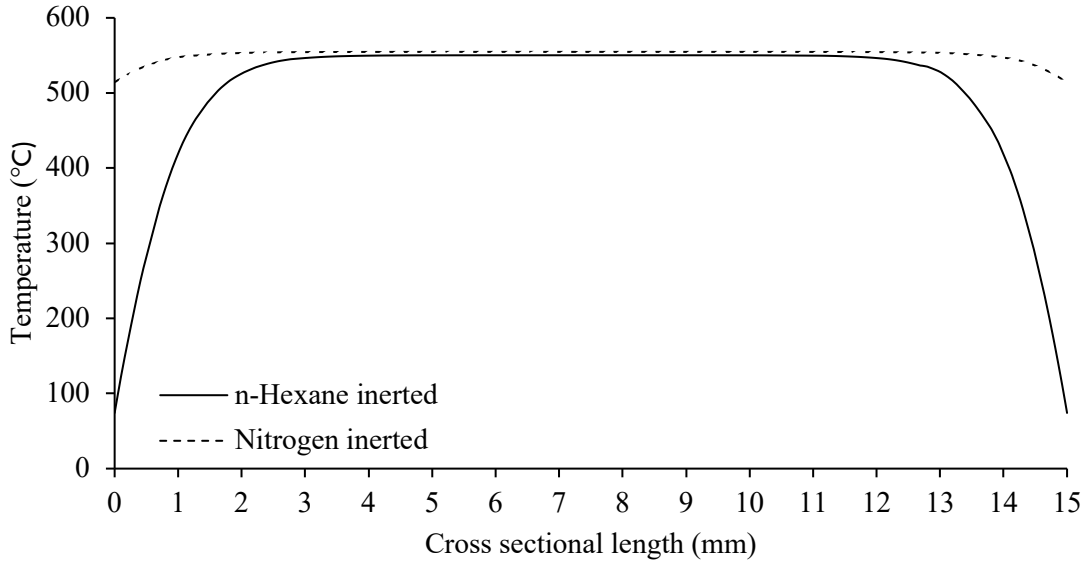


Figure 3-2 – A cross-sectional temperature profile of a 45×15×15 mm sycamore block pyrolysed at 0.5 kW, 18 seconds, in *n*-hexane and nitrogen, showcasing increased temperature control on the surface of the block when processed within a liquid medium.

In order to maintain a consistent liquid surround, the liquid needs to either be present in excess, and/or refluxed back into the pyrolysis vessel. The bulk temperature of the pyrolysis system is therefore significantly lower (liquid boiling point temperature as

opposed to pyrolysis temperatures), and potentially more controllable when a liquid medium is used as opposed to a gas inerting medium. Table 3-1 shows that the breakdown voltage for n-hexane is over ten times higher than that of air at equivalent conditions. This means that as long as the liquid atmosphere is maintained, high intensity electric fields can be utilised safely, minimising arcing or plasma formation. Power densities of 10^7-10^8 W/m^3 needed to achieve pyrolysis, such that the power density in the sample is sufficient to induce heating in microwave transparent materials, could also be obtained (Robinson et al., 2010a).

While the concept of substituting the inert gas for a microwave transparent liquid such as *n*-hexane appears to be viable when microwave heating is used, greater heat losses to the liquid can be expected due to the higher heat transfer coefficient. The increased heat transfer could limit the ability of the process to attain temperatures of 400-600 °C within the biomass, or at least result in an increased energy requirement for equivalent pyrolysis performance to a gas inerted process. The focus of this chapter is to use theoretical and experimental approaches to validate this new concept and establish the extent to which sycamore (as a model lignocellulosic biomass) can be pyrolysed. The specific objectives required to achieve this goal are:

- Determine the extent to which pyrolysis can be achieved when the biomass is immersed within a liquid, and the corresponding energy requirements compared to a gas inerted process.
- Determine the feasibility of various liquids as inerting media, and their respective energy penalties or benefits.
- Understand the temperature distribution within biomass during microwave heating when immersed within a liquid.

- Determine the yields of the pyrolysis oil product produced, and the composition of the pyrolysis oil.

3.2 Materials and methods

3.2.1 Liquid-inerted microwave pyrolysis equipment configuration

The liquid-inerted microwave pyrolysis experiments were carried out using a 0 - 2 kW microwave generator operating at approximately 2.45 GHz and a single mode cavity. An automatic three stub tuner (S-TEAM STHD v1.5) was used to maximise the absorbed power and to log applied and reflected power (absorbed power = applied power – reflected power). The sycamore sample (45 × 15 ×15 mm) was placed within a 30 mm diameter quartz tube and covered with 100 mL solvent. A microwave-transparent ceramic block (boron nitride) was placed on top of the sycamore block to reduce buoyancy and ensure the sample was contained within the waveguide section where the electric field intensity is highest. The upper section of the tube was contained within an electromagnetic choke and connected to a condenser. Vaporised solvent was condensed and allowed to reflux back into the reactor to provide a constant level of liquid over the biomass. The waveguide and choke were purged with nitrogen at 10 L/min to provide a secondary inert atmosphere to prevent combustion of the solvent in case of failure of the tube. A schematic of the experimental system is shown in Figure 3-3.

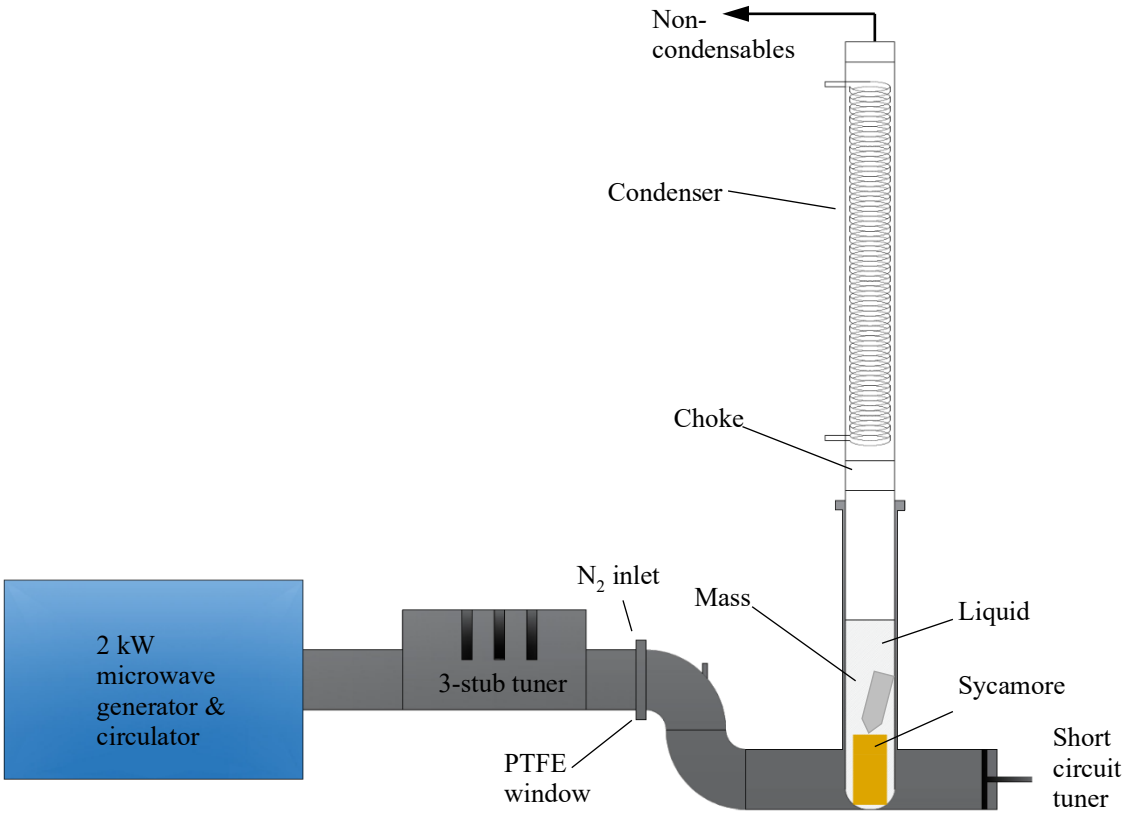


Figure 3-3 - The schematic of the single-mode liquid-inerted microwave pyrolysis system

3.2.2 Gas-inerted microwave pyrolysis equipment configuration

The single-mode gas-inerted microwave pyrolysis system was set up in a similar configuration to the liquid-inerted process. The equipment set up was modified to add a nitrogen purge within the glassware, with a collection vessel added for any condensed pyrolysis gases produced by the pyrolysis process. Figure 3-4 shows the schematic for the gas inerted process.

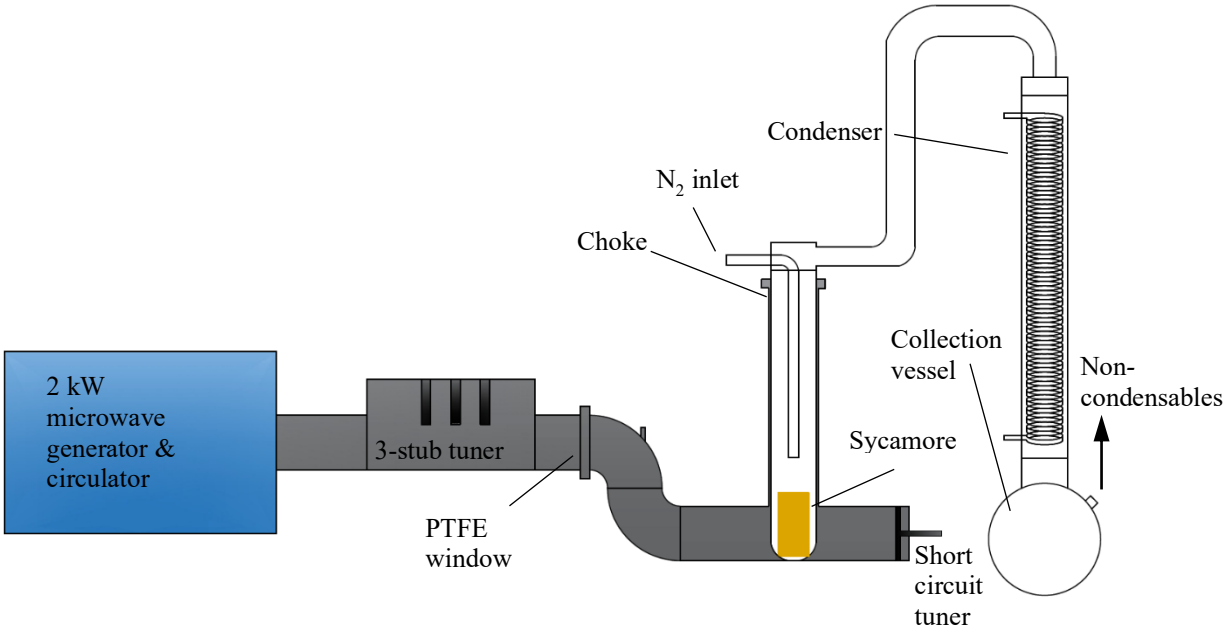


Figure 3-4 - The schematic of the single-mode gas-inerted microwave pyrolysis system

3.2.3 Pyrolysis oil collection

In the hydrocarbon solvents, the pyrolysis oil that was produced fractionated into two phases: an aqueous phase that precipitated out of the solvent into its own phase, and an organic phase, which was miscible with the hydrocarbon solvent, as shown in Figure 3-5.

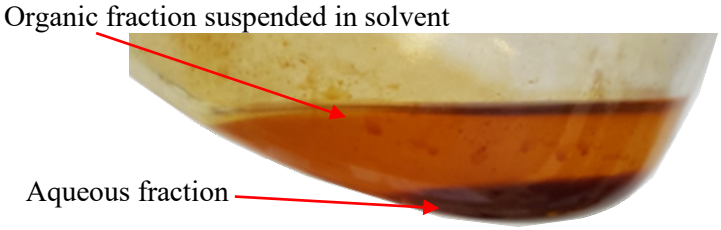


Figure 3-5 - The fractionated pyrolysis oil product, showing the aqueous and organic fractions when cyclohexane was used as an inerting liquid.

The physical state of the pyrolysis oils that were acquired post pyrolysis for each solvent investigated within this chapter are outlined in Table 3-2.

Table 3-2 – The physical state of the pyrolysis oil after pyrolysis in the inerting media investigated.

Solvent	Oil product
Cyclohexane	Organic phase oil suspended in solvent, aqueous phase fractionated and settled at the bottom of the quartz tube
2-Propanol	Single-phase solvent/oil liquid mix
Nitrogen	Single-phase pyrolysis oil

3.2.3.1 Hydrocarbon solvents

For the hydrocarbon inerted solvents (with the exception of kerosene), the solvent was poured out and collected into a pre-weighed vessel. The aqueous phase which had adhered to the quartz tube was washed with acetone and collected into a pre-weighed vessel. The aqueous and organic phase liquids were air dried for 12 hours, or until the mass of the liquid plateaued. The masses of the samples were then weighed with a four-point balance.

3.2.3.2 Oil-miscible solvents

For oil miscible solvents such as 2-propanol, the solvent-oil mixture was poured into a pre-weighed vessel. The liquid was air dried for 12 hours, or until the mass of the liquid plateaued. The masses of the samples were then weighed with a four-point balance.

3.2.3.3 Nitrogen

For the nitrogen inerted pyrolysis process, the glassware used in the pyrolysis process was pre-weighed. After pyrolysis had occurred, the mass of the glassware (reaction vessel and collection vessel) containing the pyrolysis oil was weighed in order to determine pyrolysis oil yields with a four-point balance.

3.2.4 Impedance matching

The automatic 3-stub tuner provided the option of carrying out microwave pyrolysis with a fixed or dynamic impedance matching to maximise power absorbance, with both providing advantages and disadvantages during the pyrolysis process. Fixed impedance matching provided feedback as the changing dielectric properties of the sample based on absorbed power could be observed. An advantage of dynamic impedance matching was that the power absorbed by the sample could be maximised, increasing the efficiency of the energy absorbed based on the applied power, along with a more consistent energy absorbance, however the process feedback based on absorbed power during the pyrolysis process was lost, as shown in Figure 3-6.

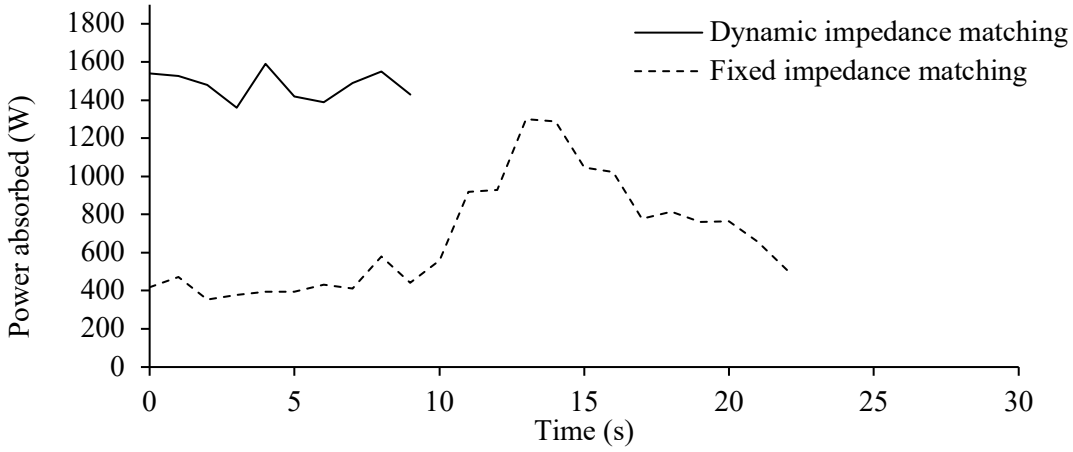


Figure 3-6 – A representative example of a dynamic and fixed impedance matching process with cyclohexane as an inerting medium, with the absorbance shown for approximately 1.5±0.1 kW applied to the system.

It can be seen that the absorbed power during the fixed impedance matching process was lower, and underwent a rise and fall over the process. This is representative of changes in the dielectric properties of the material, whereas the dynamic impedance matched process remained consistent. As the investigation within this chapter focussed on the effect of solvent on the pyrolysis process (not any optimisation at this stage), the

efficiency of applied power against power absorbed was not necessary to maximise. Therefore both fixed and dynamic impedance matching were investigated.

3.2.5 Single-mode microwave cavity characteristics

A single-mode microwave system was initially developed for the investigation into the feasibility of carrying out microwave pyrolysis within a liquid medium. Single-mode microwave cavities are predictable in terms of their electric field distribution. The design of the single-mode system allowed for very high power-densities to be obtained within the sycamore block. In order to obtain a well-defined microwave field, the sycamore block geometry must be small, limiting the size of the blocks used. The size of the sycamore blocks used were also much less than any penetration-depth limitations for a 2.45 GHz microwave system (Section 3.3.1.1).

In order to control the position of the high intensity electric field, an automatic 3-stub tuner was employed to enable real-time changes of the positions of the standing waves in the cavity. This allowed for dynamic impedance matching and maximum power absorption.

Applied and reflected power could also be recorded which enabled quantification of absorbed power by the sycamore sample. For a 2.45 GHz microwave system, the reaction vessel size was limited by the waveguide dimensions (86.36 × 43.18 mm), and also by the microwave choke, which was designed to prevent propagation of microwaves to the surrounding environment.

For a cut off frequency of 2.45 GHz, the radius of the choke must be 3.58 cm when filled with air, however the radius of the choke used was 2.1 cm, much less than the maximum geometry to prevent microwave leakage. This extra safety margin was employed to account for uncertainties in vapour/liquid flow regimes within the choking

section. The waveguide is a WR430 system, meaning the dimensions are 10.92 × 5.46 cm. With these dimensions the maximum size of the sycamore block was limited to 5.46 × 2.1 × 2.1 cm.

3.3 Liquid-solvent characterisation

3.3.1 Microwave transparency – Dielectric properties and dipole moment

The dielectric properties need to be considered when deciding on a solvent for use in a microwave process. As introduced in Section 1.4, the dielectric constant, ε', is a material's ability to store electric potential energy under the influence of an electric field. The dielectric loss factor, ε", is the material's efficiency in converting this stored energy into heat. These two factors combine to form the loss tangent, tan δ, a measure of the relative heating ability.

For a molecule to have a permanent dipole moment, it must have an asymmetric charge distribution. Molecules with a permanent dipole moment, such as water, are considered polar. If a liquid solvent has a significant dipole moment, then it will be heated under microwave radiation more readily than solvents with a low dipole moment, provided frictional forces are present (for example in a liquid, rather than a gas). For a microwave process, as the microwave passes by a molecule in the cavity, the electric field direction changes 2.45×10^9 times per second (for a frequency of 2.45 GHz). The polar molecules with a dipole moment will try to align with this oscillating field by rotating. The aligning and realigning of the molecules results in heating through frictional effects.

The dielectric properties and dipole moments of the liquids used in this study are presented in Table 3-3.

Table 3-3 - Dielectric constants, loss tangents, and dipole moments of solvents. *Not available.

Solvent	Dielectric constant at 20 °C, 2.45 GHz	Loss tangent at 20 °C, 2.45 GHz	Dipole moment	Source
Nitrogen	1.0	<0.001	*	(Haynes, 2014)
n-Hexane	2.0	<0.001	0.08	(Speight, 2017, Ameta and Ameta, 2018)
Cyclohexane	2.2	<0.001	*	(Speight, 2017, de la Hoz and Loupy, 2013)
Water	80.1	0.123	1.85	(Ameta and Ameta, 2018, Onimisi, 2015)
Acetic Acid	6.2	0.174	1.74	(Ameta and Ameta, 2018, de la Hoz and Loupy, 2013)
Isooctane	2.2	<0.001	*	(Speight, 2017)
Pentane	1.8	<0.001	*	(Speight, 2017, de la Hoz and Loupy, 2013)
2-Propanol	19.4	0.67	1.56	(Anderson et al., 2015, de la Hoz and Loupy, 2013)
Kerosene	1.8	<0.002	*	(Speight, 2017)
Glycerol	42.5	*	2.56	(Han, 2013)

The dielectric properties of the liquids must be taken into consideration as the aim of the process was for the sycamore sample to heat and for pyrolysis to occur, with the liquid being utilised as a heat sink in the microwave process. Solvents with a low dielectric constant and loss tangent would be considered more ideal, as the majority of the microwave energy would be absorbed by the sycamore allowing for quantification of the energy absorbed by the sycamore. For a microwave absorbent solvent, the energy provided to the system would be absorbed by both the solvent and sycamore, resulting in energy quantification and mass loss challenges. The energies presented in the investigations are therefore shown in terms of total energy provided to the system, calculated based on the mass of the sycamore block.

3.3.1.1 Penetration depth

The penetration depth of the liquids and the biomass used are important in the pyrolysis process. The penetration depth is defined as the distance from the surface of the material

to where the power drops to e^{-1} from its value at the surface. If the liquid used to inert the process has a very small penetration depth, then selective heating of the biomass will not occur, and the liquid will heat instead. The penetration depth with most liquids increases with an increase in temperature. This was proven in a study which revealed that selective heating of a biomass sample (okra) was feasible at 50 °C using water as the solvent (Lee et al., 2016). Penetration depths can be calculated using Equation 3-1 by (Metaxas and Meredith, 1983):

$$D_p = \frac{\lambda_0}{2\pi(2\varepsilon')^{1/2}}\left\{\left[1+\left(\frac{\varepsilon''}{\varepsilon'}\right)^2\right]^{1/2} - 1\right\}^{-1/2} \qquad 3\text{-}1$$

Where:

D_p - Penetration depth, m

λ^0 - Wavelength, m

ε' - Dielectric constant

ε'' - Dielectric loss factor

Table 3-4 – Penetration depths of the solvents investigated in this study

Solvent	Penetration depth at 20 °C, 2.45 GHz (cm)
Nitrogen	>19488.4
n-Hexane	1378.0
Cyclohexane	1313.9
Water	1.4
Acetic Acid	6.38
Isooctane	1313.9
Pentane	1452.6
2-Propanol	0.7
Kerosene	726.3

It is evident from Table 3-4 that the hydrocarbon solvents, along with acetic acid allow for penetration of microwaves deep enough into the quartz tube reactor of diameter 30 mm to allow for the sycamore block to heat from the start of the pyrolysis process. The dielectric constant of a liquid could decrease with an increase in temperature, as at higher temperatures molecules experience in increase in movement and vibrations, reducing the polarisation in the electric field, which could serve to increase the penetration depth of a liquid. The increase in temperature could also reduce the drag to the rotation of the molecules aligning with the electric field, and would reduce the dielectric loss, this could serve to either decrease the penetration depth based on Equation 3-1, or limit the increase in penetration depth. Water and 2-propanol have very small penetration depths; for pyrolysis to occur the temperature would have to rise in order to decrease the dielectric property values and, therefore, potentially increase the penetration depth. A small diameter quartz tube would also allow for pyrolysis to occur due to the short distance from the quartz tube to the sample, accounting for the small penetration depth. Another factor that would allow for pyrolysis of the sycamore block in water and 2-propanol would be boiling of the liquid; the presence of vapour around the sycamore block would dramatically increase the microwave penetration depth. The boiling regime of the liquid solvent in the pyrolysis process would therefore be important in determining whether pyrolysis would occur, irrespective of the solvent used.

3.3.2 Physical properties

The boiling point of the solvent is important due to two main factors. The first factor is related to the process itself, where the solvent must act as a heat sink and provide a consistent liquid-surrounding environment. During the microwave pyrolysis process, the centre of the sample block is expected to reach temperatures of 300 – 500 °C. Due

to heat transfer to the solvent, however, the outside of the sample block will be cooled to approximately the boiling point of the liquid. This would not be a high enough temperature to pyrolyse the outside of the sample in the case of most liquids used. If the boiling point is high (>250 °C), then it is possible that the temperature of the surrounding liquid could get to very high temperatures and start to pyrolyse the outside of the sample. A lower boiling point solvent would allow for easier separation from the pyrolysis oil, as a higher temperature boiling point solvent may have a temperature overlap with the pyrolysis oil on thermal separation, reducing separation ability.

The latent heat of vaporisation is the energy required to vaporise a certain mass of liquid at its boiling point. A high latent heat of vaporisation in a microwave transparent solvent would allow for more energy transfer before boiling occurs. Specific heat capacity and thermal conductivity of the liquid must also be considered.

The viscosity of the liquid-inerting phase is another important factor to consider. If the viscosity of the liquid is high, the bubbles that are formed during pyrolysis will take longer to disperse from around the biomass. The bubbles are formed by both as volatiles exiting the biomass sample and liquid boiling from the heat transfer from the biomass to the liquid (Plais and Augier, 2016). The viscosity would also affect convective heat transfer from the solid block to the liquid.

Table 3-5 shows the physical properties of the liquids investigated in this study.

Table 3-5 – Physical properties of the solvents investigated in this study, all values given at 20 °C (Haynes, 2014).

Solvent	Boiling point (°C)	Latent heat of vaporisation, ΔH_{vap} (kJ/kg)	Thermal conductivity, k (W/m·K)	Specific heat capacity, C_p (J/kg·K)	Dynamic viscosity (cP)
n-Hexane	68	365	0.126	2260	0.30
Cyclohexane	81	369	0.117	1860	0.87
Water	100	2260	0.598	4190	0.89
Acetic Acid	118	402	0.193	2043	1.03
Isooctane	99	307	0.100	2100	0.50
Pentane	36.1	366	0.136	2180	0.23
Kerosene	200 - 250	251	0.145	2000	1.64
2-Propanol	82.5	754	0.141	2348	2.04
Glycerol	290	830	0.292	2430	1412

3.3.2.1 Solvent safety and environmental considerations

Although the work carried out within this thesis is a study on the behaviour of the pyrolysis process within various solvents, safety and environmental factors surrounding the solvents were investigated. A solvent that would be heavily restricted by legislation, for example, would not be a feasible solvent to use on future scale-up considerations. Safety and environmental considerations, based on the GlaxoSmithKline (GSK) solvent selection guide, are presented in Table 3-6.

Table 3-6 – GSK solvent selection guide parameters for the solvents investigated in the thesis, higher values are better (EHS = Environmental, Health, and Safety) (Henderson et al., 2011).

Solvent	Waste	Environmental impact	Health	Flammability & Explosion	Reactivity/ Stability	Life Cycle Score	Legislation Flag	EHS Red Flag
n-Hexane	5	3	4	2	10	7	Substitution recommended	Flagged
Cyclohexane	5	5	7	2	10	7	-	-
Water	4	10	10	10	10	10	-	-
Acetic Acid	4	8	6	8	7	8	-	-
Isooctane	6	4	8	3	10	7	-	-
Pentane	5	6	8	2	10	7	-	Flagged
Kerosene	8	2	9	6	10	7	Substitution recommended	Flagged
2-Propanol	3	9	8	6	8	4	-	-
Glycerol	6	7	8	10	9	8	-	-

Table 3-6 shows that solvents such as *n*-hexane, when considering environmental impact and sustainability, would be less ideal than a solvent such as water, for example. Legislation flags would also direct away from the usage of such poor-performing solvents, as the potential for the use of such solvents, especially on a, future, larger scale, could be restricted. Further, EHS red flags are also used to identify solvents with potential issues regarding their boiling point, for example kerosene would require significant energy requirements for separation using distillation, and pentane would be considered very volatile and flammable at low temperatures. Despite the environmental and safety factors, the poor (environmentally) performing solvents were investigated to determine their ability to allow for selective heating of the sycamore to occur during the pyrolysis process.

3.3.3 Favourable solvent properties

Favourable solvent properties for carrying out liquid inerted pyrolysis are presented in Table 3-7, based on the properties identified from the solvents investigated in this thesis.

Table 3-7 – Favourable properties for a liquid used as an inerting medium.

Factor	Value
Dielectric properties	Low (less than wood)
Boiling point	Below pyrolysis temperatures (<200°C)
Latent heat of vaporisation	High (>2000 kJ/kg)
Thermal conductivity	High (>0.5 W/m·K)
Specific heat capacity	High (>4000 kJ/kg·K)
Dynamic viscosity	Low (<0.25 cP)

The ideal solvent in relation to the factors discussed in this section would primarily have low dielectric properties, so as to maximise the absorbance of energy in the solid and promote selective heating of the solid. A boiling point just below pyrolysis

temperatures (~200°C) would allow for adequate temperature control of the surface, without allowing for pyrolysis to occur, and maximise energy transfer from the solid to the liquid while the liquid is below its boiling point. The latent heat of vaporisation would be as high as possible, to minimise boiling and maintain a liquid surround. The thermal conductivity would be high to increase heat transfer from the solid to the liquid, and through the liquid itself, but not too high so as to cool the block and prevent pyrolysis temperatures from being reached. The specific heat capacity would be as high as possible to limit the rate of temperature increase of the liquid, and increase temperature control of the solid. The dynamic viscosity would ideally be low, so as to allow for bubble disengagement away from the solid and maintain a liquid surround. Finally, the solvent would be environmentally friendly and safe to use. As a solvent with all of the favourable properties likely does not exist, investigation into the ability of the solvents to control the sycamore temperature, and allow pyrolysis of the sycamore to occur, was carried out.

3.4 Results and discussion

3.4.1 Solvent screening and process repeatability

A range of microwave absorbent and microwave transparent solvents were identified and assessed in Section 3.3. It was identified that solvents with a low loss tangent (hydrocarbons) would be better suited as inerting media within the liquid-inerted microwave pyrolysis system than microwave absorbent solvents, such as water or 2-propanol. Initially, investigation into the repeatability of the pyrolysis process was carried out based on observing power absorbed during the pyrolysis process. All sections present the powers absorbed during processing and an image of the pyrolysed block. *n*-Hexane and cyclohexane are presented to represent hydrocarbon solvents,

whereas power absorption for octane, pentane and kerosene are presented in Appendix B.

3.4.1.1 Power absorption for n-hexane

Figure 3-7 (A-C) presents power absorption over time for applied powers of 1.0 - 1.8 kW in the presence of *n*-hexane.

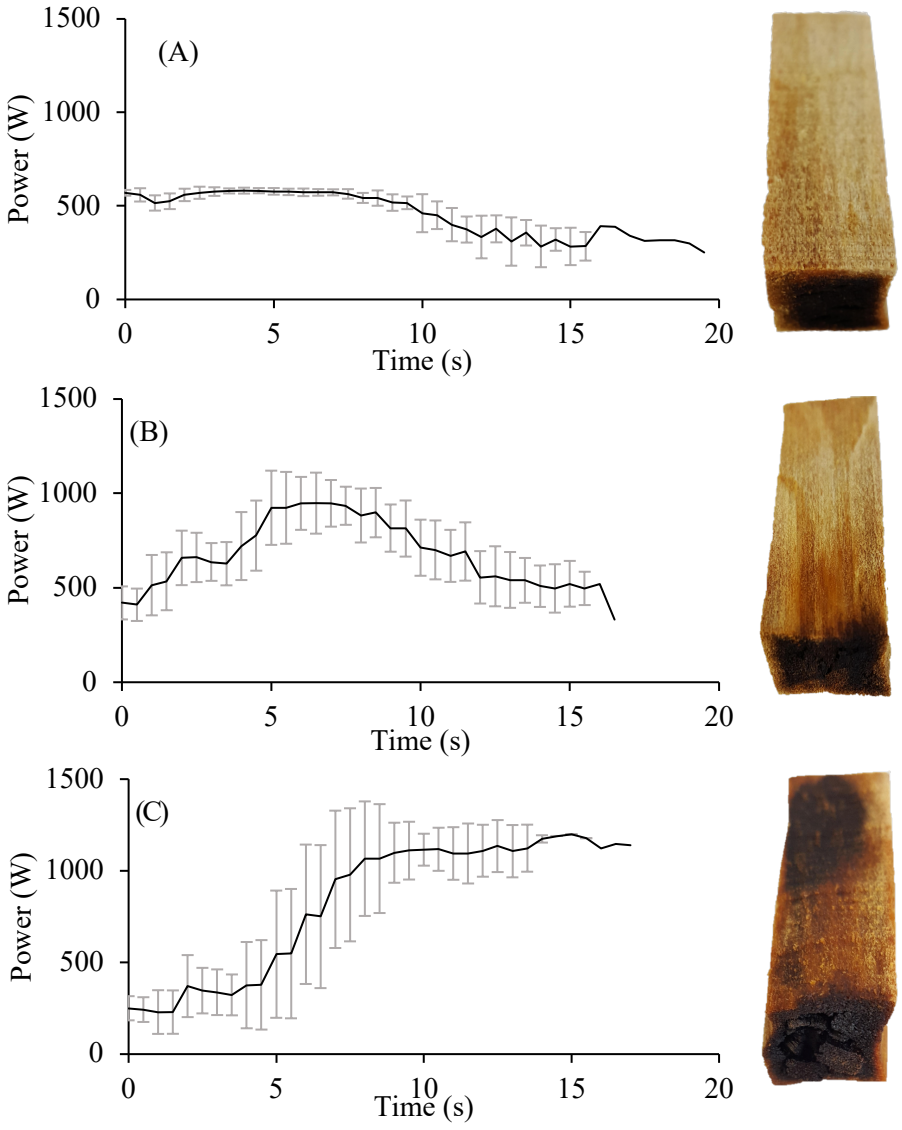


Figure 3-7 – (Left) Absorbed power for *n*-hexane based on approximately (A) 1.0 kW, (B) 1.5 kW, (C) 1.8 kW applied power over 5 runs per applied power with fixed impedance matching, and a treated block (1.0 kW applied, 15 seconds), showcasing heating within the centre of the sycamore block. (Right) Sycamore blocks after pyrolysis at the respective powers, 15 second processing time.

Figure 3-7 reveals that liquid inerted pyrolysis was successful within *n*-hexane as an inerting liquid, with successful temperature control at the surface and a charred interior. For all four applied powers tested, the data produced was repeatable; every run for each specific applied power followed a similar trend. The lower applied power of 1.0 kW exhibited greater repeatability and lower variation in the repeats than the higher powers of 1.5 and 1.8 kW, with the largest variation through the entire process being at the highest power, 1.8 kW.

3.4.1.2 Power absorption for cyclohexane

Figure 3-8 shows the powers absorbed by the sycamore sample when using cyclohexane as an inerting liquid.

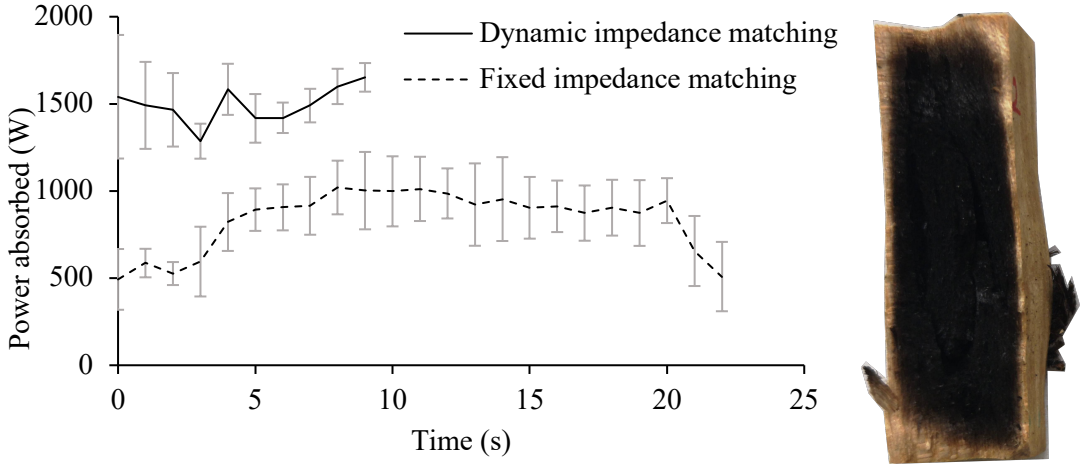


Figure 3-8 – (Left) Absorbed powers for cyclohexane as an inerting liquid, with real-time impedance matching to increase absorbance of the solid sample, and fixed impedance matching for equivalent applied powers (approximately 1.5±0.1 kW) over 10 runs. (Right) A cross section of a sycamore block treated at 1.5 kW applied power, 4 second processing time, dynamic impedance matching.

Figure 3-8 shows that pyrolysis was possible for a cyclohexane inerted process. For the dynamic impedance-matched process, in comparison to the absorbance of the fixed impedance matching process, the absorbance of the power was closer to the set-point. When dynamic impedance matching was applied, the absorbance remained consistent

around the applied value. The fixed impedance matching process showed a rise and fall over time, resultant of the changing dielectric properties of the sycamore as it was heated.

3.4.1.3 Power absorption for water

Water as a solvent in the microwave system offers a contrast to the low-loss microwave transparent hydrocarbons. The feasibility of microwave absorbent solvents to enable pyrolysis was investigated. Power absorbed by the pyrolysis system inerted by water is shown in Figure 3-9.

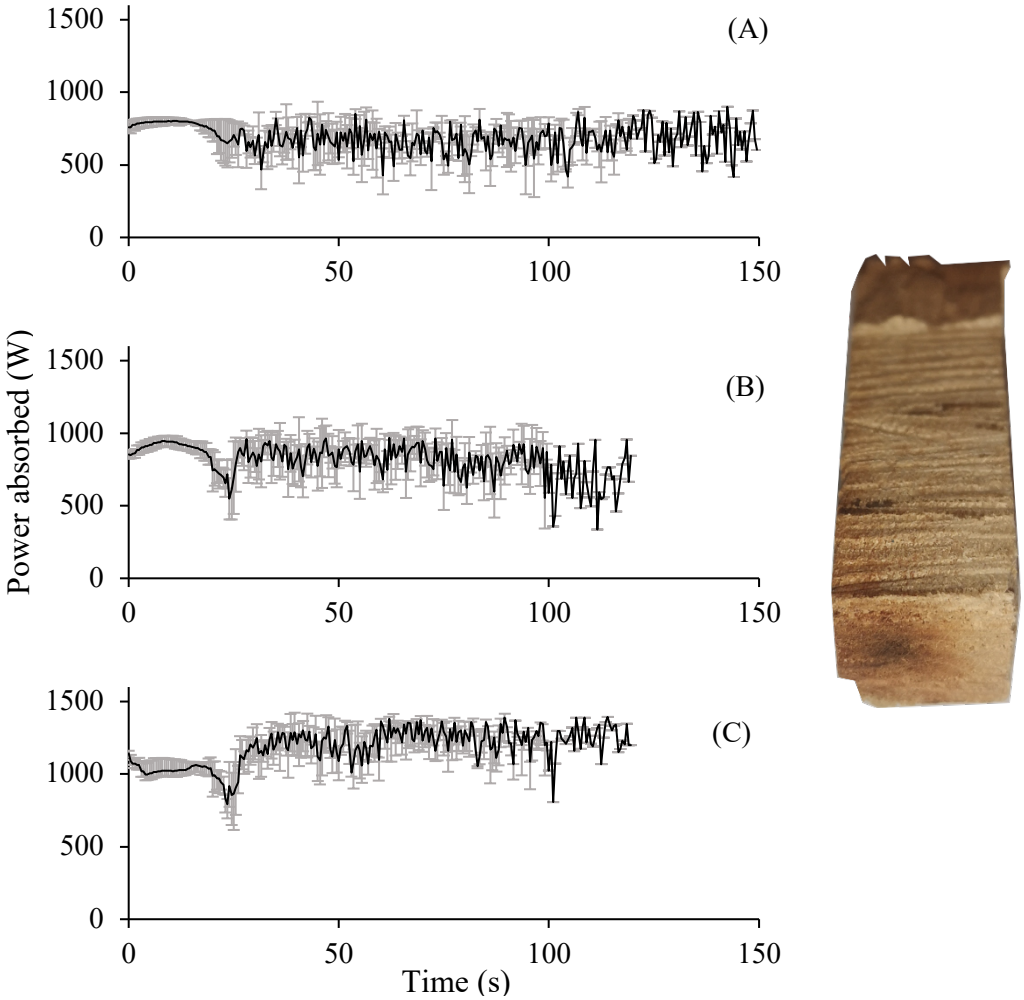


Figure 3-9 – (Left) Absorbed power for water as a solvent based on approximately (A) 1.25 kW, (B) 1.50 kW, (C) 1.80 kW applied powers with fixed impedance matching over 3 runs per applied power. (Right) A cross section of a sycamore block treated at 1.8 kW applied, 120 second processing time.

Water behaved very differently to the hydrocarbons where at all powers provided to the system, there were long periods of a consistent absorbance. At around 25 seconds for 1.50 and 1.80 kW applied power, the absorbance dropped and then rose before attaining a consistent range of power. As water is polar, it is very microwave absorbent and therefore the initial consistent absorbance is where the liquid water is absorbing the microwaves. The drop and rise in absorbance are likely related to the onset of boiling. Once the liquid starts to boil the liquid-gas regime around the sample would be changing constantly, resulting in fluctuations in absorbed power. It is also possible that as the boiling temperature of water is approached, the dielectric loss of the liquid gets lower and thus allows for selective heating of the sycamore to occur (Lee et al., 2016).

3.4.1.4 Power absorption for 2-propanol

2-Propanol offers a comparison to water as it is a microwave absorbent liquid with a small penetration depth at 20 °C, however the boiling point is lower than water (82 °C) and it has a lower latent heat (754 kJ/kg) and specific heat capacity (2348 J/kg·K). Figure 3-10 shows the absorbed power for 2-propanol based on 1.5 - 1.7 kW applied power.

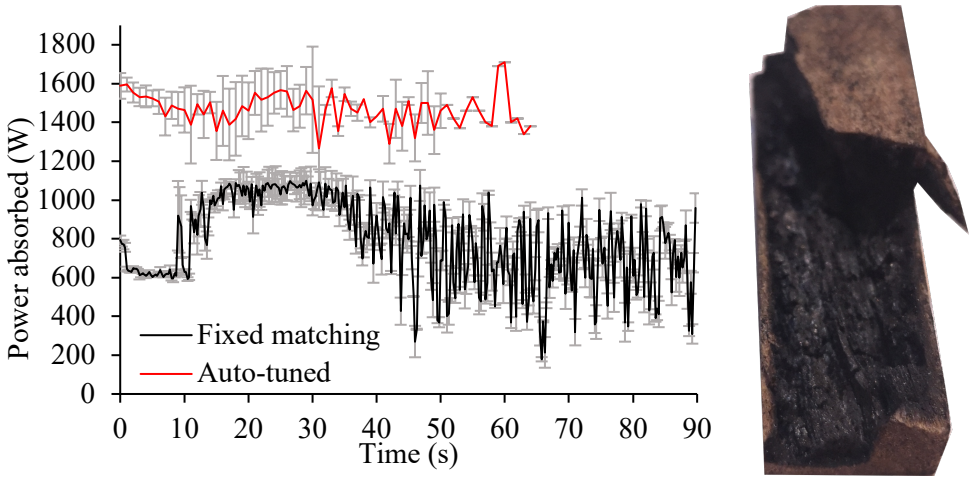


Figure 3-10 – (Left) Absorbed power for 2-propanol as an inerting liquid, with fixed impedance matching, and dynamic impedance matching to increase absorbance of the solid sample, at approximately 1.5 kW applied power over 5 runs. (Right) A cross section of a sycamore block after treating at 1.5 kW applied power, 45 second processing time, dynamic impedance matching.

With fixed impedance matching it is evident that the absorbance of 2-propanol is similar to that of water. There was an initial consistent absorbance, at which the liquid started to boil. This resulted in the fluctuations in the absorbed power. The fluctuations appear to have a larger range (around the absorbed value of approximately 600 W ±300 W) than water.

The dynamic impedance matched absorbed power shown in Figure 3-10 behaves very similarly to that of the absorbed powers for the fixed impedance matching process, a difference being that the power absorbed is much closer to the applied power (1.5 kW). The absorbed power is around 1.5 kW. The variation around the consistent absorbed power is less erratic than the fixed impedance matching process, which further demonstrates how dynamic impedance matching benefits the process in terms of repeatability and energy efficiency.

As the liquid likely absorbed microwave energy, and the energy quantified represented the total energy provided to the system, quantification of energy to the sycamore was not possible. Therefore, the ability to monitor the pyrolysis process and change in dielectric properties of the sycamore, based on reflected/absorbed power, was lost in this case.

3.4.1.5 Power absorption for acetic acid

Figure 3-11 shows that acetic acid follows the same trends at all powers tested, however at higher powers the start of the decline in absorbance occurs earlier.

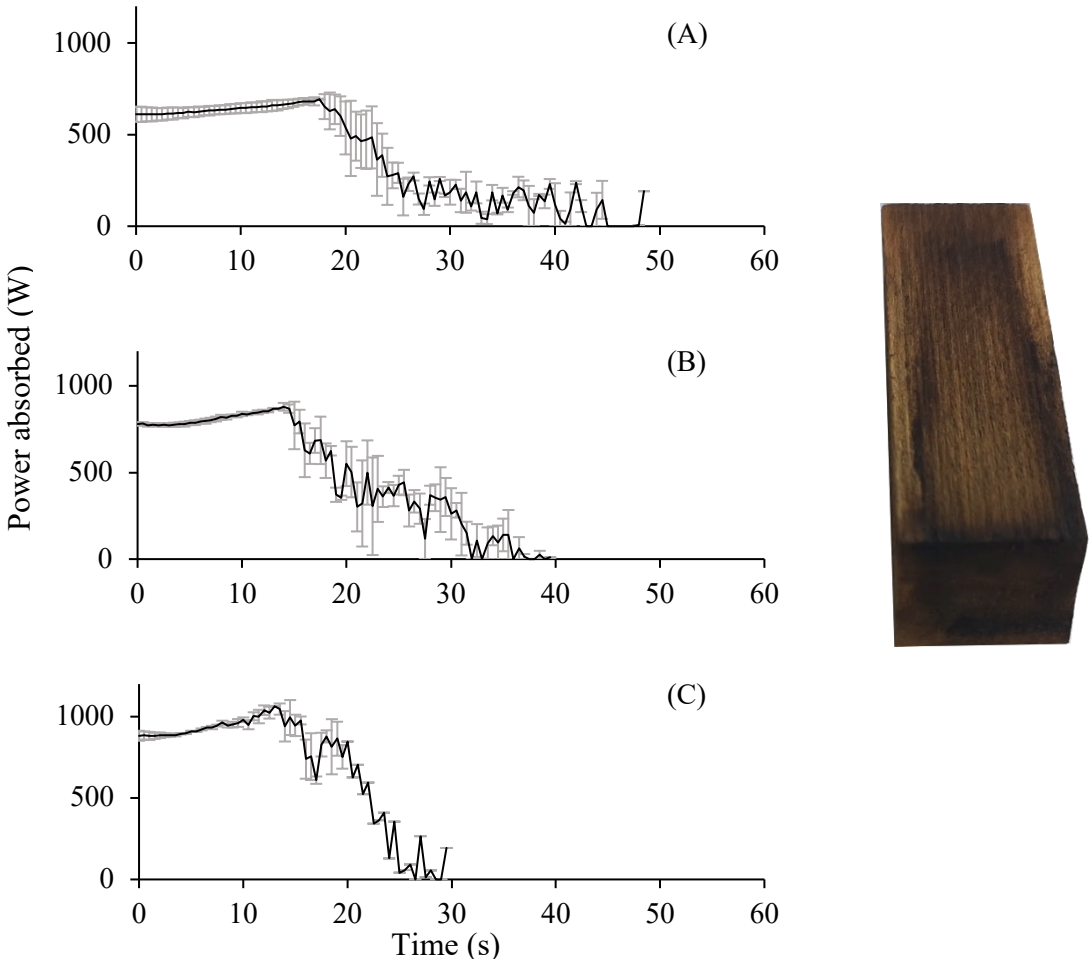


Figure 3-11 – (Left) Absorbed power for acetic acid as a solvent based on approximately (A) 1.00 kW, (B) 1.25 kW, (C) 1.50 kW applied powers with fixed impedance matching over 3 runs per applied power. (Right) A sycamore block sample post pyrolysis in acetic acid (1.5 kW applied, 12 seconds).

Figure 3-11 shows that pyrolysis was possible within acetic acid, however some surface charring of the sycamore block occurred. All of the runs were reproducible up until 15 seconds. The absorbance declined very rapidly after 15 seconds until zero absorbance was achieved. As acetic acid is a microwave absorbent solvent, the absorbed power dropping to zero is unexpected. The decline in absorbance is likely due to the changing dielectric properties and boiling regime of the liquid. In this case, the vapour produced caused displacement of the liquid from around the biomass into the condenser losing the liquid-inerting required for the process, potentially explaining the drop in absorbed power.

3.4.1.6 Power absorption for glycerol

Glycerol was investigated due to its high dielectric constant (42.5), very high boiling point (290 °C) and very high viscosity (1412 cP). Absorbed powers are shown in Figure 3-12.

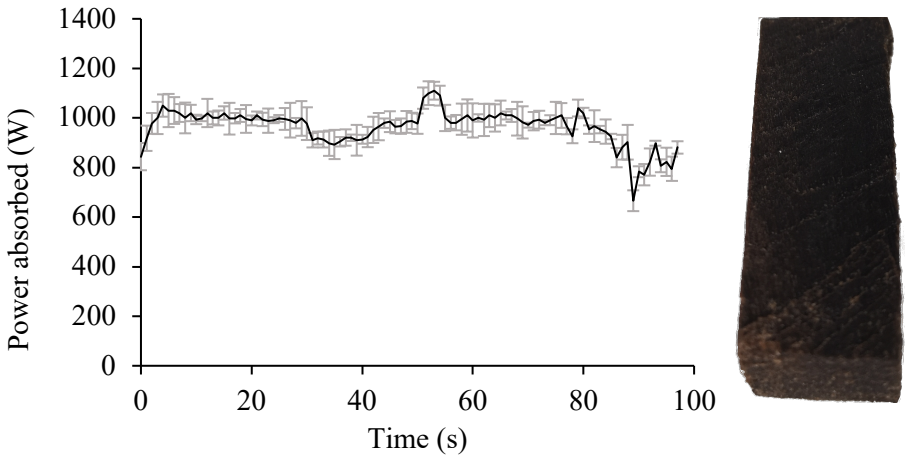


Figure 3-12 – (Left) Power absorbed for sycamore with glycerol as an inerting liquid, with dynamic impedance matching to increase absorbance of the solid sample at 1.0 kW over 4 runs. (Right) The sycamore block post pyrolysis within glycerol, (1 kW applied, 100 seconds).

During processing with glycerol, the absorbance remained high throughout the experiments and was relatively stable, with a small degree of variability (< ±100 W) around the applied power of 1.0 kW. It can be seen that the surface cooling present for the hydrocarbon inerted pyrolysis process was not present for glycerol, potentially due to the boiling point of glycerol, or the high viscosity of the liquid allowing for a large amount of bubble retention within the liquid. Despite glycerol allowing for pyrolysis to occur (due to the high boiling point and viscosity) post-pyrolysis separation of the oil from the glycerol proved to be challenging. Glycerol did not readily dry and separate from the pyrolysis oil due to its low volatility, and liquid-liquid extraction proved difficult due to the high viscosity of the liquid.

3.4.1.7 Power absorption for nitrogen

Figure 3-13 shows the absorption curves for sycamore pyrolysing within a nitrogen inerted atmosphere.

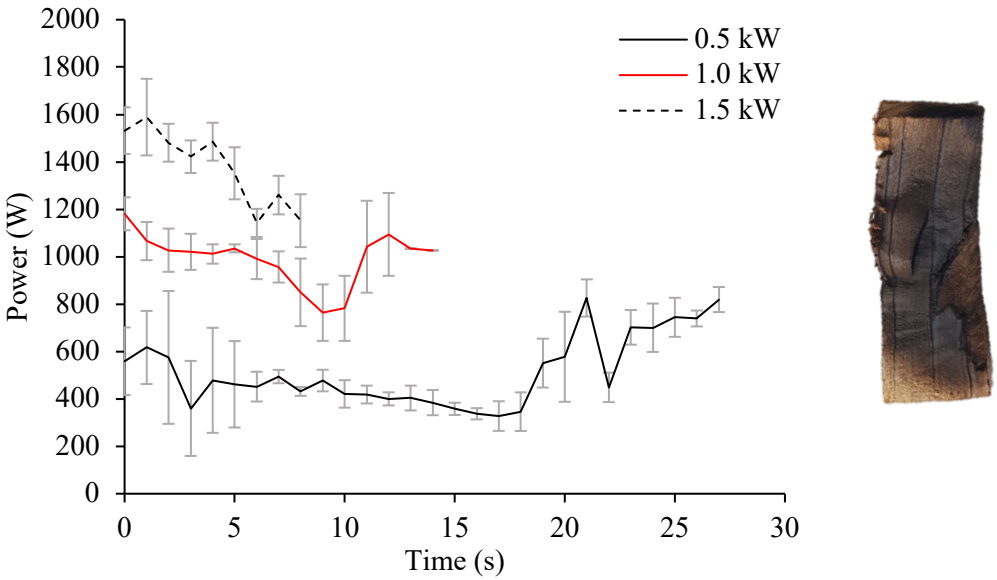


Figure 3-13 – (Left) Power absorbed for sycamore with nitrogen as an inerting medium, with dynamic impedance matching to increase absorbance of the solid sample at approximately 0.5, 1.0 and 1.5 kW applied power over 5 runs per applied power. (Right) The sycamore block after nitrogen inerted pyrolysis, 0.5 kW applied, 10 second processing time.

It is evident from Figure 3-13 that pyrolysis occurred for the nitrogen inerted process, however the surface level temperature control present in the liquid inerted microwave pyrolysis processes was not present. The absorbed power for each power applied offered repeatable behaviour. The lower power (0.5 kW applied) tests appeared to be more consistent around the set power value after 5 seconds, before which there was a large degree of variance. The power absorbed during the 1.5 kW runs all appeared to decrease as the pyrolysis process progressed, and the 1.0 kW runs decreased until around 10 seconds, at which point the absorbance increased.

3.4.1.8 Power absorption discussion

The absorbed powers provided an initial insight into the repeatability of the microwave pyrolysis process. The dielectric properties of the sycamore would change with increasing temperature. As the sycamore heats, the ability of the sycamore to both absorb the microwave energy and convert the stored energy into heat will change, affecting the power absorbed in the fixed impedance matching processes.

Investigation into both microwave transparent liquids and microwave absorbent liquids as inerting media were performed, with fixed and dynamic impedance matching. The power absorbed for every applied power are repeatable, therefore feasible repeats of the same processing conditions could provide similar process outputs in terms of solid volatilised and pyrolysis oil yields.

Carrying out microwave pyrolysis with fixed impedance-matching for a low loss material such as sycamore is feasible, but processing implications must be considered. Using fixed matching limits power absorption and therefore using power as a control variable is more difficult than when using real-time impedance matching. There is a large variation in the trends of absorbed power for each power applied and therefore an increase in applied power may not necessarily correlate to a higher power absorbed by the sample. The advantages of dynamic impedance matching would allow for more of the applied power to be absorbed by the sample in the cavity, resulting in both increased energy efficiency, power densities and lower processing times for the same specific energies (kJ/g).

For hydrocarbon solvents and both fixed and dynamic impedance matching, the slower processing times and lower heating rates of the lower power (0.5 kW) runs allowed for greater levels of repeatability. The power absorbed during the pyrolysis process within

the microwave absorbent solvents was high, due to the power applied to the system being absorbed by the solvents. It was therefore not possible to determine the amount of power absorbed selectively by the sycamore during the pyrolysis process in microwave absorbing liquids. It can, however, due to the nature of the solvents, be determined that more power or longer times would be required to heat the sycamore to the same degree when processing in a microwave absorbent solvent as when processing within a microwave transparent solvent. The absorbed power of all of the microwave absorbent solvents investigated appeared to fluctuate around a set value after a certain point, representative of the liquid boiling, as was observed empirically.

The absorbed power when pyrolysing within acetic acid, despite being a microwave absorbent solvent, reduced to zero. This is likely due to the fixed impedance matching characteristics of the pyrolysis process being carried out, coupled with the loss tangent of acetic acid decreasing with increasing temperature and boiling regime once the acetic acid was boiling. The presence of solvent within the condenser was also observed with 2-propanol. The fixed stub position was likely not suitable for the gas-solid atmosphere, resulting in a decline to zero absorbance.

Similar effects on the sycamore block were observed with glycerol, however in this case the sycamore block appeared to be significantly charred on all surfaces. This charring was likely due to the high viscosity of the liquid, leading to large bubbles and the subsequent displacement of liquid glycerol from around the biomass. Due to the loss of the liquid environment when using glycerol and acetic acid, further investigations into mass loss (for glycerol) and pyrolysis oil yields (for both glycerol and acetic acid) were not undertaken using these liquids with the single-mode experimental setup.



Figure 3-14 – The sycamore block pre pyrolysis (left) and post-pyrolysis within acetic acid (middle) and glycerol (right), showing charring on the surface of the block.

For the nitrogen inerted pyrolysis process the absorbed powers at all applied powers investigated were repeatable. With similar absorbance behaviour, a direct comparison could be made between the gas and (low loss) liquid inerted processes in terms of mass loss and pyrolysis oil yields. This is discussed in the next section.

3.4.2 Effect of solvent on solid mass loss

The liquid-inerted pyrolysis process was carried out in the presence of the selected solvents, and the change in mass recorded at a range of energy inputs. Mass loss was used to give an indicative yet quantitative measure of conversion, with a higher mass loss indicating a greater degree of pyrolysis. The inerting media investigated, as identified in Section 3.3 comprised of both microwave transparent and microwave absorbent solvents. *n*-Hexane, cyclohexane, isooctane and kerosene were chosen due to their microwave transparency whilst having differing physical properties. Acetic acid, 2-propanol and water were chosen due to their high microwave absorbance and differing physical properties, such as latent heat of vaporisation, with water being 3 times larger than 2-propanol, for example. Acetic acid was investigated due to its high dielectric constant and also as it is a prominent component of pyrolysis oil (Hu and Gholizadeh, 2019). Water was investigated due to its very high dielectric properties, along with water being a green solvent, the pyrolysis process succeeding within water would allow for a range of liquids to be investigated. To provide a comparison point in terms of pyrolysis mass loss performance in the liquid-inerted system, gas-inerted

microwave pyrolysis was carried out to determine how mass loss is affected when there was no efficient cooling on the surface of the biomass.

The mass loss data for n-hexane, cyclohexane, kerosene, pentane, acetic acid, water, 2-propanol and nitrogen are presented in Figure 3-15 – Figure 3-23.

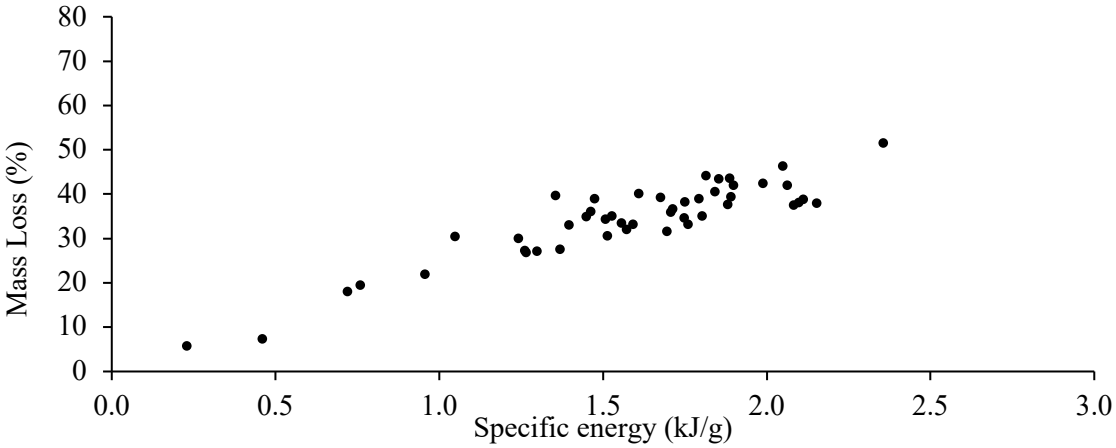


Figure 3-15 - Bulk mass loss of the sycamore blocks against specific energy absorbed by the sycamore using n-hexane as an inerting liquid for applied powers ranging from approximately 1.0 – 1.8 kW.

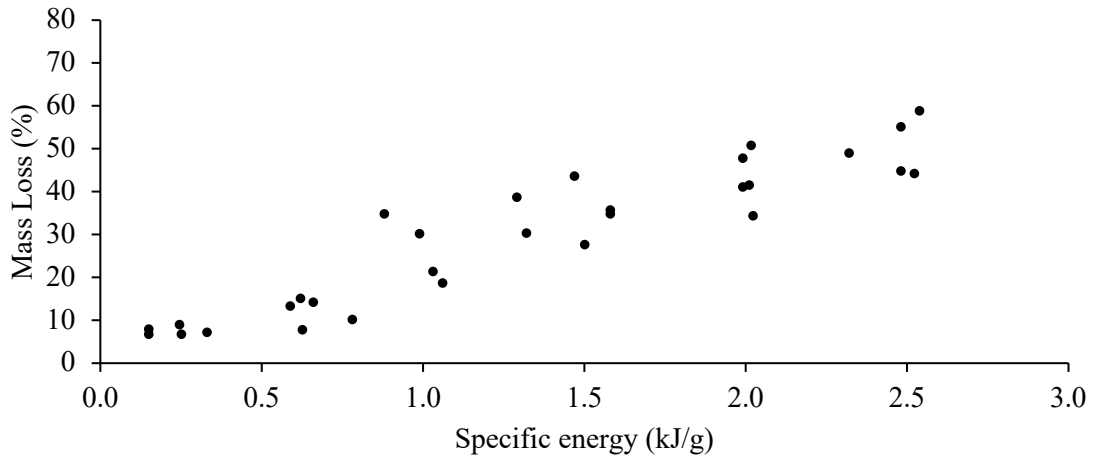


Figure 3-16 - Bulk mass loss of the sycamore blocks against specific energy absorbed by the sycamore for cyclohexane as an inerting liquid with applied powers from approximately 0.6 – 1.7 kW.

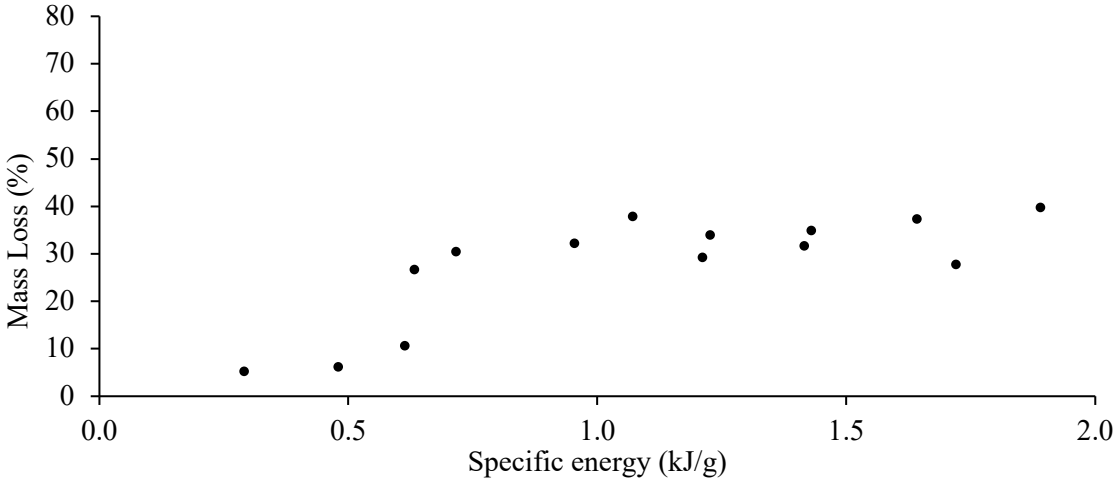


Figure 3-17 – Bulk mass loss of the sycamore blocks against specific energy absorbed by the sycamore for isooctane as an inerting liquid, with applied powers ranging from approximately 1.0 - 1.8 kW.

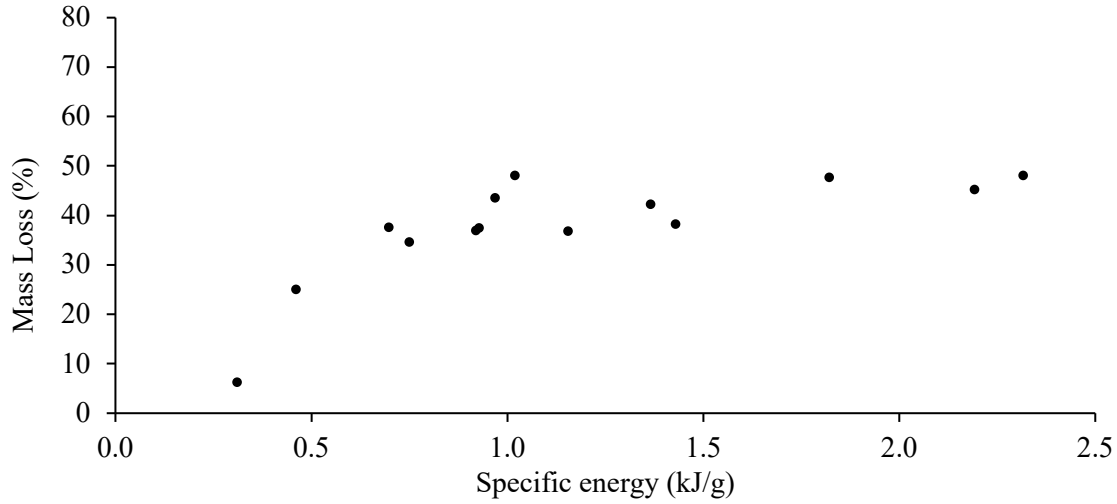


Figure 3-18 - Bulk mass loss of the sycamore blocks against specific energy absorbed by the sycamore for kerosene as an inerting liquid, with applied powers ranging from approximately 1 - 1.8 kW.

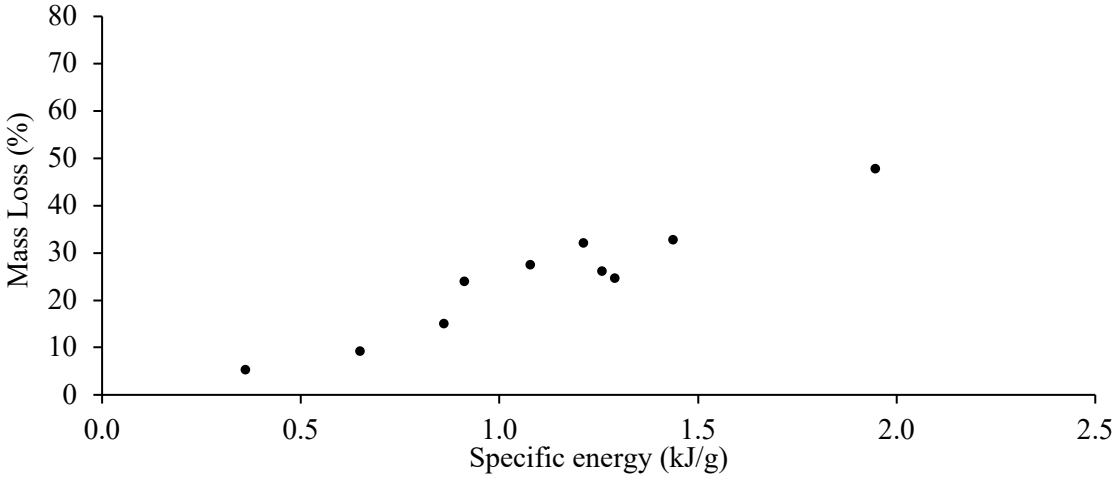


Figure 3-19 - Bulk mass loss of the sycamore blocks against specific energy absorbed by the sycamore for pentane as an inerting liquid, with applied powers ranging from approximately 1 - 1.8 kW.

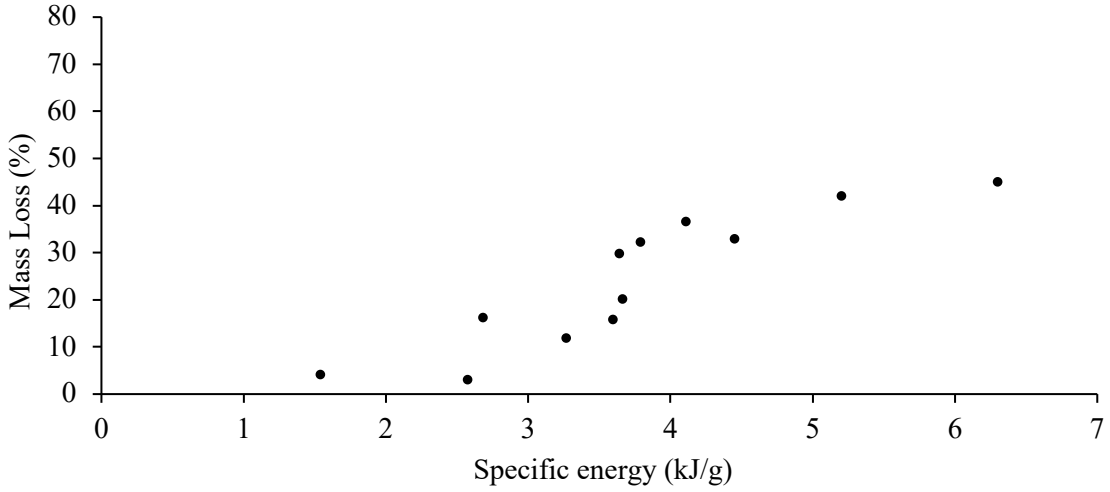


Figure 3-20 - Bulk mass loss of the sycamore blocks against specific energy absorbed by the sycamore for acetic acid as an inerting liquid, with applied powers ranging from approximately 1.0 - 1.5 kW.

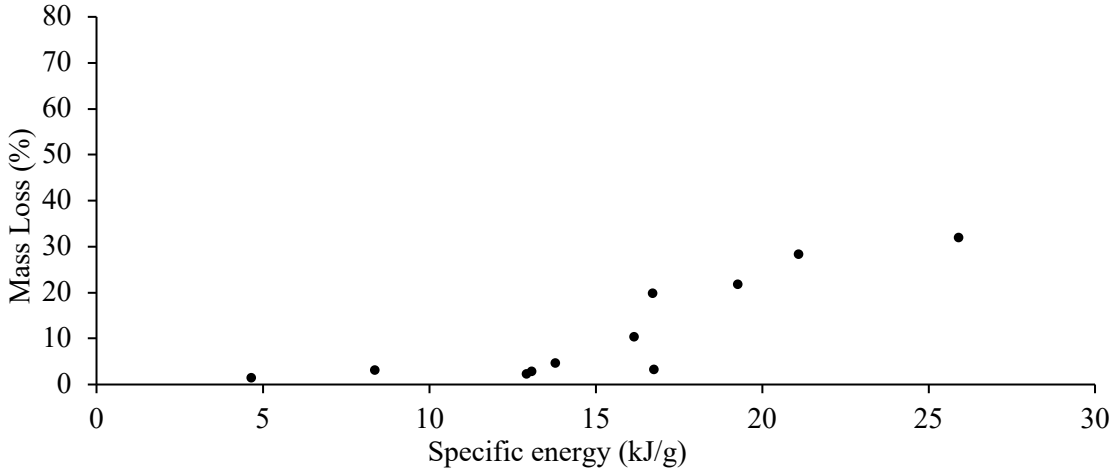


Figure 3-21 - Bulk mass loss of the sycamore blocks against specific energy absorbed by the sycamore for water as an inerting liquid, with applied powers ranging from approximately 1.25 - 1.8 kW with fixed impedance matching.

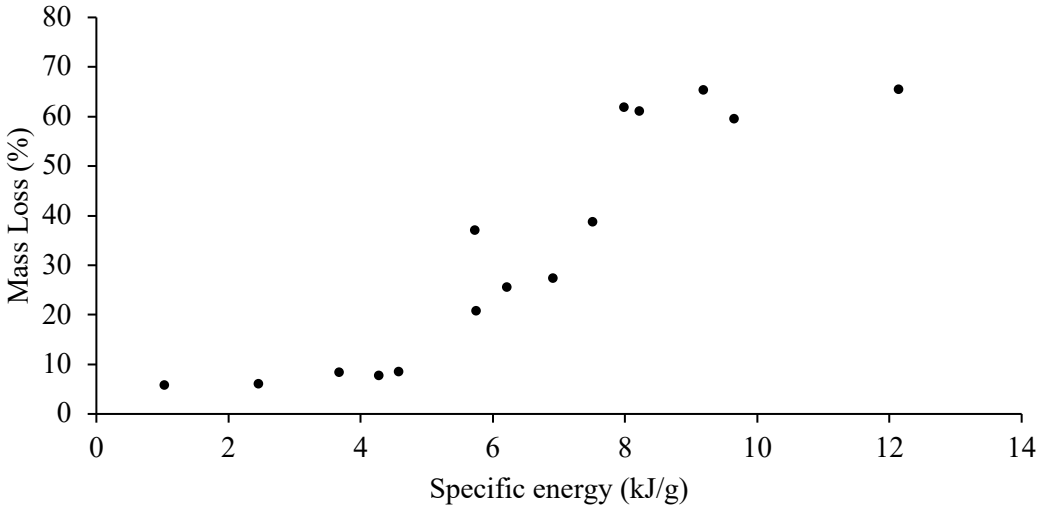


Figure 3-22 - Bulk mass loss of the sycamore blocks against specific energy absorbed by the sycamore for 2-propanol as an inerting liquid, with an applied power of 1.5 kW.

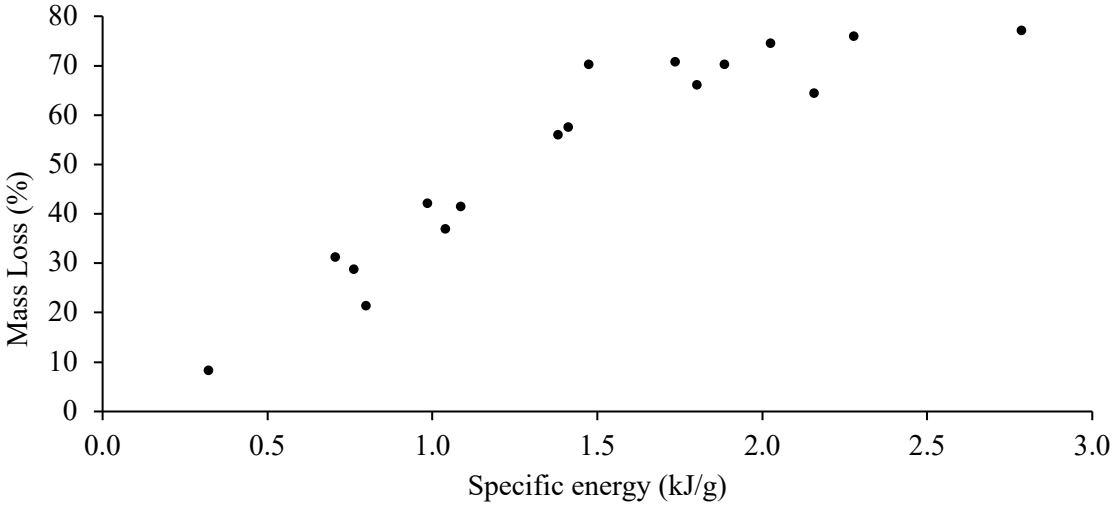


Figure 3-23 – Bulk mass loss for sycamore against specific energy absorbed by the sycamore inerted by nitrogen with applied powers ranging from approximately 0.6 – 1.5 kW.

Figure 3-15 – Figure 3-23 present that mass losses (greater than the water content of 6.4 %) were achieved for all the inerting media investigated, with mass losses reaching up to 77 %. From Figure 3-15, it is evident that the mass loss of the sycamore in n-hexane followed a linear trend with increasing energy to the sample reaching a highest mass loss at 52 % at 2.36 kJ/g. For cyclohexane, the maximum mass loss attained during the process was around 60 % at 2.5 kJ/g, with a threshold for mass loss >10 % being approximately 0.5 kJ/g. For isooctane the threshold for any appreciable mass loss (>10 %) was 0.5 kJ/g, at which point there was a sharp increase and then a plateau at approximately 40 % mass loss. For kerosene, Figure 3-18 shows that above 0.5 kJ/g, the mass loss rapidly increased until a plateau of around 40-50 % above 1.0 kJ/g. When pentane is used as an inerting liquid there is a positive linear trend between the specific energy absorbed by the sycamore block, with the highest mass loss of the sycamore block being 48 % at 1.95 kJ/g.

When using acetic acid as an inerting liquid, the threshold energy for pyrolysis to occur (>10 % mass loss) is approximately 2.5 kJ/g with mass losses reaching up to 45 %. Figure 3-20 shows that while pyrolysis can occur using acetic acid as an inerting

medium, there is an energy penalty present, with a mass loss of almost 40 % requiring 4.1 kJ/g absorbed specific energy, compared to approximately 1.5 kJ/g for the hydrocarbon solvents.

When water was used as an inerting medium, the threshold specific energy for any appreciable mass loss (>10 %) to occur was around 15 kJ/g, around 30 times the threshold energy required in the hydrocarbon solvents (0.5 kJ/g). Below the threshold energy input, the sycamore remained non-pyrolysed. At higher energy inputs above the threshold energy, it was possible to pyrolyse the biomass, with 32 % mass loss observed at 26 kJ/g.

When 2-propanol was used as the inerting medium, it appeared that a threshold energy input of around 5 - 6 kJ/g was required for any appreciable mass losses (>10 %) to occur. At lower energy inputs (2 – 5 kJ/g) the sycamore remained non-pyrolysed, with the recorded mass loss corresponding to the removal of water from the sycamore sample. At higher energy inputs (>6 kJ/g) it was possible to pyrolyse the biomass, with 65 % mass loss observed at 12 kJ/g.

For the nitrogen inerted process, it can be seen from Figure 3-23 that there appears to be a positive linear trend up to 1.5 kJ/g at which point the mass loss plateaus at around 75 %. When compared to the liquid-inerted pyrolysis process, the mass loss is much greater for equivalent specific energies. It would be expected for a gas-inerted pyrolysis process to allow for greater mass losses, due to the entire block pyrolysing, whereas in a liquid-inerted system there is a layer of non-pyrolysed wood at the surface of the block.

3.4.2.1 Mass loss discussion

To further develop the process and determine solvent feasibility, the solvents were directly compared against each other in terms of mass loss performance as shown in Table 3-8 and Figure 3-24.

Table 3-8 - The inerting media investigated, with highest mass losses presented, and energy requirements for the sycamore block reach 20 % and 40 % mass loss during the pyrolysis process

Inerting medium	**Highest mass loss achieved (%)**	**Absorbed specific energy required to obtain 20 % mass loss (kJ/g)**	**Absorbed specific energy required to obtain 40 % mass loss (kJ/g)**
Nitrogen	77.2	0.7	1.0
n-Hexane	51.6	0.8	1.6
Cyclohexane	58.9	0.8	1.5
Isooctane	39.7	0.6	1.9
Kerosene	48.1	0.4	1.0
Pentane	47.7	0.9	1.6
Acetic acid	45.0	3.6	5.0
Water	32.1	16.7	-
2-Propanol	65.5	5.8	8.0

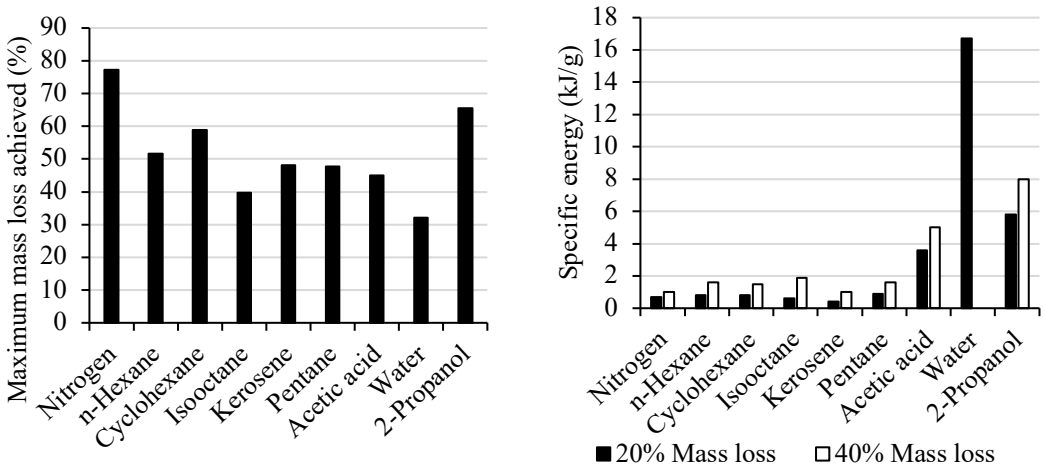


Figure 3-24 – The maximum mass loss achieved for the inerting media investigated, and specific energy requirements to achieve 20 % and 40 % mass loss during the pyrolysis process.

It is evident that all of the hydrocarbon solvents tested behaved similarly within the liquid-inerted microwave pyrolysis process, requiring around 0.5 kJ/g absorbed specific energy for pyrolysis to begin.

For the polar solvents, the energy requirements were evidently higher compared to utilising hydrocarbons as they absorb microwave energy directly and therefore reduce the energy efficiency of the process. As the temperature of water increases, the dielectric loss factor decreases (Ellison et al., 1996). Lee et al. (2016) demonstrated that selective heating of biomass can take place within water during microwave heating at temperatures above 50 °C due to this phenomenon. Each microwave absorbent solvent investigated reached its boiling point during the pyrolysis process as there was evidence of boiling, so it is likely that selective heating did indeed take place and that enough microwave energy was absorbed by the biomass to allow the centre of the particle to reach temperatures sufficient to induce pyrolysis.

More energy was clearly required for the polar solvents, however the fact that pyrolysis did occur in every solvent investigated indicates that the concept of pyrolysing within an inerting liquid could be applied using a broad spectrum of different liquids and is not confined solely to those that are microwave transparent. This represents a significant step forward from the original idea of the requirement for microwave transparent liquids. The energy needed to achieve >10 % mass loss was around 3 and 15 kJ/g for acetic acid and water respectively, approximately 6 to 30 times the requirement in the hydrocarbon liquids. Despite the energy requirement for pyrolysis being increased, 2-propanol allowed for pyrolysis to occur to a much greater degree (65.5 % mass loss) than other polar solvents (<45 % mass loss). The increased energy requirements and mass loss penalty when using water as an inerting liquid are likely related to the latent heat and specific heat capacity of the water. The latent heat of vaporisation for water (2260 kJ/kg) is around 3 – 5 times that of the other polar solvents (402 – 830 kJ/kg). The specific heat capacity (4190 J/kg·K) is around double that of the other polar solvents (2043 – 2048 J/kg·K), meaning that more energy is clearly required

to both heat the water to its boiling point and vaporise the liquid. With the lower latent heat value for propanol, when compared to water, it is possible that more liquid was boiling during the pyrolysis process. Therefore, it is possible that there was a lower incidence of a consistent liquid surround around the sycamore block, allowing for the temperatures to increase internally and pyrolysis to occur. The surface of the sycamore block remained non-pyrolysed, however. It is likely that there was, therefore, sufficient liquid in contact with the surface of the sycamore block to maintain the surface temperature of the sycamore block below pyrolysis temperatures (<300 °C).

When using kerosene as an inerting liquid, the mass losses observed at low specific energies (<1.5 kJ/g) were higher than cyclohexane and other lower temperature boiling point hydrocarbons. This was to be expected due to the higher boiling point of kerosene (200 - 250 °C), which means that the surface temperature of the sycamore would be much higher than with cyclohexane, leading to higher temperatures within the depth of the biomass and consequently more mass loss at a given energy input.

The mass loss with pentane was comparable to the other hydrocarbon solvents investigated. However due to the very low boiling point (36.1 °C) and latent heat (366 kJ/kg), significant boiling and vaporisation of the pentane occurred resulting a low volume of the liquid surrounding the sycamore block. This large amount of boiling significantly reduced the feasibility of using pentane as an inerting liquid during the pyrolysis process.

When using acetic acid as an inerting liquid, from observations after the pyrolysis process had occurred, the outside of the sample had charred suggesting it had indeed pyrolysed. The surface level pyrolysis could also be due to the boiling regime and changes in absorbance (Section 3.4.1.5), with the reduction of liquid surround, the process acted as a gas-inerted process.

Figure 3-25 presents the cyclohexane and nitrogen inerted microwave pyrolysis process and a nitrogen inerted fixed bed configuration of larch particles <4 mm, at a mass of 5 g (Robinson et al., 2015).

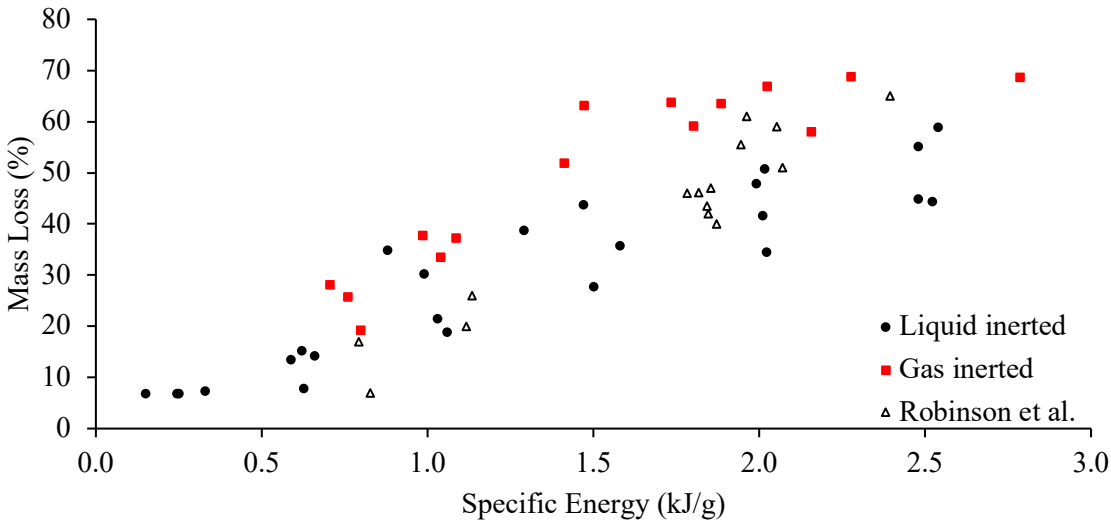


Figure 3-25 – Bulk mass loss for sycamore (cyclohexane inerted, nitrogen inerted) and a 5 g larch fixed bed of particle size <4mm (Robinson et al., 2015) inerted by nitrogen

Figure 3-25 shows that for the ranges investigated in the single-mode microwave pyrolysis system, the performance in terms of mass losses was comparable to literature. It is evident that in a like-for-like process, gas inerted processing allowed for greater mass losses across all specific energies that were investigated. This greater mass loss performance is to be expected, as there was no layer of non-pyrolysed wood at the surface of the biomass and therefore the potential for mass loss was greater. With the potential mass loss being lower, there was also an energy penalty for liquid-inerted pyrolysis when compared to the gas-inerted pyrolysis process, around 10-20 % for equivalent specific energies using hydrocarbon solvents, showing that efficient cooling is occurring in the liquid inerted process.

3.4.3 Pyrolysis oil yields

The pyrolysis oil yields for each of the inerting media investigated are presented as yields based on the original non-pyrolysed sycamore block masses on a dry weight basis.

Pyrolysis oil was produced in small volumes (<1.5 mL) that could not be directly collected due to the low volume and high viscosity. The aqueous phase fraction adhered to the sides of the quartz tube and could not be poured. Using a pipette was also not feasible due to aforementioned viscosity and wetting properties. For this reason, the suspended organic fraction was separated and the aqueous fraction was collected by washing with acetone. The acetone fraction was subsequently dried to leave the aqueous fraction of the pyrolysis oil and the solvent phase was dried to leave the organic phase of the pyrolysis oil. To provide an estimate of pyrolysis oil lost during the drying and separation stages, the mass of the quartz tube (with oil adhered to the sides) was weighed before and after washing and compared to the oil masses after washing and separation. Estimated losses during the washing and separation stages for approximately 2.5±0.04 kJ/g, 21±3 % aqueous oil yield (3 repeats) are presented in Table 3-9.

Table 3-9 – Estimated losses during the collection and subsequent separation of the aqueous pyrolysis oil phase for approximately 2.5±0.04 kJ/g, 21±3 % aqueous pyrolysis oil yield (3 repeats).

Stage of separation	Mass (g)	Loss (g)	Loss (%)
1a) Initial aqueous phase mass in quartz tube	0.76 ±0.13	0	0
1b) Aqueous phase mass precipitated out of the organic phase over time (1 hr)	0.58 ±0.05	0	0
2) Aqueous phase after washing and drying	1.20 ±0.15	0.16 ±0.02	10.6 ±0.9

Table 3-9 shows that for the highest yield of aqueous pyrolysis oil attained during the cyclohexane inerted process (18 - 24 %), the losses during transfer for the aqueous phase oil were around 0.16g (9 - 11 % of the total yield). If it is assumed that the losses during separation remained consistent throughout all specific energies investigated, for lower pyrolysis oil yields, the potential transfer loss percentage became much higher. Equivalent losses for a 10 % pyrolysis oil yield would have a potential transfer loss potential of 30 % of the recorded value.

For the organic phase, recording the mass produced immediately after pyrolysis was not possible as it was readily miscible within the organic solvent. Therefore, using Raoult's law, estimations were made on the amount of organic phase lost as vapour during separation of the organic phase and the solvent.

$$p = \overset{*}{p}_a x_a + \overset{*}{p}_b x_b \qquad 3\text{-}2$$

$$y_a = \left(\frac{p - \overset{*}{p}_b}{\overset{*}{p}_a - \overset{*}{p}_b} \right) \frac{\overset{*}{p}_a}{p} \qquad 3\text{-}3$$

Where:

$\overset{*}{p}_x$	-	Partial vapour pressure of component x
p	-	Total vapour pressure of the mixture
x_x	-	Liquid composition of component x, mole basis
y_x	-	Vapour composition of component x, mole basis

As pyrolysis oil has a complex composition, representative substitutes for the oil were used: acetic acid was chosen as it is a component of pyrolysis oil, with a boiling point at the lower range of the pyrolysis oil boiling point (118°C). Kerosene was also chosen as a representative organic liquid with a boiling point within the middle to upper range for pyrolysis oil (200 – 250°C). Assuming an upper estimate of 5 % organic phase oil

in the solvent the compositions of the solvent and the organic components are shown in Table 3-10.

Table 3-10 – Vapour composition of the organic phase-solvent mix based on 5 % organic pyrolysis oil phase by mass.

Selection		Vapour Composition (%)		Organic phase lost (%)
'Oil'	Solvent	'Oil'	Solvent	
Kerosene	n-Hexane	0.17	99.83	3.47
Acetic acid	n-Hexane	0.46	99.54	9.15
Kerosene	Cyclohexane	0.30	99.70	6.02
Acetic acid	Cyclohexane	0.79	99.21	15.86

It is evident that up to 15 % of the organic phase oil from pyrolysis could be lost as vapour during the separation process.

Pyrolysis oil collection was viable in 2-propanol; both the aqueous and organic phases of the pyrolysis liquid produced during the pyrolysis process was readily miscible with 2-propanol, and therefore the oil yield was able to be determined on separation of the solvent from the oil. Pyrolysis oil collection was possible for the gas-inerted process, where the liquid and volatiles produced were directly condensed into the system and therefore could be weighed immediately, providing an accurate liquid yield that was not possible in the liquid-inerted system using the current setup.

Figure 3-26 - Figure 3-28 show the overall liquid yields of pyrolysis oil from the liquid-inerted microwave pyrolysis process in cyclohexane, 2-propanol and nitrogen based on the starting sycamore block mass, with the mass losses for reference. As the cyclohexane inerted process fractionated the pyrolysis oil into an aqueous and organic phase, the individual fraction yields could be determined, and so are presented in Figure 3-26.

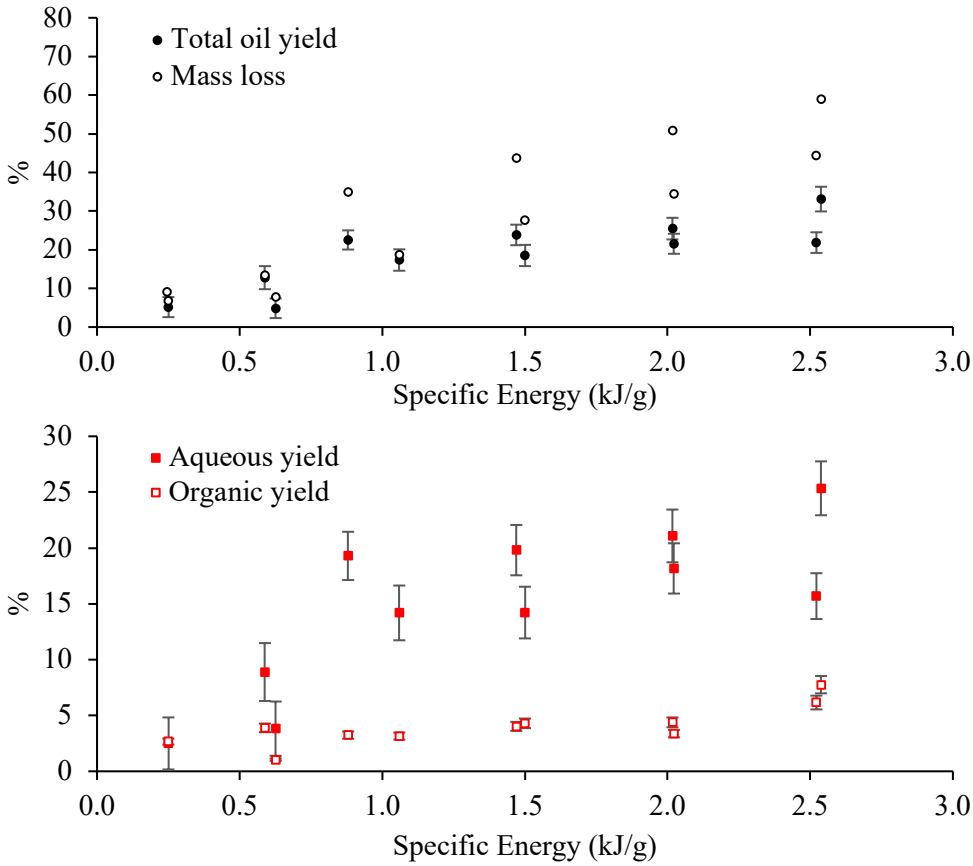


Figure 3-26 –Pyrolysis oil yields from the liquid-inerted microwave pyrolysis process in cyclohexane at applied powers of approximately 0.6 – 1.5 kW, with mass loss included for reference, error bars represent potential variation due to the separation process.

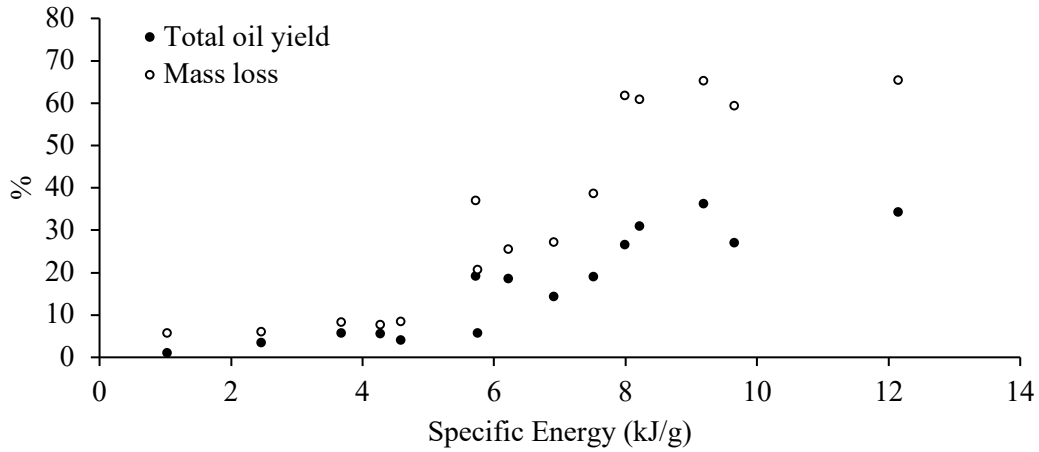


Figure 3-27 – Total pyrolysis oil yields from the liquid-inerted microwave pyrolysis process in 2-propanol, with mass loss included for reference.

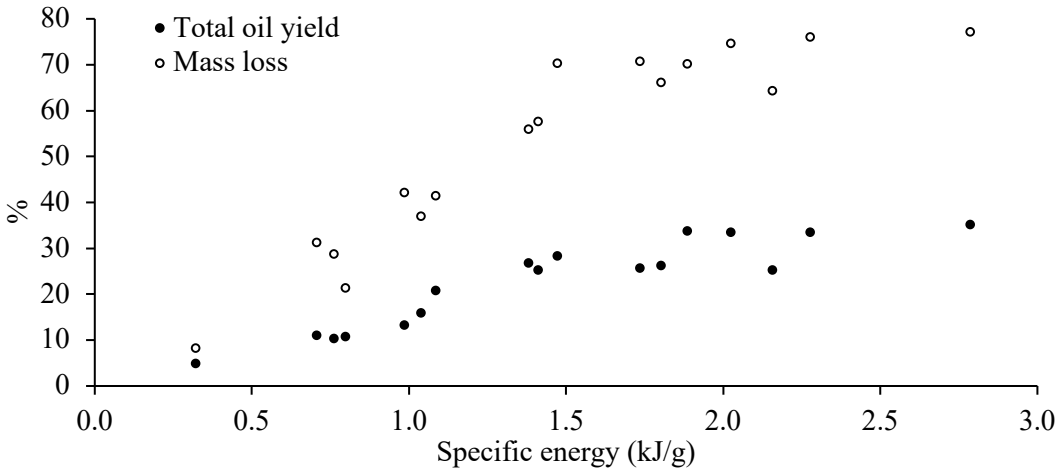


Figure 3-28 – Total pyrolysis oil yields from the nitrogen-inerted microwave pyrolysis process with approximately 0.5 – 1.5 kW applied power, with mass loss included for reference.

Figure 3-26 illustrates that when using cyclohexane as an inerting medium, the maximum pyrolysis oil yield achieved was 30.3 % at 2.54 kJ/g, representative of 52 % of the total solid volatilisation. It is evident that for all oil yields attained, there is a higher yield of the aqueous phase pyrolysis oil than the organic phase.

The trend of the pyrolysis oil yields for the liquid-inerted microwave pyrolysis using 2-propanol as an inerting liquid followed a similar trend to the mass-losses of the sycamore. The liquid yields produced are approximately comparable to the cyclohexane inerted process, however, as was present with the mass losses, there was a significant energy penalty to achieve comparable pyrolysis oil yields. The maximum oil yield was 36.4 % at 9.18 kJ/g, representative of 65.3 % mass loss.

Figure 3-28 shows a positive trend in terms of pyrolysis oil yield and specific energy for the nitrogen inerted process, with the highest oil yield being 35.2 % at 2.79 kJ/g, representative of 77.2 % mass loss.

3.4.3.1 Pyrolysis oil yield in relation to mass loss

Observing the total pyrolysis oil yield in relation to the mass loss during the pyrolysis process allowed for the determination of the solid volatilised that was converted to

pyrolysis oil, and as such determine the solid volatilised to gas (by difference). Determining this factor would allow for a visual representation of the solid volatilised to a liquid, and, therefore, a visual representation of solid volatilised to gas.

Figure 3-29 presents the total pyrolysis oil yields in relation to the solid mass losses for cyclohexane, and the aqueous and organic phase yields.

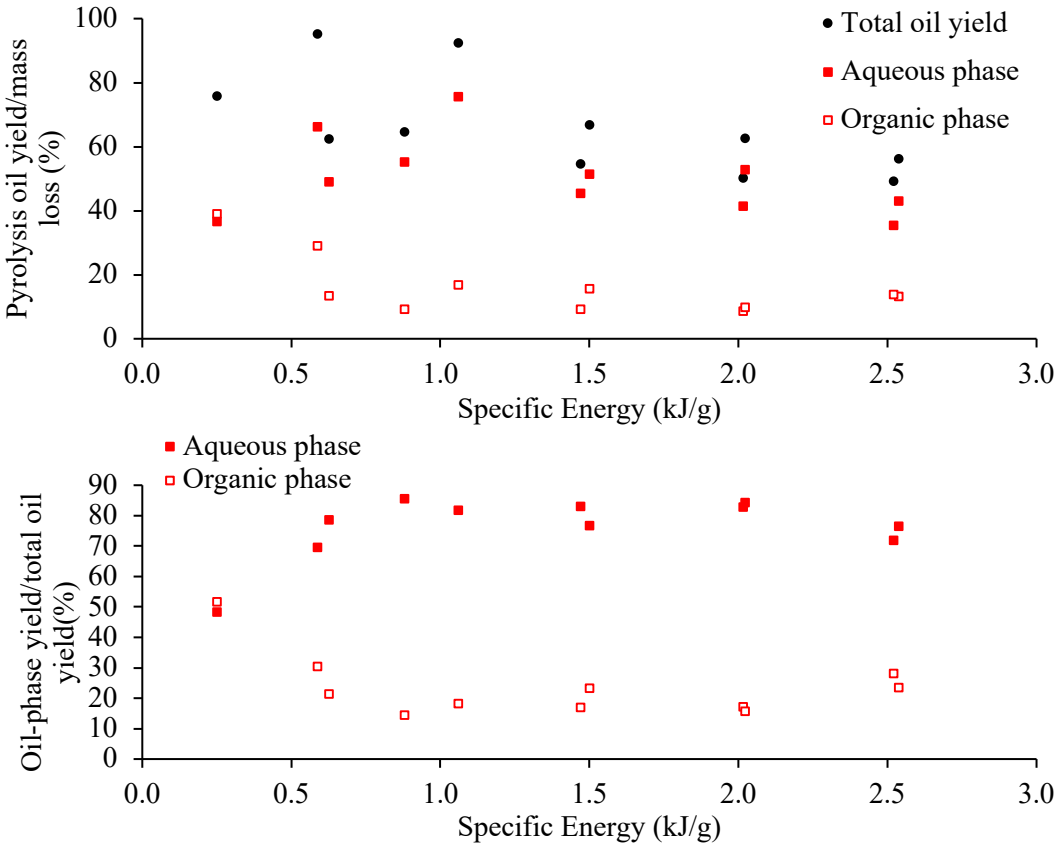


Figure 3-29 – Pyrolysis oil yields in relation to the mass loss, and in relation to the total oil yields for the cyclohexane inerted microwave pyrolysis process.

It is evident that for the cyclohexane inerted microwave pyrolysis process, there is a slight negative trend, decreasing from 75 – 95 % at 0.2 – 1 kJ/g, to approximately 50 % at 2.5 kJ/g. Apart from the values at 0.25 kJ/g, there was a higher concentration of the aqueous phase in the total oil yield for all specific energies investigated. Figure 3-30 presents the total oil yield in relation to the mass loss achieved during the pyrolysis process within 2-propanol.

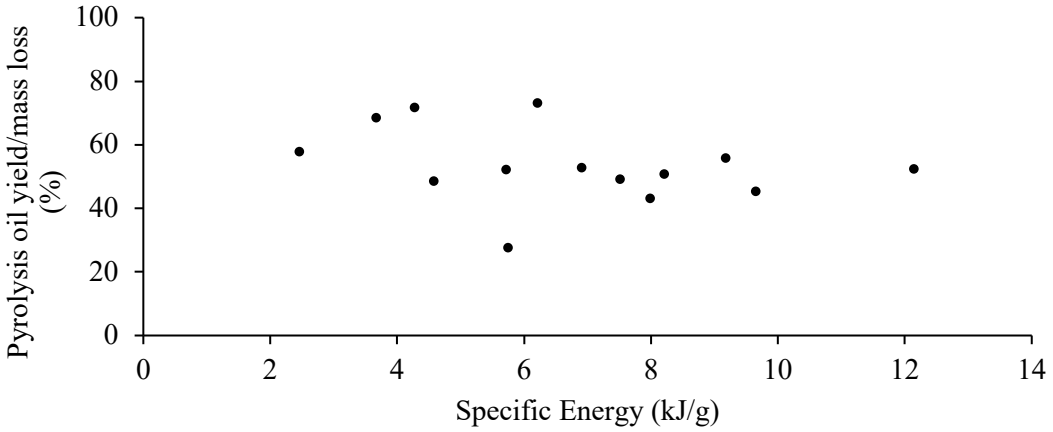


Figure 3-30 – Pyrolysis oil yield in relation to the mass loss for the 2-propanol inerted microwave pyrolysis process.

For 2-propanol, there is a declining trend, decreasing from 60 – 70 % at 2 – 4 kJ/g to 45 – 50 % at 10 – 12 kJ/g. For the nitrogen inerted process, the pyrolysis oil yield in relation to the mass loss stays relatively stable across all specific energies investigated at a value of approximately 35 – 50 %, as shown in Figure 3-31.

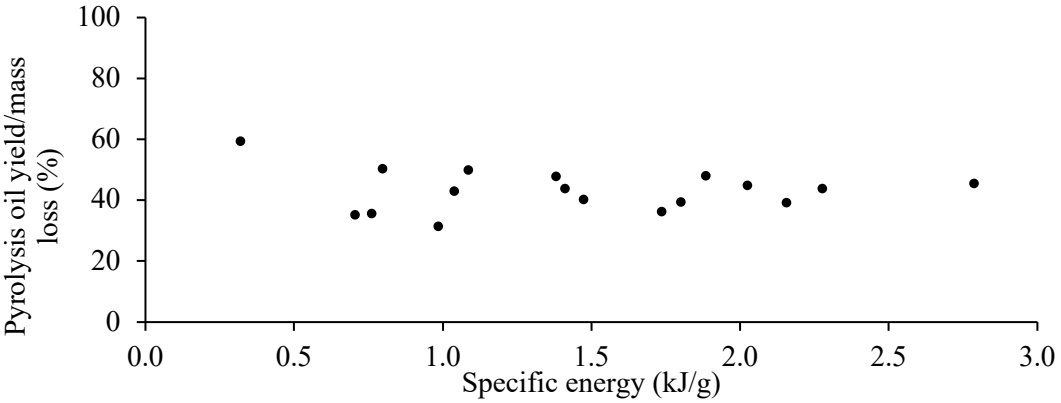


Figure 3-31 – Pyrolysis oil yield in relation to the mass loss for the nitrogen inerted microwave pyrolysis process.

For all inerting media tested, the total pyrolysis oil yields followed the mass loss trends, increasing with increasing specific energies up to a plateau value of 30 – 35 %. The oil yields, however, did not increase linearly with mass loss, with the percentage of mass loss going towards oil production reducing with increasing specific energy. Pyrolysis produces three main products, pyrolysis oil, pyrolysis gas and solid residue/char. The

solid and pyrolysis oil masses were measured post pyrolysis therefore it can be assumed that any masses unaccounted for are represented by the gaseous product, after accounting for the potential oil lost during collection. It is consequently evident that with increasing specific energy, the pyrolysis process shifts from favouring oil production, to beginning to favour gas production, likely due to increasing temperatures within the biomass and longer residence times of the process.

The gas inerted microwave pyrolysis process had a lower oil/mass loss ratio than the liquid inerted processes. The lower ratio could be due to the absence of the liquid, resulting in a hotter surrounding than the liquid inerted process. A liquid inerted environment temperature would only increase to the temperature of the boiling point of the liquid. A gas inerted atmosphere, however, would allow the surface of the sycamore to keep increasing in temperature, reducing surface temperature control. Despite having a cold gaseous surround, contact condensation of the pyrolysis volatiles in the liquids provide a higher cooling ability and as such, more volatiles were lost as vapour in the gas inerted process.

For the cyclohexane inerted process, the aqueous phase fraction for all specific energies tested remained higher than the organic phase. The aqueous phase occupied approximately 80 % of the total oil yield for all conditions investigated.

3.4.4 Pyrolysis oil composition

Following pyrolysis, the pyrolysis oil product naturally fractionated into an aqueous and organic phase. The solvent used affected how the pyrolysis oil product fractionated; for water as a solvent, the aqueous phase was miscible with the water, and a separate organic fraction formed. For hydrocarbons the organic phase was miscible with the solvent and the aqueous phase fractionated out. For the gas inerted process, the oil

produced was single-phase, and for the propanol inerted process, the liquid product was single-phase.

Preliminary GC-MS analysis on the *n*-hexane inerted liquid fractions obtained post-pyrolysis was carried out by a collaborator from the University of the Basque Country, with the aim of identifying and quantifying prominent compounds in the aqueous and organic fractions. GC-MS analysis on the nitrogen, 2-propanol and water inerted processes were carried out by a collaborator at the University of Nottingham. The water content of the aqueous phase was determined to be 40-50 % by mass, whereas the organic phase contained <5 % water. Table 3-11 and Figure 3-32 present prominent compounds in each fraction, along with groups of compounds identified (the tabulated version of the prominent groups can be seen in Appendix B.2).

Table 3-11 – Prominent major compounds of the pyrolysis oil products for varying inerting media, with analysis carried out by each collaborator denoted.

Compound	**Peak area (%)**					
	n-Hexane (aqueous)	**n-Hexane (organic)**	**Nitrogen (1.08 kJ/g)**	**Nitrogen (1.89 kJ/g)**	**2-Propanol**	**Water**
Levoglucosan	13.2	-	-	-	5.3	-
Furfural	0.8	7.1	2.0	0.8	3.3	6.4
4-Vinyl-guaiacol	-	6.2	0.9	4.3	4.3	5.7
Guaiacol	0.5	4.5	6.4	5.3	1.6	7.3
Syringol	2.0	6.9	9.1	7.1	6.6	14.1
Eugenol	-	2.0	-	-	0.8	1.4
Cresol	-	-	0.7	0.5	1.0	-
Isoeugenol	0.4	7.7	-	-	-	-
Sinapaldehyde	-	-	2.0	-	-	3.1
Syringaldehyde	1.7	-	2.5	2.7	1.4	3.0
	Spain		University of Nottingham			

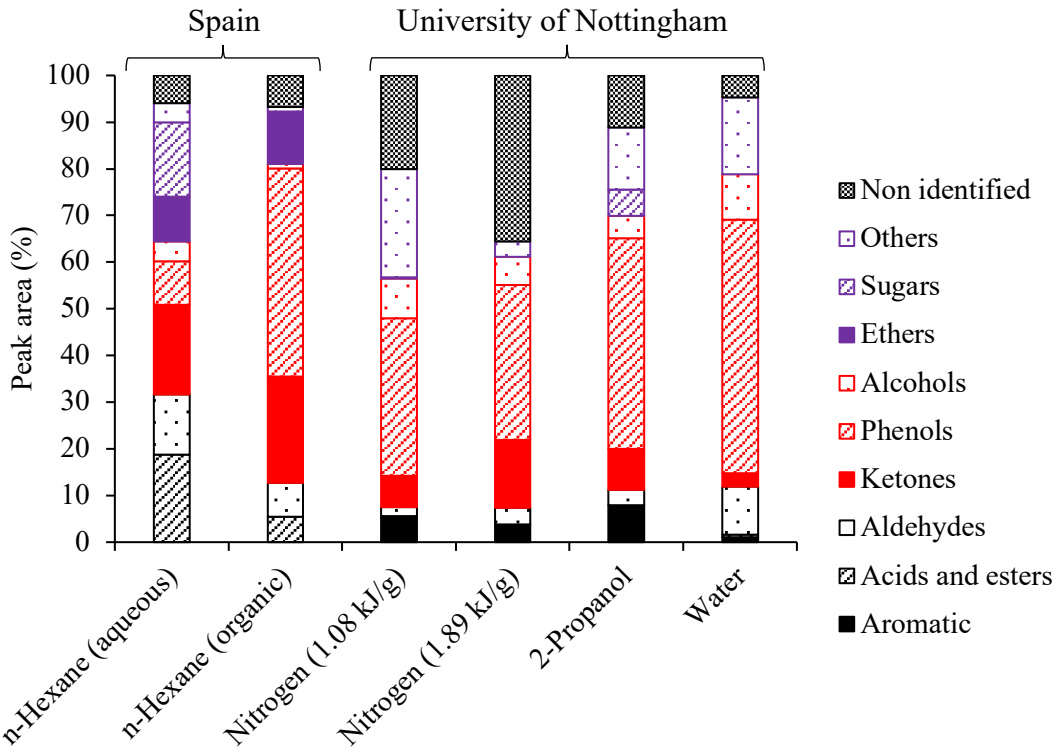


Figure 3-32 - Group abundance in the inerting media used, based on peak area, with analysis carried out by each collaborator denoted.

Figure 3-32 evidently shows that the fractions of liquids contained different compounds. For the n-hexane inerted process, the aqueous phase consisted of sugars, such as levoglucosan, a product of cellulose pyrolysis (Patwardhan et al., 2009). Interestingly, levoglucosan was not detected within the nitrogen inerted oil, however due to the large percentage of non-identified compounds, it is possible that it was still present. Acids and esters, along with aldehydes were present in both phases, with a greater percentage in the aqueous phase. The organic phase was phenol-rich with a very low alcohol content and the absence of sugars. The organic phase favoured compounds such as furfural, guaiacol and isoeugenol. The large amount of sugars present in the aqueous-phase oil for the *n*-hexane inerted process suggests that the pyrolysis oil did not undergo significant degradation during the pyrolysis process, as levoglucosan is known to decompose during pyrolysis (Hu and Gholizadeh, 2019, Zhang et al., 2012, Kim and Choi, 2018).

For the nitrogen inerted processes, levoglucosan was not detected and for the 2-propanol oil, the levoglucosan concentration was lower than the n-hexane inerted process. The lower concentration in 2-propanol could be due to the single-phase liquid containing all oil compounds present, whereas with phase fractionation, only a certain percentage of the oil would be present as the phase total. The lower levoglucosan percentage could also be due to how the sycamore block was heated during pyrolysis. 2-Propanol readily boiled during the microwave pyrolysis process, leaving an alternating gas/liquid atmosphere around the sycamore block and therefore allowing for high mass losses to be attained. These high mass losses could have resulted in much higher temperatures within the sycamore block being reached and possibly resulting in levoglucosan degradation. For the water inerted process there was no levoglucosan present, possibly due to the temperatures reached not being sufficient enough to reach significant cellulose degradation temperatures. It was evident that there were significant compositional differences in the oil phases and oils from different inerting media. There was a large potential error however, with the single-mode system due to the small volumes of oil produced. Therefore, a system with the potential to produce larger volumes of oil would be extremely beneficial.

The categorisation of pyrolysis oil compounds is challenging due to the large number of compounds typically present and multiple functional groups existent in certain compounds (Kostas et al., 2019b). Syringaldehyde, for example, could be classified as aromatic, aldehyde or phenol due to its multiple functional groups. For certain pyrolysis oil samples such as the nitrogen inerted oil samples, there was a high percentage (20 – 35 %) of unidentified compounds, this could be due to the high number of compounds and isomers present, coupled with the NIST Library software not readily identifying every compound present. It is also possible that the different methods carried out by the

Using multiple collaborators to analyse the pyrolysis oil could have led to challenges when comparing the pyrolysis oil composition. Interpretation of the analysis could potentially differ between operators, and introduce discrepancies in the compositional results. Therefore, future work would involve carrying out analysis on the same GC system, and the same column, as well as the same method, to reduce these discrepancies. Sample transport and transport time could also have affected the compositional data due to degradation or evaporation of volatile and semi-volatile compounds (Diebold, 1999). Direct analysis after processing, with minimal transport, would, therefore, be beneficial to determine an accurate compositional analysis of the pyrolysis oil.

3.4.5 Processing implications – solvent recycling

When considering scale-up opportunities for the liquid inerted microwave pyrolysis system, processing factors that are not of major importance in laboratory-scale research become more apparent. In a scaled-up continuous process using large amounts of solvent, solvent costs, solvent-pyrolysis-liquid separation requirements in terms of energy, cost and health and safety become much more of a priority. As it is not feasible to introduce fresh solvent continuously, a single step that would allow for adequate cost/material-feasibility of the pyrolysis process would be to recycle the liquid solvent back into the system. Separation must occur to isolate the aqueous and organic phases of the pyrolysis oil product from the liquid solvent, and so direct recycling of the solvent is not likely to be a plausible option. A ‘worst case’ scenario would be when the organic phase is present at a high concentration in the liquid solvent and possibly further increases as more organic phase is added in subsequent pyrolysis steps. These factors would require further investigation, particularly into specific behaviours where the

liquid solvent may become more saturated with the organic phase fraction as the run numbers increase.

Figure 3-33 shows mass losses for five repeats in the same cyclohexane solvent, at the same processing conditions.

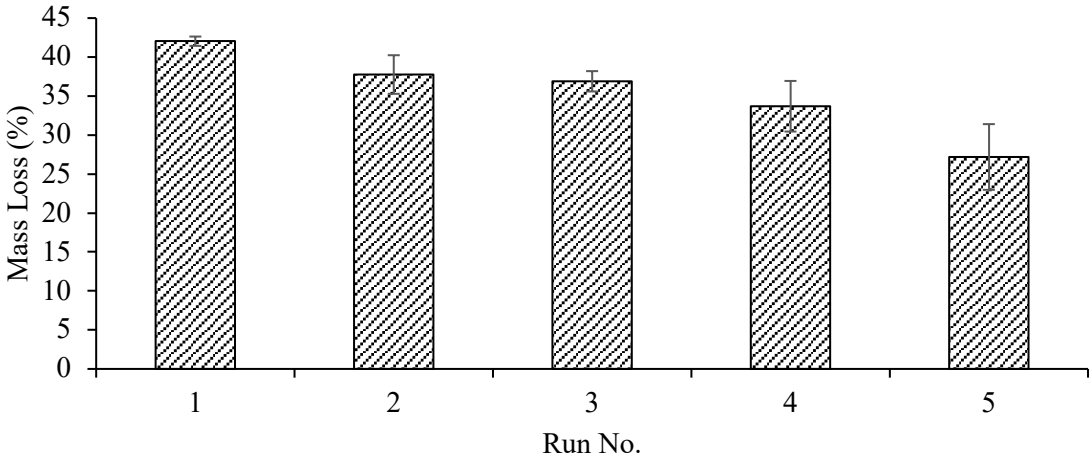


Figure 3-33 – Bulk mass loss for sycamore with cyclohexane as an inerting medium, five successive runs at 1.5 ±0.06 kJ/g, 1.5 kW applied power (three repeats) with dynamic impedance matching to maximise the absorbed power.

Figure 3-33 shows that there is a tangible performance decrease in terms of mass loss over successive runs with a recycling of liquid. The first recycle run provides mass losses of 42 %, which is congruent with mass loss data for the same specific energy in Section 3.4.2. The final recycle run provides a mass loss of around 27 %, equivalent to mass loss performance of around 0.75 kJ/g in a clean liquid solvent, resulting in an energy to mass loss efficiency penalty of around 50 %. This data shows that in order to carry out liquid inerted microwave pyrolysis with a high energy efficiency, the liquid that is used must be largely uncontaminated with pyrolysis oil. To increase the purity of the liquid solvent being used, a larger volume of liquid could be used in relation to the sycamore block, or in terms of a flow process, high liquid throughput could be achieved to continually provide fresh solvent to surround the biomass sample.

Alongside mass loss performance, data was also collected to determine how much liquid was lost during processing. The sycamore block became saturated with the liquid solvent after processing and therefore quantification of the 'lost' solvent was carried out. Figure 3-34 shows the percentage mass of cyclohexane left as a percentage of the starting mass after each successive run.

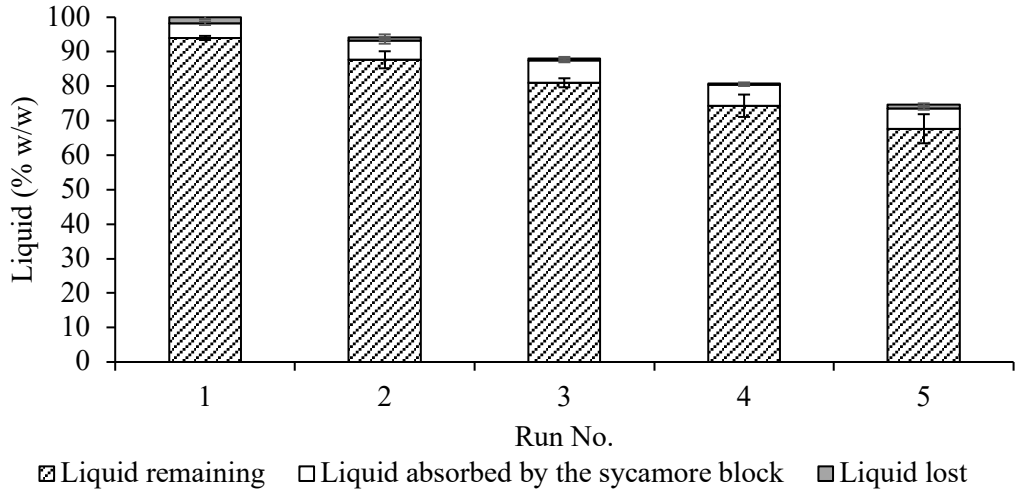


Figure 3-34 – Liquid solvent mass as a percentage of the starting liquid mass when pyrolysing sycamore with cyclohexane as an inerting medium, five successive runs at 1.5 ±0.06 kJ/g, starting volume 100 mL (77.9g), 1.5 kW applied power.

Figure 3-34 illustrates that for each successive recycling run, the total liquid lost remained consistent at around 6 mL (4.67 g), regardless of which successive recycle run was undertaken. The majority of the lost liquid was absorbed into the biomass, with only a small percentage (~1 %) being lost as vapour during the process. It would therefore be necessary when considering a flow process, for a make-up liquid solvent stream to be introduced to the process. This would prevent the process from losing the required solvent over time, approximately 0.8g of solvent per g of feedstock.

Table 3-12 shows how much liquid is lost and where the liquid is lost for every recycle run.

Table 3-12 - Average values for the liquid solvent lost post-pyrolysis averaged out over every successive run.

Per run:	Total liquid lost	Liquid absorbed by sample	Liquid lost as vapour	Wet/dry post pyrolysis sample mass
Mass (g)	5.04 ± 0.39	4.38 ± 0.66	0.76 ± 0.55	-
%	6.47 ± 0.50	5.62 ± 0.84	0.97 ± 0.70	208.91 ± 12.86

For all recycle runs, the amount of liquid absorbed by the biomass remained consistent regardless of the amount of mass lost through pyrolysis. Table 3-12 shows that post pyrolysis, the mass of the block with the absorbed liquid is over twice the dry sample mass. This absorbance of the liquid could be a combination of external pressure of the liquid on the biomass due a liquid head of ~10 cm above the block, and the liquid readily flowing through the biomass/char structure due to pyrolysis. Theoretically, if there was consistent production of volatiles during pyrolysis, then the biomass would be free of solvent due to the pressure gradient that would be produced until the microwave processing has stopped. Therefore, it is likely that the liquid was absorbed into the biomass post-processing. The quick absorbance could be due to quick cooling of the biomass, reducing the internal pressure of the biomass, and also due to the new charred structure within the biomass, where liquid would flow more freely within. Resultant of the liquid absorbance in a high throughput process, a drying/stripping process would need to be developed in order to separate the absorbed liquid from the char. The process would need to utilise a makeup stream of 0.8 g of solvent per g of feedstock to prevent solvent losses. Alternatively, the solid could also immediately be removed from the process to minimise solvent uptake, lowering the makeup stream requirement.

3.4.6 Estimating internal sycamore temperature

It was established in Section 1.3.1 that lignin, cellulose and hemicellulose thermochemically decompose at a differing range of temperatures. Estimating the temperature within the sycamore block would allow for insights into the potential lignin, cellulose and hemicellulose decomposition within the sycamore block during pyrolysis, and potential oil compounds present in the oil produced. Using the temperature prediction method introduced in Section 2.6.1, the internal temperature of the biomass could be determined using the amount of absorbed power absorbed over time, assuming that the sample is being heated homogenously by the microwaves. The predicted internal and surface temperature at the centre of the sycamore blocks, and the cross sectional temperature profile of the sycamore block is presented in Figure 3-35, below.

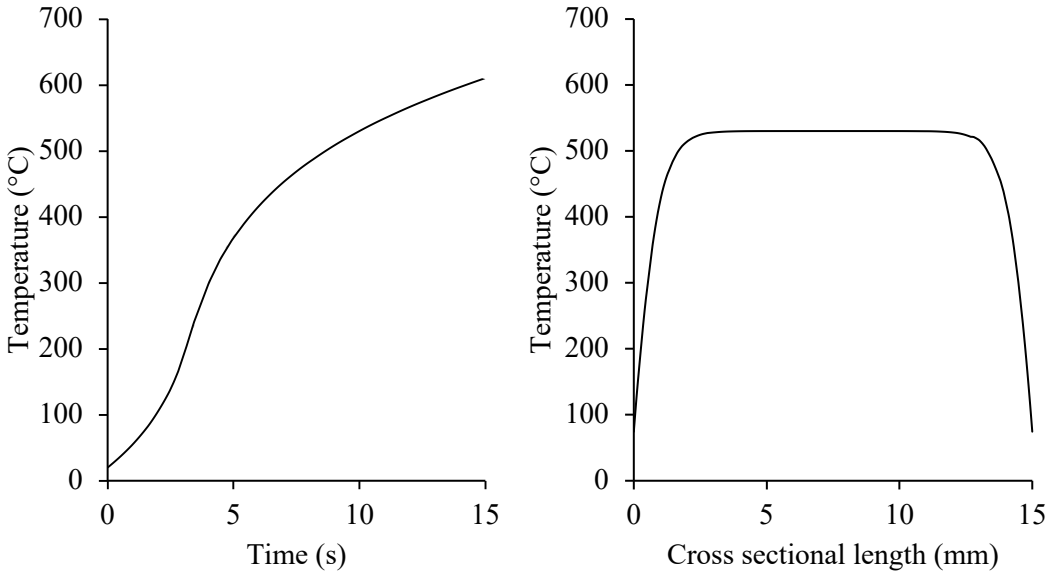


Figure 3-35 - Predicted internal temperature in the centre of the block over time, and a cross sectional temperature profile at 10 seconds based on 0.6 kW absorbed power with *n*-hexane as an inerting liquid.

Figure 3-35 shows that pyrolysis temperatures of 300 °C over 66 % of the sectional area can be obtained within 4.5 seconds of processing, with a predicted energy

requirement of just 0.5 kJ/g. This energy requirement correlates with the empirical observations for the hydrocarbon inerted liquids, where mass losses greater than the moisture content (6.4 %) started to be achieved.

3.4.6.1 Cross sections of the sycamore blocks post-pyrolysis

Figure 3-36 shows cross sections of pyrolysed blocks at 1.5±0.1 kW applied power 3 – 10 seconds (representative of 0.5 – 2.5 kJ/g).

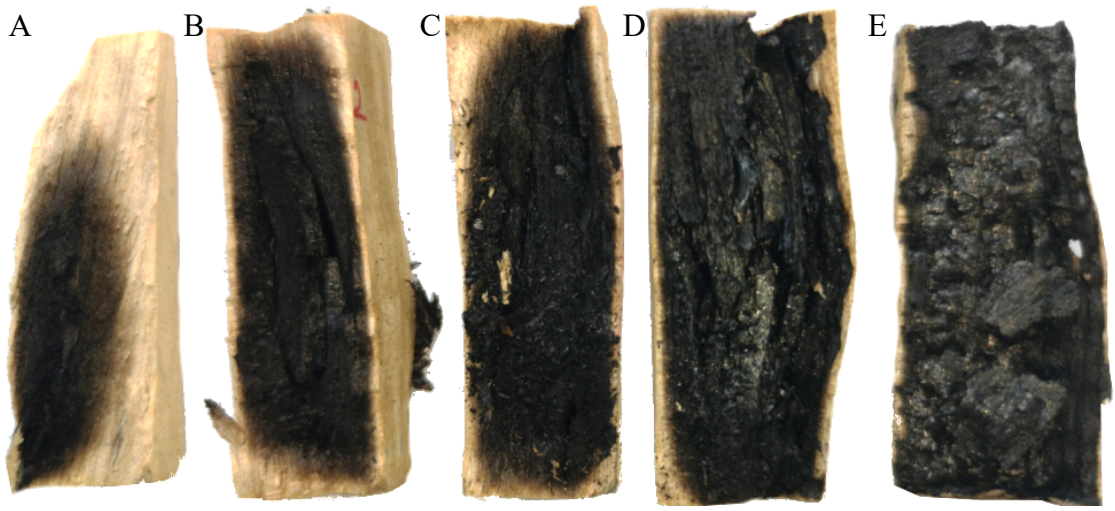


Figure 3-36 - Cross sections of the pyrolysed sycamore at approximately A) 0.5 kJ/g, B) 1.0 kJ/g, C) 1.5 kJ/g, D) 2.0 kJ/g, E) 2.5 kJ/g, 1.5 kW applied power within cyclohexane and dynamic impedance matching.

It can be seen in Figure 3-36 that the sycamore heated internally with the surface of the block remaining non-pyrolysed, indicative of sufficient heat transfer and cooling on the surface of the sycamore. As the specific energy (and therefore mass loss) increased, the inside of the sycamore block became more charred. In blocks A, B and C, the char appears to follow the grain of the wood, remaining uniform. For blocks D and E, the char appears to be much less ordered and more brittle, indicative of more of the internal structure of the sycamore being thermochemically broken down. For blocks B-E, it is a possibility that internal pressures sufficient to distort the overall shape of the sycamore

blocks had been achieved, as block B had char forced out of the surface of the block, and blocks C-E have an expanded mid-section

In order to determine the internal temperatures obtained within the sycamore block, the block was cut open and selected for TGA and compositional analysis post-pyrolysis. An example of the cross-section of a sycamore block following pyrolysis within n-hexane at 1.5kW applied power and 12 seconds is shown in Figure 3-37, and the same conditions carried out computationally are shown in Figure 3-38.



Figure 3-37 - Cross-sectional images of sycamore blocks after pyrolysis (1.5 kW applied, approximately 0.6 kW absorbed, 12 seconds) within n-hexane (45 x 15 x 15 mm).

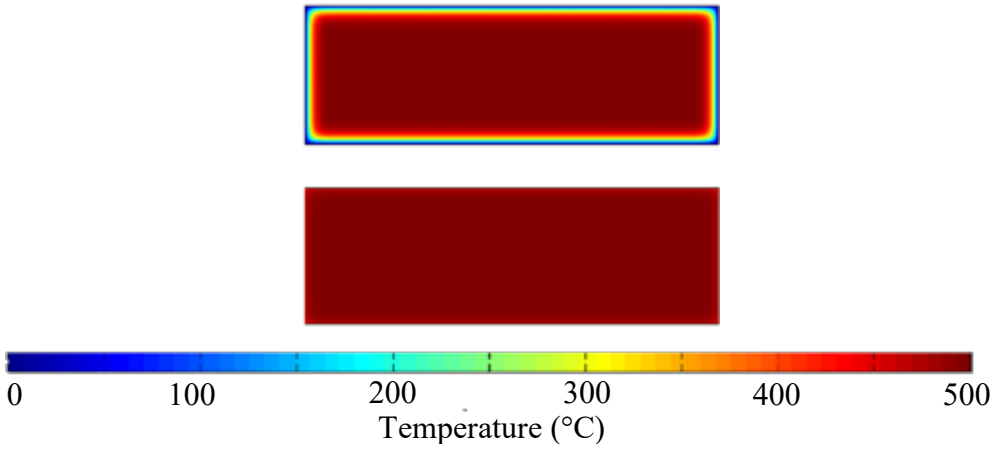


Figure 3-38 – Computed temperature cross section of the sycamore block 1.5 kW applied power (0.6 kW absorbed power), 12 seconds, within n-hexane (top), and nitrogen (bottom).

Figure 3-37 illustrates that the centre of the sycamore block was charred, whilst the outer edges parallel to the grain remained non-pyrolysed. The cross-section appeared

to be similar to the simulated temperature distribution for *n*-hexane in Figure 3-38, with the same outer layer of non-pyrolysed material visible in both simulation and experiment. The outer layer of non-pyrolysed wood was not visible in the nitrogen simulation in Figure 3-38, showcasing inefficient temperature control on the surface of the sycamore block when using a gas-inerted atmosphere, and coinciding with the surface-level pyrolysis of the nitrogen inerted process showcased in Section 3.4.1.7.

Evidently, there appeared to be an effect of the grain direction which is likely to influence the heat transfer coefficient as grain direction will influence both heat transfer through the block and mass transfer of the volatiles leaving the block. It is clear from Figure 3-38 that temperatures high enough to pyrolyse biomass could be achieved within the core of the block, if the block was heated volumetrically, despite the surrounding liquid medium environment not exceeding temperatures above 68 °C for n-hexane as a liquid. It is also visually evident from Figure 3-37 that there were varying degrees of pyrolysed sycamore within the block, with section (i) appearing to have undergone the lowest degree of pyrolysis compared to sections (ii) and (iii).

3.4.6.2 Thermogravimetric analysis

It was not possible to directly measure temperatures that had been reached within the biomass block during heating. In order to gain an inference to temperature and an understanding of the degree of pyrolysis within the block of sycamore, thermogravimetric analysis was performed on the three internal sections of the post-pyrolysis sycamore block as shown in Figure 3-37.

Due to the visual differences in the pyrolysed block in Figure 3-37, analysis was carried out to compare the TGA curves for the sections in the post-pyrolysis sycamore, as shown in Figure 3-39.

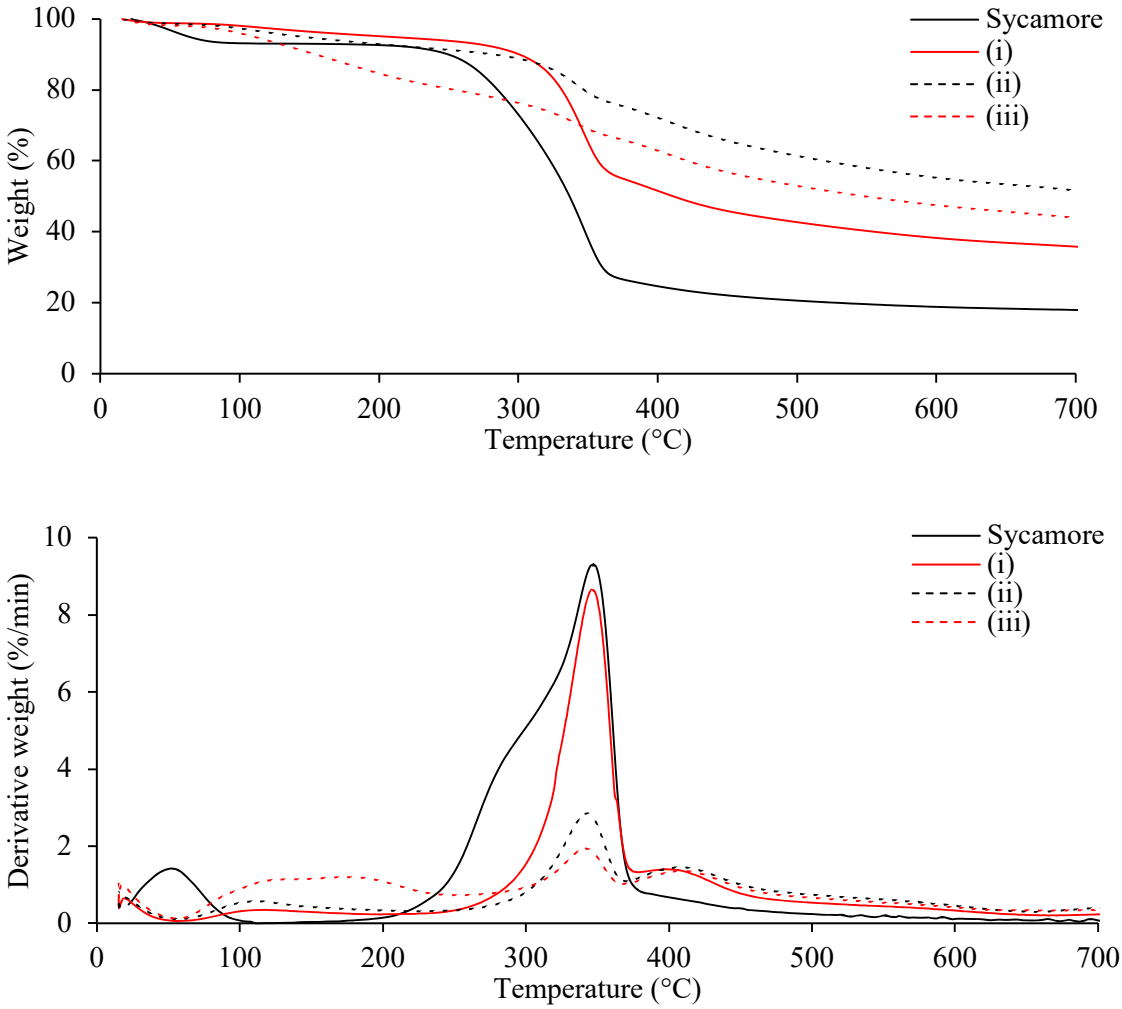


Figure 3-39 - Weight and derivative weight changes for three subsections of the pyrolysed sycamore, and non-pyrolysed sycamore with a heating rate of 10 °C/min.

As shown in Figure 3-39, the difference in the peak at 340 °C between sections (i), (ii) and (iii) confirms that differing degrees of pyrolysis had taken place within the block of sycamore, likely due to different reductions in cellulose composition within the pyrolysed sample. For all sections analysed, the initial shoulder at 200 - 270 °C present in the sycamore sample was not present, likely due to complete degradation of hemicellulose and the initial stage of cellulose degradation.

As the samples were from the same sycamore feedstock, the fixed carbon composition of the pyrolysed chars would all represent the equivalent composition of the non-pyrolysed sycamore. Using the fixed carbon (FC) ratios, the mass remaining in the char

(in relation to the sycamore) could be determined using Equation 3-4, and the temperature can be determined from this mass remaining, using the sycamore TGA curve.

$$\text{Mass remaining (\%)} = \frac{100}{\left(\frac{FC_{Char}}{FC_{Sycamore}}\right)} \qquad 3\text{-}4$$

The mass losses and temperatures reached within the charred section using Equation 3-4 were 50, 59 and 65 %, and 336, 347 and 353 °C for sections (i), (ii) and (iii) respectively. The temperatures reached coincide with the start and end of the derivative weight peak around 340 °C, explaining why the 340 °C peak is prominent for section (i), but not for (ii) and (iii) (Figure 3-39).

Along with analysing the heating profile within the sycamore block, investigations into how the processing conditions affected the solid volatilised were determined. Table 3-13, Figure 3-40 and Figure 3-41 present the composition and temperature reached for the non-pyrolysed sycamore, and samples taken from the centre of the sycamore block post pyrolysis, representative of position (ii) in the sycamore block (Figure 3-37).

Table 3-13 – The composition (dry basis) of the centre of the sycamore and centre of the pyrolysed samples for approximately 0.6 – 1.5 kW applied power to the system.

Specific energy (kJ/g)	Bulk mass loss (%)	Volatiles (%)	Fixed carbon (%)	Ash (%)	Temperature reached (°C)
0.00	0.0	82.0	16.9	1.2	20
0.59	13.4	51.5	46.2	2.4	346
0.88	34.9	45.3	52.5	2.2	350
1.06	18.8	50.2	47.7	2.1	348
1.47	43.7	36.8	60.0	3.3	366
1.50	27.7	35.5	62.2	2.3	372
2.02	34.5	32.7	64.6	2.7	382
2.02	50.8	24.7	70.8	4.5	413
2.52	44.3	20.9	75.2	3.8	438
2.54	58.9	17.7	78.2	4.1	456

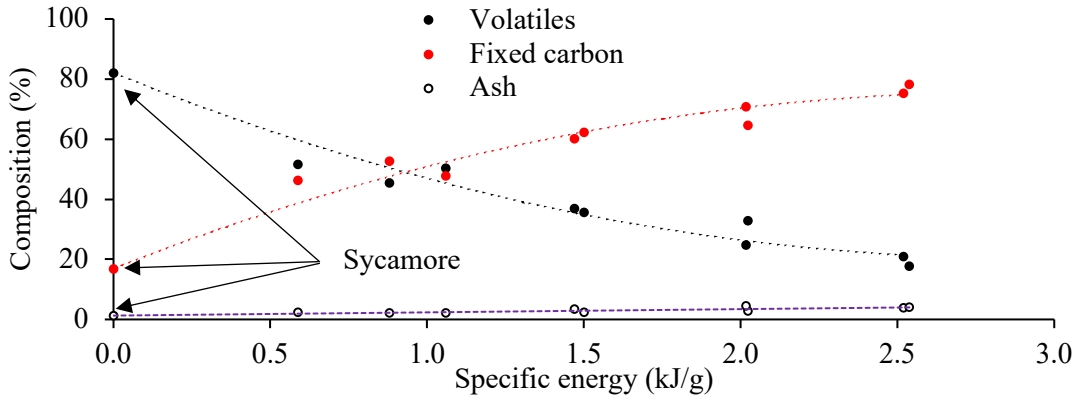


Figure 3-40 – Composition (dry basis) of the non-pyrolysed sycamore and centre of the pyrolysed samples.

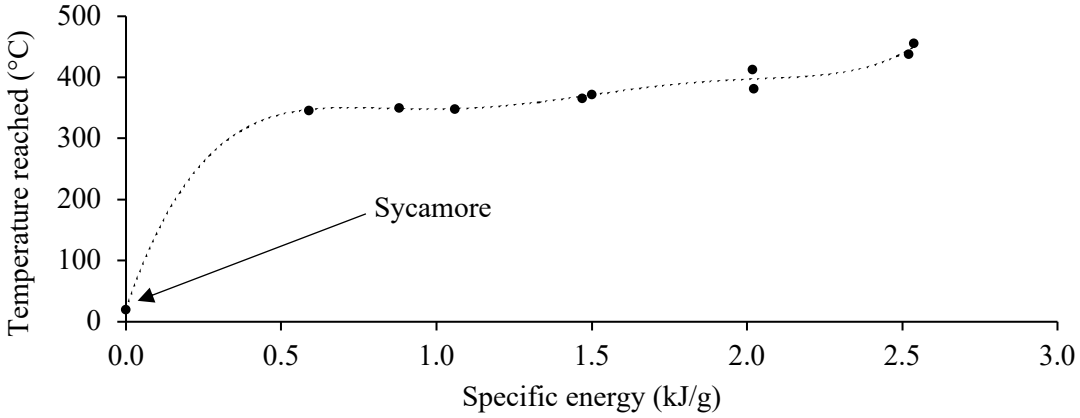


Figure 3-41 – Predicted temperatures reached within the centre of the pyrolysed samples, with non-pyrolysed sycamore for reference.

As the specific energy increased, the volatiles present decreased, and the fixed carbon and ash content increased. It is shown in Table 3-13, Figure 3-40 and Figure 3-41 that irrespective of mass loss, the specific energy absorbed by the sycamore block was the determining factor for temperature reached within the sycamore block. For example, for approximately 1.5 kJ/g, the mass losses ranged from 28 % - 44 %, however the composition of the char remained consistent, with temperatures reached being similar.

Overall, it was evident from the TGA data that temperatures of 250 - 380 °C had been exceeded, which is the temperature range of pyrolysis for the majority of the sycamore mass. It was also determined, however, that the internal temperature of the sycamore (predicted by TGA) plateaued around 350 - 430 °C throughout the specific energy range investigated. Interestingly, similar specific energies had different mass losses, due to varying absorbed powers and processing times, however the internal temperature predicted by TGA was not affected. It could therefore be determined that there would be processing differences between varying powers, and so an investigation was carried out to observe the pyrolysis process as it was occurring.

3.4.7 Observations of gas bubble behaviour

To observe the process of pyrolysis within a liquid medium, the reactor configuration was modified to allow for a camera to be placed at the side of the reactor. Figure 3-42 shows a side-view of the processing conditions investigated, at two powers (approximately 0.6 kW and 1.5 kW), absorbed as in Section 3.4.2, for cyclohexane, kerosene and nitrogen as inerting media.

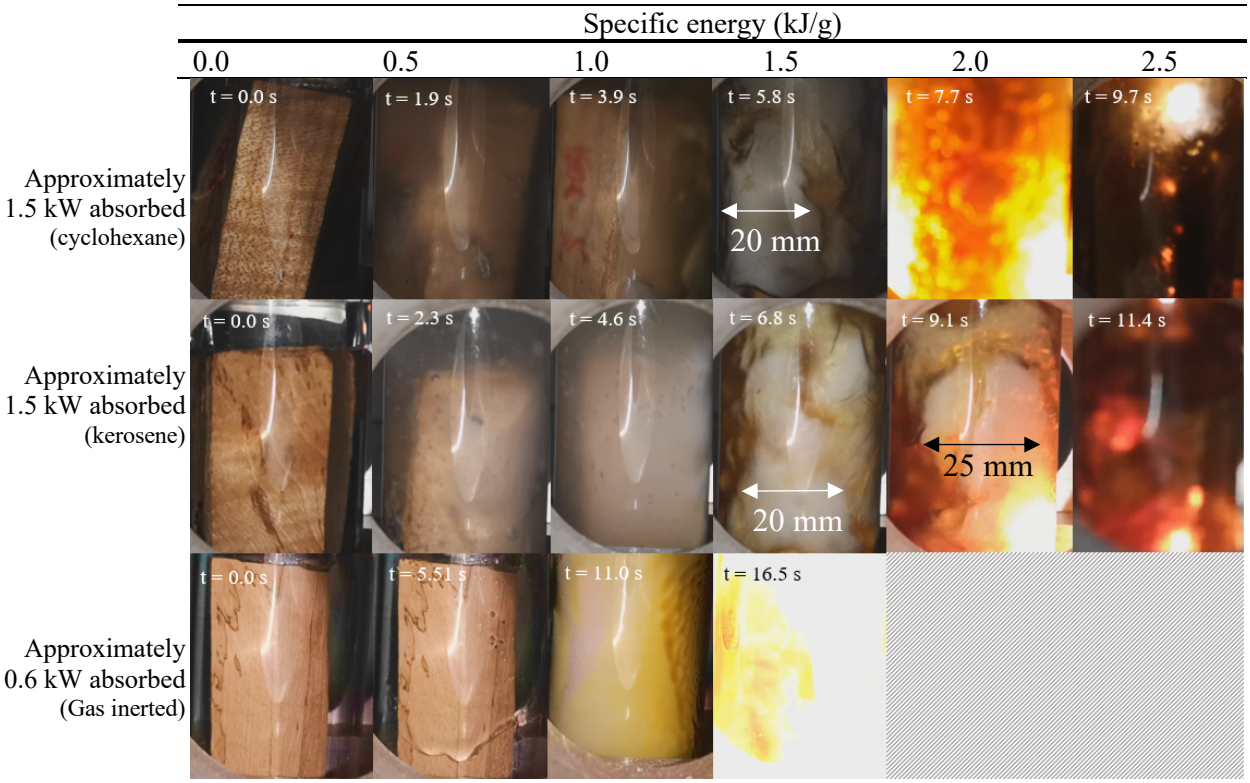


Figure 3-42 - Behaviour of the nitrogen and liquid inerted (cyclohexane and kerosene) single-mode microwave pyrolysis system at approximately 0.6 kW and 1.5 kW absorbed, over specific energies of 0.0 – 2.5 kJ/g.[1]

For each process investigated, the process followed the same steps: 1) Drying of the biomass, evidenced by the cloudy liquid formation for the liquid-inerted processes and water present on the wall of the quartz tube for the gas-inerted process at 0.5 kJ/g. 2) Pyrolysis, shown at 1.5 kJ/g for the liquid-inerted processes, and 1.0 kJ/g for the gas inerted process. 3) If the process is left running for a sufficient amount of time, plasma formation occurs, as shown by the glow of ionised gas in Figure 3-42. A prominent gaseous surround would reduce both the cooling efficiency of the liquid-inerted microwave pyrolysis process, and the electric field stability surrounding the sycamore block. This reduced electric field stability results in arcing and plasma formation due to dielectric breakdown around the biomass in the gas pockets. Dielectric breakdown

[1] The differences in time for the cyclohexane and kerosene equivalent specific energies are due to differences in the sycamore starting mass.

occurs when the charge build-up exceeds the electrical limit or dielectric strength of a material, which results in the gas becoming partially ionized and changing from being an electrical insulator to an electrical conductor (Haynes, 2014). Therefore, despite the liquid surround delaying the arcing process, it was not sufficient to prevent it entirely. The plasma formation and large amounts of pyrolysis-gas leaving the biomass all result in higher temperatures of the surface of the sycamore, reducing temperature control of the pyrolysis process.

In the nitrogen-inerted system, volatiles production began earlier than the liquid-inerted processes. This was likely due to the sycamore reaching pyrolysis temperatures more quickly than when a liquid was used. An obvious change was the presence of large pyrolysis-condensate volume, during the gas-inerted process the pyrolysis-vapours fill the quartz tube within 0.6 seconds, as shown in Figure 3-43.

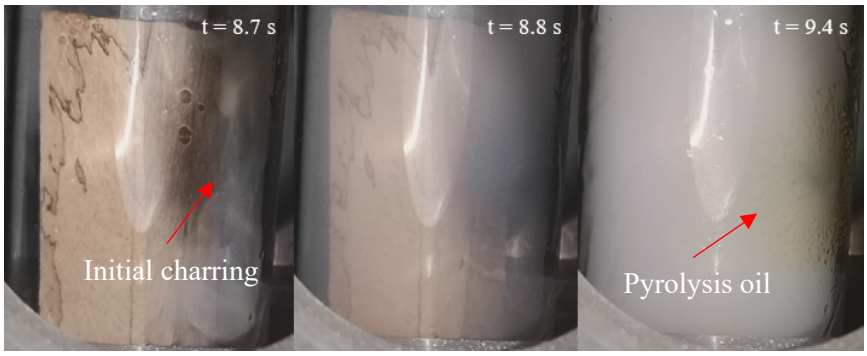


Figure 3-43 – Condensate formation in the gas-inerted microwave pyrolysis system, approximately 0.6 kW absorbed, representative of 0.79 – 0.85 kJ/g specific energy.

As is highlighted in Figure 3-43, the sycamore began to darken and started to char, with condensate filling the tube within 0.6 seconds from the onset of volatiles production. Pressure sufficient to move the pyrolysis oil out of the biomass was present, as evidenced by the pyrolysis liquid hitting the glass and spreading along the wall (Figure 3-43, 9.4 seconds). It is evident that the reduction in vapour volume in the liquid-inerted process is a combination of contact condensation; the pyrolysis volatiles are leaving the

biomass at pyrolysis temperatures of approximately 300 - 500 °C and immediately come into contact with liquid at its boiling point; in the case of cyclohexane, 81 °C and kerosene, 200-250 °C.

The computational simulations introduced in Section 2.6.1 use the assumption that subcooled nucleate boiling occurs on the surface of the biomass, and that there would only be a significant gas-phase once the critical heat flux of the biomass is overcome, which is not evident from the empirical observations. With the liquid-inerted pyrolysis concept, vapour will be produced from the surface of the biomass. This vapour can be produced in two ways: volatiles produced during pyrolysis of the biomass and boiling of the solvent. Different boiling regimes exist and would affect the vapour production during the pyrolysis process. When a liquid boils, it goes through stages as shown in Figure 3-44.

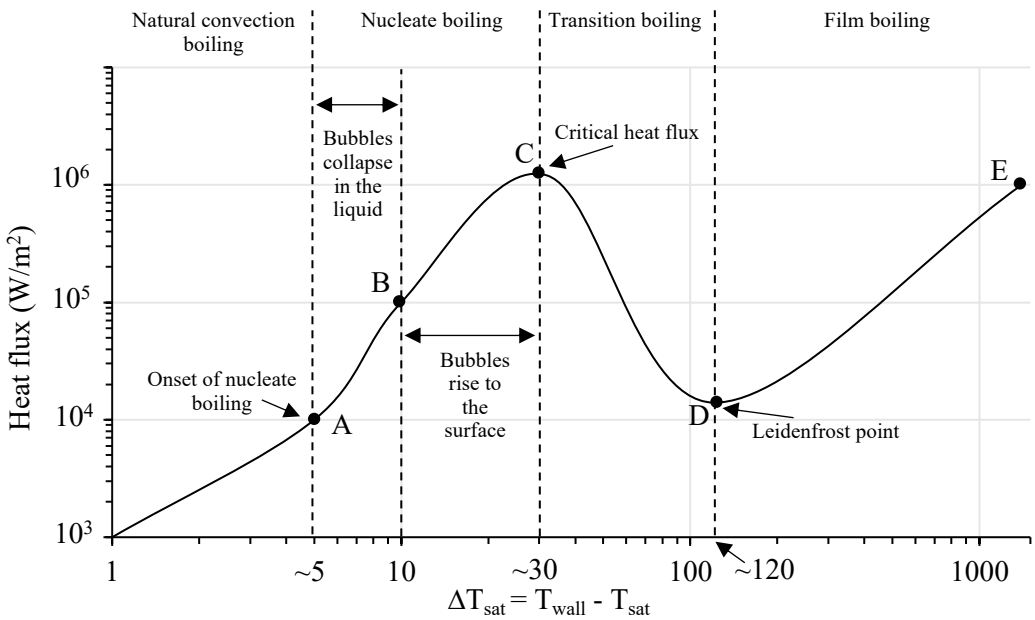


Figure 3-44 – Pool boiling curve for water, adapted from Serth (2007).

There are four main regimes for a liquid undergoing heating and boiling:

1) Natural convection boiling – No bubbles form until the heating surface (the sycamore block surface in the case of the pyrolysis process) are approximately 5°C greater than the liquid saturation (boiling) temperature (point A).
2) Nucleate boiling – Bubbles form at sites on the surface of the heating medium, with the rate of bubble formation and nucleation sites increasing as the temperature increases. Between regions approximately 5 - 10°C above the saturation temperature (points A – B), the bubbles are dissipated in the liquid shortly after leaving the surface of the nucleation site due to the lower bulk temperature of the liquid. The space vacated by the bubbles is replaced by the liquid surround, and as the rate of boiling increases, the agitation and mixing caused by this process leads to a greater heat flux and heat transfer coefficient. Between approximately 10 - 30°C above the saturation temperature (points B – C), the bubble formation rate causes continuous columns of vapour within the system which can coalesce to form slugs of vapour, the bubbles move all the way to the surface of the liquid, where the vapour content is released. The large heat flux is caused by the combined effects of liquid entrainment and vaporisation.
3) Transition boiling – Unstable vapour films begin forming over the heating medium, releasing large patches of vapour at regular intervals above the critical heat flux temperature (point C). The vapour film acts as insulation around the heating medium due to the low thermal conductivity relative to the liquid, reducing the heat flux from the surface to the liquid. At the Leidenfrost point (point D), nucleate boiling is completely replaced by film boiling.
4) Film boiling – The heating medium surface is completely covered by a stable vapour film. The increase in heat flux after the Leidenfrost point is due to the

increasing temperature differential between the heating medium and the bulk vapour/liquid. This increases heat transfer through the vapour film as radiation.

The volatiles produced during the pyrolysis process caused a gas phase larger than that expected from boiling of the solvent alone. This volatiles production would cause the behaviour of the boiling regime at the surface of the sycamore block to behave as if the critical heat flux had been overcome (film boiling on the surface), and therefore heat transfer would be reduced, explaining the presence of char at the surface of the biomass where the volatiles had left the block.

To reduce to rate of volatiles leaving the sycamore block, and therefore also reduce to heat transfer rate from the sycamore block to the solvent, a lower absorbed (approximately 0.6 kW applied power with dynamic impedance matching) was investigated, as shown in Figure 3-45.

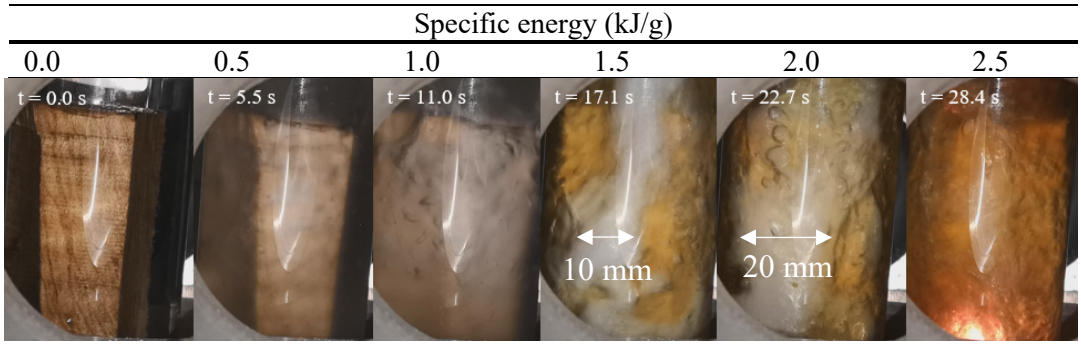


Figure 3-45 – Behaviour of the cyclohexane inerted microwave pyrolysis process at approximately 0.6 kW absorbed power.

The power provided to the sample had a significant effect on the behaviour of the process in terms of gas production and pyrolysis performance. For the lower power cyclohexane runs, the volume of gas produced for equivalent specific energies was lower, as at 1.5 kJ/g, there was more liquid surrounding the 0.6 kW sample than the 1.5 kW sample. The lower volume of gas produced was likely due to the lower power; a lower power provided to the sample would result in the lignocellulosic constituents of

the biomass breaking down at a slower rate, producing volatiles at a lower rate, and with the lower heating rate, the cooling requirement of the surrounding liquid was lower resulting in a lower boiling rate of the liquid. Figure 3-44 and Figure 3-45 shows that for the higher power investigated, 1.5 kW, due to the greater power density provided to the sample, plasma formation occurred during the process much earlier (2.0 kJ/g), and to a greater extent than the lower power of 0.6 kW in the liquid inerted process.

Despite the liquid-inerted process providing temperature control on the surface of the sycamore blocks, the process as a whole was not always liquid inerted due to vapour formation. This changing regime may result in the microwave pyrolysis process behaving similarly to a nitrogen inerted process. To avoid significant vapour pockets around the biomass a number of changes to the process are required. This includes a larger diameter reactor to promote dispersion, smaller bubbles (low viscosity, high boiling point and latent heat), or a less intense electric field (reducing the power input).

3.5 Conclusions

The overarching aim of the research described within this chapter was to determine the feasibility of carrying out microwave pyrolysis within a liquid medium and to assess the solid and liquid products.

It was found that that the process allowed for pyrolysis to occur in all liquid inerting environments investigated. The process was repeatable, based on power absorbed, for all solvents investigated. There was an evident advantage in terms of bulk mass loss of the solid when using hydrocarbon liquids as the inerting media as opposed to microwave absorbent liquids such as water. Hydrocarbon liquids allowed for around 60 % solid mass loss achievable at approximately 2.5 kJ/g, whereas for all the microwave absorbent liquids used there was an evident energy penalty, and a mass loss penalty for

all microwave absorbent solvents except 2-propanol, which obtained mass losses of up to 65 %. Regardless of the energy penalty however, it was shown that a range of solvents could be used, and the process was not confined to solely low loss (microwave transparent) solvents. The pyrolysis oil product produced fractionated into solvent miscible and non-miscible phases, depending on the solvent used. This allows for many possibilities for processing, depending on what pyrolysis oil product is needed based on the fractionation that occurs, and what thermochemical interactions may possibly be required.

At the range of specific energies investigated, the equivalent gas inerted process produced higher mass losses than the liquid inerted system, as is to be expected due to the efficient surface-liquid heat transfer in the liquid environment in the liquid-inerted system. The liquid inerted system allowed for a controlled heating profile within the sycamore, charring in the centre and remaining non-pyrolysed at the surface, as opposed to the gas-inerted system, where the whole block pyrolysed, and the fixed bed process in literature, where non-homogenous heating was observed (Robinson et al., 2015).

It was observed that depending on the liquid-solvent used, the pyrolysis oil product fractionated into a solvent-miscible and solvent-immiscible phase. For hydrocarbons, the organic phase was miscible, and aqueous phase precipitated out. The two phases contained different types of compounds, with the organic phase consisting of mostly phenols, and the aqueous phase containing more acids and esters. It was also identified that the liquid yields from the liquid-inerted process were lower than the gas-inerted process. This was likely due to the gas-inerted process allowing for direct collection of the pyrolysis oil, whereas the liquid-inerted process required post-process separation to obtain the two separate oil fractions, resulting in transfer and separation losses.

Significant vapour present around the sycamore block was observed during the pyrolysis process, largely due to the geometry of the reactor used, this reduced the benefit of the liquid surround. Therefore, a process that can exploit the liquid inerted behaviour, and maintain a more consistent liquid surround was required to be developed. Also a factor of the geometry of the reactor, despite pyrolysis oil yields being relatively high (>30 %), due to the small masses of the sycamore blocks processed, the overall masses of pyrolysis oil produced remained low (<2 g), and therefore development of the process to obtain larger pyrolysis oil volumes that could be directly collected was required.

When considering the solvents used in this chapter, the physical and dielectric properties all resulted in variations in terms of mass-loss performance, pyrolysis oil yield, bubble disengagement, and potential heat transfer. On a comparison of liquids, hydrocarbons were most suited to maximising mass loss and pyrolysis oil yields. The ideal pyrolysis liquid would likely have features of multiple different liquids tested, however, depending on the process requirements. If a process required a single-phase product, for example, then hydrocarbons would not be suitable, and alcohols would be more suited.

4. Controlling the boiling regime

4.1 Introduction

Chapter 3 demonstrated that microwave pyrolysis in a liquid inerted medium was feasible, with energy requirements not outside the realm of that for gas inerted pyrolysis. It was also found that pyrolysis could occur particularly well in liquids with a low loss tangent such as cyclohexane. Liquids with both high and low loss tangents enabled pyrolysis to occur, with low loss liquids such as n-hexane requiring much less energy, around 2.5 kJ/g for 60 % mass loss, than high loss liquids, such as water requiring more than 25 kJ/g for 30 % mass loss. A liquid with a low loss tangent, such as n-hexane, is largely microwave transparent and can therefore serve as a heat-sink to cool the biomass which is being selectively heated in the system. The single-mode system, however, had limitations, including the maximum size of processable biomass and the volume of liquid surrounding the biomass during processing.

The single-mode liquid inerted microwave pyrolysis system, due to the geometry of the equipment, did not allow for sufficient liquid to surround the biomass, resulting in large areas surrounding the biomass being occupied by gas. This large gas hold-up was suspected to compromise the benefits of the liquid inerted system. Along with the poor control exhibited on the process in terms of maintaining a liquid surround, the relatively small sample sizes used resulted in small product volumes, and a high risk of transfer losses when calculating yield. It was determined that moving from a single-mode cavity to a multi-mode cavity would be beneficial to increase the size of the biomass block (from 45×15×15 mm to up to 50×50×50 mm) to produce more measurable quantities of product, and to increase the liquid volume (100 mL to 1 L) to promote bubble disengagement.

4.1.1 Limitations of the single-mode microwave pyrolysis system and benefits of the multi-mode scaled-up system

4.1.1.1 Bubble regime and volume of liquid surrounding the biomass

When the biomass was undergoing pyrolysis, it was noted that bubble formation on the surface in relation to the surrounding liquid was large in terms of volume. There were significant periods of time where the vapour was surrounding the biomass, rather than a liquid. For the process to behave as intended, the liquid at the surface of the biomass needs to be kept at its boiling point, with liquid constantly replenishing that which is being lost due to boiling on the surface of the biomass. The amount of available fresh solvent was low due to the reactor-tube diameter of 30 mm. This means that the ideal liquid behaviour, using the liquid as a heat sink, with the heat transfer from the biomass to the liquid would be limited as the bubble formation would reduce the amount of liquid surrounding the biomass. Because of this design, the system at various points would behave in parts as if it was gas inerted due to the gas surrounding, rather than liquid inerted if at any point the bubbles formed are greater than 15 mm in diameter.

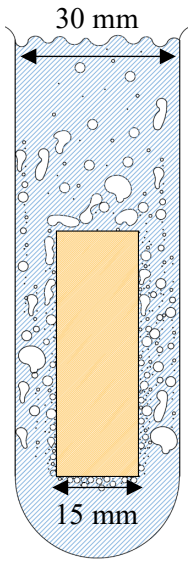


Figure 4-1 - A schematic representation of how bubble regime leads to limited volumes of liquid surrounding the biomass, tube diameter 30mm, biomass block 45×15×15 mm

4.1.1.2 Vapour volume quantification

It was observed that there was a large production of volatiles produced during the pyrolysis process. An estimation of the volume of gas produced, from the boiling solvent, based on the energy input to the biomass can be calculated using the enthalpy of vaporisation for the liquid and the ideal gas law, along with heat fluxes calculated by the computational simulations (Section 2.6.1). The assumptions used to underpin these calculations were as follows:

- The liquid was assumed to be at 20 °C initially, and any further energy provided to the liquid past its boiling point acted to vaporise it.
- Below the boiling point of the solvent, no vapour was produced.
- The temperature of the liquid was homogenous.
- The system was open and remains at atmospheric pressure.
- The gas phase was assumed to be ideal.

Heat transfer equations than can then be used to calculate the temperature increase up to the boiling point, after which the flowrate of vapour can be calculated:

Solvent temperature below $T_{Boiling:}$

$$T_{solvent} = \frac{\dot{Q}}{h\,A} + T_{surface} \qquad 4\text{-}1$$

Solvent vapour produced at $T_{Boiling}$:

$$V = \frac{\dot{Q}\,R\,T}{\Delta H_{Vap}\,p} \qquad 4\text{-}2$$

Where:

$\dot{Q}$	-	Power absorbed by the biomass, W
h	-	Heat transfer coefficient, W/m^2·K
A	-	Area, m^2
ΔH_{vap}	-	Enthalpy of vaporisation, J/mol
$\dot{V}$	-	Flowrate of gas, m^3/s
R	-	Constant, 8.3145 J/mol·K
T	-	Temperature, K
p	-	Pressure, Pa

Figure 4-2 shows the volume of vaporised n-Hexane based on three absorbed powers by the sycamore block.

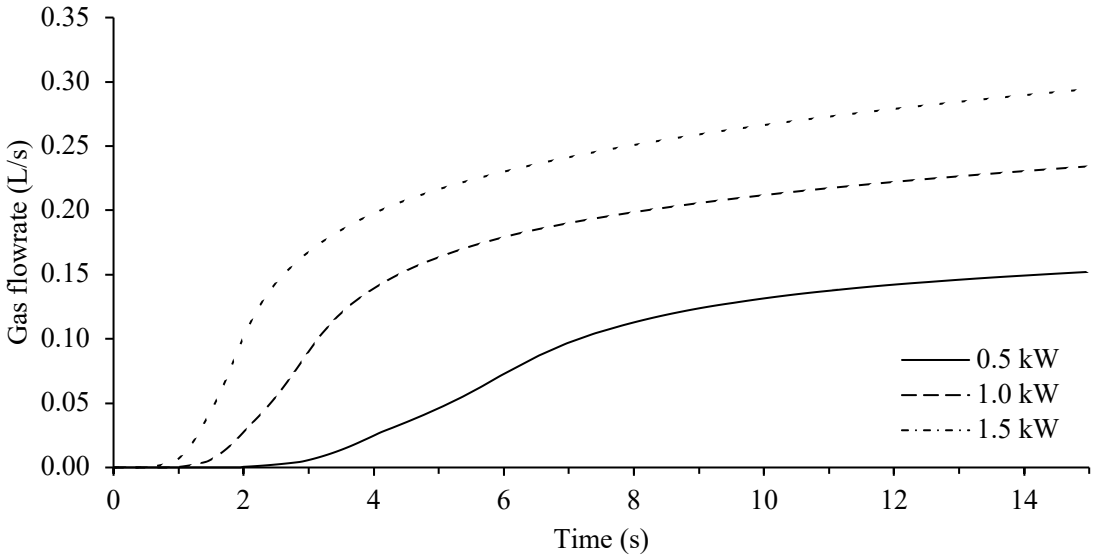


Figure 4-2 – Flowrate of *n*-hexane vaporised based on heat transfer from the 45×15×15mm sycamore block to the solvent in the single-mode liquid-inerted microwave system at 0.5 – 1.5 kW absorbed power.

Initially, volumetric heating of the sycamore occurred with heat being transferred to the liquid via convection. Once the solvent reaches its boiling point, the liquid starts to boil, with vapour production increasing due to the higher heat flux from the higher block temperature (as explained in Section 3.4.7). The gas flowrate then begins to plateau as the heat flux and boiling liquid approach equilibrium.

Taking into account only boiling solvent during the pyrolysis process, at 0.5 kW absorbed, 0.15 L/s was produced. With the quartz tube allowing for 100 mL of liquid, the vapour production during the pyrolysis process was larger than the vessel volume. With the bubble formation limited to the surrounding area of the sycamore block, there was very little room between the biomass and the vessel walls, resulting in displacement of the liquid from around the biomass and in some cases entrainment into the condenser. The estimate of volatiles production was underestimated, however, due to not taking into account volatiles production. Therefore, the gaseous/volatile atmosphere would result in larger volumes of gas. It can be confirmed that this was visible empirically when carrying out the pyrolysis experiments, with the large volumes of gas surrounding the biomass (Section 3.4.7), and with liquid being carried up by the vapour to the condenser. Due to this gas behaviour, the benefit of having a liquid surround was greatly reduced in the single-mode system.

4.1.1.3 Design to control the boiling regime

It was important to have a system design that allowed for a large amount of liquid around the biomass to replenish the liquid on the surface of the biomass and prevent the large volume of vapour surrounding the sycamore block, as identified in Section 3.4.7. The new configuration design of a 100 mm diameter beaker enabled larger volumes (1 L) of liquid to surround the biomass, therefore increasing the likelihood of liquid replenishment at the surface. If the diameter is sufficient, the volatiles produced from the biomass, along with the boiling liquid would move both away and up from the biomass, as opposed to the single-mode system where the tube diameter was so small that the gas had no other pathway except to completely surround the sycamore block when dispersing from the surface of the sycamore block.

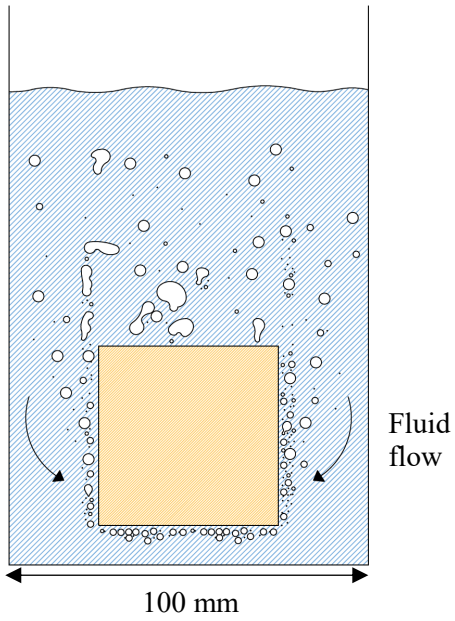


Figure 4-3 - A schematic showing how the liquid replenishes the biomass surface in the scaled-up system

For the single-mode liquid inerted microwave pyrolysis system, the size of the biomass was limited to 45 × 15 × 15 mm due to the diameter of the quartz tubes. The biomass could be made longer in the vertical direction; the longer block would lead to only partial heating as more of the biomass would be located away from the high intensity electric field within the cavity.

In the single-mode system, due to the low mass of the sycamore blocks used (5 – 7 g), small of volume of pyrolysis oil were produced (< 2g). This presented processing issues due to the oil's high viscosity. Attempts at pouring led to the adhesion of the oil to the glassware and no pyrolysis oil being collected at all. Pipetting also resulted in oil remaining within the pipette tip and not being able to eject. To collect the liquid, the sample and glassware were washed with a suitable solvent, such as acetone or methanol, which would then produce 2 - 3 mL of collectable liquid. The volume of liquid produced would mean that any mass quantification methods would involve a lot of potential error (>100 % of the yield for low oil yields), as any water content change or unseparated solvent would drastically change the liquid yield measured, along with any

volatile components of the pyrolysis-liquid product being lost as the acetone-liquid mix was dried. Any losses of liquid product on such a scale would be representative of a large percentage of the total liquid (>10 % at the highest yields attained), therefore creating potential for error and lowered confidence in the liquid yields. As such, a process that would allow for greater oil volumes was necessary, as any transfer losses would represent a smaller percentage of the total yield.

4.2 Aims and objectives

The aim of using the multi-mode system was to understand the product yield and quality that could be obtained when conducting pyrolysis within a liquid. The objectives required to achieve this aim were:

1. Design and build a system to avoid gas build-up and vapour slugging.
2. Understand the effect of sycamore block size on yield of the pyrolysis oil product.
3. Understand how the pyrolysis process is affected by the choice of solvent.
4. Understand how the process affects the composition of the residual solid.
5. Understand the effect of energy input and power density on pyrolysis oil quality.

4.3 Materials and methods

4.3.1 Microwave experimental system

Sycamore blocks were cut into 30 × 30 × 30 mm, and 50 × 50 × (50, 40, 25 & 15) mm, representative of average masses of 12g, 72g, 62g, 35 g and 19g, respectively, with a moisture content of 6 % (ASTM D4442). Solvents (cyclohexane, kerosene, 2-propanol - reagent grade) were provided by Fisher Scientific. Microwave pyrolysis experiments were carried out utilising a 0 – 6 kW microwave generator at 2.45 GHz and a multi-

mode cavity. An automatic three stub tuner (S-TEAM STHD v1.5) was used to maximise the absorbed power and to log forward and reflected power. The sycamore block was placed in a 100 mm diameter flanged quartz beaker with a height 250 mm and covered with 1L solvent (cyclohexane, kerosene, 2-propanol and water). The sycamore block had a tendency to float, so it was weighted down by a glass mass to prevent floating and allow sufficient liquid to surround the biomass. The beaker was placed in a 240 × 240 × 300 mm reactor cavity. A flanged 100 mm lid was then placed on the beaker and connected within an electromagnetic choke to a condenser. The reactor cavity and choke were purged with 10 L/min nitrogen to maintain an inert environment should there be a failure of the quartz beaker. A schematic of the reactor for the experimental system is shown in Figure 4-4.

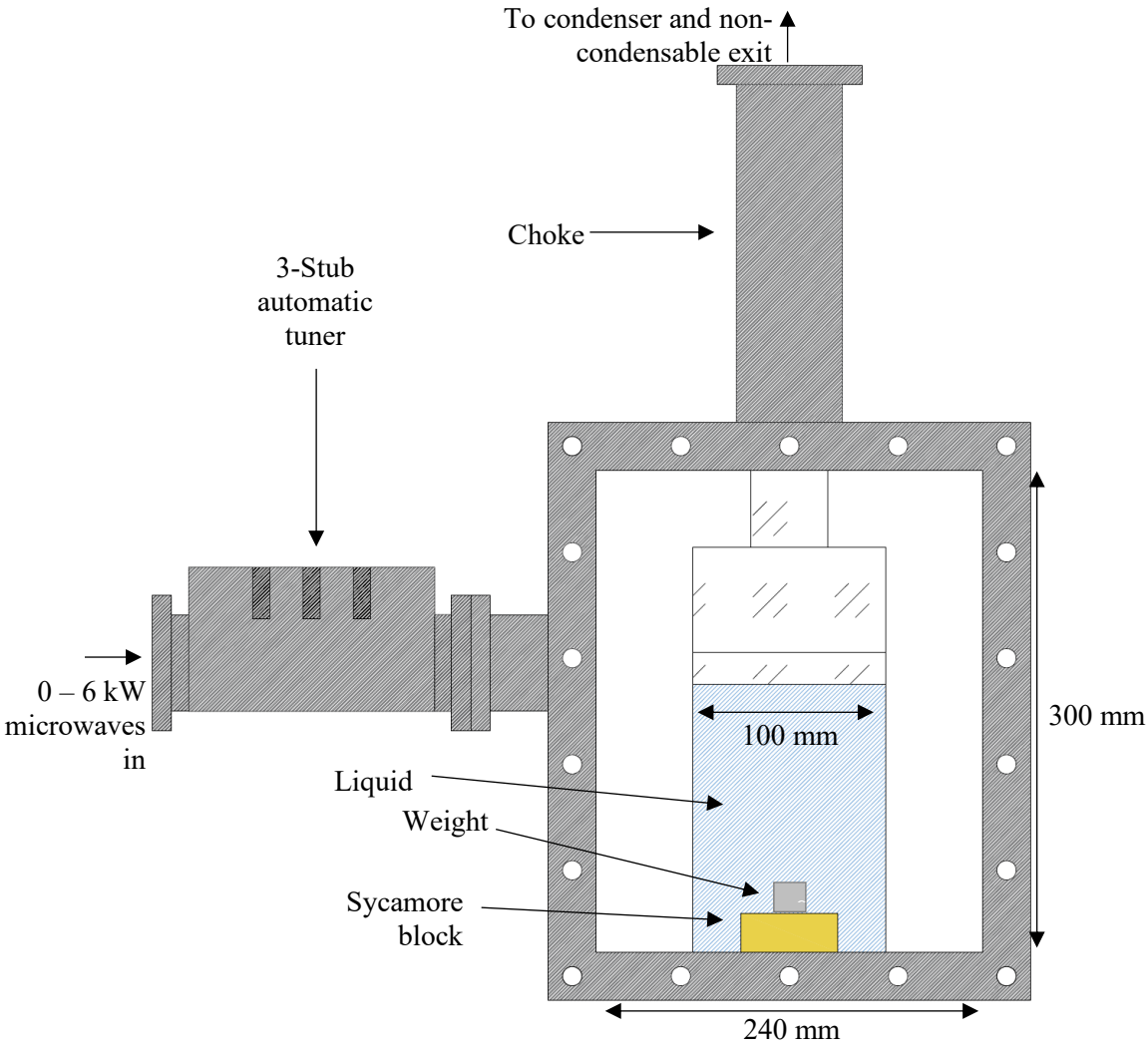


Figure 4-4 - Liquid-inerted multi-mode microwave pyrolysis system

Experiments were carried out at 0.5-6 kW for 5-300 seconds, to give an energy input range of 0.4 – 5.5 kJ/g. After the pyrolysis process the remaining sycamore sample was washed with acetone and dried at 105 °C until a constant mass was obtained. Pyrolysed samples were then weighed and percentage mass losses were calculated.

4.3.2 Pyrolysis oil collection

4.3.2.1 Cyclohexane

For cyclohexane, the aqueous phase oil produced was collected using a syringe and weighed. The solvent phase was poured into a pre-weighed vessel and air dried until

the solvent was removed. Any residual aqueous phase oil was washed with acetone and placed into a pre-weighed vessel and air dried to remove the acetone. The dried oil masses were then weighed.

4.3.2.2 Kerosene

Due to the physical properties of kerosene, having a low volatility and high boiling point (200 - 250 °C), the organic fraction oil could not be separated by drying. For calculation of pyrolysis yields, the organic pyrolysis oil fraction required liquid-liquid separation to obtain a dryable fraction using methanol. The extracted organic phase was then placed into a pre-weighed vessel and the sample was air dried until the solvent was removed. The residual oil was then weighed. The aqueous phase fraction appeared to contain a small fraction of kerosene that on drying of the aqueous phase separated from the pyrolysis oil. This separated kerosene could be removed, and the aqueous oil weighed. Figure 4-5 shows the aqueous phase oil with kerosene, and the organic phase pyrolysis oil fraction after washing with methanol.

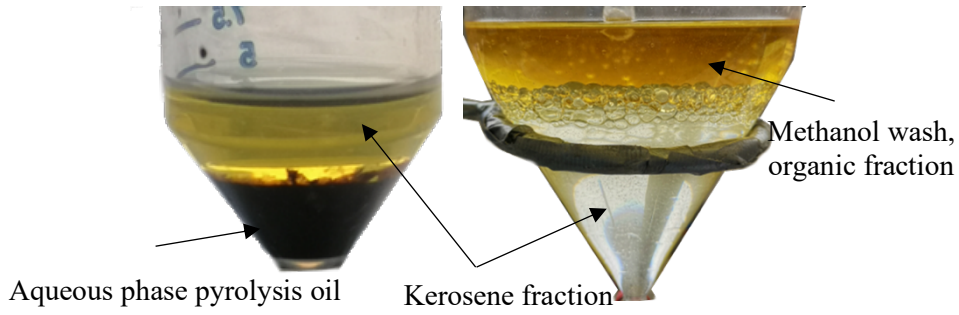


Figure 4-5 - (Left) Aqueous phase pyrolysis oil with kerosene separated out after 24h of air drying. (Right) the organic kerosene fraction after washing with methanol.

4.4 Results and discussion

4.4.1 Power absorption for the multi-mode system

The automatic three-stub tuner allowed for recording of applied, reflected and therefore absorbed power by the system. To first determine the repeatability of the liquid-inerted multi-mode microwave pyrolysis system, the power absorption for various applied powers in various solvents (previously investigated in the single-mode system) were investigated.

The solvents investigated were microwave transparent solvents (cyclohexane and kerosene), and microwave absorbent solvents (2-propanol and water).

4.4.1.1 Cyclohexane

Cyclohexane was chosen as an inerting liquid as it was investigated in the research process described in Chapter 3, and therefore direct comparisons could be made with the single-mode liquid inerted microwave pyrolysis system. Cyclohexane was also found to allow for pyrolysis to occur with a very little energy penalty in comparison to a gas-inerted process in the single-mode system. Figure 4-6 shows absorbance for two applied powers, showcasing consistent absorbance throughout the pyrolysis process. Two powers (0.5 and 3.0 kW) are chosen for Figure 4-6, representative of different power densities within the sycamore block. All other powers investigated (0.5 – 5.5 kW, 0.5 kW intervals) are presented in Appendix C.

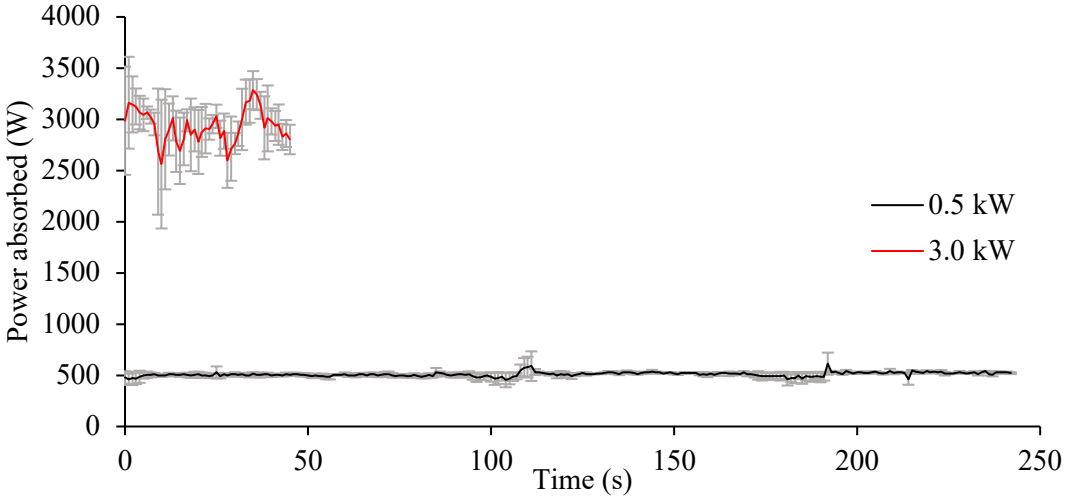


Figure 4-6 – Power absorbed by the system for approximately 0.5 and 3.0 kW applied power in the multi-mode microwave pyrolysis system, sycamore block of dimensions 50×50×25 mm and using cyclohexane as an inerting liquid for 10 runs per applied power.

It can be seen from Figure 4-6 that for both powers presented, the power absorption remained consistent around the set point. Repeatability was better for the lower applied power (0.5 kW), showing a maximum standard deviation from the set-point during the process of ±0.14 kW at 111 seconds, with an average standard deviation of ±0.02 kW throughout the entire process. Despite the higher variation around the set-point for the higher power (±0.23 kW for the whole process, ±0.6 kW maximum at 9 seconds), the process was evidently repeatable for all powers, with a low deviation from the set-point (≤8 % for 3.0 kW applied, ≤4 % for 0.5 kW applied).

4.4.1.2 Kerosene

Kerosene was investigated due to its similar dielectric properties to cyclohexane, being almost microwave transparent, yet having a higher boiling point and viscosity. Results are presented for approximately 0.5 and 3.0 kW applied powers in Figure 4-7, with other powers investigated (5.0 kW) in Appendix C.

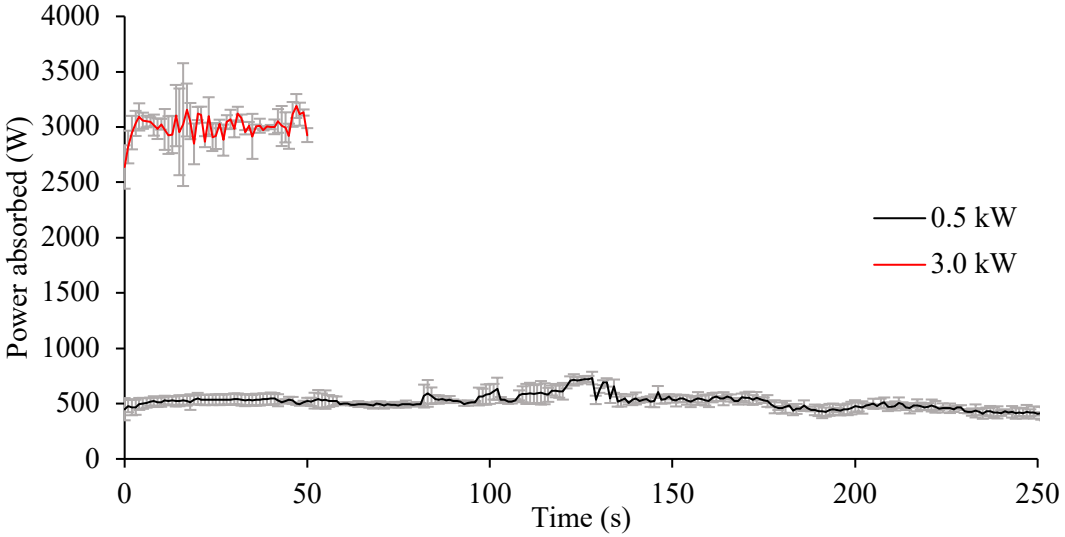


Figure 4-7 - Power absorbed by the system for approximately 0.5 and 3.0 kW applied power in the multi-mode microwave pyrolysis system, sycamore block of dimensions 50×50×25 mm and using kerosene as an inerting liquid for 8 runs per applied power.

Figure 4-7 shows that for the powers investigated, the trends were similar to that of cyclohexane. The 0.5 kW applied power showed less variation around the set value during the process, with a maximum variation of ±0.12 kW at 83 seconds, ±0.04 kW over the whole process. The 3.0 kW applied power runs showed a maximum variation of ±0.5 kW at 16 seconds, ±0.1 kW over the whole process, however the variation of the 3.0 kW runs was less than when using cyclohexane as an inerting liquid. For the powers investigated, the microwave pyrolysis process was repeatable when using kerosene as an inerting liquid with the average standard deviation of ≤4 % for 3.0 kW applied, ≤8 % for 0.5 kW applied.

4.4.1.3 2-Propanol

Figure 4-8 shows the absorbance, and percentage of applied power absorbed by the system when using 2-propanol as an inerting liquid.

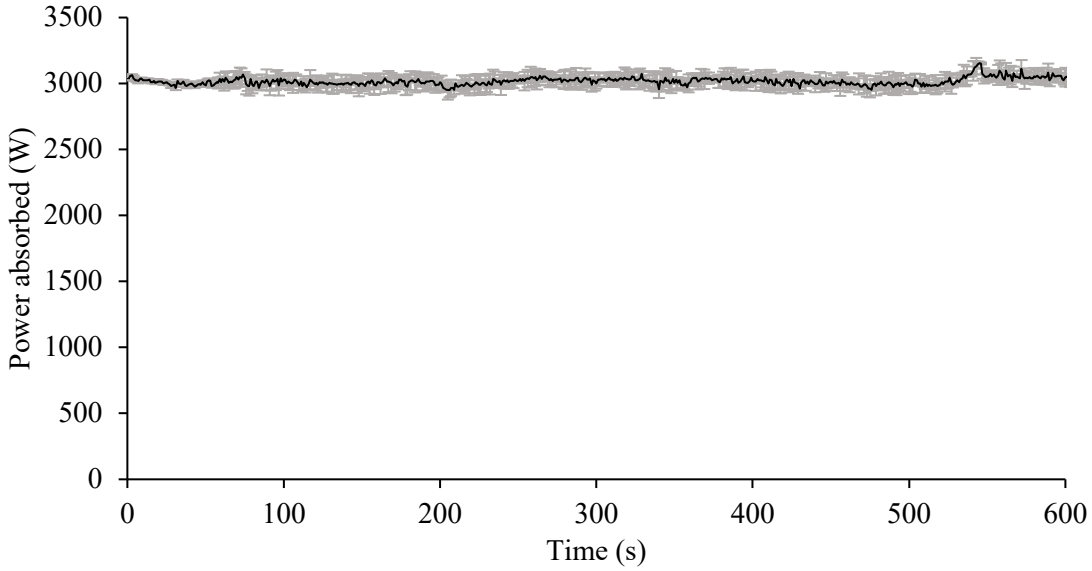


Figure 4-8 - Power absorbed by the system for approximately 3.0 kW applied power in the multi-mode microwave pyrolysis system, sycamore block of dimensions 50×50×25 mm and using 2-propanol as an inerting liquid over 5 runs.

It can be seen that when using 2-propanol as an inerting liquid within the multi-mode liquid inerted pyrolysis system, due to the high dielectric properties of 2-propanol readily absorbing microwave energy, the absorbed power remained consistent around the set-point of 3.0 kW, with an average standard deviation of ±0.04 kW over the whole process.

4.4.1.4 Water

Along with 2-propanol, water was also investigated in the multi-mode liquid-inerted microwave pyrolysis process to determine whether water would be a valid solvent to use on scale-up of the process, power absorbed for approximately 3.0 kW applied power is presented in Figure 4-9.

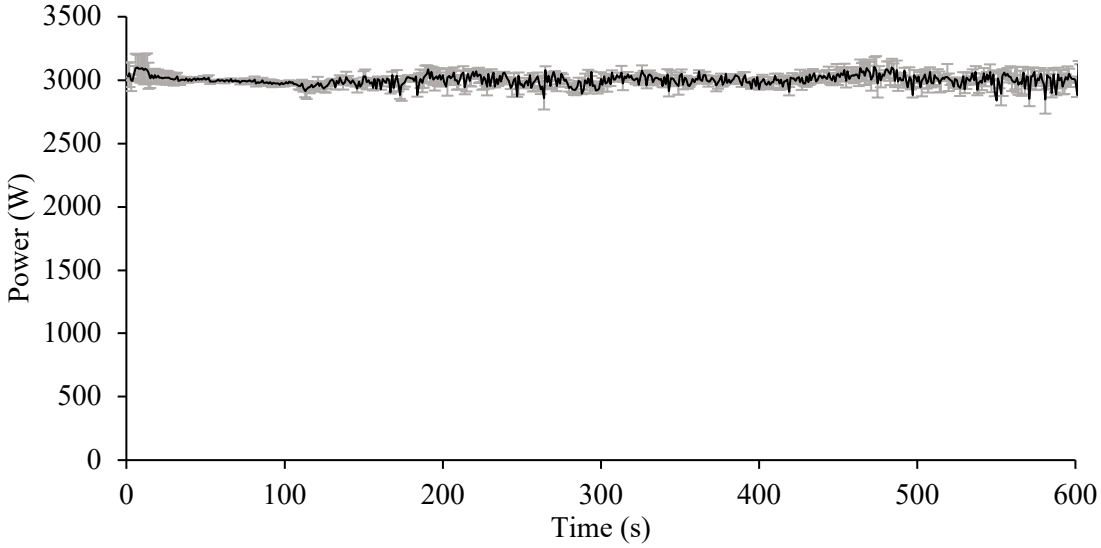


Figure 4-9 – Power absorbed by the system for 3.0 kW applied power, in the multi-mode microwave pyrolysis system, sycamore block of dimensions 50×50×25 mm and using water as an inerting liquid, averaged over 5 runs.

Figure 4-9 shows that for 3.0 kW applied power, the absorbed power remained consistent around the set point of 3.0 kW for the entire processing time with an average standard deviation of ±0.03 kW. The absorbed power value is stable until approximately 113 seconds in the process, at which point the variation around the set point increases, representative of the onset of boiling. Considering the energy required to heat water, it can be calculated that heating 1 L of water from 20 to 100 °C would require approximately 336 kJ of energy, representative of 112 seconds at a power of 3 kW, coinciding with the absorbance data presented in Figure 4-9.

4.4.1.5 Power absorption discussion

A summary of the power absorbed at each set point, along with the representative variations around the set points are presented in Table 4-1.

Table 4-1 - Average absorbed power and standard deviation over the entire pyrolysis process for the solvents investigated.

Solvent	0.5 kW set point average power absorbed (kW)	3.0 kW set point average power absorbed (kW)	Standard deviation as a percentage of the absorbed power (%)	
			0.5 kW	3.0 kW
Cyclohexane	0.51 ±0.02	2.93 ±0.23	3.9	7.8
Kerosene	0.50 ±0.04	3.00 ±0.12	8.0	4.0
Water	-	2.99 ±0.03	-	1.0
2-Propanol	-	3.02 ±0.04	-	1.3

For all solvents investigated, there was confidence in the repeatability due to the small amount of variation around the absorbed power. The average standard deviation for all the processes remained within ±8 % of the set-point values. The more microwave absorbent solvents (2-propanol and water) showed less variation around the set point when compared to the hydrocarbon solvents, largely due to the solvents themselves readily absorbing the microwave energy. In comparison to the single-mode system, the absorbance was more consistent in the multi-mode system. The consistent absorbance was potentially due to the reactor geometry, with microwave propagation occurring within the multi-mode reactor and being less likely to be reflected to the magnetron.

4.4.2 Block geometry testing in the multi-mode system

As the pyrolysis reactor was larger, the process allowed for a wider range of sycamore block geometries that could be investigated. To determine how the sycamore block size affected pyrolysis performance, various dimensions of blocks were examined.

The power applied to the samples was kept consistent throughout all geometries. The block size investigation involved determining how well various block geometries performed in terms of mass loss, liquid yields, and energy requirements required for pyrolysis to occur. Mass losses for the geometries (30 × 30 × 30 mm and 50 × 50 × (15, 25, 40 & 50) mm) that were tested in the multi-mode system are presented in Figure 4-10.

4.4.2.1 Mass loss

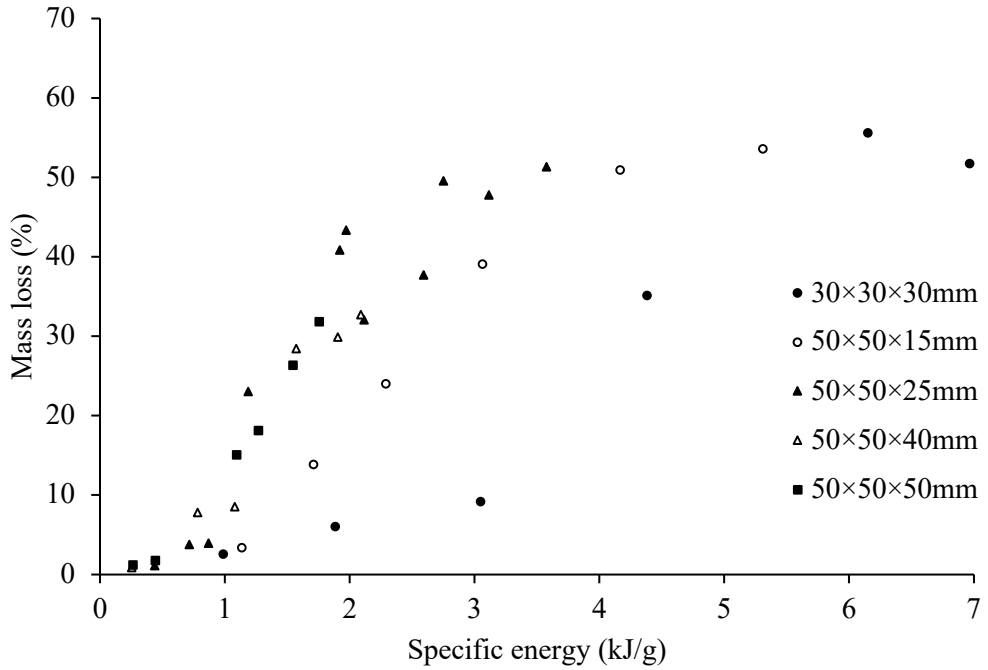


Figure 4-10 – Overall block mass loss against specific energy for 1.5 kW applied power, 10 - 82 seconds for the sycamore block geometries investigated in cyclohexane.

Figure 4-10 shows that there was a positive trend between specific energy and mass loss for all geometries investigated, with the maximum mass loss being 55.6 % at 6.15 kJ/g. It appears that for all geometries tested, there was a linear mass loss increase past a threshold limit (approximately 1.0 kJ/g), until around 50 % mass loss, at which point the mass loss plateaued. This trend was similar to the single-mode system, however the energy requirements were slightly higher, as the threshold for the single-mode was

around 0.5 kJ/g, where the multi-mode required around 1 kJ/g. For the 30×30×30 mm blocks, there was poor performance in terms of mass loss below 3 kJ/g (<6 % mass loss).

4.4.2.2 Pyrolysis oil yield

The pyrolysis oil volume was measured in each experiment. As was previously identified in Chapter 3, the pyrolysis oil product fractionated into two phases; aqueous and organic. The total yields in relation to the non-pyrolysed block masses were considered to identify how well the block sizes allowed for pyrolysis oil yield. Figure 4-11 shows the total pyrolysis oil yield against energy for the block geometries investigated for 1.5 kW applied power.

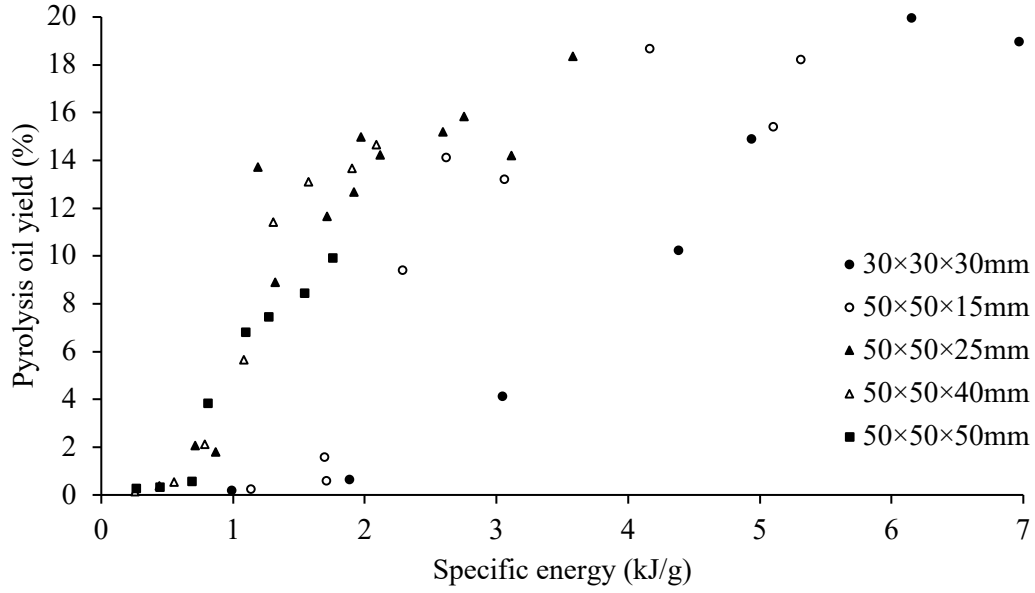


Figure 4-11 – Pyrolysis oil yield against Specific Energy at an applied power level of 1.5 kW, 10 - 82 seconds for the sycamore block geometries investigated.

Figure 4-11 presents a positive trend for all sycamore geometries tested, with the maximum liquid yield being 20.0 % at 6.15 kJ/g for the 30×30×30 mm block. A pyrolysis oil yield of 18.4 % occurred at 3.58 kJ/g for the 50×50×25 mm block, which was close to the maximum but required just 58 % of the energy.

4.4.2.3 Geometry testing discussion

For the smaller block sizes (30×30×30 mm) it is evident that pyrolysis did occur, but mass losses above 50 % required a larger specific energy than larger blocks. Either efficient heat transfer from the biomass to the liquid surround must be overcome at lower specific energies, or as the block is small in relation to the cavity, the real-time impedance matching is not sufficient for these block sizes. It is apparent that on a mass loss basis at the specific energies investigated, the larger blocks pyrolyse more, possibly due to the lower surface area to volume ratio in the larger blocks resulting in less efficient surface cooling. As a processing consideration, for specific energies comparable with the small-scale liquid inerted system, whilst obtaining potential mass losses above 40 %, 50×50×25 mm blocks were chosen. Based on mass losses, the 50×50×25 mm blocks represented a compromise between increased masses, and therefore potential increased collectable pyrolysis oil masses, and raw-material required for each process run. Pyrolysis oil yields were also high in the 50×50×25 mm blocks, further confirming the use of the geometry for further absorbed power and pyrolysis behaviour investigations.

It appeared that the maximum pyrolysis oil yields identified during the investigation were not representative of the highest mass losses. For all geometries tested, there appeared to be lower pyrolysis oil yields at the higher specific energies above the maximum pyrolysis oil yield, which implies that attaining the absolute maximum mass loss is not necessarily beneficial to the process as more energy is needed to achieve the same or lower pyrolysis oil yield. The decrease in pyrolysis oil yields was likely due to increased carbonisation, and increased temperatures within the sycamore block as a result of the higher absorbed energy.

4.4.3 Effect of heating conditions

With the geometry of the sycamore block kept constant, other processing parameters, such as power applied and processing times and their effect on mass loss and pyrolysis oil yield could be investigated.

4.4.3.1 Mass loss, non-polar solvents

Figure 4-12 shows the effect of energy input against mass loss and pyrolysis oil yield of sycamore blocks for applied powers ranging from approximately 0.5 – 5.5 kW within cyclohexane. Kerosene was also investigated in the multi-mode system due to its higher viscosity (1.64 cP) and boiling point (200-250 °C) compared to cyclohexane (0.87 cP, 81 °C). Mass loss data and pyrolysis oil yield against specific energy applied to the sycamore blocks for 0.5 - 5.0 kW are presented in Figure 4-13.

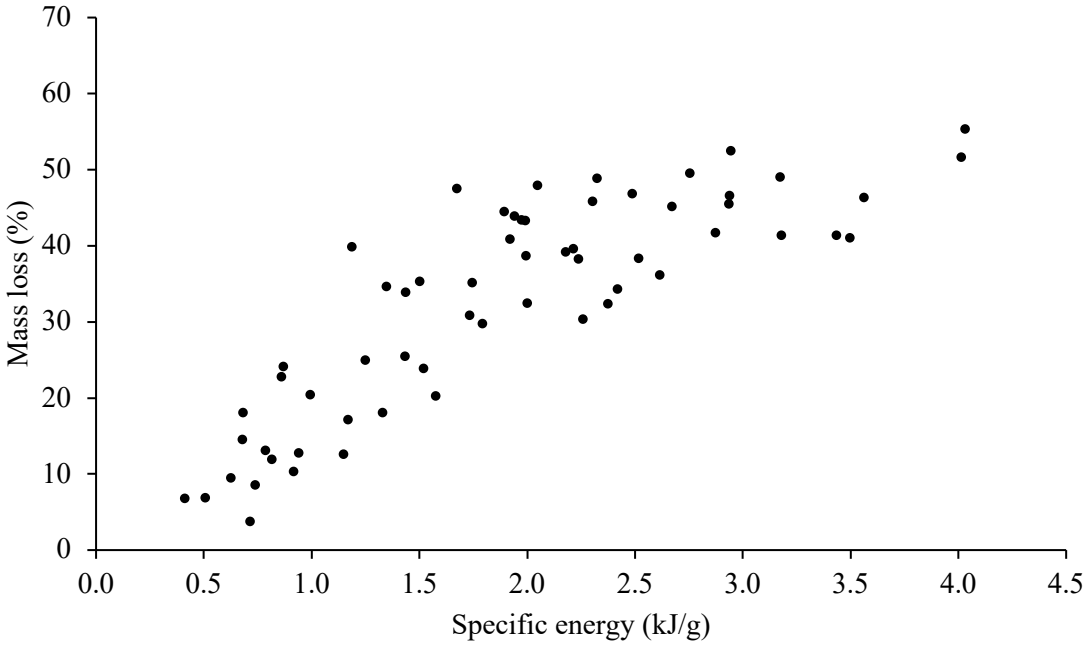


Figure 4-12 - Solid mass of sycamore blocks against absorbed specific energy at applied power levels of 0.5 – 5.5 kW using cyclohexane as an inerting liquid.

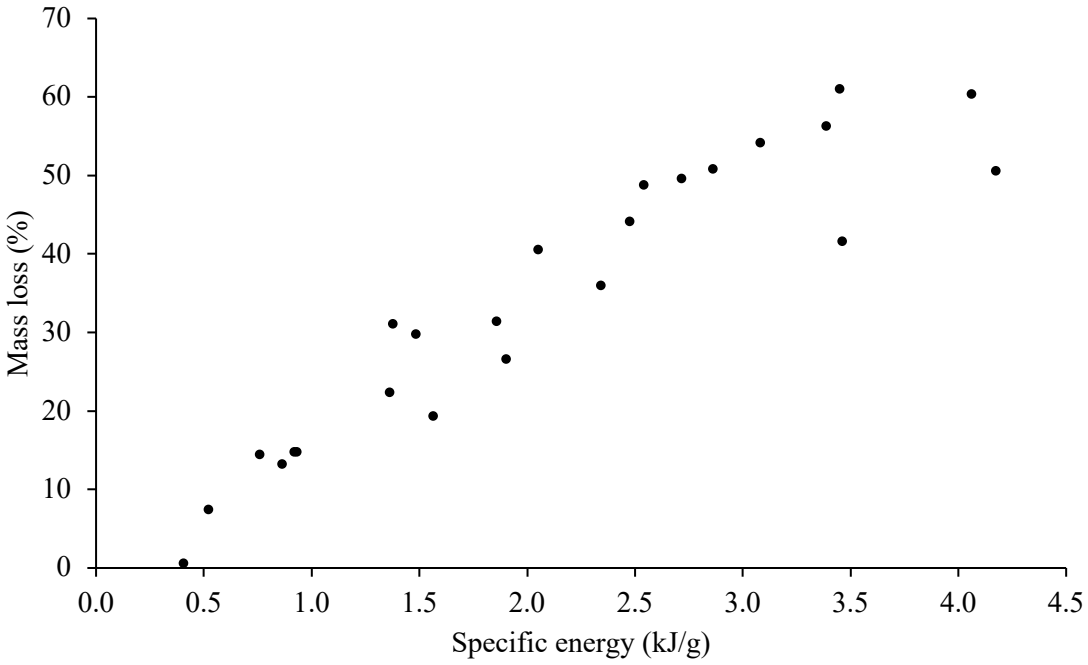


Figure 4-13 - Solid mass loss of sycamore blocks against absorbed specific energy at applied power levels of 0.5 – 5.0 kW using kerosene as an inerting liquid.

There was a positive trend between the energy input and the bulk mass loss for both the cyclohexane and kerosene inerted processes, with higher energy input leading to greater mass loss. The maximum mass loss obtained was 55.3 % at 4.03 kJ/g for cyclohexane, with much of the data reaching close to this maximum as low as 1.67 kJ/g. The maximum mass loss achieved was 61.1 % at 4.06 kJ/g for kerosene. For both solvents, there appeared to be a linear increasing trend, followed by a plateau. The plateau for cyclohexane of around 55 % was lower than the single-mode liquid inerted microwave pyrolysis process (approximately 62 %).

4.4.3.2 Water and 2-propanol as inerting liquids

During the single-mode liquid-inerted microwave pyrolysis process investigations, water and 2-propanol allowed for pyrolysis to occur, despite being microwave absorbent liquids. This was not the case in the multi-mode system, and despite high absorbance of the power to the system, it appeared that all the power applied went to

heating and boiling the solvent, rather than heating the sycamore blocks at all. Figure 4-14 shows the 2-propanol, water and cyclohexane inerted sycamore blocks post-pyrolysis.



Figure 4-14 – The sycamore blocks after processing within 2-propanol (left), water (middle), cyclohexane (right), with the water and 2-propanol blocks exhibiting no mass loss, cyclohexane 44 % mass loss.

4.4.3.3 Mass loss discussion

The mass losses are summarised in Table 4-2.

Table 4-2 – Highest mass loss achieved and energy requirements for pyrolysis and 50 % mass loss to occur for the solvents investigated in the multi-mode system, with comparisons for the single-mode system presented.

Inerting medium	Highest mass loss achieved (%)	Threshold specific energy for pyrolysis to occur (>10 % mass loss) (kJ/g)	Absorbed specific energy required for 50 % mass loss (kJ/g)
Cyclohexane (multi-mode)	55.3	0.7	2.9
Cyclohexane (single-mode)	58.9	0.6	2.0
Kerosene (multi-mode)	62.8	0.7	2.9
Kerosene (single-mode)	48.1	0.5	-
2-Propanol (multi-mode)	-	-	-
2-Propanol (single-mode)	65.5	6.0	8.0
Water (multi-mode)	-	-	-
Water (single-mode)	32.1	16.2	-

The multi-mode liquid inerted microwave pyrolysis process is comparable to the smaller-scale liquid-inerted microwave pyrolysis process with the mass loss trends following a similar pattern for both hydrocarbon solvents tested. The cyclohexane and

kerosene inerted processes both exhibited a threshold energy value for pyrolysis of approximately 0.5-0.7 kJ/g. The highest mass loss on the small-scale system was 60 % at 2.54 kJ/g, the multi-mode system starts to reach higher levels of volatilisation (<40 %) at equivalent specific energies to the single-mode system. There does, however, appear to be a mass loss penalty of around 10 % at equivalent specific energies for the multi-mode system in cyclohexane when compared to the single-mode liquid-inerted process. The mass loss penalty would be expected if there was efficient surface cooling of the biomass due to a more controlled boiling regime compared to the single-mode system. The mass loss penalty could also be due to the larger sycamore particle size, coupled with the less-defined multi-mode microwave field. As the block size was larger than the single-mode system, the benefit of the liquid-inerted microwave process was negated as the block was likely heating heterogeneously, with the rest of the block relying on heat transfer via conduction to heat (Figure 4-15).



Figure 4-15 - A cross section of a sample pyrolysed at approximately 0.5 kW applied, 60 seconds in cyclohexane, showcasing uneven heating of the sycamore block

The uneven heating would result in a reduction in overall energy to heat efficiency, heating more at certain points, resulting in an overall penalty to mass loss. Despite the energy penalty within cyclohexane for the multi-mode system when compared to the single-mode system, there was no such penalty when utilising kerosene as an inerting liquid. This is likely due to the higher boiling temperature of kerosene when compared to cyclohexane. The surface temperature of the sycamore block when submerged in

cyclohexane would be kept around the boiling temperature of 81 °C, not high enough to allow for pyrolysis to occur. In kerosene, however, the temperature of the surface would likely be kept around the boiling range of 180 - 250 °C, high enough for hemicellulose to start to thermochemically decompose, along with the onset of lignin decomposition.

For 2-propanol and water, pyrolysis was not able to occur at all, contrary to the results of the single-mode liquid-inerted microwave pyrolysis process. The penetration depth at room temperature for both 2-propanol and water are very low, 0.7 and 1.4 cm respectively. The nature of the multi-mode reactor design with large volume of surrounding liquid meant that the electric field intensity within the block was inherently lower than the single mode system, which coupled with the increased cooling efficiency through control of the boiling regime meant that temperatures high enough to achieve pyrolysis did not occur.

4.4.4 Pyrolysis oil yield

The pyrolysis oil yields and gas yields (by difference) using cyclohexane are presented in Figure 4-16, and kerosene in Figure 4-17. The pyrolysis oil and gas yields as a percentage of the total volatiles produced are presented in Appendix C.

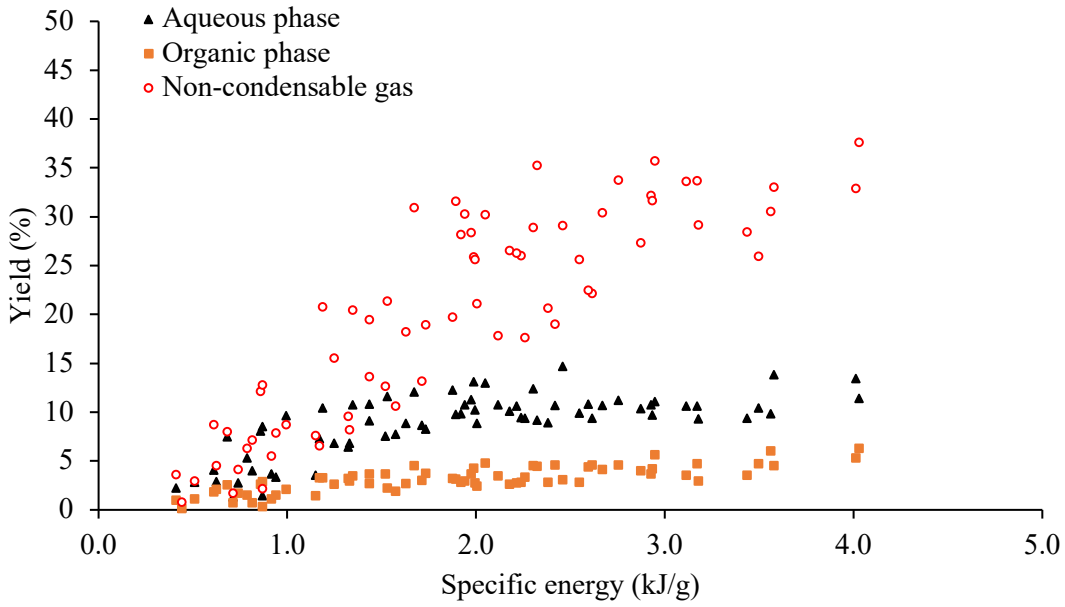


Figure 4-16 –Aqueous and organic pyrolysis oil yields for cyclohexane as an inerting liquid, with non-condensable gas yields shown (by difference).

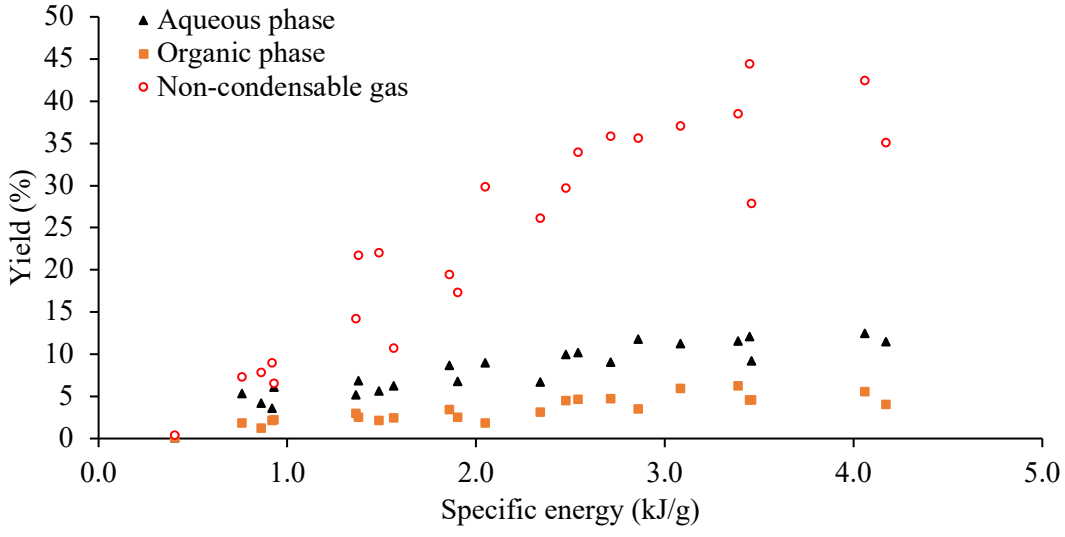


Figure 4-17 – Aqueous and organic pyrolysis oil yields for kerosene as an inerting liquid, with non-condensable gas yields shown (by difference).

It is evident from Figure 4-16 and Figure 4-17 that there was a positive trend between the pyrolysis oil yield and energy input for both absorbed powers investigated in cyclohexane and kerosene. On addition of the two phases, the maximum total oil yield obtained was 17.9 % at 4.0 kJ/g for cyclohexane, with oil yields obtained close to the maximum at around 2.0 kJ/g. The maximum oil yield was 18 % at 4.1 kJ/g for kerosene, with the majority of data lying between 10-18 % liquid yield at 1.0 – 4.0 kJ/g (Appendix C). The yields plateaued around 18 % at 2.0 kJ/g and above, suggesting that there was an oil yield limit that could be obtained in the multi-mode liquid-inerted system for the sycamore block geometries investigated. For both cyclohexane and kerosene as inerting liquids, the organic phase oil yield increased linearly, whereas the aqueous phase yield increased before plateauing around approximately 12 – 14 %. For both cyclohexane and kerosene, as the mass loss increased, the non-condensable gas yields increased alongside, suggesting that the internal temperature of the sycamore block would be reaching temperatures that would lead to secondary degradation of the volatiles produced.

During the pyrolysis process, the three products are pyrolysis oil, solid (char and non-pyrolysed sycamore) and gas. It is therefore evident that at lower specific energies, the pyrolysis oil yield and gas yield were in the same order of magnitude, however the gas yield became much greater than the oil yields at higher specific energies (<1.5 kJ/g).

A summary of the pyrolysis oil yields, in comparison to the single-mode pyrolysis system are presented in Table 4-3.

Table 4-3 – Summary of the oil yields obtained in the multi-mode system, with the single-mode results as a comparison.

Solvent	Maximum oil yield (%)	Specific energy required for maximum oil yield (kJ/g)	Energy required for 15 % oil yield
Cyclohexane (multi-mode)	18.8	4.01	1.67
Kerosene (multi-mode)	18.0	4.06	2.54
Cyclohexane (Single-mode)	30.3	2.54	1.10

The pyrolysis oil yields in the multi-mode system appear lower than the single-mode yields. This is likely due to reduced temperature control within the bulk of the sycamore block due to the lower surface area to volume ratio, and heterogeneous heating profile of the block. Despite a reduction in yields in terms of the starting sycamore mass, due to the sycamore block mass being much higher (40g compared to 5-7 g), the overall volumes of oil produced were higher.

It was evident that the multi-mode microwave pyrolysis process was less favourable to pyrolysis oil production than the single-mode system, with values changing from 57 - 30 % from 0.5 - 4.0 kJ/g, compared to 95 - 49 % from 0.5 - 2.5 kJ/g in the single-mode system (Appendix C). Despite having lower favourability to oil production, the multi-mode system allowed for larger volumes of pyrolysis oil to be produced. The reduction in oil yield could be due to the non-homogenous heating profile identified, resulting in higher temperatures within the sycamore block at the point of pyrolysis, shifting to gas production at lower specific energies than the single-mode system, as shown in Figure 4-18 for cyclohexane as an inerting medium.

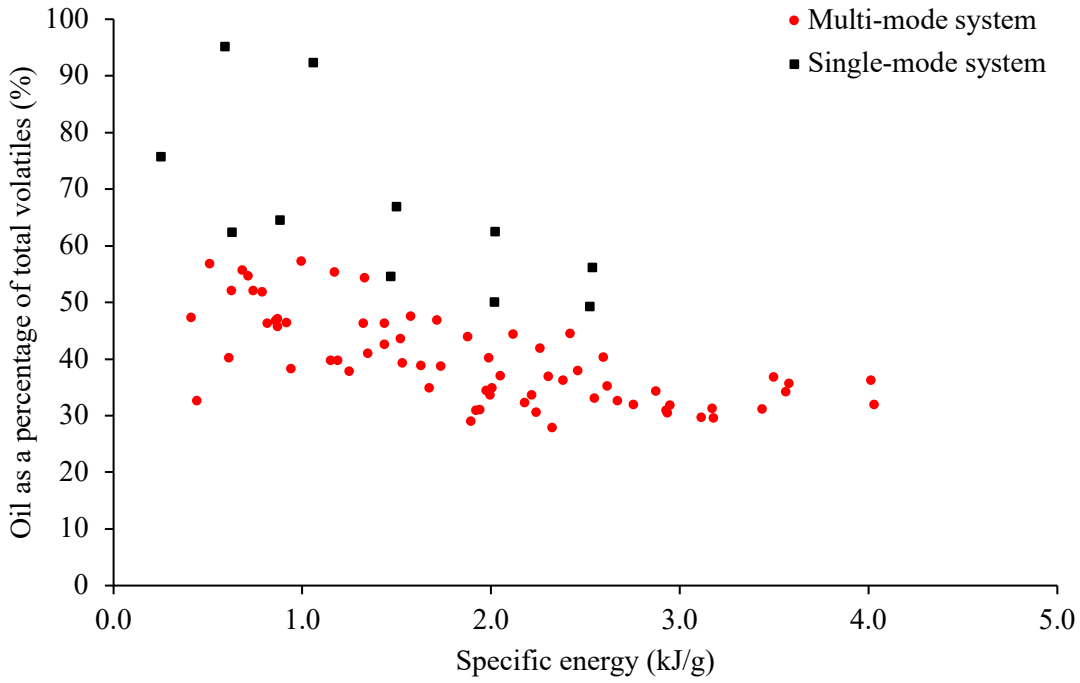


Figure 4-18 – The total oil yield as a percentage of volatiles for the single-mode system and the multi-mode system, with cyclohexane as an inerting medium.

It is evident that the yield of pyrolysis oil was higher for the single-mode system when compared to the multi-mode system. The computational model indicated that pyrolysing at 3.0 kW for 40s (heating homogenously) would reach an internal temperature of approximately 700 °C, as shown in Figure 4-19.

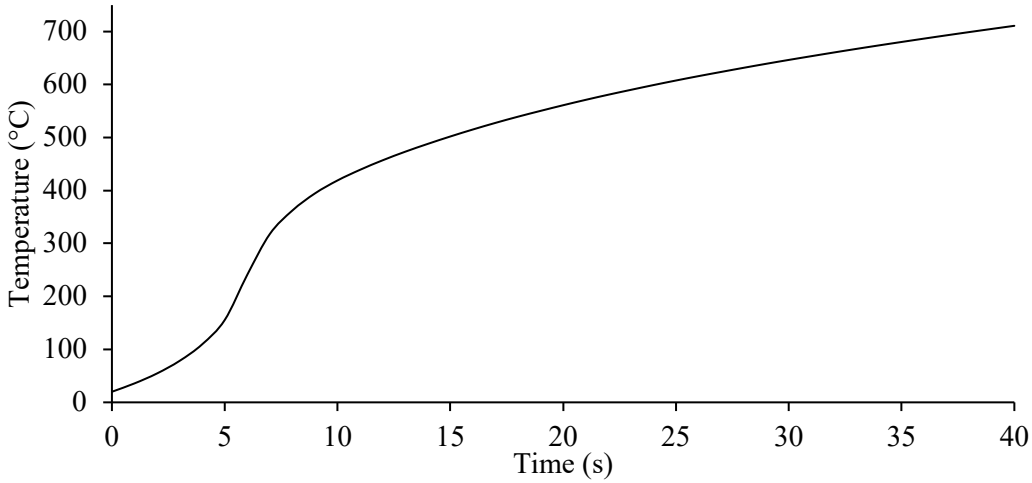


Figure 4-19 - Internal temperature plot of a 50 × 50 × 25 mm sycamore block, heated under the conditions 3 kW absorbed, 40 seconds.

Higher temperatures could lead to volatiles secondary degradation within the sycamore block itself, reducing the overall pyrolysis oil yield during processing. As was shown by the TGA curve for sycamore (Section 3.4.6.2), temperatures greater than 500 °C are not beneficial to the pyrolysis process as the majority of the sycamore mass is lost before this temperature. The oil yield as a percentage of the total volatiles produced was larger for cyclohexane than kerosene for all specific energies investigated. The higher boiling point of kerosene (200 – 250 °C) could reduce the potential for contact condensation of the pyrolysis oil produced and would not condense the more volatile or lower boiling point components of the pyrolysis oil, reducing the observed yield. The higher viscosity (1.64 cP) and lower latent heat (251 kJ/kg) of kerosene compared to cyclohexane (0.87 cP, 365 kJ/kg) could also reduce the cooling efficiency at the surface of the sycamore due to higher vapour volumes at the surface of the block, allowing for internal temperatures to be higher. Due to the decrease in the efficiency of oil yield at higher specific energies, a balance must be made between pyrolysis oil yield and the energy requirement to obtain the yield.

The non-homogenous heating also presents issues during volatiles production. If the volatilised section of the sycamore block is surrounded by the non-pyrolysed sycamore, the volatiles flow is restricted, and the volatiles may condense within the fibres of the sycamore itself due to the temperature control at the surface of the block, reducing the oil yield within the liquid surround. Oil and solid analysis was carried out to estimate the temperatures reached during the process, and the effect on pyrolysis oil fractions,

4.4.5 Pyrolysis oil composition

GC-MS analysis was carried out on the pyrolysis oil fractions produced by the multimode system. The pyrolysis oil produced fractionated into a solvent miscible phase and an aqueous phase that was not miscible with the hydrocarbon solvent used.

Table 4-4, and Figure 4-20 present prominent compounds identified within the oil fractions, and group categorisations of the oil product from the multi-mode liquid inerted pyrolysis process (the tabulated version of the prominent groups can be seen in Appendix C.3), with compositions from the single-mode process for comparison.

Table 4-4 – Prominent major compounds for the multi-mode liquid inerted microwave pyrolysis process in various inerting media, with the single-mode oils presented for comparison, and analysis carried out by each collaborator denoted.

	Peak area (%)					
Compound	**Single-mode n-hexane (aqueous)**	**Single-mode n-hexane (organic)**	**Cyclohexane 1.33 kJ/g (aqueous)**	**Cyclohexane 1.87 kJ/g (aqueous)**	**Cyclohexane 1.33 kJ/g (organic)**	**Cyclohexane 1.87 kJ/g (organic)**
Levoglucosan	13.2	-	19.2	19.1	-	-
Furfural	0.8	7.1	1.1	7.1	0.2	-
4-Vinyl-guaiacol	-	6.2	0.4	-	5.6	6.2
Guaiacol	0.5	4.5	-	-	7.9	4.3
Syringol	2.0	6.9	4.7	2.3	0.1	8.7
Eugenol	-	2.0	-	1.8	17.2	6.9
Cresol	-	-	1.0	0.9	0.5	0.9
Isoeugenol	0.4	7.7	-	-	14.0	-
Sinapaldehyde	-	-	-	3.0	-	0.7
Syringaldehyde	1.7	-	4.4	4.4	0.6	3.8
	Spain (single-mode)			University of Nottingham (multi-mode)		

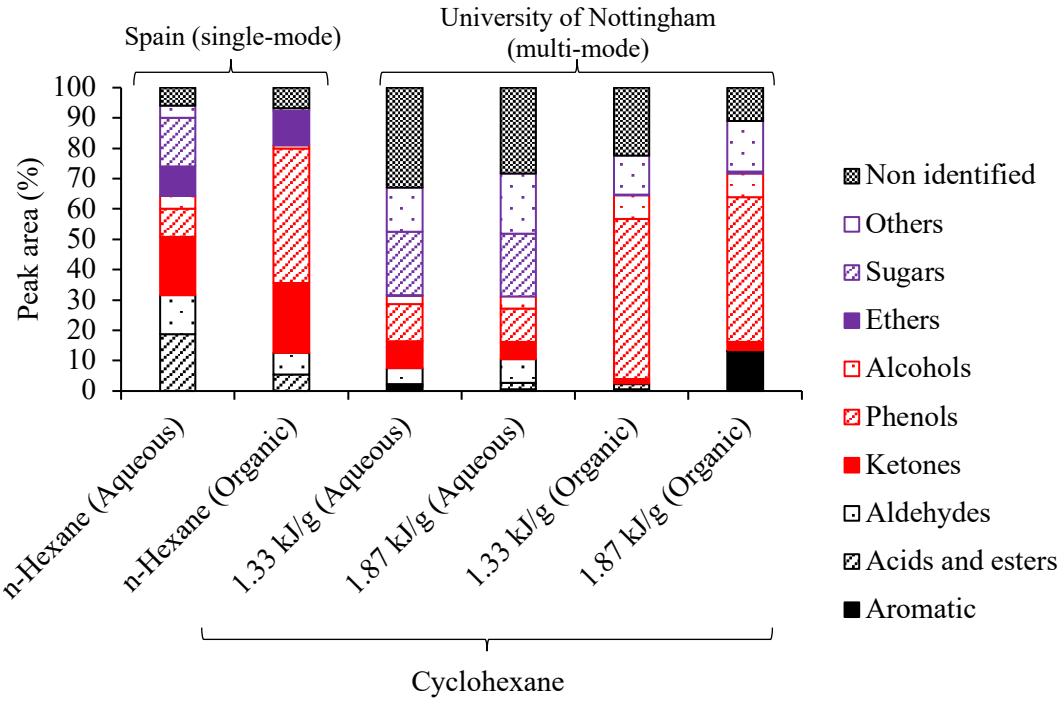


Figure 4-20 - Compound groups for the multi-mode liquid inerted microwave pyrolysis process in various inerting media, with the single-mode oils presented for comparison, with collaborators denoted.

It is evident from Figure 4-20 that the composition of the organic and aqueous oil fractions had differing compositions. The aqueous phase oil fractions contained sugars, ketones and small amounts of phenols. The organic fraction comprised of mostly phenols, with no sugars present. Both cyclohexane inerted multi-mode pyrolysis oils had similar compositions despite having different mass losses (18 % and 35 % for 1.08 and 1.87 kJ/g respectively). The aqueous phase fractions from the multi-mode system had a similar concentration of levoglucosan (approximately 19 %), larger than the single-mode system aqueous phase oil (13 %). The larger levoglucosan concentration could be due to potentially higher temperatures being obtained internally within the sycamore block due to the non-homogenous heating profile, resulting in greater levels of cellulose decomposition. Despite the heterogeneous heating profile, however, the temperature control on the surface of the block could increase the temperature control of the block, preserving the levoglucosan produced, as excessive temperatures would

lead to levoglucosan degradation (Pecha and Garcia-Perez, 2015). Furfural was present in the higher specific energy (1.87 kJ/g) aqueous phase fraction at a greater concentration than the low specific energy oil (1.08 kJ/g). Furfural is formed from both the thermal degradation of hemicellulose, cellulose, and levoglucosan (Kim and Choi, 2018). With the higher concentration of levoglucosan, and also furfural, it could be possible that there was sufficient temperature control to preserve the levoglucosan and degrade the hemicellulose more in the multi-mode system, when compared to the single-mode system.

The oil produced when using kerosene, while collected, was not included in the oil comparison. As kerosene is not volatile and has a high boiling range (200 - 250°C), thermal separation or drying was not an option for obtaining the organic oil fraction, and therefore the sample was liquid-liquid extracted with dichloromethane (DCM) (as methanol could have potentially have been present in the pyrolysis oil). This DCM extraction would likely have not removed all of the compounds present in the kerosene, and therefore the number of compounds present in the resulting sample would be reduced. Due to the liquid-liquid extraction, it is possible that the organic compounds extracted by the DCM were also diluted, resulting in difficulty identifying them. As identified in Section 3.4.4, the operators and methods may have introduced compositional discrepancies, and so future work would involve remedying said discrepancies.

4.4.6 Solid analysis pre and post pyrolysis

4.4.6.1 Lignin, cellulose and hemicellulose concentration

Determining the cellulose, hemicellulose and lignin content of biomass before and after pyrolysis was carried out to identify and confirm the degree of pyrolysis that had

occurred. A lower composition of these components would suggest that temperatures sufficient to break down each constituent had been reached. Uneven heating occurred within the sycamore block, therefore for this analysis, samples were taken from the pyrolysed section of the biomass. Table 4-5 shows the composition of the non-pyrolysed sycamore used throughout the pyrolysis investigations.

Table 4-5 -The composition of the sycamore used in this study.

Sample	Lignin (%)	Cellulose (%)	Hemicellulose (%)
Sycamore	33.6 ±0.06	35.9 ±1.8	18.1 ±0.8

The compositional analysis accounted for 87.6 % of the wood, with the rest of the composition unaccounted for. The unknown composition is likely a combination of moisture, proteins, lipids and other extractives (Miranda et al., 2017, Gutiérrez et al., 2004, Piispanen and Saranpää, 2002).

Figure 4-21 presents the hemicellulose, cellulose and lignin compositions of the char present in the sycamore block before and after pyrolysis.

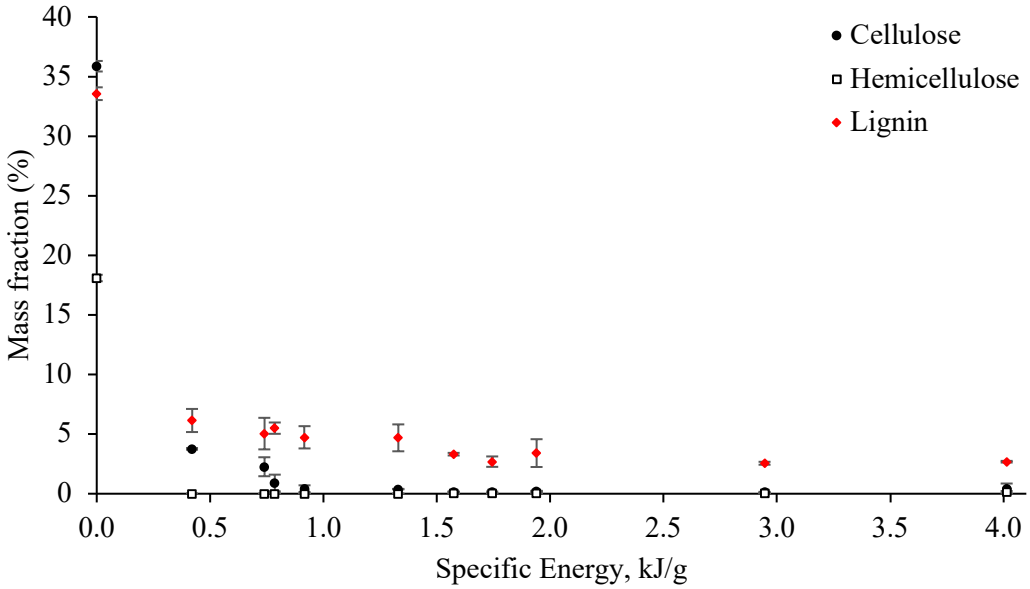


Figure 4-21 – Hemicellulose, cellulose and lignin content against mass loss for the pyrolysed sycamore char.

As highlighted in Figure 4-21, for all processing conditions investigated, it is evident that complete hemicellulose and cellulose breakdown had occurred in the charred section at mass losses above 10 %, and almost complete (<5 % composition) decomposition of lignin had occurred. Therefore, when pyrolysis was occurring, >10 % mass loss, it is likely that temperatures of 200 - 400 °C had been reached at the point of heating within the sycamore block.

For the multi-mode pyrolysis samples, in comparison to the single-mode liquid inerted pyrolysis process, the lignin composition within the char was much lower, as shown in Figure 4-22.

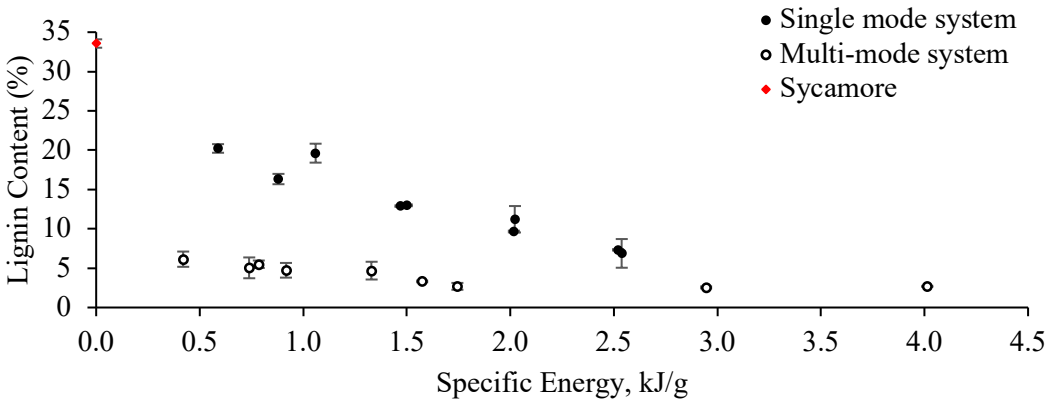


Figure 4-22 – Lignin composition of the single-mode and multi-mode system, 0 – 4 kJ/g.

The lower lignin concentration is possibly due to the higher temperatures that were reached, and reduced homogeneity of the point of heating within the sycamore block. The temperatures reached within the single-mode system were approximately 346 - 456°C (Section 3.4.6.2) at specific energies and mass losses of 0.59 - 2.54 kJ/g and 13 - 62 %, respectively. The heating profile was more evenly distributed over the sycamore block within the single-mode system as evidenced by the even char formation, whereas the multi-mode block heating from a certain point may have resulted in the point of pyrolysis being insulated by the rest of the sycamore block. The point of heating may

have resulted in higher temperatures than expected, therefore investigations into the internal temperature reached were required.

It is therefore possible that the single-mode liquid inerted system allowed for a greater degree of selective decomposition of the cellulose and hemicellulose composition. The single-mode system would allow for better internal temperature control due to the small block size, however due to the large volume of gas pockets, the surface temperature control was reduced. The pyrolysis oil yields were therefore higher than the multi-mode system, but the quality could have been reduced due to the aforementioned lack of surface temperature control. The multi-mode system had poor internal temperature control due to the heterogeneous heating profile and larger block size. Consequently, the selective decomposition identified for the single-mode system was not seen in the multi-mode system, although due to the good surface temperature control, the liquid quality was improved.

It was determined that the heterogenous heating profile resulted in a lack of selective decomposition within the sycamore block in the multi-mode system for the microwave transparent solvents. To determine the composition of the block as a whole, and determine if the overall composition of the sycamore was significantly reduced, the entire pyrolysed block (including the outer non-pyrolysed section) was also milled into a homogenised powder and analysed, and the compositional analysis is shown in Figure 4-23.

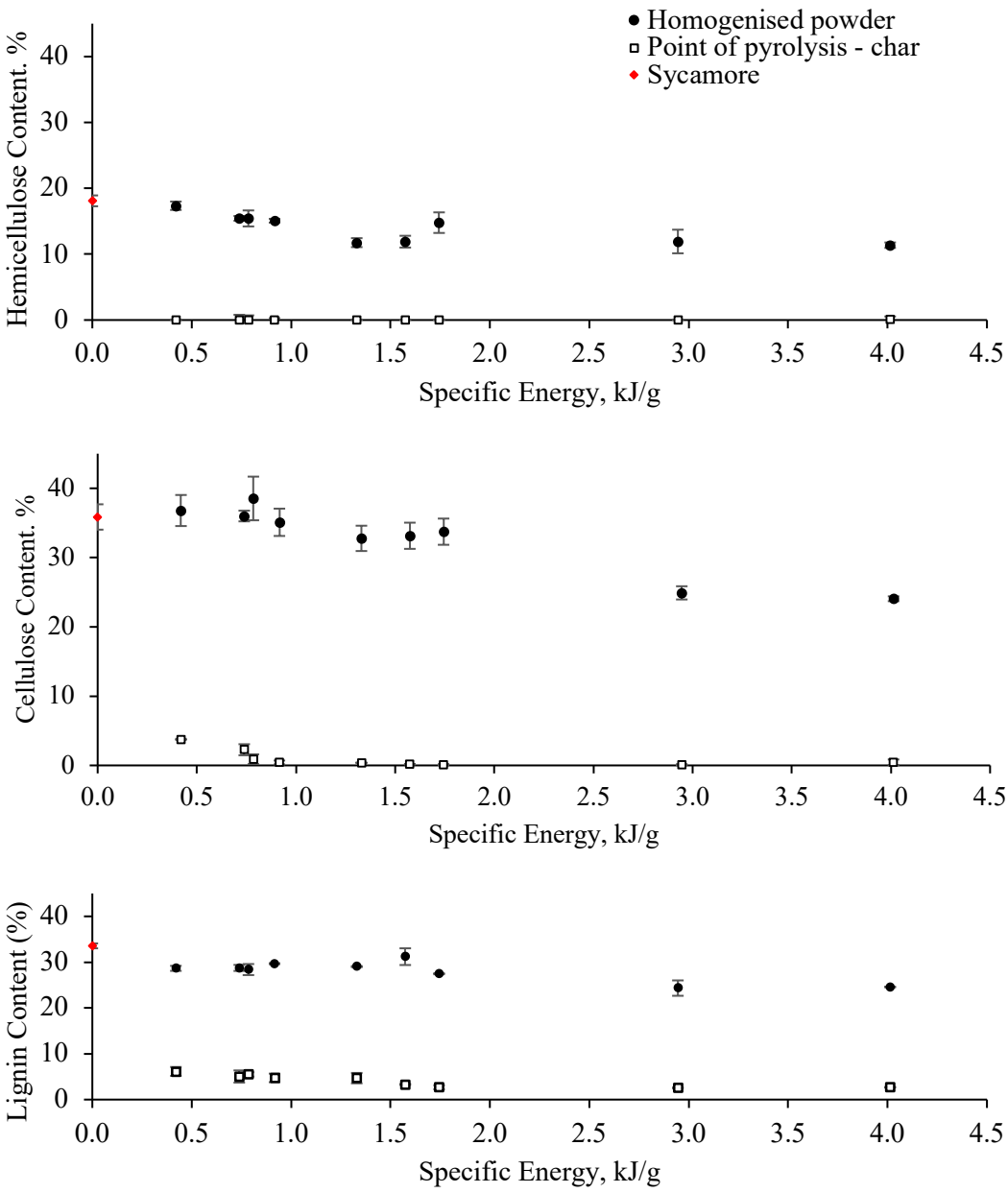


Figure 4-23 – The composition of the blocks as a whole for the specific energies investigated, with the composition of the chars for reference.

The homogenised block compositions remained close to that of the non-pyrolysed wood at all specific energies investigated. This is largely due to the fact that the relative density of wood is much greater than that of the char. With the increased relative density, and the assay using a set mass rather than a volume, it is likely that the majority of the mass of the homogenised powder came from the wood fraction, rather than the char fraction.

At low mass losses (6 – 13 %), the cellulose content of the homogenised powder appeared to be higher than the non-pyrolysed sycamore. This is likely because as the wood was charred, hemicellulose content decreased around this charred section due to the low breakdown temperature of hemicellulose. If the mass is reduced, and the hemicellulose content decreases with cellulose remaining present within the bulk structure due to increased temperature control throughout the block, then proportionally the cellulose concentration would increase. There is also the consideration that the pyrolysis process could have removed extractives and other sycamore constituents not tested for (proteins, lipids) due to the fact that the pyrolysis process was carried out in a solvent. This removal of other sycamore constituents could enrich the overall concentration of cellulose in the sample, where pyrolysis has not occurred to a large degree (<35 % mass loss). Generally, due to the heterogeneity of the heating profile within the sycamore block in the multi-mode system, pyrolysis occurring did not alter the overall block composition significantly, with the largest composition decline being 11 % for cellulose.

4.4.6.2 Empirical temperature estimations and compositional analysis

Using the computational simulation based on energy absorbed, internal temperatures of the sycamore block during pyrolysis could be estimated. The internal temperature prediction, however, was based on homogenous heating, which was not observed empirically in the multi-mode system, contrary to the single mode system, where the blocks appeared more evenly heated, and so temperature predictions likely were not representative of actual temperatures obtained. Figure 4-24 shows the temperature predictions compared to the empirical cross sections of the sycamore block for approximately 0.5 kW absorbed, 30 – 120 seconds.

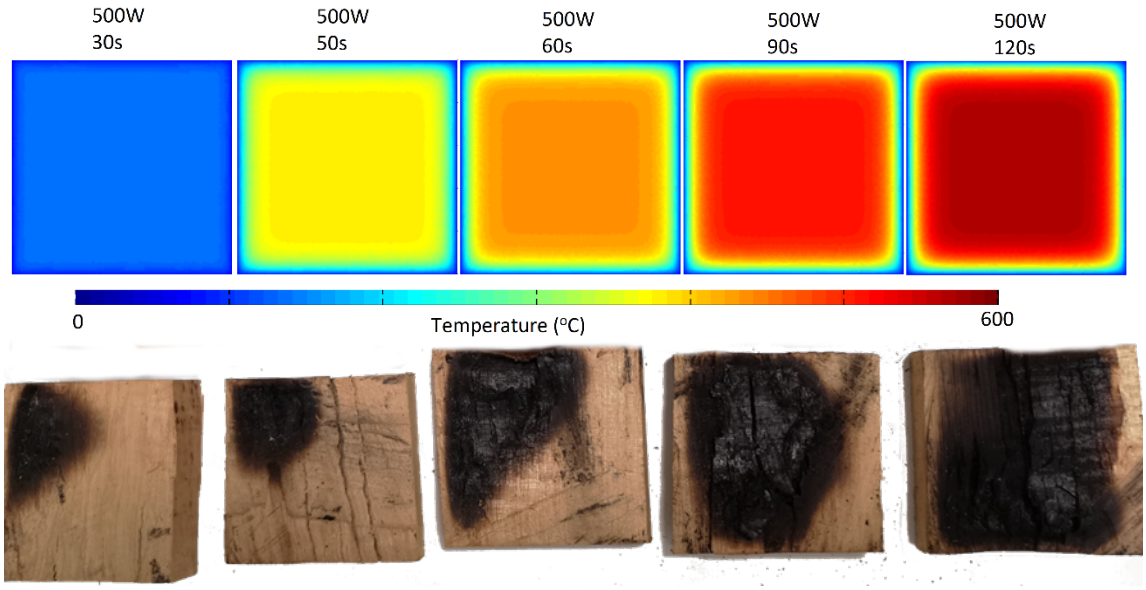


Figure 4-24 - Temperature estimates based on simulations for various processing conditions on 50×50×25 mm sycamore blocks within cyclohexane, and cross-sections of the empirical counterparts within cyclohexane, showcasing heating from a certain point in the biomass.

As highlighted in Figure 4-24, the higher specific energy cross sections match the heating profile of the simulations more closely. The more even heating profile of the higher specific energy samples is likely due to heat transfer by conduction through the block from the point of pyrolysis. If the biomass was heating from a specific point (based on the observations for lower specific energies) there was sufficient time for heat transfer to occur through the biomass, leading to pyrolysis throughout the internal sections of the block. Based on homogenous heating throughout the sample for the 0.5 kW, 30 second run, it was estimated that pyrolysis temperatures (> 250 °C) would not be reached due to the uniform heating throughout the biomass and cooling on the surface. Empirically, however, due to the heterogeneous energy dissipation and heat transfer, it is evident that adequate pyrolysis temperatures are reached in certain areas. Instead of relying on simulations due to the discrepancy in heating profiles, the internal temperatures obtained during the pyrolysis process were estimated using TGA.

Char samples were taken from the centre of the point of pyrolysis within the sycamore block. Proximate analysis could then be carried out to determine the volatilisation at the point of pyrolysis, and therefore provide an estimate of temperatures exceeded. Figure 4-25 shows the TGA derivative mass losses for a sample of the char samples analysed.

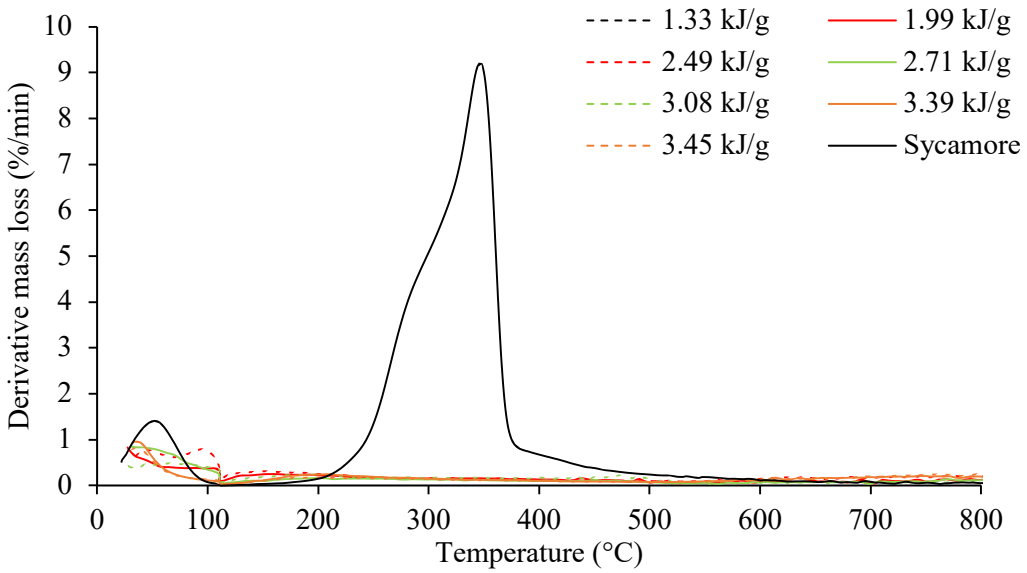


Figure 4-25 – Derivative mass loss curves for the pyrolysed sections of the sycamore block, heating rate 10 °C/min.

It is evident that for all processing parameters investigated, significant temperatures had been achieved in the chars (>400°C). For all chars investigated, there were no peaks in the derivative mass losses in the temperature ranges for hemicellulose, cellulose and lignin (200 – 400°C). Temperatures reached were predicted using the fixed carbon ratio between the chars and sycamore (Equation 3-4, Section 3.4.6.2).

Table 4-6 summarises the proximate analysis data and internal temperatures reached for chars taken from samples with varying degrees of pyrolysis (17 – 56 % total mass loss). Table 4-6 and Figure 4-26 present the compositional analysis of the sycamore on a dry basis, pre and post pyrolysis, and Figure 4-27 presents the temperatures reached

within the sycamore at the point of pyrolysis with various processing conditions (0 – 4 kJ/g).

Table 4-6 - Proximate analysis for chars (dry basis) at the point of pyrolysis at specific energies of 0 – 4 kJ/g.

Specific energy (kJ/g)	Bulk mass loss (%)	Volatiles (%)	Fixed C (%)	Ash (%)	Temperature reached (°C)
0	0.00	82.12	16.79	1.09	20
1.33	18.03	16.15	79.62	4.23	471
1.57	16.74	12.31	83.32	4.37	504
1.74	35.18	10.13	85.81	4.06	530
1.99	43.32	11.25	84.10	4.65	512
2.49	46.86	13.81	82.21	3.99	500
2.71	49.60	8.86	87.46	3.68	540
2.95	52.45	9.72	86.06	4.22	533
3.08	54.23	10.51	85.40	4.09	525
3.39	56.34	11.97	84.09	3.94	511
4.01	51.65	10.00	85.44	4.56	526

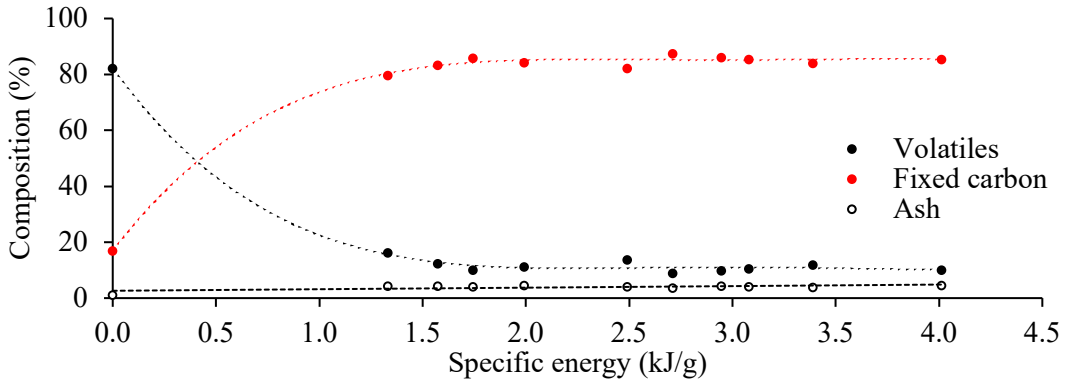


Figure 4-26 – Proximate composition (dry basis) of the non-pyrolysed sycamore and centre of the pyrolysed samples.

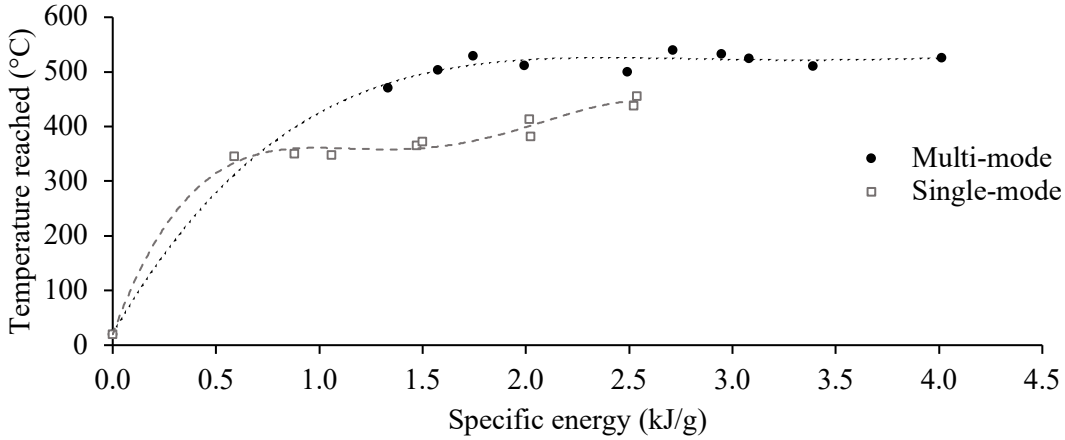


Figure 4-27 – Temperatures estimated by TGA within the centre of the pyrolysed samples within cyclohexane, with non-pyrolysed sycamore and the single-mode results for reference.

The temperatures reached at the point of pyrolysis ranged from 445 to 530°C, coinciding with decomposition of cellulose, hemicellulose and lignin within the sycamore block, validating the compositional concentrations identified in Section 4.4.6.1. The temperatures obtained were higher than the single-mode system, which highlights the loss of internal temperature control within the sycamore block. There were also significantly higher fixed carbon contents for the chars when compared to the single-mode system for equivalent specific energies, 79 – 86 % for the multi-mode system, compared to 46 – 78 % for the single-mode system. It can therefore be determined that the internal temperature control present in the single-mode system was effectively lost at the point of pyrolysis in the multi-mode system.

4.5 Conclusions

A process was developed to attempt to maintain a consistent liquid surround around the sycamore blocks during the pyrolysis process. It had been shown that microwave pyrolysis of sycamore within a liquid inerted environment can be scaled from a small-scale single-mode system, sycamore block mass of 5 - 7 g, to a larger scaled multimode system of block masses up to 75 g. With the scaled process, there was also the ability to collect the liquid produced without significant difficulty due to the greater pyrolysis oil production, which was not present in the smaller scale single-mode system.

There were multiple objectives which were met in terms of understanding how processing conditions could alter the pyrolysis process when scaled-up to increase potential yields. These included understanding the effect of block geometry and energy requirements for bulk mass losses and liquid yields. The multi-mode liquid-inerted pyrolysis system allowed for mass losses of up to 61 %, with liquid yields reaching 20 % based on processing conditions. The energy requirement for pyrolysis to produce a large volume of oil (>45 % mass loss, >15 % pyrolysis oil yield) was around 2 kJ/g,

which was comparable to both nitrogen-inerted systems, and the smaller-scale single-mode liquid inerted system.

It was found that on scaling up the sycamore block geometry, the even heating profile that was observed within the single-mode liquid-inerted pyrolysis process was not present. It was seen that for the processing conditions observed, the sycamore blocks heated from a certain point within the biomass, heating unevenly and reaching potentially higher temperatures at the point of heating than the single-mode pyrolysis process. This uneven heating presents that direct scale-up of the sycamore block geometry would not be optimal, and scale-up in terms of a high-throughput continuous system would be more suited to homogenous heating of the sycamore block.

On adding the potential for a greater liquid surround, scaling up both the quartz beaker and the sycamore block resulted in potential heating by convection within the block itself, discounting the benefit of the more consistent liquid surround. The pyrolysis oil yield in relation to the total volatilisation, for all specific energies investigated, was lower (<60 %) than the single-mode system (<90 %). The decrease in pyrolysis oil yield: mass loss ratio for both cyclohexane and kerosene could be due to high internal temperatures being reached within the biomass when pyrolysing at higher powers and longer times (>550°C), confirmed by the lignocellulosic composition analysis and TGA. This resulted in a larger percentage of gaseous pyrolysis vapour production. The excessively high temperatures within the sycamore blocks could be due to multiple factors; at higher specific energies, the large potential vapour formation could have aided in overcoming the critical heat flux at the surface of the sycamore block. The geometry of the sycamore block coupled with the non-uniform electric field could have also contributed to the higher temperatures, with the point of pyrolysis being insulated by the rest of the block.

It was identified that despite the heterogeneous heating profile of the sycamore block in the multi-mode system, due to the larger volume of liquid surrounding the block, there was potential for increased surface level temperature control and bubble disengagement. The oil produced had a higher concentration (based on peak area) of levoglucosan, suggesting that the temperature of the oil produced was controlled to prevent secondary degradation, despite the heterogeneous internal heating profile. The single-mode system likely had improved internal temperature control due to the more homogeneous heating profile and smaller block size, however the multi-mode system likely had poorer internal temperature control, resulting in lower oil yields, but superior external temperature control, due to the reactor design.

There was scope for further investigation into the overarching understanding of the process of a liquid-inerted microwave pyrolysis process. A process understanding needed to be established for the processing parameters being investigated such as applied power and processing time relationships. The processing parameters that were required to be investigated included potential temperatures reached internally in the multi-mode system due to heterogeneous heating, potential internal pressures due to volatiles production, and theoretical maximum volatilisation achievable during pyrolysis.

5. New insights into microwave pyrolysis mechanisms

5.1 Introduction

Chapters 3 and 4 demonstrated that liquid inerted microwave pyrolysis was possible in both a single and multi-mode configuration. It was found that microwave absorbent solvents such as water and 2-propanol allowed for pyrolysis to occur in a single-mode system, but not multi-mode, likely due to the penetration depths of the solvent during processing.

The investigations for Chapters 3 and 4 were related to determining the effect of different inerting media on the pyrolysis process, and scaling-up the process to better collect and quantify the pyrolysis oil products. Each process had advantages and limitations; the single-mode system appeared to have superior temperature control internally, but due to the scale of the system, resulted in poor temperature control at the surface of the block and the scale was small (5 – 7 g samples). The multi-mode system allowed for much larger blocks and oil masses to be produced but forfeited efficient temperature control within the biomass, whilst retaining the potential for increased surface temperature control due to more effective bubble disengagement and larger liquid volume around the block. Whilst many observations in the two previous chapters could be rationalised with physical explanations such as electric field strength, thermal conductivity and convective heat flux, there are a number of phenomenon that are not as easily explained. These include the selective depolymerisation of the sycamore, the ease to which pyrolysis can be achieved in materials with a low dielectric loss, and the temperature regulation in cases where thermal runaway would be expected to occur.

The aim of this chapter is to gain further insights into the mechanisms of microwave pyrolysis and attempt to provide an explanation for the observed phenomena.

5.2 Materials and methods

5.2.1 Microwave pyrolysis

For the investigations into power density effects, the methods outlined in Chapter 3, Section 3.2.1 and Chapter 4, Section 4.3.1 were utilised, for the single-mode and multi-mode systems, respectively.

5.2.2 Microwave cavity modelling

To simulate the electric field, the introduction of the microwaves was made by a rectangular port (WR340, 86.4 × 43.2 mm) (Figure 5-1). The simulations coupled the power input and frequency of the microwaves to the microwave system, the resultant electric field strength and distribution, and the power distribution across the sycamore block resultant of the electric field strength. The power density distribution could then be utilised as a heat source, as opposed to a homogenous power profile across the entire block. The models were carried out at a frequency of 2.45 GHz, with a power input range of 0.5 – 3 kW. The 'Electromagnetic Waves, Frequency Domain' environment was used in COMSOL Multiphysics 5.3 to simulate the microwave field.

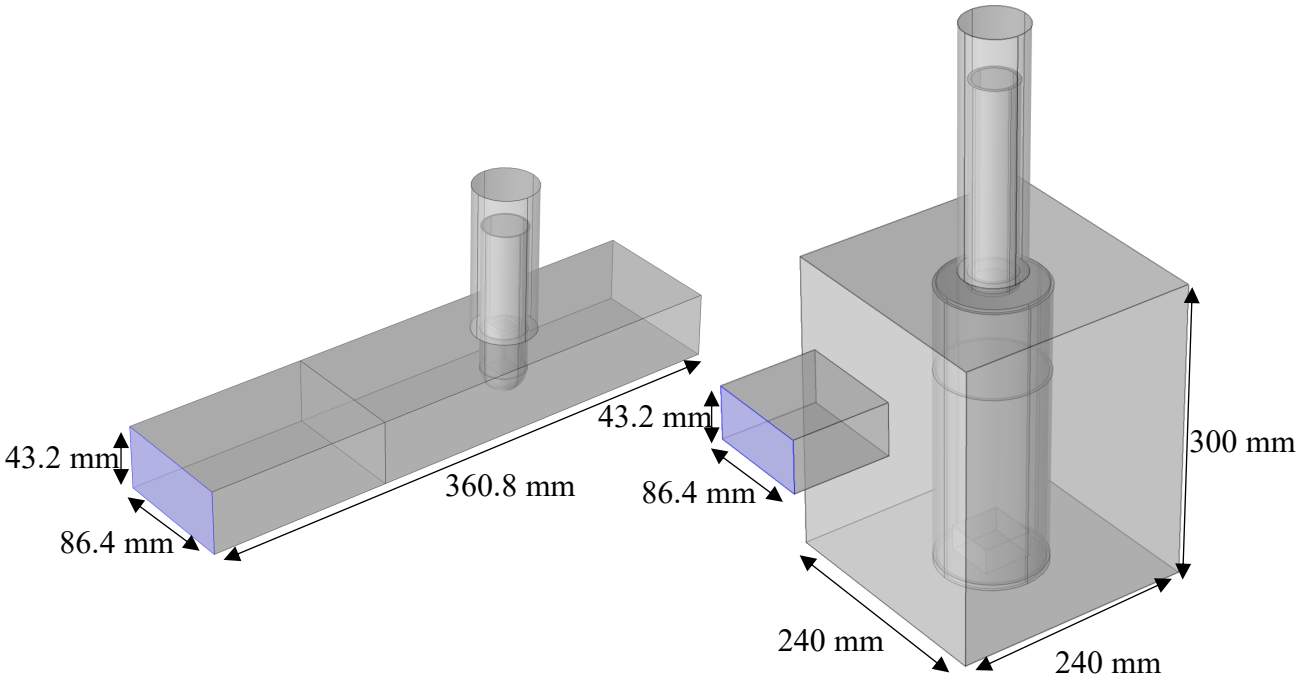


Figure 5-1 – (Left) The single-mode and (right) the multi-mode liquid inerted microwave pyrolysis systems, with the microwave inlet port highlighted in blue.

The electric field vector was calculated using Maxwell's equations:

$$\nabla \times \mu^{-1}(\nabla \times E) - k_0^2\left(\varepsilon_r - \frac{i\sigma}{\omega\varepsilon_0}\right)E = 0 \qquad 5\text{-}1$$

And the power taken up by the material was calculated using (Meredith, 1998):

$$P = 2\pi f \varepsilon_0 \varepsilon'' E^2 V \qquad 5\text{-}2$$

Where:

P	-	Power, W
∇	-	$\left(\frac{\delta}{\delta x}, \frac{\delta}{\delta y}, \frac{\delta}{\delta z}\right)$
μ	-	Relative permeability
i	-	$\sqrt{-1}$
ε_r	-	Relative permittivity
ε_0	-	Permittivity of free space
ε''	-	Dielectric loss factor
σ	-	Electrical conductivity, S/m

E	-	Electric field strength, V/m
k_0	-	Wave number ($k_0 = \omega/c_o$)
ω	-	Wave angular frequency, rad/s
c_0	-	Speed of light in a vacuum, m/s
f	-	Frequency of the applied field, Hz
V	-	Volume of the material, m^3

The dielectric properties of the sycamore were determined by the cavity perturbation method (Section 2.3.1). Figure 5-2 shows the dielectric constant, and loss factor of the sycamore.

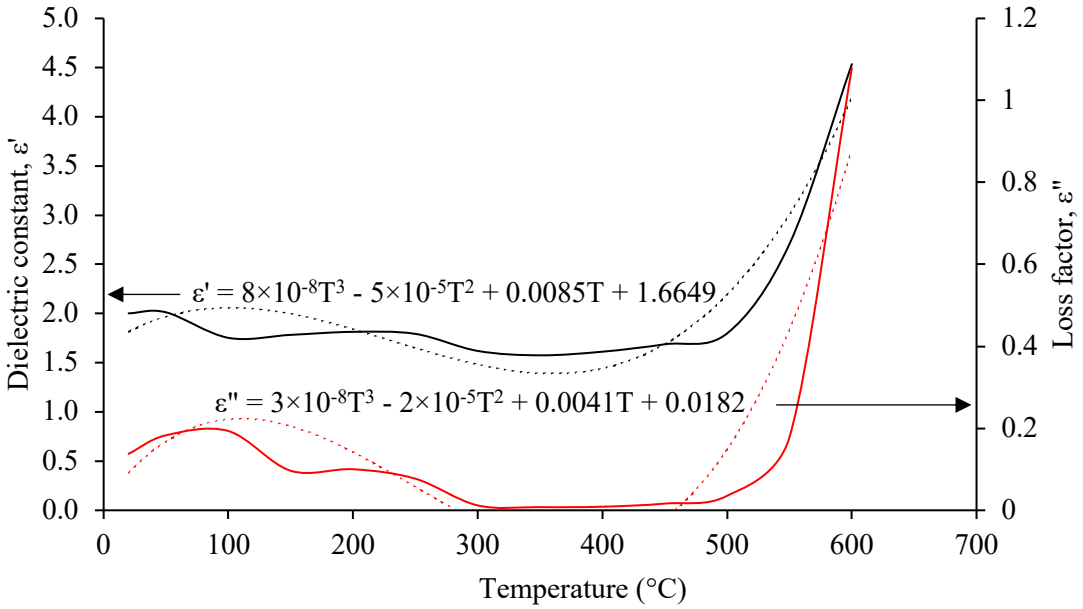


Figure 5-2 – The measured dielectric constant and loss factor of the sycamore.[1]

The sycamore block was modelled as if it was submerged within cyclohexane inside a quartz tube/beaker, and the modelling parameters are presented in Appendix D, Table D-1.

[1] As the loss factor trendline had negative values between 280 – 450°C, a minimum value of 0.001 (the minimum value measured) was applied to the line of best-fit equation for the purposes of the simulations.

5.3 Results and discussion

5.3.1 Effect of power density on pyrolysis performance

Chapter 3 involved a feasibility study, determining whether pyrolysis was feasible in a wide range of polar and non-polar solvents, and Chapter 4 involved investigation into mass losses and pyrolysis oil yields in a process designed to reduce the gaseous surround around the sycamore block, irrespective of power density effects present. The investigations were focused on specific energy as the main process variable. The same energy, however, can be achieved with different power and time combinations; 2 kW absorbed power for 5 seconds would result in the same total energy provided to the sample as 1 kW for 10 seconds. A lower power, longer time process would offer the potential for increased temperature control during the pyrolysis process, potentially reducing the mass lost by the sycamore block.

Figure 5-3 presents mass loss data for the single-mode cyclohexane inerted process. The power density effect on the pyrolysis oil produced was also investigated (Figure 5-4). Mass losses and total pyrolysis oil yields for 0.5 and 3.0 kW applied to the multi-mode system are presented in Figure 5-5 (cyclohexane inerted) and Figure 5-6 (kerosene inerted).

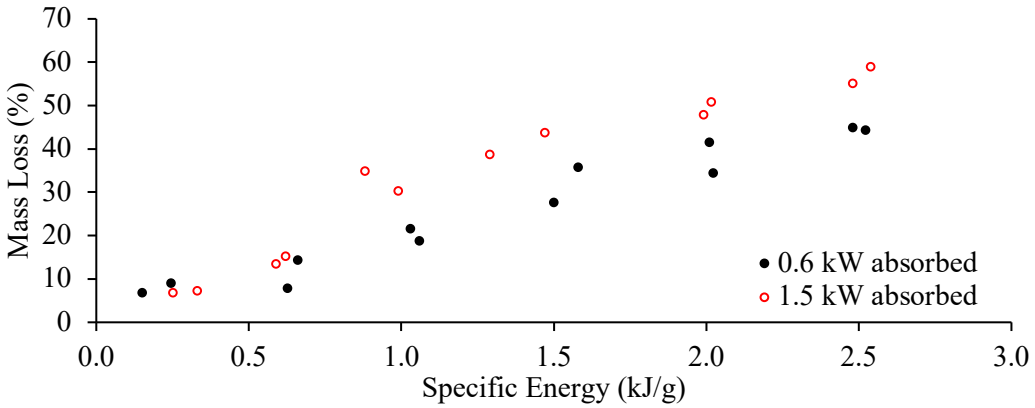


Figure 5-3 - Bulk mass loss of the sycamore blocks against absorbed specific energy for cyclohexane as an inerting liquid for approximately 0.6 and 1.5 kW absorbed power in the single-mode system.

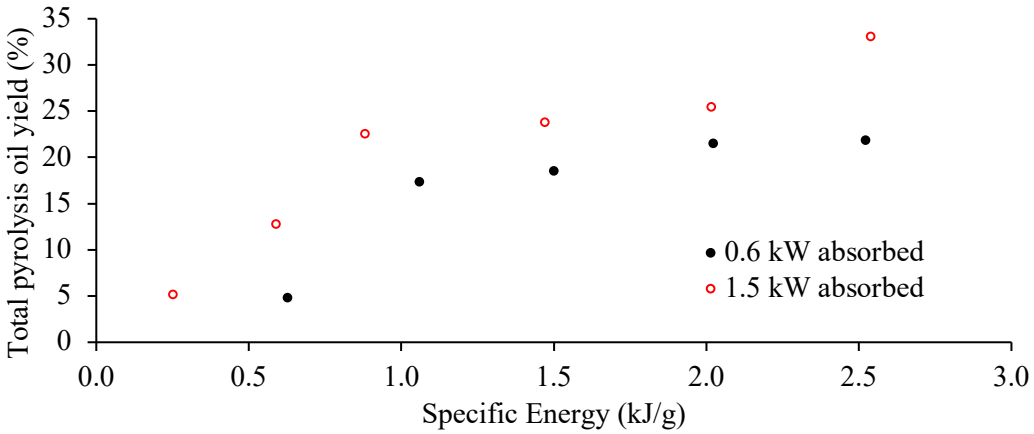


Figure 5-4 – Total pyrolysis oil yields of the sycamore blocks against absorbed specific energy for cyclohexane as an inerting liquid for approximately 0.6 and 1.5 kW absorbed power in the single-mode system.

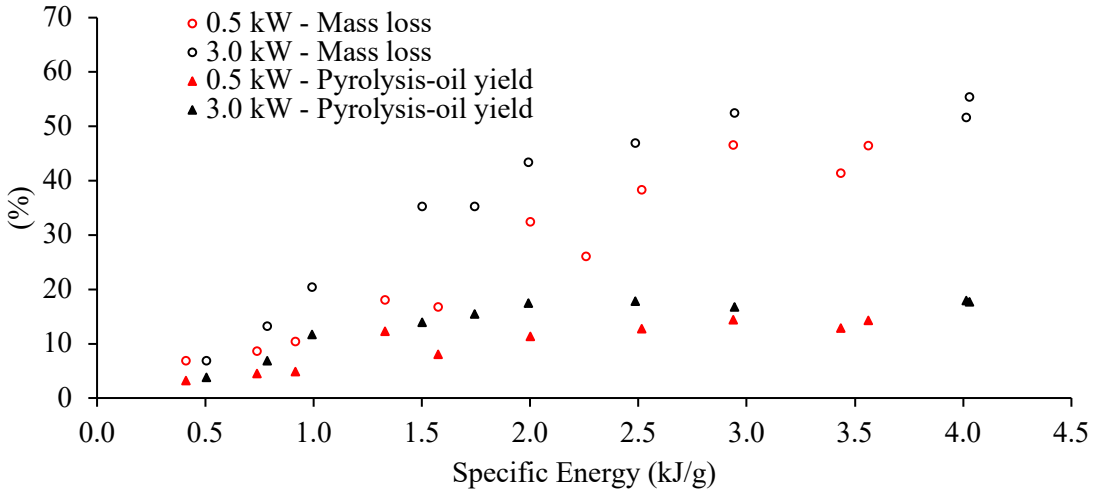


Figure 5-5 - Solid mass loss and pyrolysis oil yield (based on the non-pyrolysed sycamore mass) of sycamore blocks against absorbed specific energy at applied power levels of 0.5 and 3 kW using cyclohexane as an inerting liquid, dynamic impedance matching.

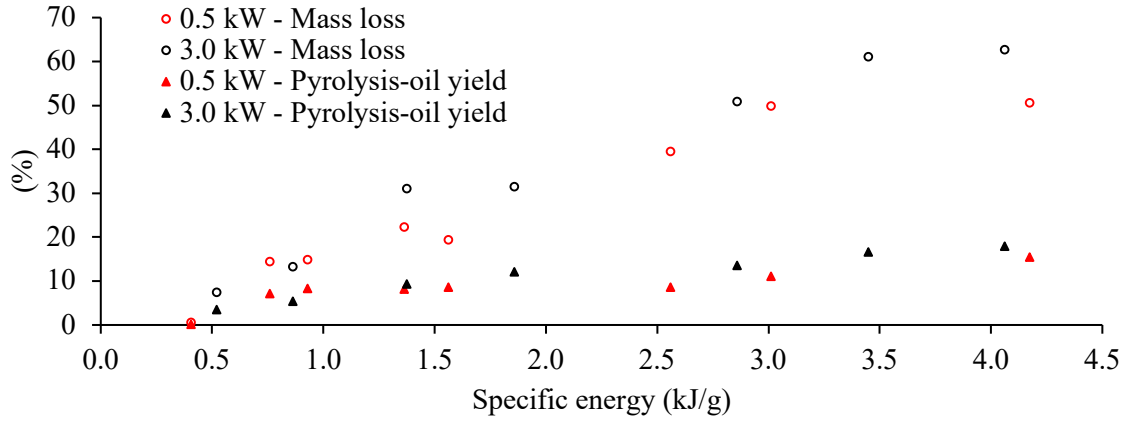


Figure 5-6 - Solid mass loss and pyrolysis oil yield (based on the non-pyrolysed sycamore mass) of sycamore blocks against absorbed specific energy at applied power levels of 0.5 and 3 kW using kerosene as an inerting liquid, dynamic impedance matching.

Figure 5-3 shows that there was an evident power density effect based on the power absorbed; throughout the specific energy ranges investigated, 1.5 kW process provided a 14-16 % increase in mass loss performance compared to 0.6 kW. The maximum mass loss attained during the process was around 60 % at 2.5 kJ/g. It is evident that the power density effect that was present in the mass loss results was also present for pyrolysis oil yields within the process. For equivalent specific energies, 1.5 kW applied produced higher total yields of pyrolysis oil than the 0.6 kW process in the single-mode system. The maximum pyrolysis oil yield achieved was 30.3 % at 2.5 kJ/g, representative of 58 % of the total solid volatilisation for the 1.5 kW process, compared to 21.5 % at 2.0 kJ/g in the 0.6 kW process. For the multi-mode system, for both kerosene and cyclohexane, there appeared to be a power density effect during processing, with the higher power applied (3.0 kW) resulting in higher mass losses and oil yields than the lower power applied (0.5 kW).

Evidently, the power applied to the system in a microwave pyrolysis process therefore had an effect on both mass loss and oil yields. In both the single-mode and multi-mode systems, the mass losses and oil yields were increased at higher powers absorbed by the sycamore block. It was apparent, however, that the power density effect was less pronounced in the multi-mode system, with the majority of lower power run mass losses being approximately 8 – 10 % less than the higher power for the cyclohexane inerted system. It was identified in Chapter 4 that the heating profile of the sycamore within the multi-mode system was less homogenous than the single-mode system. This heterogeneous heating profile would result in heating by conduction in parts of the block, negating the benefit of the liquid surround. Therefore, the power applied, and consequently heating rate, would not be as important in determining the temperature reached for the multi-mode system as compared to the single-mode system.

The increase in mass loss and pyrolysis oil yield with increased power was more prominent in the cyclohexane inerted process when compared to the kerosene inerted process in the multi-mode system, potentially due to the lower latent heat and higher boiling point of kerosene (251 kJ/kg, 200 - 250 °C) compared to cyclohexane (369 kJ/kg, 81 °C). This lower latent heat and higher boiling point would reduce the cooling potential of the liquid surround, resulting in higher surface temperatures, and potentially higher internal temperatures of the sycamore block.

For the multi-mode system, despite the higher mass losses and oil yields at higher powers applied, it can be inferred that at higher specific energies (>1.5 kJ/g), the solid volatilised would produce a higher yield of gas than oil, as the mass losses increase at a greater rate than the oil yields. For all powers and specific energies investigated for the single-mode system, it appears that the pyrolysis oil yield was always >50 % of the mass lost.

As it was determined that higher powers resulted in higher mass losses and pyrolysis oil yields, it was necessary to understand the underlying heat and mass transfer implications within the sycamore block, and to further understand the behaviour of the microwave pyrolysis process. The volatiles generation rate would be much greater if a high power density was employed, due to the same volume of vapour being produced in a shorter time than would be the case for a lower power density. The volatiles generation rate could have an effect on the physical properties of the sycamore block, affecting internal temperatures, pressures and dielectric properties, which could further affect the compositional breakdown of the sycamore block. The heating rate, and subsequent volatile generation rate is also a key differentiator between microwave pyrolysis and that carried out conventionally. Efforts to understand the effects of power

density could therefore be extrapolated to a broader understanding of microwave versus conventional pyrolysis, and this is further investigated in Sections 5.3.2 - 5.3.4.

5.3.2 Factors affecting temperature predictions of the sycamore block

Throughout the thesis, theoretical temperature predictions were presented based on an absorbed power basis. This method provided a basis for determining temperatures reached based on the sycamore physical properties, as the power absorbed was known from empirical data. It was evident from empirical observations, however, that the heating profile within the sycamore block during pyrolysis was heterogeneous; the power absorbed was assumed to be homogenous throughout the entire volume of the sycamore block for the heating model. In reality, however, some parts of the block were more pyrolysed than others due to the spatial power density distribution.

To better understand the extent of heterogeneous heating of the sycamore block during the pyrolysis process, computational simulations were carried out using the method outlined in Section 5.2.2.

Figure 5-7 presents the power density within the sycamore block during the pyrolysis process within the single-mode system for 1.5 kW applied power.

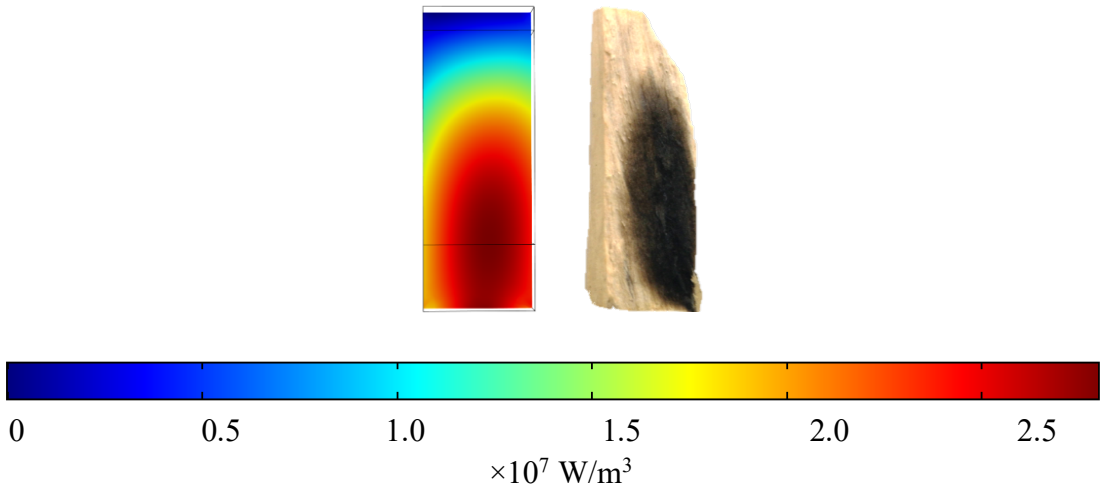


Figure 5-7 – (Left) The power density (W/m^3) distribution within the sycamore block in the single-mode liquid inerted microwave pyrolysis process at 1.5 kW applied power. (Right). A cross section of a sycamore block pyrolysed at 1.5 kW applied power, 0.5 kJ/g.

It can be seen from Figure 5-7 that the simulated power density distribution was similar to the empirical heating profile. This power density distribution supports the observation that the heating of the sycamore block during the pyrolysis process was not completely uniform. An example of the simulated and empirical heating profile for the multi-mode system is presented in Figure 5-8.

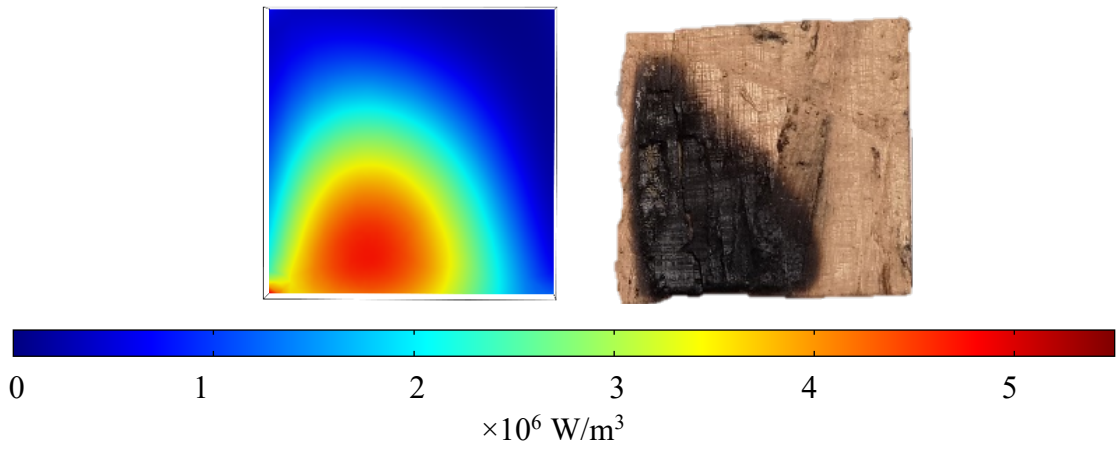


Figure 5-8 - (Left) The power density (W/m^3) distribution within the sycamore block in the multi-mode liquid inerted microwave pyrolysis process at 0.5 kW applied power. (Right). A cross section of a sycamore block pyrolysed at 0.5 kW applied power, 0.92 kJ/g.

Figure 5-8 shows that the power density distribution was similar to the empirical counterpart. The simulated profile shows a prominent heterogeneous heating profile, and therefore the block would experience higher temperatures at certain points of the block, as was observed empirically. The heating area appeared roughly similar to the single-mode system, however due to the size of the block, the degree of heterogeneity was greater.

Due to the heterogeneous heating profiles identified, the temperature reached during processing was determined at specific points for both the single-mode and multi-mode computational simulations, as presented in Figure 5-9.

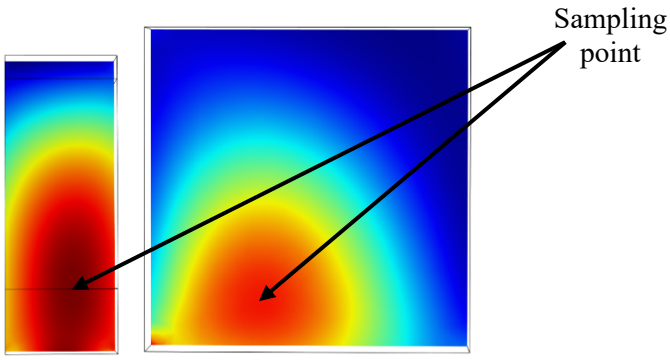


Figure 5-9 – Sampling points within the sycamore block for the single-mode and multi-mode computational simulations.

Figure 5-10 presents the internal sycamore block temperature as predicted by (1) the average absorbed power, (2) the spatial power density distribution and (3) with TGA for comparison over the pyrolysis processing time for the single-mode system.

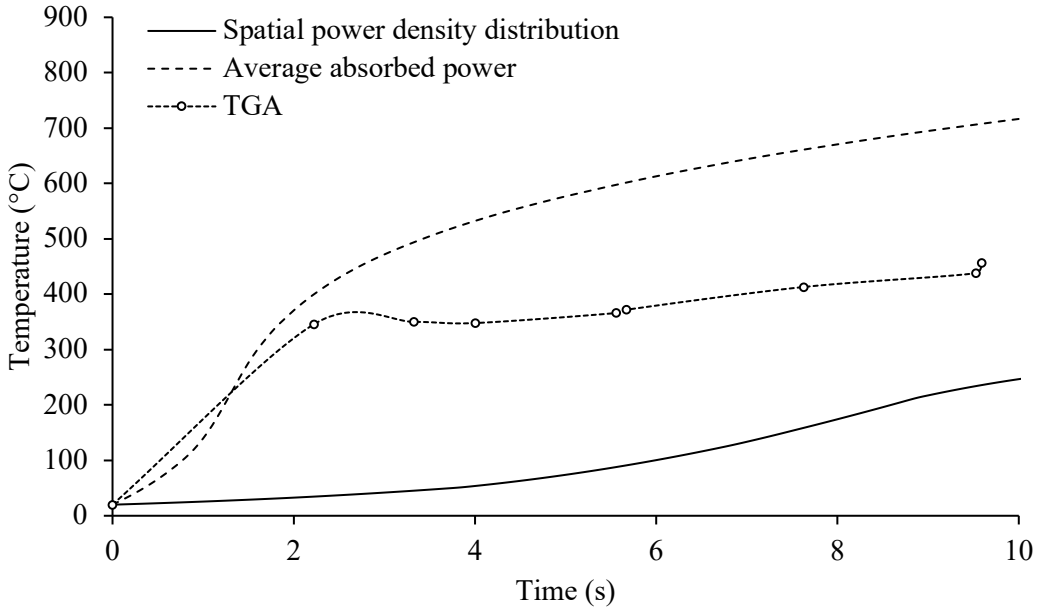


Figure 5-10 – Internal temperatures at the sampling point for a block heated by 1.5 kW power absorbed, and heated in the theoretical microwave field with 1.5 kW applied power, with temperatures predicted by TGA for comparison for the single-mode system.

It is evident from Figure 5-10 that for the single-mode microwave system, the internal temperature when predicted by the microwave field was dramatically underestimated for the entire processing time of the pyrolysis process. The peak temperature of the sycamore block obtained from the microwave heating model was 233 °C, compared to 456 °C predicted by TGA and 716 °C estimated by setting the power absorbed by the sycamore block. As the heating profile was predicted by the dielectric properties of the wood, it was possible that there were discrepancies between the measured dielectric properties of the sycamore from the cavity perturbation method, and during the pyrolysis process itself.

For the applied microwave field simulation, the absorbed power by the sycamore block was reliant on the dielectric properties, which due to the low values resulted in poor absorbance, as shown in Figure 5-11 (for the single-mode system).

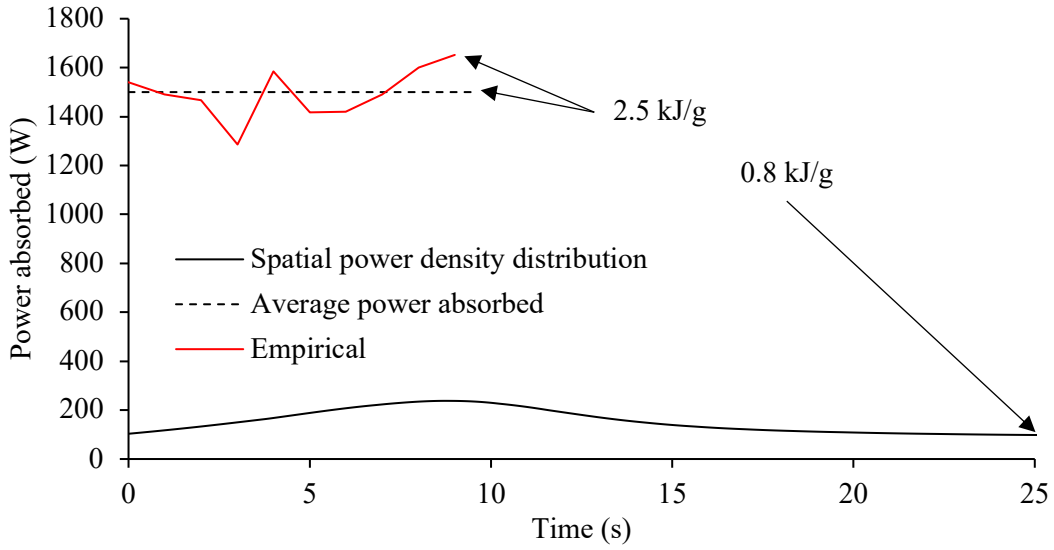


Figure 5-11 – The power absorbed of the microwave field model, power absorbed model, and empirical data for approximately 1.5 kW applied power (cyclohexane inerted), for the single-mode system.

Figure 5-11 shows that the poor absorbance in the spatial power density distribution model meant that the pyrolysis time of the theoretical process would be longer than the absorbed power model and empirical data for equivalent specific energies. The average absorbed power model and empirical processing time was approximately 10 seconds, whilst the spatial power density model processing time would be approximately 94 seconds, resulting in a greater surface cooling potential and a temperature plateau of 280 °C (Figure 5-10) due to the poor absorbance.

Figure 5-12 presents the internal sycamore block temperature as predicted by (1) the average absorbed power, (2) the spatial power density distribution and (3) with TGA for comparison over the pyrolysis processing time for the multi-mode system.

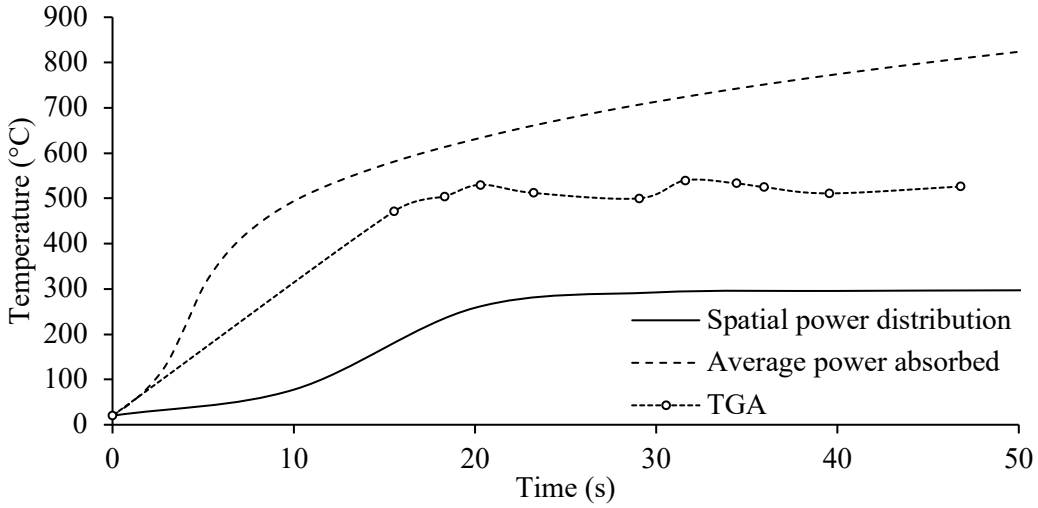


Figure 5-12 – The internal temperature at the sampling point for a block heated by 3.0 kW power absorbed, and heated in the theoretical microwave field with 3.0 kW applied power, with temperatures predicted by TGA for comparison for the multi-mode system.

Much like the single-mode system microwave model predictions, throughout the processing time range, the temperature of the sycamore block was underestimated for the microwave field model. This lower temperature would be likely due to the dielectric loss factor reaching its minimum value of 0.001 at around 280 °C and therefore the absorbance of the sycamore block was minimised, with minimum further heating occurring. For both the single-mode and multi-mode models, the power absorbed model overestimated the internal block temperatures, and the microwave field models underestimated the temperatures. The overestimation was possibly due to processing factors such as volatiles generation within the block that occurred due to the fast processing time not being accounted for in the determination of the specific heat capacity and thermal conductivity measurements, as they were conventionally heated and are much slower processes. The difference in predicted temperatures for the models and TGA suggest that the physical and dielectric properties of the sycamore used in simulations are not representative of those within a microwave heating environment.

During processing the power absorbed by the block could be quantified, and therefore the power absorbed model could be altered to fit the empirical absorbed power. The

addition of dielectric properties and a microwave field to predict power absorbed, when the heat transfer profile and dielectric properties were not completely explained, would therefore add a layer of complexity and source of error. As such, it was necessary to investigate potential sources of sensitivity to the sycamore physical properties, and also determine any differences in the dielectric properties of the sycamore block during microwave pyrolysis, compared to the cavity measurements.

The temperature of the sycamore block was dependent on multiple factors: specific heat capacity, thermal conductivity and heat transfer to the surroundings. The thermal conductivity determines heat transfer through the sycamore block, and therefore a higher thermal conductivity would result in lower temperatures achieved within the centre. For the single-mode system, the thermal conductivity required to match the internal temperature plateau of 450 °C, predicted by TGA at 2.5 kJ/g, was 41 times greater than the estimated value of 0.155 W/m·K. Changing the specific heat capacity to reach the peak value of 450 °C at 2.5 kJ/g required a value 3.5 times the value calculated by DSC, and drastically reduced the heating rate within the sycamore block, as shown in Figure 5-13.

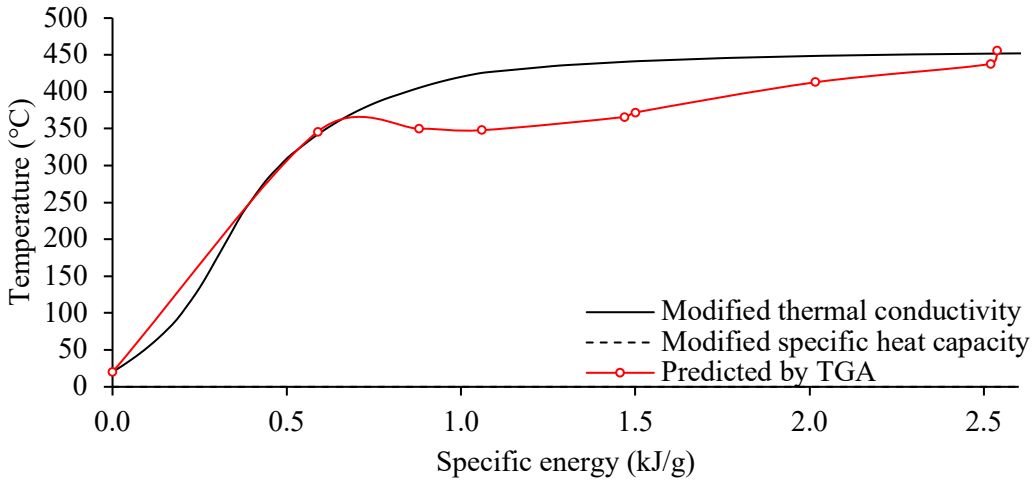


Figure 5-13 – The temperature at the centre of the 4.5 × 1.5 × 1.5 cm sycamore block, 1.5 kW absorbed power, with modified thermal conductivity (k×41), and modified specific heat capacity (C_p×3.5), with internal temperature predicted by TGA for reference.

Heat transfer through wood is anisotropic due to the grain direction within the structure itself (Hunt and Gu, 2006). With the thermal conductivity of wood in the grain direction being up to 3 times greater than the tangential direction and with char having a similar value to the estimated value of 0.155 W/m·K (Hankalin et al., 2009), variability in the heat transfer could be expected. The range of thermal conductivities for wood grain directions, however, are well outside the value required to limit the temperature of the sycamore to 450 °C, and as such, other factors such as volatiles generation could have an effect on the heating rate. For the models used to determine the internal temperature, the energy to the sample went towards the sensible heat, and as such raising the temperature of the block. If significant volatiles were present within the system, then it could be possible that the energy provided to the system would vaporise any liquid intermediates produced. It is therefore possible that due to the fast processing time of the microwave pyrolysis process, the large amount of volatiles production could potentially alter the physical and dielectric properties of the block as a whole.

5.3.3 Dielectric properties from the pyrolysis process

The cavity perturbation method, introduced in Section 2.3.1, was used to determine dielectric properties as a function of temperature. It was identified, however, that the properties determined by the cavity perturbation method were likely to be different to those that exist during microwave heating, due to the heating rate and volatiles production discrepancies between the microwave pyrolysis process and the cavity perturbation method. The absorbance and heating rate of the empirical blocks was both higher and quicker, respectively, than the microwave simulation results for the single-mode system. It was therefore necessary to estimate the dielectric properties of the sycamore block during the pyrolysis process and identify any differences to the cavity perturbation method dielectric properties.

The dielectric loss factor is a function of Equation 5-2 (Section 5.2.2), which considers power density absorbed by the sample and electric field strength. The absorbed power recorded during the pyrolysis process, coupled with the volume of the sycamore block could be used to determine the power density (W/m^3) at any point during the process. The electric field strength (V/m) was also required to predict the loss factor. To determine the electric field strength for all powers applied to the single-mode system, the empty single-mode system, and the system with the sycamore sample, quartz tube and cyclohexane liquid was simulated in COMSOL Multiphysics 5.3. The peak electric field strength in relation to the power applied to the single-mode system, along with the average electric field within the sycamore block is presented in Figure 5-14.

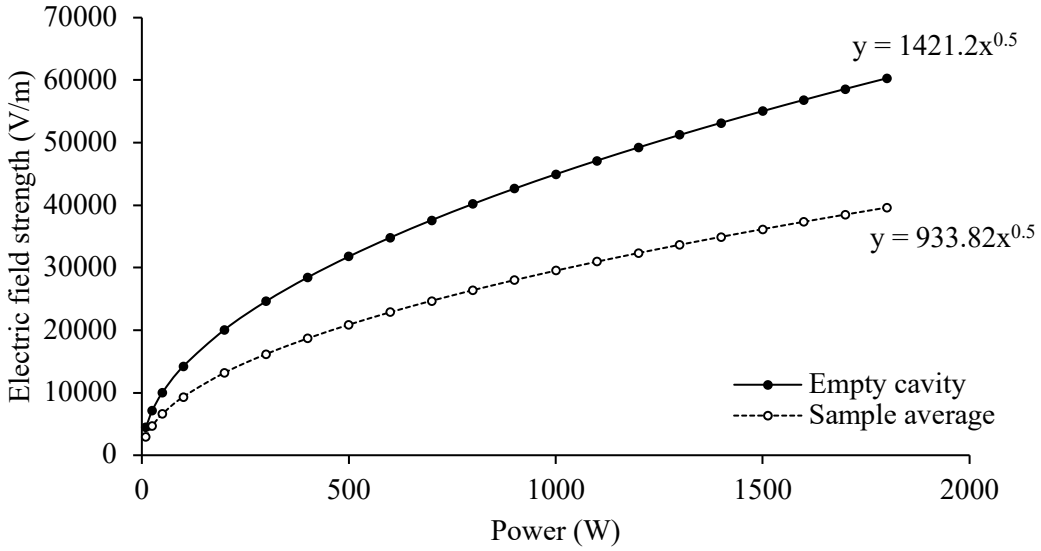


Figure 5-14 – The relationship between applied power and the peak electric field strength within the single-mode microwave pyrolysis system without the sample present, and with the sample present at 20 °C.

Figure 5-14 shows that when a sample is present in the microwave cavity, the electric field strength is lower, which is due to the higher loss factor of sycamore compared to air. Using the measured dielectric properties and the electric field strength, the theoretical absorbed power could be determined over the pyrolysis process temperatures (0 - 550°C) (Figure 5-15).

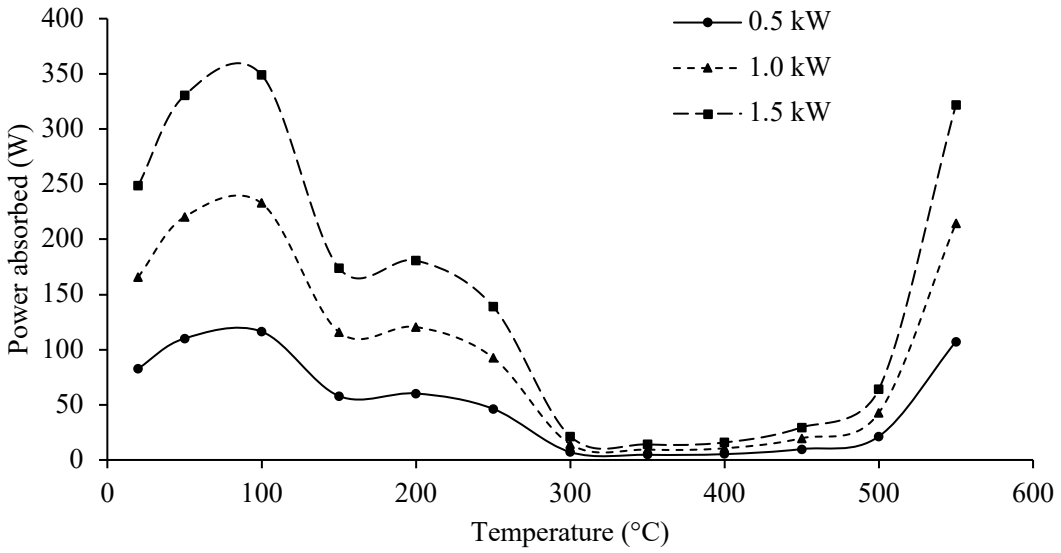


Figure 5-15 – Theoretical power absorbed by the sycamore block, based on applied powers of 0.5 – 1.5 kW, over the temperature range of 0 - 550°C.

It can be seen that from Figure 5-15, above temperatures of 300°C, not taking into account any solvent absorbance, the absorbed power would be expected to decrease to almost zero. This implies that little further heating would take place beyond 300 °C, which is consistent with the predicted temperatures using the microwave model (Figure 5-11 and Figure 5-12), but clearly inconsistent with the outcome of the empirical pyrolysis experiments predicted by TGA. The cavity perturbation technique heated conventionally and slowly (5 °C/min), which was very different to the rapid heating that actually occurred during microwave pyrolysis. It was possible, therefore, that the dielectric properties, measured by cavity perturbation, were not truly representative of the properties during the pyrolysis process. Therefore, analysis was carried out to estimate the magnitude of the dielectric properties that would be required to fit with the microwave pyrolysis observations.

Equation 5-2 (Section 5.2.2) was rearranged to form Equation 5-3, which was used determine the dielectric loss factor during the pyrolysis process.

$$\varepsilon'' = \frac{P}{2\pi f \varepsilon_0 E^2 V} \qquad 5\text{-}3$$

The loss factor was calculated for every time point within the pyrolysis process over 22 runs of varying powers applied and absorbed (0.6 – 1.8 kW applied power). The cavity perturbation method was conventionally heated, with dielectric properties measured at set temperatures rather than specific energies. To match the cavity perturbation measurements to process specific energies, temperatures estimated within the biomass at specific energies (determined by TGA, Section 3.4.6.2) were equated to the cavity dielectric properties at the same temperatures to provide comparisons to the pyrolysis process. The dielectric loss factor of the sycamore block during the pyrolysis process compared to the cavity perturbation method values is presented in Figure 5-16.

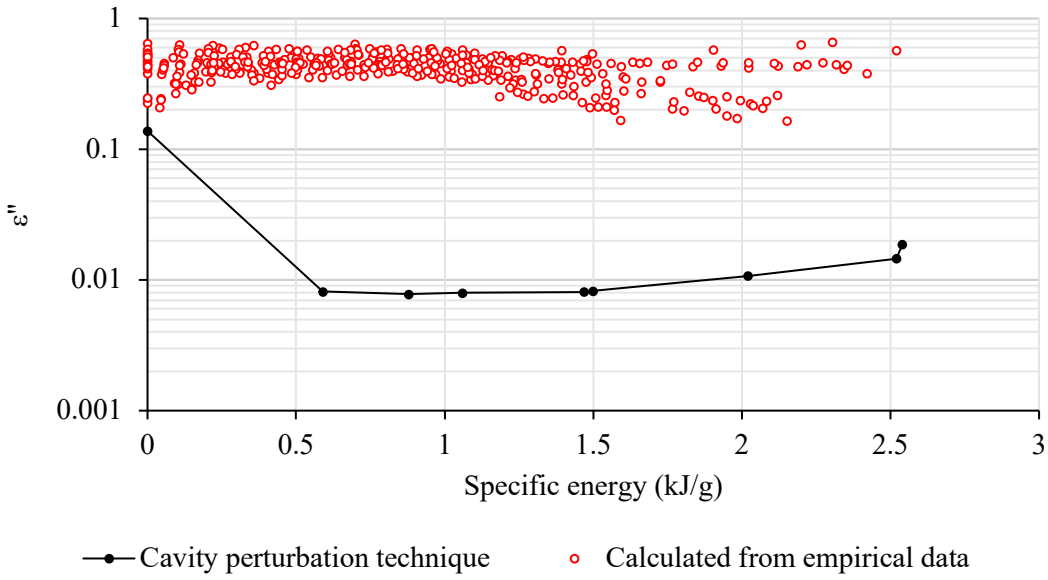


Figure 5-16 – The dielectric loss factor for sycamore within the single-mode liquid inerted pyrolysis process over 22 runs, 0.6 – 1.8 kW applied power.

Figure 5-16 presents that initially, the loss factor calculated by the cavity and the process were within the same order of magnitude, 0.14 – 0.58. Once the pyrolysis process began, however, the loss factor for the cavity perturbation method decreased

by a magnitude of 10, while the calculated loss factors from the process itself remained similar to the starting values.

For all processing conditions investigated, the dielectric loss factor of the sycamore block based on power absorbed was significantly higher than equivalent loss factors presented by the cavity perturbation method. The higher dielectric loss factor could be due to the short processing times (<30 seconds) compared to the cavity perturbation method. The volatiles production during the microwave pyrolysis process would be significant within this time frame, which could affect the dielectric properties of the sycamore block during the process (the rate of volatiles production is explained further in Section 5.3.4). The cavity perturbation method ramped at 5°C/min, likely allowing for very slow volatiles production. Therefore, any influence of the volatiles produced on the dielectric properties of the sycamore would have been lost. Levoglucosan was previously identified as a prominent compound within pyrolysis oil, and could be considered representative of volatiles from cellulose (Suuberg and Oja, 1997), the dielectric properties of levoglucosan over 20 - 350 °C were previously measured by J. Robinson (Appendix D, Table D-2). Liquid levoglucosan has a dielectric constant and loss factor of approximately 4 and 0.4, respectively, and around the boiling point of levoglucosan (~300 °C), the dielectric constant and loss factor are 1.658 and 0.022 respectively, larger than the cavity measurement equivalents for sycamore. It is possible that higher pressures, due to significant volatiles production, within the sycamore block would result in the volatiles boiling at higher temperatures than atmospheric pressure. This would therefore result in the microwave energy being absorbed by the volatiles, and energy provided to the sample going towards volatilisation of the liquid intermediate, potentially causing a temperature plateau as predicted empirically by TGA. The pressure investigation on volatiles produced is explained further in Section

5.3.4. It was therefore necessary to investigate the dielectric properties of the wood during a rapid microwave heating process, rather than a slow conventional process.

Initial testing on the measuring the dielectrics of the sycamore during microwave pyrolysis was carried out by collaborators at the University of Valencia. A sycamore cylinder of diameter. 9.8 ±0.1 mm and 10 mm height was placed into a cavity and heated with microwaves, with the dielectric properties measured at specific time points. The dielectric constant and loss factor in comparison to the cavity perturbation method are presented in Figure 5-17.

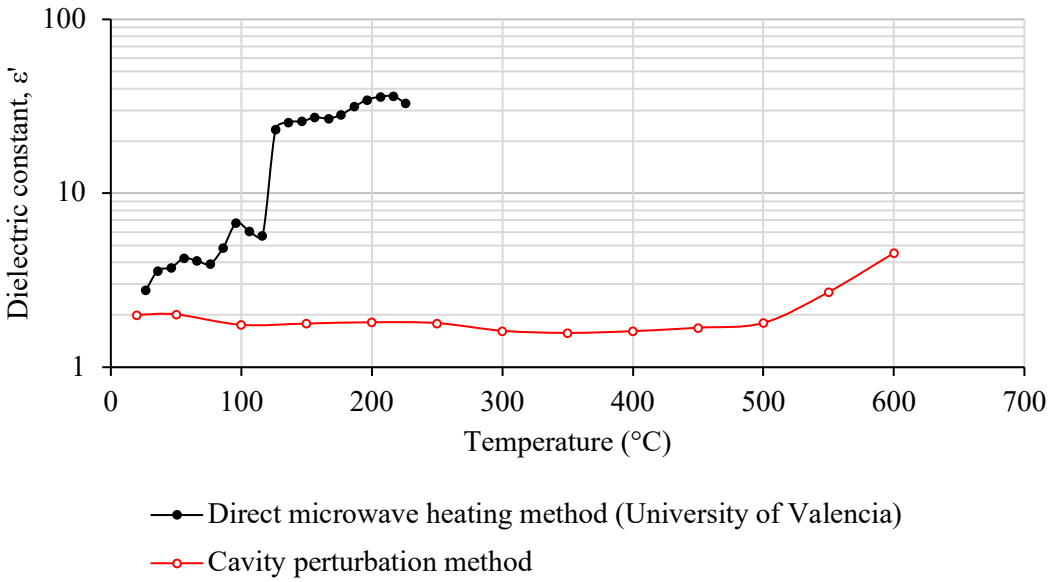


Figure 5-17 – The dielectric constant of the sycamore over the temperature range 0 – 600 °C for the microwave method and the cavity perturbation method.

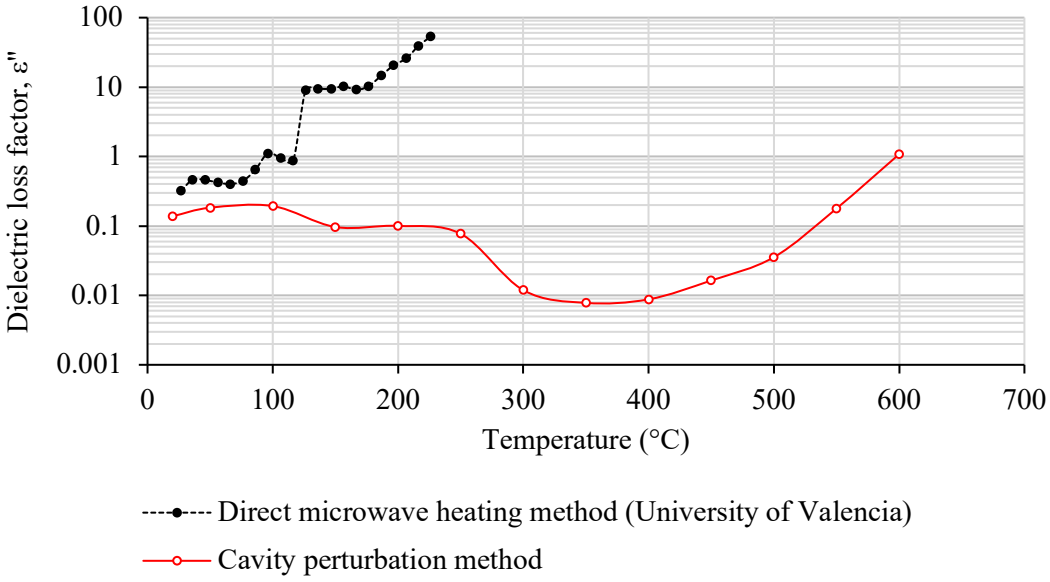


Figure 5-18 - The dielectric loss factor of the sycamore over the temperature range 0 – 600 °C for the microwave method and the cavity perturbation method.

It is highlighted in Figure 5-17 and Figure 5-18 that the dielectric properties of the sycamore when undergoing microwave pyrolysis were dramatically different to when the sample was heated conventionally. At room temperature (20°C), the dielectric properties were within the same order of magnitude, however the microwave dielectrics increased gradually until 116°C, until increasing by a factor of 50 - 60. The maximum dielectric constant and loss factor from the cavity method were 4.53 and 2.62, respectively, at 600°C, whereas for the microwave method they were 32.88 and 53.13, respectively, at 226°C. After 226°C for the microwave cavity method, the volatiles generation and pressure caused the sycamore cylinder to be ejected from the sample holder, preventing further measurement.

It was shown in Figure 5-18 that the dielectric properties of the sycamore were consistent across the pyrolysis process. Therefore, an approximate predicted value of 2.8 for the dielectric constant, and 0.5 for the loss factor, approximately the initial

dielectric properties of the sycamore was used. The internal temperature of the sycamore block, 1.5 kW applied power, 10 seconds is shown in Figure 5-19.

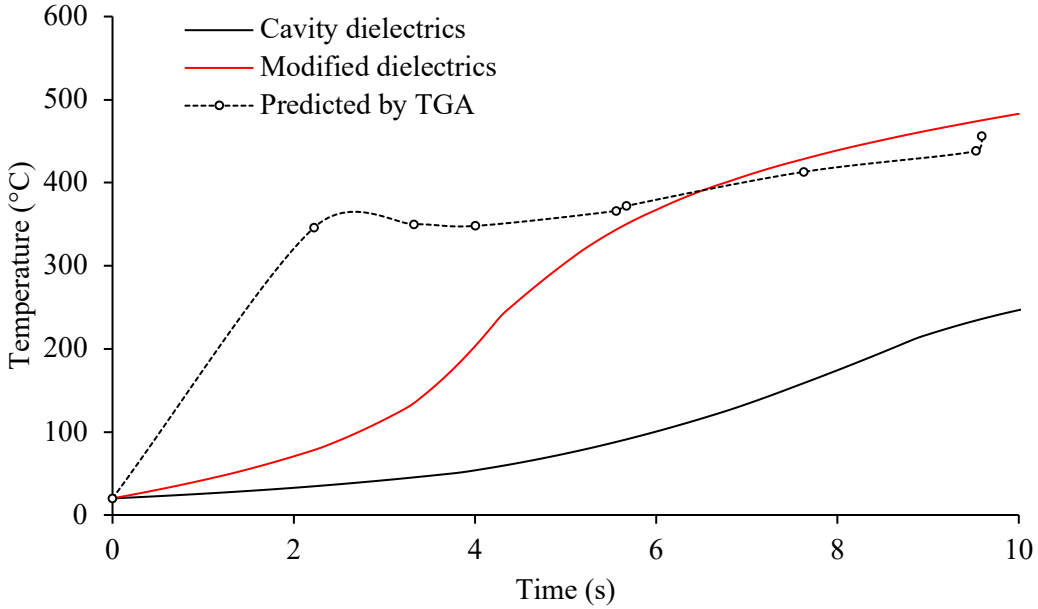


Figure 5-19 – The internal temperature at the sampling point for a sycamore block heated in the theoretical microwave field with 1.5 kW applied power, with the cavity dielectrics and modified dielectrics, with temperatures predicted by TGA for comparison for the single-mode system.

Figure 5-19 highlights that in terms of the internal heating rate of the sycamore block, the peak temperature reached within the sycamore block matched the empirical predictions more closely when using dielectric properties derived from the process itself than from the microwave heating cavity method. The heating rate of the sycamore block below 5 seconds was still slower than the prediction by TGA, and therefore factors that were not considered by the models, such as volatiles production, could have an effect on the dielectric properties and physical properties of the block as a whole, and subsequently the heating rate of the block.

The disparity between the cavity perturbation dielectric properties, the empirical dielectric properties based on the Meredith (1998) equation, and the microwave cavity dielectric properties throughout the pyrolysis temperature range highlight the

challenges with using conventional heating methods to predict microwave processing parameters. Potential significant internal pressures were identified by observations; the sycamore block warped (Section 3.4.6.1), significant volatile volumetric production was observed (Section 3.4.7), and the sycamore block ejected from the microwave dielectric measurement system. As it was identified that prominent oil compounds have higher dielectric properties than the sycamore block during the cavity perturbation method, and the microwave dielectric measurement method showed high dielectric properties, the potential internal pressure within the sycamore block during the pyrolysis process was therefore determined to be investigated.

5.3.4 Pressure generation within the sycamore during pyrolysis

It was identified in Section 5.3.3 that there was a discrepancy with the dielectric properties of the sycamore block during microwave pyrolysis when compared to the cavity perturbation method. The primary reason for this is that microwave absorbent volatiles produced during the pyrolysis process are maintained within the biomass due to mass transfer restrictions. The mass lost from the sycamore during the pyrolysis process was due to the thermochemical decomposition of the sycamore constituents (cellulose, hemicellulose and lignin), and subsequent volatiles ejection from the sycamore block structure. The mass lost from the sycamore therefore occurred due to a pressure gradient within the sycamore block, a high pressure inside would have been required to force the volatiles out of the block structure. High pressures could therefore act to sustain the presence of microwave-absorbent volatiles (e.g. Levoglucosan) at temperatures in excess of their normal boiling point. Testing this hypothesis requires that the rate of volatiles generation is quantified, which can therefore be used to estimate the likely pressure that will occur within a given geometry during the pyrolysis process.

Internal pressures of the sycamore block during the pyrolysis process could not be directly measured, although it was evident that during the process, warping of the block structure and significant volatiles ejection from the block occurred. Two approaches are investigated in terms of predicting internal pressures:

1) Using mass loss data for the pyrolysis process and the time of processing, a volatiles generation rate could be determined, and as such pressures calculated using literature values for permeability.

2) Using established kinetic decomposition models available from literature, based on temperature.

For the first model, the gradient of the mass loss curve based on the processing time of the pyrolysis process represented the rate of volatiles production. Figure 5-20 presents the mass loss data for 1.5 kW absorbed for the single-mode system as a function of time.

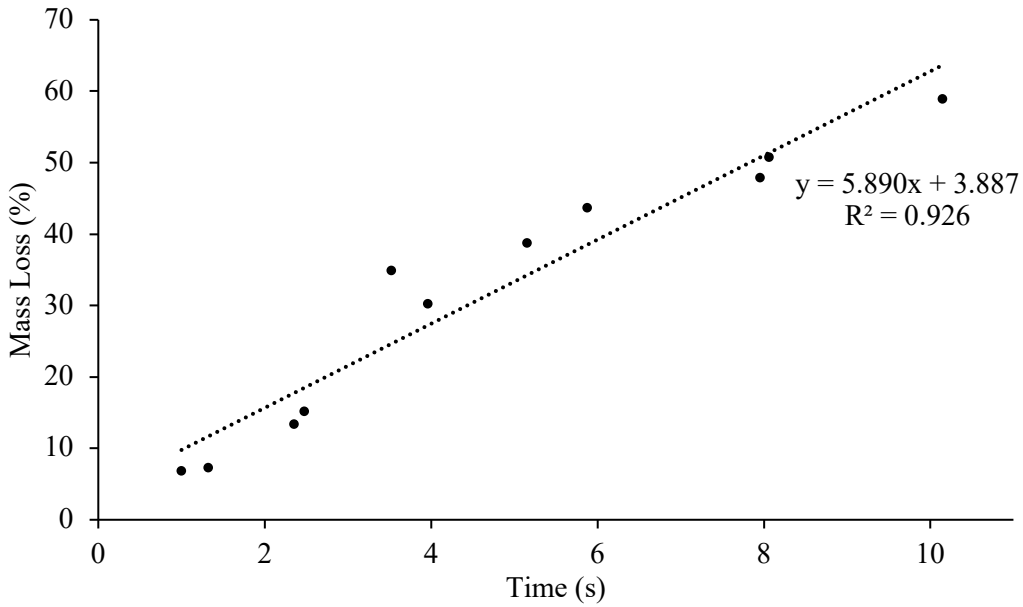


Figure 5-20 – The mass loss data for approximately 1.5 kW absorbed power, 6 ±0.25 g sycamore block mass.

Figure 5-20 shows that approximating the mass loss on a linear basis, the rate of mass loss could be approximated to 5.89 %/s (0.35 g/s on a mass basis or 35 kg/m^3·s on a density basis).

Using Darcy's law (on a mass concentration generation basis), which describes fluid flow through a porous medium, internal pressures of the sycamore could be estimated using equations 5-4 and 5-5.

$$\frac{\delta}{\delta t}\left(\varepsilon_p \rho\right) + \nabla(\rho \boldsymbol{u}) = Q_m \qquad 5\text{-}4$$

$$\boldsymbol{u} = -\frac{\kappa}{\mu} \nabla p \qquad 5\text{-}5$$

Where:

Q_m	-	Volatiles mass concentration generation rate, kg/m^3·s
ε_p	-	Porosity
ρ	-	Mass concentration of the volatiles produced, kg/m^3
u	-	Velocity of volatiles, m/s
κ	-	Intrinsic permeability, m^2 (m$^3_{gas}$/m$_{wood}$)
μ	-	Dynamic viscosity, Pa·s
∇p	-	Pressure gradient vector, Pa/m

The first investigation involved pressure generation based on volatiles generation, with no change in the overall sycamore block structure, and no temperature calculations carried out. The simple model would allow for determination of the peak pressure within the sycamore block, as at the onset of volatilisation and mass loss, the sycamore block would be at its initial permeability and porosity values. The simple process is shown in Figure 5-21. The initial parameters for the wood and volatiles, such as porosity, permeability and dynamic viscosity are presented in Appendix D, Table D-1.

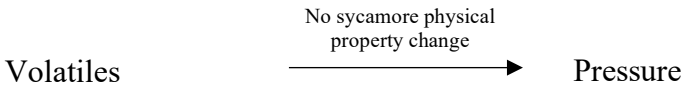


Figure 5-21 – The simple schematic for determining peak pressure within the sycamore block during microwave pyrolysis.

Figure 5-22 presents the pressure within the sycamore block based solely on volatiles generation.

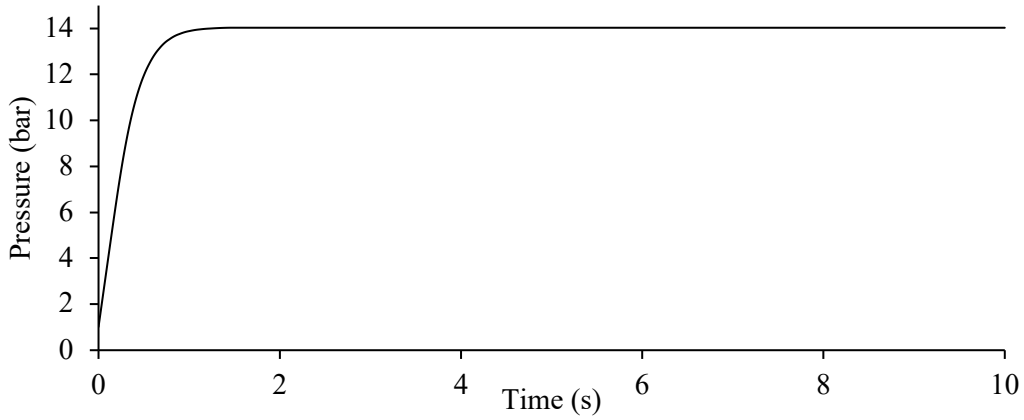


Figure 5-22 – Pressure generation within the 4.5 × 1.5 × 1.5 cm sycamore block during the pyrolysis process, with no physical changes to the sycamore block.

It is evident that when no physical changes occured within the sycamore block during the pyrolysis process, the pressure reached a peak of approximately 14 bar and plateaued. The plateau would likely not occur in reality, as due to the decomposition of the sycamore structure, the porosity and permeability of the sycamore block would increase.

The volatiles generation model applied with increasing permeability and porosity of the sycamore block presents a process as shown in Figure 5-23. The permeability and porosity changes over the process are stated in Appendix D, Table D-4.

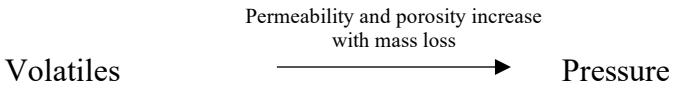


Figure 5-23 – The schematic for determining peak pressure within the sycamore block during microwave pyrolysis, with permeability and porosity changes applied.

Figure 5-24 presents the pressure within the sycamore block based on volatiles generation with increasing permeability and porosity as the block becomes more pyrolysed.

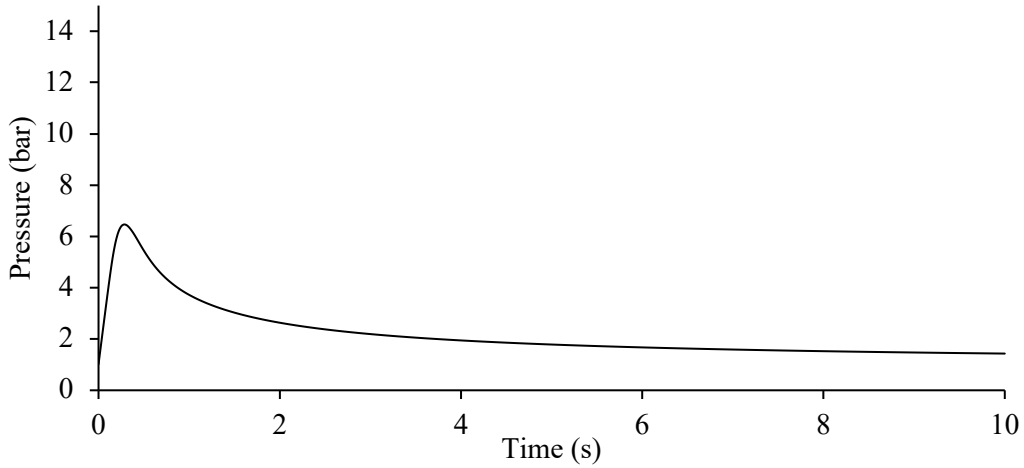


Figure 5-24 – Pressure generation within the 4.5 × 1.5 × 1.5 cm sycamore block during the pyrolysis process, permeability and porosity increases considered.

Figure 5-24 illustrates that if the porosity and permeability increase linearly with the mass loss of the sycamore block, then the peak pressure obtained is less than 50 % of the pressure obtained if the sycamore block structure is assumed to be unchanged (6.25 bar compared to 14 bar). The equation for the permeability of the block was much more sensitive to the degree of pyrolysis than porosity; the range of the permeability values was 5×10^{-16} - 1×10^{-13} m^2 (Di Blasi, 2000), meaning the permeability at complete pyrolysis was 200 times greater than the starting value, whereas the porosity value ranged from 0.4 – 0.76 (based on the processing parameters in Appendix D.3). The permeability of the wood as a whole varies based on physical properties, moisture

content, tangential and radial grain directions, and even where the wood sample was taken from (Hansmann et al., 2002). The value range for permeabilities, however, were within the range determined for wood from literature (Lihra et al., 2007). It was therefore evident that the pressure generation within the sycamore block was very sensitive to the permeability of the sycamore block, as the permeability at the peak pressure (1.29 seconds) was 4.4 times the starting value. Figure 5-25 displays the sensitivity of the peak pressure obtained within the sycamore blocks, for both the single-mode and multi-mode scale blocks, in terms of the permeability of the sycamore block.

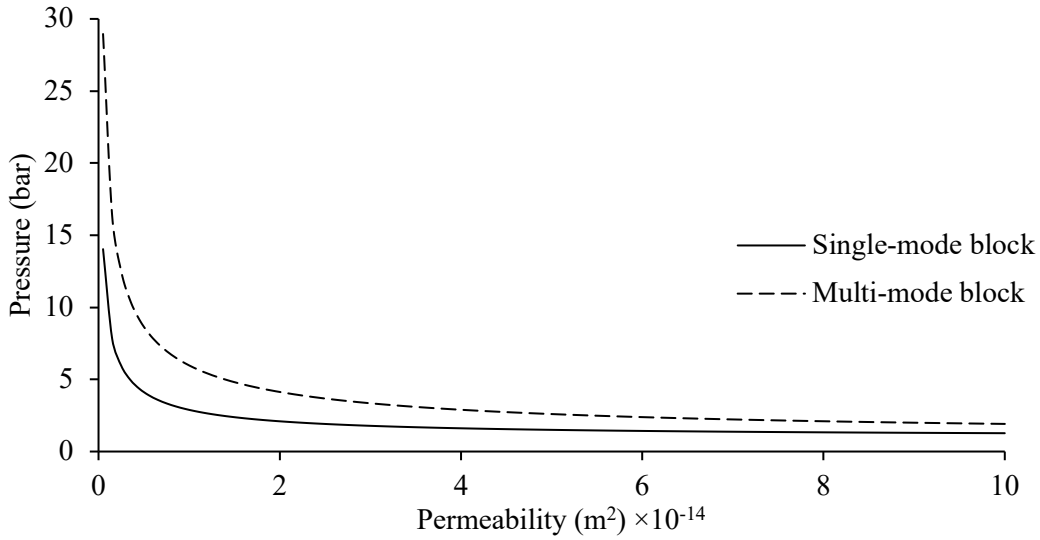


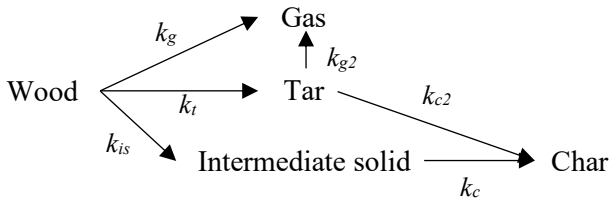
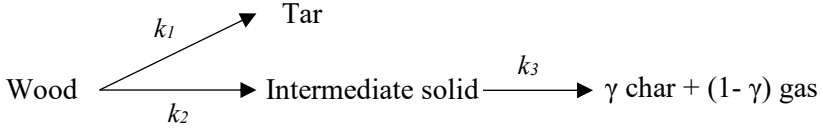
Figure 5-25 – The peak pressure within the 4.5 × 1.5 × 1.5 cm, and 5.0 × 5.0 × 2.5 cm sycamore block against the processing permeability range.

There is evident pressure sensitivity to the permeability and block size during the pyrolysis process, with the multi-mode block exhibiting around double the pressure obtained within the single-mode block. As the sycamore block starts to pyrolyse and become charred, it is possible that the permeability increase due to the compositional breakdown results in less restriction to the flow of volatiles, as shown by the pressure/volatiles flow relationship in Equation 5-5, reducing the internal pressure of the sycamore block. Further investigation into established decomposition models was

therefore determined to be necessary to provide a point of comparison to the volatiles generation model; the literature models utilised Arrhenius rate equations for the decomposition of the biomass based on temperatures reached. The initial volatiles generation model assumed linear volatiles production, whereas there would likely be variability based on the biomass constituent decomposition (cellulose, hemicellulose and lignin).

Four literature models are presented, the first model involved the decomposition of wood to gas, tar and char via an intermediate solid (Park et al., 2010), the second model involved the decomposition of lignin (Chan and Krieger, 1981), cellulose (Capart et al., 2004) and hemicellulose (Varhegyi et al., 1989) to volatiles and char. The third model also involved cellulose, hemicellulose and lignin to char and volatiles (Ding et al., 2018). The fourth model involved decomposition of wood to tar and char (Kilzer and Broido, 1965, Park et al., 2010, Mok and Antal, 1983). For all four literature models investigated, the volatiles generation rate was calculated by Arrhenius rate equations, coupled with the mass concentration (kg/m^3) of the reacting material, to produce volatiles as a rate ($kg/m^3 \cdot s$). The volatiles generation rate was then used in Equations 5-4 and 5-5 to determine pressures within the sycamore block during pyrolysis. Heat transfer within the sycamore was calculated using absorbed power as a heat source, Darcy's law was used to determine pressures achieved within the sycamore block, and the volatiles produced were assumed to be produced in the pores of the sycamore block. The wood decomposition models are shown in Table 5-1.

Table 5-1 – The four models presented and their respective kinetic parameters.

		Kinetics	Reference
Model 1		$k_i = A_i e^{\frac{-E_i}{RT}}$ i = g, t, is, c, g2, c2	(Park et al., 2010)
Model 2	Cellulose$_A$ $\xrightarrow{A}$ (1-γ_A) volatiles + γ_A char Cellulose$_B$ $\xrightarrow{B}$ (1-γ_B) volatiles + γ_B char	$\frac{d\omega_i}{dt} = -Ae^{\frac{-E}{RT}}\omega_i{}^{n_i}(1-0.99\omega_i)^{m_i}$, $i = A,B$, $\omega_i = \frac{\rho_{cli}}{\rho_{cli,0}}$, $\rho_{cl} = \rho_{clA} + \rho_{clB}$	(Capart et al., 2004)
	Hemicellulose $\xrightarrow{k_1}$ (1-γ_1) volatiles + γ_1 intermediate solid Intermediate solid $\xrightarrow{k_2}$ (1-γ_2) volatiles + γ_2 char	$k_i = A_i e^{\frac{-E_i}{RT}}$ i = 1, 2, l	(Varhegyi et al., 1989)
	Lignin $\xrightarrow{k_l}$ (1-γ_l) volatiles + γ_l char	$k_i = A_i e^{\frac{-E_l}{RT}}$	(Chan and Krieger, 1981)
Model 3	Cellulose $\xrightarrow{C}$ (1-γ_A) volatiles + γ_A char Hemicellulose $\xrightarrow{H}$ (1-γ_h) volatiles + γ_h char Lignin $\xrightarrow{L}$ (1-γ_l) volatiles + γ_l char	$\frac{d\omega_i}{dt} = -\left(\frac{\rho_{i,0}}{\rho_w}\right)\omega_i{}^{n_i}Ae^{\frac{-E}{RT}}$ $i = C, H, L$, $\omega_i = \frac{\rho_i}{\rho_{i,0}}$	(Ding et al., 2018)
Model 4		$k_i = A_i e^{\frac{-E_i}{RT}}$ i = 1, 2, 3	(Kilzer and Broido, 1965, Park et al., 2010, Mok and Antal, 1983)

For all four models investigated, the temperature increase of the sycamore block was determined from absorbed power, for models 2 and 3, the lignocellulosic composition and moisture content were considered in the absence of extractives. The compositional data presented in Section 4.4.6.1 accounted for 87.6 % of the total wood mass, with the moisture content of 6.4 % included, 94 % of the total mass was accounted for. To reach a total of 100 %, the extractives content was discounted, and the lignocellulosic composition was altered to account for 93.6 % of the composition. The new composition assumed for models 2 and 3 is shown in Table 5-2.

Table 5-2 – The modified composition of the sycamore block for models 2 and 3.

Sample	Lignin (%)	Cellulose (%)	Hemicellulose (%)	Moisture (%)
Sycamore	35.9	38.4	19.3	6.4

For all four models, water evaporation kinetics by Ding et al. (2018) were applied, as shown in Figure 5-26, the kinetic parameters are presented in Appendix D, Table D-5.

$$H_2O_{Liquid} \xrightarrow{k_{H2O}} H_2O_{Vapour}$$

Figure 5-26 – The drying process of all four models, $k_{H2O} = A_{H2O} e^{\frac{-E_{H2O}}{RT}}$, (Ding et al., 2018).

Models 1 and 4 assume that there is competition between gas, tar and char yield during the pyrolysis process, with gas yield increasing with longer residence times. The lignocellulosic models 2 and 3 assume that each biomass constituent is responsible for its own generation of volatiles and char. The kinetic parameters for each model and the heat of pyrolysis (Δh) during the pyrolysis process, and the material properties of the wood and volatiles are shown in Appendix D, Table D-6 – Table D-10. The mass generation and mass conservation reactions during the process are shown in Table 5-3.

Table 5-3 – Governing equations for models 1 – 4 (Park et al., 2010, Chan and Krieger, 1981, Capart et al., 2004, Varhegyi et al., 1989, Kilzer and Broido, 1965, Mok and Antal, 1983).

	Model 1	**Model 2**	**Model 3**	**Model 4**
Solid mass generation	$\frac{\delta\rho_a}{\delta t} = S_a = -(k_t + k_g + k_{is})\rho_a$ $\frac{\delta\rho_{is}}{\delta t} = S_{is} = k_{is}\rho_a - k_c\rho_{is}$ $\frac{\delta\rho_c}{\delta t} = S_c = k_c\rho_{is} + k_{c2}\rho_t$	$\frac{\delta\rho_{hcl}}{\delta t} = S_{hcl} = -k_1\rho_{hcl}$ $\frac{\delta\rho_{is}}{\delta t} = S_{is} = \gamma_1 k_1\rho_{hcl} - k_2\rho_{is}$ $\frac{\delta\rho_{clA}}{\delta t} = S_{clA} = \rho_{clA,0}\frac{d\omega_A}{dt}$ $\frac{\delta\rho_{clB}}{\delta t} = S_{clB} = \rho_{clB,0}\frac{d\omega_B}{dt}$ $\rho_{cl} = \rho_{clA} + \rho_{clB}$ $\frac{\delta\rho_l}{\delta t} = S_l = -k_l\rho_l$ $\frac{\delta\rho_c}{\delta t} = S_c = \gamma_2 k_2\rho_{is} + \gamma_A k_A\rho_{clA} + \gamma_B k_B\rho_{clB} + \gamma_A k_l\rho_l$	$\frac{\delta\rho_H}{\delta t} = S_H = \rho_{H,0}\frac{d\omega_H}{dt}$ $\frac{\delta\rho_C}{\delta t} = S_C = \rho_{C,0}\frac{d\omega_C}{dt}$ $\frac{\delta\rho_L}{\delta t} = S_L = \rho_{L,0}\frac{d\omega_L}{dt}$ $\frac{\delta\rho_c}{\delta t} = S_c = \gamma_C k_C\rho_C + \gamma_H k_H\rho_H + \gamma_L k_L\rho_L$	$\frac{\delta\rho_a}{\delta t} = S_a = -(k_1 + k_2)\rho_a$ $\frac{\delta\rho_{is}}{\delta t} = S_{is} = k_2\rho_a - k_3\rho_{is}$ $\frac{\delta\rho_c}{\delta t} = S_c = \gamma k_3\rho_{is}$
Gas phase masses	$\frac{\delta(\varepsilon\rho_t)}{\delta t} = S_t = k_t\rho_a - (k_{c2} + k_{g2})\rho_t$ $\frac{\delta(\varepsilon\rho_g)}{\delta t} = S_g = k_g\rho_a + k_{g2}\rho_t + k_{H2O}\rho_{H2OV}$	$\frac{\delta(\varepsilon\rho_v)}{\delta t} = S_v = (1-\gamma_1)k_1\rho_{hcl} + (1-\gamma_2)k_2\rho_{is} + (1-\gamma_A)k_A\rho_{clA} + (1-\gamma_B)k_B\rho_{clB} + (1-\gamma_l)k_l\rho_l + k_{H2O}\rho_{H2OV}$	$\frac{\delta(\varepsilon\rho_v)}{\delta t} = S_v = (1-\gamma_C)k_C\rho_C + (1-\gamma_H)k_H\rho_H + (1-\gamma_L)k_L\rho_L + k_{H2O}\rho_{H2OV}$	$\frac{\delta(\varepsilon\rho_t)}{\delta t} = S_t = k_1\rho_a + k_{H2O}\rho_{H2OV}$
Total pressure	$\frac{\delta}{\delta t}\left(\frac{\varepsilon P}{T}\right) = \frac{R}{M_t}S_t + \frac{R}{M_g}S_g + \frac{R}{M_{H2O}}S_{H2O}$	$\frac{\delta}{\delta t}\left(\frac{\varepsilon P}{T}\right) = \frac{R}{M_v}S_v + \frac{R}{M_{H2O}}S_{H2O}$	$\frac{\delta}{\delta t}\left(\frac{\varepsilon P}{T}\right) = \frac{R}{M_v}S_v + \frac{R}{M_{H2O}}S_{H2O}$	$\frac{\delta}{\delta t}\left(\frac{\varepsilon P}{T}\right) = \frac{R}{M_t}S_t + \frac{R}{M_g}S_g + \frac{R}{M_{H2O}}S_{H2O}$
Heat generation	$Q = -\left(k_t\Delta h_t + k_g\Delta h_g + k_{is}\Delta h_{is}\right)\rho_a - \left(k_{g2}\Delta h_{g2} + k_{c2}\Delta h_{c2}\right)\rho_t - k_c\Delta h_c\rho_{is} - \Delta h_{H2O}k_{H2O}\rho_{H2OL}$	$Q = (S_{hcl} + S_{is})\Delta h_{hcl} + (S_{clA} + S_{clB})\Delta h_{cl} + S_l\Delta h_l - \Delta h_{H2O}k_{H2O}\rho_{H2OL}$	$Q = (S_{hcl} + S_{is})\Delta h_{hcl} + (S_{clA} + S_{clB})\Delta h_{cl} + S_l\Delta h_l - \Delta h_{H2O}k_{H2O}\rho_{H2OL}$	$Q = -(k_1\Delta h_1 + k_2\Delta h_2)\rho_a - k_3\rho_{is}\Delta h_3 - \Delta h_{H2O}k_{H2O}\rho_{H2OL}$

Table 5-4 – Variable properties of the wood for models 1 – 4 (Park et al., 2010).

	Model 1	**Model 2**	**Model 3**	**Model 4**
Porosity	$\varepsilon = 1 - \frac{\rho_a + \rho_{is} + \rho_c}{\rho_{wood}}(1 - \varepsilon_{wood})$	$\varepsilon = 1 - \frac{\rho_{cl} + \rho_{hcl} + \rho_l + \rho_{is} + \rho_c}{\rho_{wood}}(1 - \varepsilon_{wood})$	$\varepsilon = 1 - \frac{\rho_{cl} + \rho_{hcl} + \rho_l + \rho_c}{\rho_{wood}}(1 - \varepsilon_{wood})$	$\varepsilon = 1 - \frac{\rho_a + \rho_{is} + \rho_c}{\rho_{wood}}(1 - \varepsilon_{wood})$
Gaseous flow velocity	$u = -\frac{\kappa}{\mu}\nabla\delta P$			
Wood permeability	$\kappa = (1 - \eta)\kappa_{wood} + \eta\kappa_c$			
Degree of pyrolysis	$\eta = 1 - \frac{\rho_a + \rho_{is}}{\rho_{wood}}$	$\eta = 1 - \frac{\rho_{cl} + \rho_{hcl} + \rho_l + \rho_{is}}{\rho_{wood}}$	$\eta = 1 - \frac{\rho_{cl} + \rho_{hcl} + \rho_l}{\rho_{wood}}$	$\eta = 1 - \frac{\rho_a + \rho_{is}}{\rho_{wood}}$

One of the benefits microwave pyrolysis offers over conventional pyrolysis is the opportunity for utilising larger particle sizes. Figure 5-27 shows the internal temperature increase for a 4.5×1.5×1.5 cm sycamore block heated homogenously at 1.5 kW power absorbed, versus the same particle placed in a 1000 °C furnace.

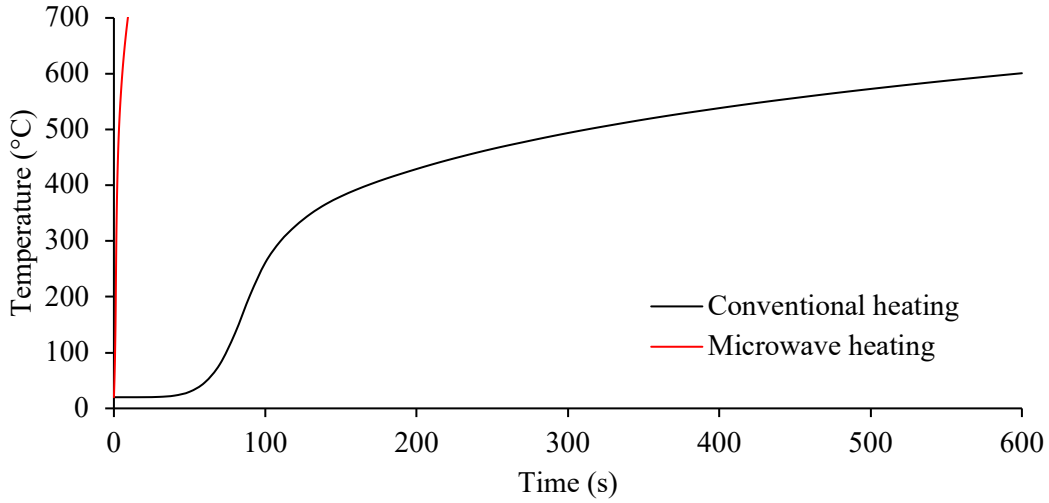


Figure 5-27 – Internal temperature prediction (modelled) over time for a 4.5×1.5×1.5 cm block in a furnace at 1000 °C, and heated by microwave with 1.5 kW absorbance.

It can be seen from Figure 5-27 that utilising a block size similar to the microwave pyrolysis process (4.5×1.5×1.5 cm) would not be possible in a conventional process when considering similar time-scales. Despite the evidence that the temperature prediction model overestimated internal temperatures based on average power absorbed and the physical properties of the sycamore block, in a conventionally heated process, an internal temperature of 500 °C would require 320 seconds to achieve. To present a comparison of pressures reached during a conventional process, a particle size of 1 mm diameter placed in a 1000°C furnace is presented as a comparison to the microwave pyrolysis process, along with literature values, where possible.

The pressure generation within the centre of the sycamore blocks/particles for the literature models are presented in Figure 5-28.

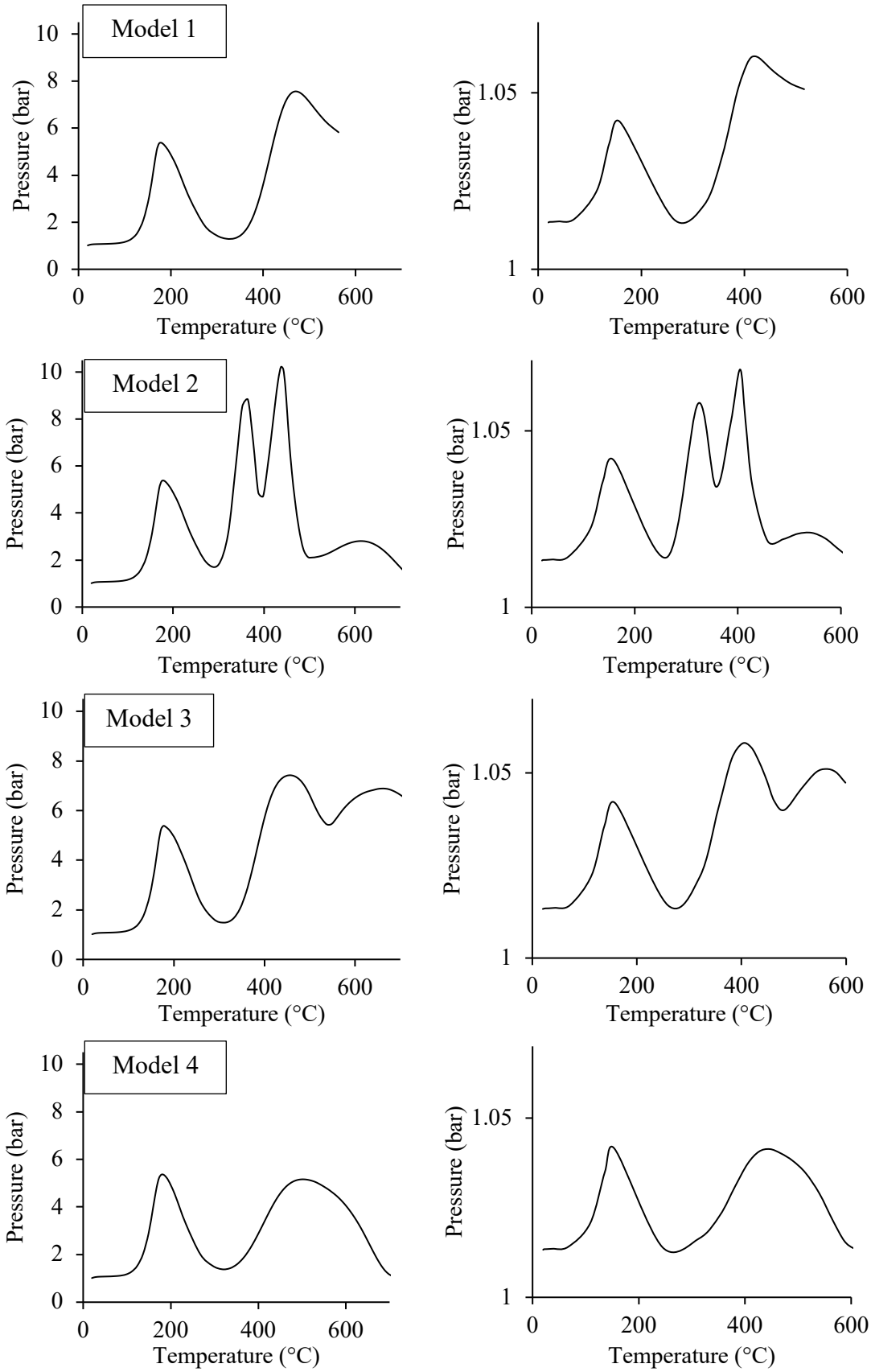


Figure 5-28 - Pressure generation within the sycamore block, models 1 - 4 for (left) a microwave pyrolysis process, sycamore block 1.5 kW applied, 4.5×1.5×1.5 cm, 10 second processing time and (right) a 1mm diameter spherical sycamore particle placed in a 1000 °C furnace, 20 second processing time.

For all models, there was an initial pressure peak from 100 – 300 °C due to water boiling and leaving the sycamore block structure, followed by pressure peaks corresponding to either lignocellulosic (models 2 and 3) or wood (models 1 and 4) breakdown. Models 1 and 4 appear to have a single pressure peak, corresponding with the wood breakdown and volatiles generation. The pressure generation for model 2 from the volatiles production appears to be discretised into hemicellulose, cellulose and lignin pressure peaks, likely due to the separate models for each constituent being combined into one model. Due to the kinetic parameters of model 3, the pressure generation appears more uniform than the model 2, with the first volatiles peak corresponding to cellulose and hemicellulose, and the second peak corresponding to lignin breakdown.

For all four models investigated, significant internal pressures (5.1 – 10.2 bar) were achieved during the microwave pyrolysis process. For the conventionally heated processes, pressures achieved were not significantly larger than atmospheric pressure (<1.07 bar). The lack of pressure generation within the conventionally heated process was likely due to the processing time (20 seconds), along with the heating profile of the particle. For a conventionally heated process, the outside would heat before the inside, and as the wood pyrolysed, the porosity and permeability would increase, decreasing the resistance to the flow of volatiles produced. For a microwave pyrolysis process, the block would heat volumetrically, and as a result the volatiles would be produced throughout the entire block, and therefore internally in the block. These volatiles would have to pass through non-pyrolysed wood at the surface of the block in the case of a liquid inerted process, resulting in much higher pressures internally compared to conventional. Experimental values for model 1, with a 25.4 mm diameter sphere in a 906 °C furnace reached a peak pressure of approximately 1.6 bar after 100 seconds (Park et al., 2010). This value, despite being higher than the theoretical values for the

smaller (1 mm) particle size, are still below the minimum theoretical pressure obtained (5.1 bar) during the microwave pyrolysis process.

If volatiles are produced and subsequently vaporised, it could be possible that the pressure generation within the sycamore block would be more consistent, rather than limited to discrete degradation peaks as shown in Figure 5-28. The increased temperature control of the sycamore block both internally and on the surface of the block would also limit the increase of porosity and permeability within the sample, as the structure would break down less than that of a sample that would keep increasing in temperature.

Empirically, the internal temperatures of the sycamore block plateaued around 450°C within the single-mode system, and 550°C within the multi-mode system. The high pressures obtained within the sycamore block during pyrolysis, coupled with volatiles production could explain the temperature plateaus within the sycamore block identified in Section 3.4.6.2. Above approximately 350°C, cellulose degradation occurs within the sycamore block, resulting in volatiles production. Levoglucosan is a prominent degradation product of cellulose (Patwardhan et al., 2009) and was identified within the pyrolysis oil produced by the liquid-inerted microwave pyrolysis process (Section 3.4.4). The boiling point of levoglucosan is approximately 290°C at atmospheric pressure (Pecha and Garcia-Perez, 2015) and would be higher at raised pressures. If cellulose degradation resulted in significant levoglucosan production within the sycamore structure, it could be possible that the energy provided to the sycamore block would be directed towards vaporising the levoglucosan, rather than heating the block, as shown by the dielectric properties of levoglucosan in Section 5.3.3. Using vapour pressures determined by Oja and Suuberg (1999), and an integrated form of the

Clausius-Clapeyron equation (Equation 5-6), the boiling point/pressure relationship for levoglucosan could be determined.

$$\ln(p) = A - \frac{B}{T} \qquad 5\text{-}6$$

Where:

p	-	Pressure, Pa
A, B	-	Constants
T	-	Temperature, K

Using pressure relationship equation, the boiling point for liquid levoglucosan across the predicted pressure ranges from the volatiles generation and literature models are presented in Figure 5-29.

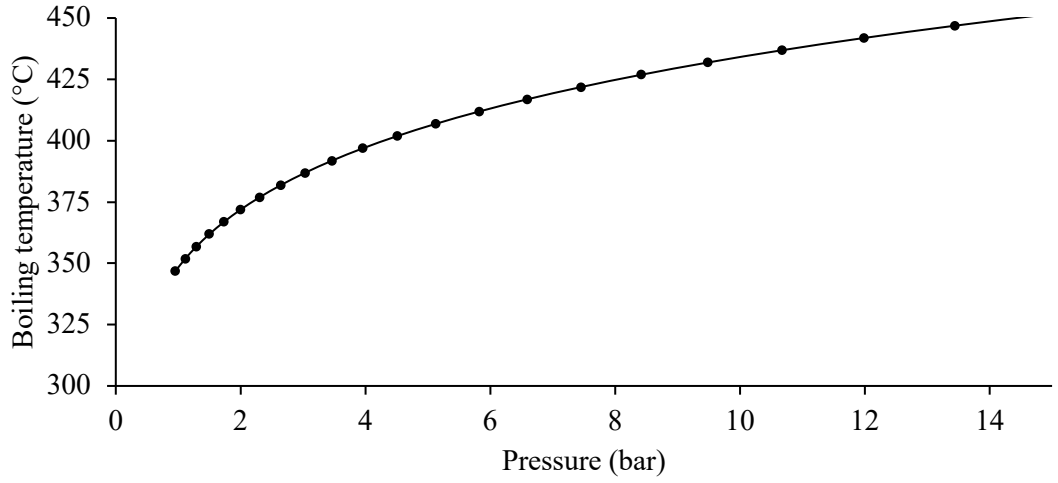


Figure 5-29 – The boiling temperature of levoglucosan at elevated pressures.

Figure 5-29 shows that in the pressure range determined from both the volatiles generation and literature models (5 – 14 bar), the boiling point of levoglucosan was elevated to 400 - 450 °C, approximately the temperature predicted by the TGA for the single-mode process plateau. It is therefore feasible that significant internal pressures could result in the liquid intermediate produced remaining as a liquid at elevated temperatures during the pyrolysis process. The energy provided to the block would

therefore go towards vaporizing the liquid intermediate, reducing the heating rate of the block as a whole, and potentially explaining the temperature plateau observed by the TGA predictions. The presence of a liquid intermediate within the block could also explain the discrepancy in the dielectric properties between the cavity perturbation method, and the (Meredith, 1998) equation predictions and real-time microwave method values. In summary, it is evident that microwave pyrolysis behaves differently than conventionally heated processes, as the heating rate, particle size and temperature gradients would result in processing factors (pressure, dielectrics) beyond simple differences in the heating method. As pressure generation would have an effect on the pyrolysis process, and is a result of volatiles generation, processing parameters would have to be controlled. Aiming for high mass losses would therefore require a high power density, which would result in a high heating rate, leading to higher pressures, resulting in higher internal temperatures and consequently higher mass losses.

5.4 Conclusions

It was identified that processing parameters that determine the energy provided to the sample (power, time) could be varied to further increase potential mass losses and pyrolysis oil yields. Higher powers applied to the process for both the single-mode and multi-mode liquid inerted process resulted in higher mass losses and pyrolysis oil yields, with the added advantage of reduced processing times during pyrolysis.

It was also recognised that due to the non-homogenous heating profile provided by the microwave field, internal temperatures at certain parts of the sycamore block would be hotter than others. For the single-mode system, the cavity dielectric properties slowed the heating rate and reduced the power absorbed by the sycamore block when compared to empirical data over the pyrolysis processing time. Due to the poor power absorbance, temperatures estimated by the models were dramatically underestimated, with

temperatures plateauing at approximately 280 °C for both the single-mode and multi-mode systems, compared to empirical predictions of 450°C for the single-mode system and 550°C for the multi-mode system. The prediction of temperatures by setting the power absorbed to be equivalent to empirical absorbed powers resulted in the models overestimating internal temperatures reached. The overestimation would likely be due to all of the energy provided to the sycamore block in the models heating the block, rather than volatilising any liquid intermediates produced during the process. The volatiles production, due to their potential presence, could have also affected the dielectric properties of the sycamore block.

The dielectric properties of the sycamore block appeared to vary from those determined by the cavity perturbation method, further showcasing the challenges of predicting and understanding the change in dielectrics over the microwave pyrolysis process. It is possible that the quick processing times of the microwave pyrolysis process (<30 seconds) reduced the accuracy of the methods used to determine the sycamore physical and dielectric properties (approximately 1.5 – 2 hours), as the slower processes would allow for the slower rate of volatiles production to not significantly affect the properties.

When modelling a microwave process heating the sycamore block, with modified dielectric properties representative of values determined empirically, despite final temperatures being similar, the heating rate was different to empirical values. Namely, the heating rate of the dielectric-property-altered model had a slower heating rate. There could potentially still be differences in the physical properties that would affect the heating rate, specifically the thermal conductivity and specific heat capacity. As specific heat capacity determines the energy requirement for a material to heat, DSC at various heating rates could be carried out to determine the specific heat capacity at various temperatures for various heating rates, to determine any differences. The

specific heat capacity at varying heating rates could then be used to identify any trends between the heating rate and specific heat capacity values and curves.

Due to volatiles production, predicted internal pressures within the single-mode sycamore block would reach around 5 – 14 bar, leading to increased temperature control and dielectrics different to those measured. The pressure determined from the volatiles production was very sensitive to the permeability of the sycamore block, along with the block size. The volatiles production and the high pressures would potentially lead to the energy absorbed by the sample going towards volatilising the liquid product, rather than heating the sycamore block itself. Energy provided to the sycamore block would, therefore, go towards the latent heat of vaporisation of volatiles produced, rather than the sensible heat of the sycamore block. Using both volatiles generation data estimated from mass loss, and kinetics determined from literature provided a preliminary estimation for pressures and compositional breakdown. The pressures predicted within the sycamore block, coupled with the vapour pressures of levoglucosan, a representative oil component, provided a potential explanation for the temperature plateaus and dielectric properties of the sycamore block during the pyrolysis process. Further investigation would be necessary into the correlation between particle sizes and predicted internal temperatures during microwave pyrolysis.

6. Conclusions and recommendations for future work

6.1 Overview

This final Chapter addresses the main aims and objectives of this thesis, including the principal findings, associated implications and also recommendations of future work for microwave pyrolysis of biomass within a liquid inerted medium.

The main outputs from this thesis include:

- Processing feasibility analysis on a bench-top scale single-mode and scaled-up multi-mode liquid inerted microwave pyrolysis process, in the form of:
    - Power absorbance behaviour and process repeatability.
    - Solvent screening with both microwave transparent and microwave absorbent liquids
    - Mass loss behaviour of the solid used as a metric for pyrolysis performance.
    - Liquid yields from the pyrolysis process and the compositional analysis
    - Analysis on the bio-char to determine temperatures reached during the pyrolysis process and compositional breakdown of the sycamore.
- Empirical observations of the liquid boiling regime during the single-mode liquid inerted microwave pyrolysis process.
- Assessment of the boiling regime control on scale-up of the liquid inerted microwave pyrolysis process.
- Identification of processing implications unique to microwave pyrolysis, such as volatiles generation, high pressures and its effect on processing parameters such as temperature control and dielectric properties.

- Investigation into processing parameters and their effect on liquid inerted microwave pyrolysis (power, time, block geometry).
- Identification of the challenges in using conventionally heated methods (differential scanning calorimetry, cavity perturbation method) to predict processing parameters involved with microwave heating, such as the dielectric properties and specific heat capacity of the sycamore.

6.2 Overall discussion and final conclusions

A liquid inerted microwave pyrolysis process was investigated to provide an alternative processing route to overcome the processing challenges associated with both conventional pyrolysis and gas-inerted microwave pyrolysis. It was determined from the initial solvent screening study that the liquid inerted pyrolysis process was entirely feasible in a wide range of solvents, including water (Chapter 3), with mass losses of up to 60 % in hydrocarbon solvents, and 35 % in water. The success of the solvents showcased the robustness of the microwave process to utilise liquids that would not be initially considered feasible due to their microwave absorbance. There was a significant advantage in terms of the potential mass loss when considering processing energy requirements when using hydrocarbon solvents. Hydrocarbon solvents allowed for mass losses of up to approximately 60 %, compared to 30 – 45 % in microwave absorbent solvents such as water and acetic acid, with the exception of 2-propanol which reached mass losses of up to 65 %. This could have been due to the observed boiling regime as the solvent was entrained within the condenser. Due to the microwave absorbent nature of water, 2-propanol and acetic acid, the energy requirements for the pyrolysis process were approximately 5 – 26 times that of gas or hydrocarbon inerted pyrolysis. There was an evident mass loss penalty when using liquid to inert the pyrolysis process as opposed to the gas inerted process, which allowed for mass losses

of up to 77 %. The mass loss penalty was likely due to the non-pyrolysed surface layer observed during liquid inerted pyrolysis, along with the increased heat transfer to the surroundings as when compared to a gas environment.

In terms of the liquid pyrolysis oil produced during the pyrolysis process, the solvent used had processing implications on the separation of the pyrolysis oil from the solvent. For the hydrocarbon solvents used, the aqueous phase oil fractionated out of the solvent, and the organic compounds within the oil were readily miscible with the solvent. The fractionation effect also occurred with water, with the organic phase fractionating out and the aqueous oil compounds being readily miscible with the water. Solvents such as 2-propanol and acetic acid appeared to be readily miscible with both oil phases, resulting in a single-phase liquid product. For the single-mode liquid inerted microwave pyrolysis system, however, due to the low mass of the sycamore blocks used (5.7 g average), the pyrolysis oil volume produced presented challenges in oil collection. Due to the high viscosity of the pyrolysis oil, coupled with the aforementioned low volumes, there was potential for significant percentages of oil product to be lost on liquid washing and drying.

Despite the single-mode system allowing for selective heating and pyrolysis of the sycamore to occur, the batch system presented challenges in maintaining a consistent liquid surround. It was observed on a number of occasions that volatiles production resulted in a gaseous environment around the biomass block. This gaseous surround results in surface heating of the block, discounting the benefits of having a liquid surround. In order to control the boiling regime surrounding the sycamore block and produce a directly collectable pyrolysis oil volume, the reactor was scaled-up into a larger-diameter multi-mode configuration.

The scaled-up system presented benefits over the single-mode system, but also presented new challenges that were not present in the single-mode system. The reactor configuration allowed for masses over ten times that of the single-mode system (5.7 g to around approximately 75 g). The reactor also allowed for a larger quartz vessel to be placed within, allowing for larger liquid volumes (1 L) compared to the single mode system (100 mL). The mass losses obtained within the multi-mode system were comparable to the single-mode system (up to approximately 60 %), and as such due to the larger block masses, directly collectable pyrolysis oil volumes were produced. Challenges that were not identified in the single-mode system were identified in the multi-mode system, however; the electric field within the multi-mode reactor was less well-defined than the single-mode system, resulting in a non-homogenous heating profile within the sycamore block. It appeared that the sycamore block heated from a certain point, as opposed to the more even heating profile identified in the single-mode system. This uneven heating resulted in increased temperatures being reached during the pyrolysis process, and almost complete lignocellulosic breakdown at low specific energies (<1 kJ/g). It was therefore determined that in order for a scalable process to be developed, the focus should therefore be on a higher frequency biomass throughput, rather than pyrolysing larger blocks.

The final investigation within this thesis was concerned with further understanding the microwave pyrolysis process. It was identified that for both the single-mode and multi-mode reactor configurations, higher powers and shorter times allowed for higher mass losses and pyrolysis oil yields to be obtained. Temperature prediction methods internally within the sycamore block (based on power absorbed, and the electric field) were compared to temperatures obtained predicted by TGA. For both the single-mode and multi-mode systems, it was observed that the heating profile estimated using the

microwave heating model had a slower heating rate than the TGA predicted equivalent. The maximum temperature plateaus obtained in the microwave models were the same for both the single-mode and multi-mode models (280 °C) due to the dielectric loss factor being very low at around that temperature. The temperature plateaus were lower than the temperature plateau predicted by TGA for the empirical processes: 450 °C and 550 °C for the single-mode and multi-mode processes respectively. Using models that use the power absorbed as an independent variable resulted in internal temperatures being overestimated when compared to the empirical predictions by TGA. It was therefore determined that the physical properties, such as specific heat capacity and thermal conductivity that were determined from a conventionally heated method may not be accurate when describing a fast-heating microwave pyrolysis process. The temperature plateau could have also been due to volatiles production coupled with increased internal pressures, causing the energy provided to the sycamore block to go towards the latent heat of the volatiles rather than the sensible heat of the block.

The dielectric properties during the process were also inferred from the power absorbed by the sycamore block during the pyrolysis process and measured during microwave heating. It was determined that the values both from the pyrolysis process and the microwave heating method both had dramatically different dielectric properties to the cavity perturbation method. The disparity in values suggested that there were heat and mass transfer characteristics that occurred during the pyrolysis process which were not considered in the slow-heating cavity perturbation method (5°C /s).

Initial estimations into pressures obtained within the sycamore block during the microwave pyrolysis process were investigated using volatiles generation rates based on mass losses, and kinetic data available from literature. It was determined that pressures of approximately 5 – 14 bar could be obtained within the sycamore block.

The high pressures within the block could potentially explain the temperature control and varied dielectric properties observed within the sycamore block over the pyrolysis specific energy ranges investigated. If a high boiling point volatile was produced during the pyrolysis process, such as levoglucosan, it is feasible that high pressures could result in a liquid volatiles being present, and energy provided to the block would vaporise the volatiles, rather than heating the block further. This would allow for potential temperature control within the sycamore block based on powers, heating rates and therefore pressures, allowing for potential selective decomposition of the lignocellulosic constituents of the biomass.

6.3 Recommendations for future work

6.3.1 Processing considerations – continuous processing

As was identified in the solvent screening study in Chapter 3, the solvent used during the liquid-inerted pyrolysis process would affect the liquid product produced. An aqueous phase solvent such as water would be readily miscible with the aqueous phase of the pyrolysis oil, and the organic phase would readily phase separate. The effect would be the opposite with an organic solvent such as cyclohexane, and in the presence of a solvent such as acetic acid or 2-propanol, both phases of the pyrolysis oil would be readily miscible with the solvent.

When considering process scale-up and development, for a liquid inerted microwave pyrolysis process the upstream processes and reactor configuration would likely not have an effect on the liquid product produced on an overarching process basis. As long as a solid is pyrolysed within a liquid, there would be three major products: solid, liquid and gas. Due to the nature of the liquid surround, it is likely that any gas produced and lost from the system could be considered non-condensable. Therefore, the products that

would flow downstream from the reactor could be considered to be residual solid and liquid.

The preliminary processing considerations for downstream operations based on the type of solvent used (organic, aqueous or oil-miscible) are presented in Figure 6-1.

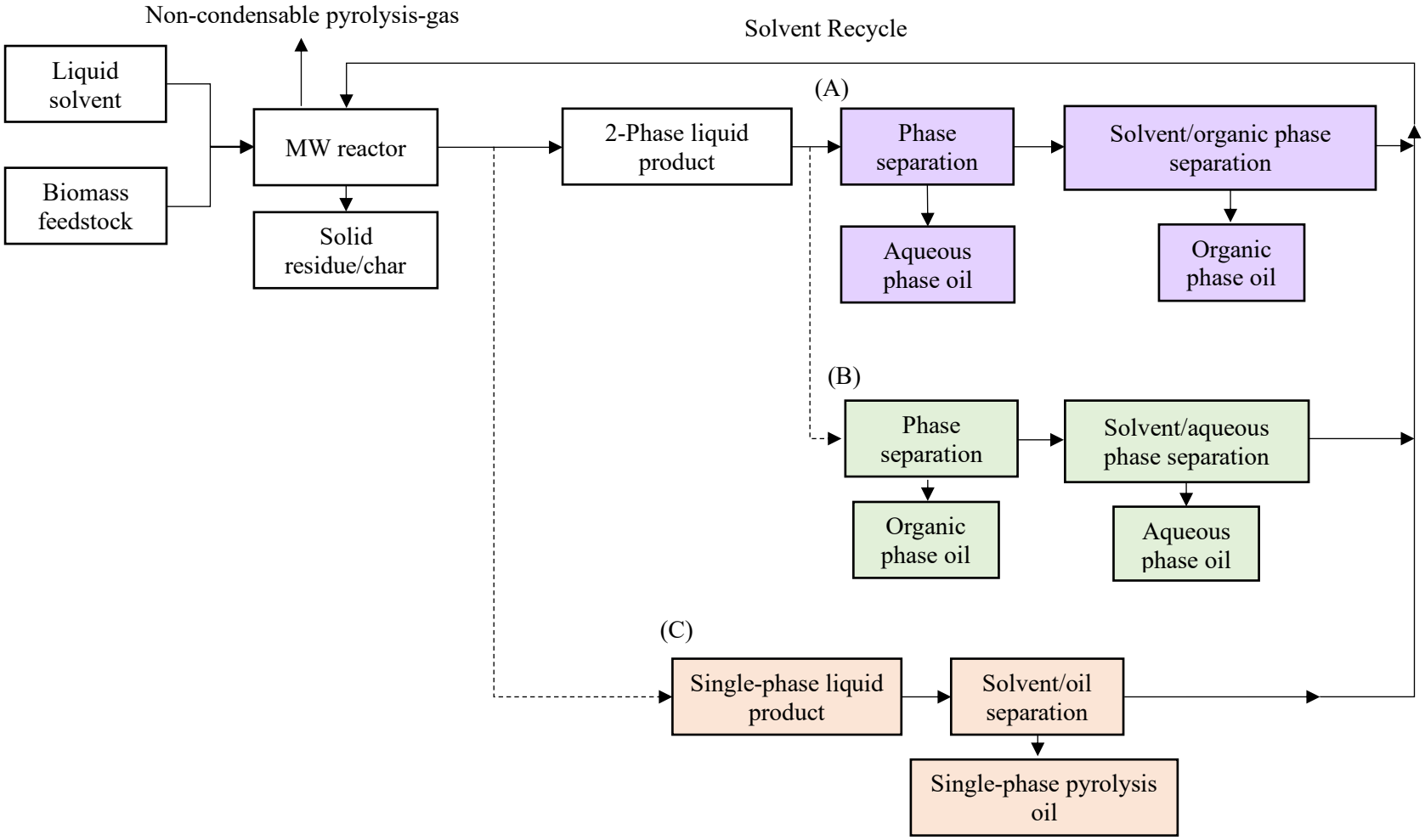


Figure 6-1 – Process flow diagram for a continuous pyrolysis process with (A) organic phase solvent, (B) aqueous phase solvent and (C) oil-miscible solvent.

Alongside the downstream considerations for the liquid and solid product post-pyrolysis, a continuous flow reactor would be required to be developed. Each pyrolysis process would have to be designed to account for both liquid-liquid properties, and liquid-solid interactions such as the solid's ability to float both pre- and post-pyrolysis. It was concluded from the research within this thesis that direct geometric scale-up of the sycamore block to obtain larger volumes of oil presented challenges in that the sycamore block heated from a specific point, with the rest of the block potentially heating by conduction. A reactor that would allow for a continuous throughput by high quantity, small particles rather than larger particles would be required. Due to the pyrolysis processes investigated within this thesis being batch systems, separation of the solvent and oil was carried out in batch. On development of a continuous process, however, development of a continuous separation method would have to be carried out.

6.3.2 Maximum and minimum geometry possible for liquid inerted microwave pyrolysis

The investigations of both the single-mode and multi-mode liquid-inerted microwave pyrolysis process were carried out with consistent block sizes, 15×15×45 mm and 25×50×50 mm respectively. Working with a standardised block size was useful for comparisons to be made and system behaviour to be analysed, however in terms of potential real-life implications, the results and conclusions present challenges. Firstly, it is unlikely that uniform woody biomass would be processed. To reduce processing and capital costs, the biomass to be pyrolysed would be minimally treated in terms of block size and moisture content. Therefore, it is likely that a waste-stream product from another process, such as forestry residues would be a viable option. Forestry residues are not a standardised size, and therefore the pyrolysis process needs to be analysed to

present the minimum and maximum possible block sizes that could feasibly be pyrolysed.

The maximum possible block size is largely down to the wavelength of the applicator used, as increasing the wavelength (by using a lower frequency generator such as 896 MHz) will in turn increase the penetration depths of the microwaves. The penetration depth of sycamore changes dramatically over the temperature range due to the changing physical properties of sycamore during pyrolysis such as char formation. The penetration depth of non-pyrolysed sycamore is 20- and 42 cm for 2.45- and 0.896 GHz respectively at 20 °C. This penetration depth limit, at the onset of the pyrolysis process, is much larger than the sycamore block sizes used (maximum 5×5×5 cm for the multimode system).

The size of the reactor, and the electric field distribution would also be a large factor in how the blocks would heat. With the single-mode system, the waveguide and heating area of the system was largely limited by the wavelength of the microwaves, and so would require a small block size, high throughput system. A multi-mode system would allow for significantly larger blocks; however, the pyrolysis process would likely be conduction limited; temperature control was significantly reduced if the internal section of the block being heated was insulated by the non-pyrolysed surround, as identified in Chapter 4.

Theoretically, if a block is placed in a location in the cavity with an intense microwave field, then energy transfer will occur. As the block size decreases, due to efficient heat transfer to the surrounding liquid increasing as the surface area to volume ratio increases, and there being a 1 mm layer of non-treated wood as shown in Section 3.4.6, it is possible that the internal temperatures reached would not be hot enough for pyrolysis to occur. For very small blocks, it would be feasible to process more than one

block simultaneously, however this then presents the issue of heterogeneous heating throughout all the samples, as presented in the fixed bed study of (Robinson et al., 2015). Another possible outcome is that if the smaller size of biomass does pyrolyse due to the very high power-density, a combination of volatiles production and surface boiling of the liquid may cause the critical heat flux of the surrounding liquid may be overcome. There is also the consideration of processing with multiple very small particles entrained in a liquid, as the particles pyrolyse and heat, there would be gas produced both by the biomass and the liquid surround of the biomass boiling, this would create gas pockets that would negate the benefit of the liquid surround. Future work would therefore involve investigation into determining an optimal particle geometry range that could feasibly allow for pyrolysis to occur by volumetric heating in a continuous system.

6.3.3 Kinetic studies on a microwave pyrolysis process

Models were introduced in Chapter 5 as a means of estimating internal pressures and compositional breakdown of the sycamore block during the microwave pyrolysis process. The models presented used conventionally heated kinetics (Park et al., 2010, Capart et al., 2004, Varhegyi et al., 1989, Chan and Krieger, 1981, Ding et al., 2018, Mok and Antal, 1983, Kilzer and Broido, 1965). Due to the known composition of the sycamore used within the research, there is potential for development of a kinetic model to accurately describe the pyrolysis process, both in terms of power absorbed, and in terms of heating from the electric field profile. There was a temperature plateau present for both the single-mode and multi-mode microwave pyrolysis processes. It is therefore evident that there were potential mass transfer, temperature and pressure relationships unique to microwave heating that were not identified during the aforementioned kinetic studies for conventional heating. Due to the volumetric nature of microwave heating

alongside the non-pyrolysed surface layer of the sycamore block identified from the liquid inerted pyrolysis process, it is evident that there are potential mass transfer gradients that are required to be investigated.

6.3.4 Comprehensive pyrolysis oil product analysis and categorisation

Pyrolysis oil is a complex mixture of hundreds of compounds with various functional groups (Czernik and Bridgwater, 2004), and multiple functional groups present challenges for compound categorisation (as identified in Chapters 3 and 4). Therefore, for model biomasses, key marker compounds at high probabilities of >80 % should be identified and used as markers for pyrolysis performance, for example, levoglucosan from cellulose, phenols from lignin and furfural from hemicellulose and levoglucosan. Various other methods analysis methods could be utilised, such as NMR, HPLC and other GC methods such as GC-FID. Standards of prominent compounds could be used to confirm their presence in the oil, and increase the confidence in the compositional data for the oil. As identified in Section 3.4.4, a more consistent method could be developed, with all analysis being carried out immediately after pyrolysis, to reduce the incidence of oil decomposition over time. The same column should also be used for all pyrolysis oils tested, so as to keep the identification of compounds consistent.

6.3.5 Dielectrics during the microwave process

It was identified in Chapter 5 that the dielectrics of the sycamore throughout the microwave pyrolysis process potentially differed to the measurements determined from the cavity perturbation method. Preliminary values determined from the pyrolysis process using the (Meredith, 1998) equation, and from a microwave heating dielectric measurement process were significantly different to the cavity perturbation values. As the dielectric properties of the feedstock determine the material's ability to heat using

microwaves, it would be imperative to determine the dielectric properties throughout the microwave pyrolysis process. The material's dielectric properties would also affect microwave field models, and therefore the ability of a model to predict both temperatures reached, and the electric field distribution and heating profile of the blocks would be affected.

6.3.6 Alternative feedstock investigation

Sycamore was used as a model feedstock throughout the thesis to maintain consistent behaviour between processing runs, and allow for the focus of the research to involve the investigation of processing parameters. Investigation into different feedstocks should be carried out to determine pyrolysis behaviour. Differing feedstocks have the potential to provide pyrolysis oils with varying compositions. Pelletised feedstocks, such as pelletised powdered wood, would likely not be feasible in a liquid inerted system due to the internal pressures produced within the particle, which could result in the pellet disintegrating. Feedstocks to be used would, therefore, involve single-particle, untreated particles, potentially similar to the geometry of the sycamore used in this thesis. Examples of potential feedstocks could involve forestry waste, other woods such as softwoods (e.g. pine), alternative lignocellulosic feedstocks such as grasses, or even non-lignocellulosic feedstocks, such as seaweed.

6.3.7 Solvent recycle

Preliminary work was carried out in this thesis to determine the energy penalty of recycling the solvent between runs. It was determined that solvent would be lost, and there was a mass loss/energy penalty for successive runs. Future work would involve investigating solvent recycle over multiple successive runs to identify if a plateau could occur in terms of a mass loss/energy penalty. Further future work could involve

investigating solvent recycle in the multi-mode system of Chapter 4. As it was identified that the solvent became more saturated with pyrolysis oil in each successive run, investigation into solvent clean-up methods could be investigated. Potential solvent clean-up methods could involve thermal separation (in the case where the boiling temperatures of the solvent and pyrolysis oil do not overlap) and stripping processes. It was also identified that the sycamore blocks absorbed some solvent post-pyrolysis. Therefore, investigation into recovering solvent lost to the sample, such as thermal separation and condensation, could be investigated.

6.3.8 Selective decomposition analysis

As identified in Chapter 5, temperature limitations inherent to the microwave pyrolysis process (due to volatiles generation and pressure) could allow for selective decomposition within the sycamore block itself. These temperature limitations should be investigated for various block sizes to identify any correlations between size and internal temperature. Processing parameters that would enable selective decomposition of either hemicellulose, or hemicellulose and cellulose (or separately in a staged process) within the microwave pyrolysis process also need to be identified.

References

ÁBREGO, J., ATIENZA-MARTÍNEZ, M., PLOU, F. & ARAUZO, J. 2019. Heat requirement for fixed bed pyrolysis of beechwood chips. *Energy,* 178**,** 145-157.

AÇıKALıN, K. & KARACA, F. 2017. Fixed-bed pyrolysis of walnut shell: Parameter effects on yields and characterization of products. *Journal of Analytical and Applied Pyrolysis,* 125**,** 234-242.

ADAM, M. 2017. *Understanding Microwave Pyrolysis of Biomass Materials.* Doctor of Philosophy Doctoral Thesis, University of Nottingham.

ADAM, M., BENEROSO, D., KATRIB, J., KINGMAN, S. & ROBINSON, J. P. 2017. Microwave fluidized bed for biomass pyrolysis. Part II: Effect of process parameters. *Biofuels, Bioproducts and Biorefining,* 11**,** 613-624.

AGUADO, R., OLAZAR, M., GAISÁN, B., PRIETO, R. & BILBAO, J. 2002. Kinetic Study of Polyolefin Pyrolysis in a Conical Spouted Bed Reactor. *Industrial & Engineering Chemistry Research,* 41**,** 4559-4566.

AL-ARNI, S., BOSIO, B. & ARATO, E. 2010. Syngas from sugarcane pyrolysis: an experimental study for fuel cell applications. *Renewable Energy,* 35**,** 29-35.

AMETA, S. & AMETA, R. 2018. *Advanced Oxidation Processes for Wastewater Treatment: Emerging Green Chemical Technology*, Elsevier Science.

ANDERSON, J., BERTHOD, A., PINO, V. & STALCUP, A. 2015. *Analytical Separation Science*.

ANTAL, M. J. & GRØNLI, M. 2003. The Art, Science, and Technology of Charcoal Production. *Industrial & Engineering Chemistry Research,* 42**,** 1619-1640.

ANTAL, M. J., JR. & VARHEGYI, G. 1995. Cellulose Pyrolysis Kinetics: The Current State of Knowledge. *Industrial & Engineering Chemistry Research,* 34**,** 703-717.

ASOKAN, M. A., SENTHUR PRABU, S., KAMESH, S. & KHAN, W. 2018. Performance, combustion and emission characteristics of diesel engine fuelled with papaya and watermelon seed oil bio-diesel/diesel blends. *Energy,* 145**,** 238-245.

AYALUR CHATTANATHAN, S., ADHIKARI, S. & ABDOULMOUMINE, N. 2012. A review on current status of hydrogen production from bio-oil. *Renewable and Sustainable Energy Reviews,* 16**,** 2366-2372.

BALAT, M. 2011. An Overview of the Properties and Applications of Biomass Pyrolysis Oils. *Energy Sources, Part A: Recovery, Utilization, and Environmental Effects,* 33**,** 674-689.

BALAT, M., BALAT, M., KıRTAY, E. & BALAT, H. 2009. Main routes for the thermo-conversion of biomass into fuels and chemicals. Part 1: Pyrolysis systems. *Energy Conversion and Management,* 50**,** 3147-3157.

BARHAM, J. P., KOYAMA, E., NORIKANE, Y., OHNEDA, N. & YOSHIMURA, T. 2019. Microwave Flow: A Perspective on Reactor and Microwave Configurations and the Emergence of Tunable Single-Mode Heating Toward Large-Scale Applications. *The Chemical Record,* 19**,** 188-203.

BENEROSO, D., ALBERO-ORTIZ, A., MONZÓ-CABRERA, J., DÍAZ-MORCILLO, A., ARENILLAS, A. & MENÉNDEZ, J. A. 2016. Dielectric characterization of biodegradable wastes during pyrolysis. *Fuel,* 172**,** 146-152.

BENEROSO, D., BERMUDEZ, J. M., ARENILLAS, A., DE LA PERIA, F., GARCIA, J. L., PRIETO, M. A. & MENENDEZA, J. A. 2015a. Oil fractions from the pyrolysis of diverse organic wastes: The different effects of conventional and microwave induced pyrolysis. *Journal of Analytical and Applied Pyrolysis,* 114**,** 256-264.

BENEROSO, D., BERMUDEZ, J. M., ARENILLAS, A. & MENENDEZ, J. A. 2015b. Influence of carrier gas on microwave-induced pyrolysis. *Journal of Analytical and Applied Pyrolysis,* 113**,** 153-157.

BHATTACHARJEE, N. & BISWAS, A. B. 2019. Pyrolysis of orange bagasse: Comparative study and parametric influence on the product yield and their characterization. *Journal of Environmental Chemical Engineering,* 7**,** 102903.

BORGES, F. C., DU, Z., XIE, Q., TRIERWEILER, J. O., CHENG, Y., WAN, Y., LIU, Y., ZHU, R., LIN, X., CHEN, P. & RUAN, R. 2014. Fast microwave assisted pyrolysis of biomass using microwave absorbent. *Bioresource Technology,* 156**,** 267-274.

BP 2019. BP Statistical Review of World Energy. United Kingdom: BP.

BRASSARD, P., GODBOUT, S. & RAGHAVAN, V. 2017. Pyrolysis in auger reactors for biochar and bio-oil production: A review. *Biosystems Engineering,* 161**,** 80-92.

BRIDGWATER, A. & PEACOCKE, G. Engineering developments in fast pyrolysis for bio-oils. Proceedings Biomass Pyrolysis Oil Properties and Combustion Meeting. NREL, 1994. 110-27.

BRIDGWATER, A. V. 1994. Catalysis in thermal biomass conversion. *Applied Catalysis A: General,* 116**,** 5-47.

BRIDGWATER, A. V. 2012. Review of fast pyrolysis of biomass and product upgrading. *Biomass and Bioenergy,* 38**,** 68-94.

BRIDGWATER, A. V., MEIER, D. & RADLEIN, D. 1999. An overview of fast pyrolysis of biomass. *Organic Geochemistry,* 30**,** 1479-1493.

BRIDGWATER, A. V. & PEACOCKE, G. V. C. 2000. Fast pyrolysis processes for biomass. *Renewable and Sustainable Energy Reviews,* 4**,** 1-73.

BUDARIN, V. L., CLARK, J. H., LANIGAN, B. A., SHUTTLEWORTH, P. & MACQUARRIE, D. J. 2010. Microwave assisted decomposition of cellulose: A new thermochemical route for biomass exploitation. *Bioresource Technology,* 101**,** 3776-3779.

BUFFI, M., CAPPELLETTI, A., RIZZO, A. M., MARTELLI, F. & CHIARAMONTI, D. 2018. Combustion of fast pyrolysis bio-oil and blends in a micro gas turbine. *Biomass and Bioenergy,* 115**,** 174-185.

CAMPUZANO, F., BROWN, R. C. & MARTÍNEZ, J. D. 2019. Auger reactors for pyrolysis of biomass and wastes. *Renewable and Sustainable Energy Reviews,* 102**,** 372-409.

CAPART, R., KHEZAMI, L. & BURNHAM, A. K. 2004. Assessment of various kinetic models for the pyrolysis of a microgranular cellulose. *Thermochimica Acta,* 417**,** 79-89.

CASTELLVÍ BARNÉS, M., LANGE, J. P., VAN ROSSUM, G. & KERSTEN, S. R. A. 2015. A new approach for bio-oil characterization based on gel permeation chromatography preparative fractionation. *Journal of Analytical and Applied Pyrolysis,* 113**,** 444-453.

CHAN, R. W.-C. & KRIEGER, B. B. 1981. Kinetics of dielectric-loss microwave degradation of polymers: Lignin. *Journal of Applied Polymer Science,* 26**,** 1533-1553.

CHANDRAN, R., KALIAPERUMAL, R., BALAKRISHNAN, S., BRITTEN, A. J., MACINNIS, J. & MKANDAWIRE, M. 2019. Characteristics of bio-oil from continuous fast pyrolysis of Prosopis juliflora. *Energy***,** 116387.

CHEN, L., YU, Z., XU, H., WAN, K., LIAO, Y. & MA, X. 2019. Microwave-assisted co-pyrolysis of Chlorella vulgaris and wood sawdust using different additives. *Bioresource Technology,* 273**,** 34-39.

CHIARAMONTI, D., BONINI, M., FRATINI, E., TONDI, G., GARTNER, K., BRIDGWATER, A. V., GRIMM, H. P., SOLDAINI, I., WEBSTER, A. & BAGLIONI, P. 2003. Development of emulsions from biomass pyrolysis liquid and diesel and their use in engines—Part 2: tests in diesel engines. *Biomass and Bioenergy,* 25**,** 101-111.

CHIONG, M. C., CHONG, C. T., NG, J.-H., LAM, S. S., TRAN, M.-V., CHONG, W. W. F., MOHD JAAFAR, M. N. & VALERA-MEDINA, A. 2018. Liquid biofuels production and emissions performance in gas turbines: A review. *Energy Conversion and Management,* 173**,** 640-658.

CHOI, J.-H., JANG, S.-K., KIM, J.-H., PARK, S.-Y., KIM, J.-C., JEONG, H., KIM, H.-Y. & CHOI, I.-G. 2019. Simultaneous production of glucose, furfural, and ethanol organosolv lignin for total utilization of high recalcitrant biomass by organosolv pretreatment. *Renewable Energy,* 130**,** 952-960.

CHOI, Y. S., JOHNSTON, P. A., BROWN, R. C., SHANKS, B. H. & LEE, K.-H. 2014. Detailed characterization of red oak-derived pyrolysis oil: Integrated use of GC, HPLC, IC, GPC and Karl-Fischer. *Journal of Analytical and Applied Pyrolysis,* 110**,** 147-154.
CHUKWUNEKE, J. L., EWULONU, M. C., CHUKWUJIKE, I. C. & OKOLIE, P. C. 2019. Physico-chemical analysis of pyrolyzed bio-oil from swietenia macrophylla (mahogany) wood. *Heliyon,* 5**,** e01790.
CHURCH, R. H., WEBB, W. E. & SALSMAN, J. B. 1988. Dielectric properties of low-loss minerals.
CINTAS, P., VERONESI, P., LEONELLI, C., KEGLEVICH, G., MUCSI, Z., RADOIU, M., DE LA HOZ, A., PRIETO, P., WADA, Y. & MOCHIZUKI, D. 2017. *Microwave Chemistry*, Walter de Gruyter GmbH & Co KG.
CZERNIK, S. & BRIDGWATER, A. V. 2004. Overview of Applications of Biomass Fast Pyrolysis Oil. *Energy & Fuels,* 18**,** 590-598.
DAI, L., WANG, Y., LIU, Y., RUAN, R., YU, Z. & JIANG, L. 2019. Comparative study on characteristics of the bio-oil from microwave-assisted pyrolysis of lignocellulose and triacylglycerol. *Science of The Total Environment,* 659**,** 95-100.
DAOUK, E., VAN DE STEENE, L., PAVIET, F., MARTIN, E., VALETTE, J. & SALVADOR, S. 2017. Oxidative pyrolysis of wood chips and of wood pellets in a downdraft continuous fixed bed reactor. *Fuel,* 196**,** 408-418.
DAS, O. & SARMAH, A. K. 2015. Mechanism of waste biomass pyrolysis: Effect of physical and chemical pre-treatments. *Science of The Total Environment,* 537**,** 323-334.
DAZA SERNA, L. V., ORREGO ALZATE, C. E. & CARDONA ALZATE, C. A. 2016. Supercritical fluids as a green technology for the pretreatment of lignocellulosic biomass. *Bioresource Technology,* 199**,** 113-120.
DE LA HOZ, A. & LOUPY, A. 2013. *Microwaves in Organic Synthesis*, Wiley.
DEMIRBAS, A. 2000. Recent advances in biomass conversion technologies. *Energy Edu Sci Technol,* 6**,** 19-41.
DEMIRBAS, A. 2006. Effect of temperature on pyrolysis products from four nut shells. *Journal of Analytical and Applied Pyrolysis,* 76**,** 285-289.
DEMIRBAS, A. 2007. Effect of Temperature on Pyrolysis Products from Biomass. *Energy Sources, Part A: Recovery, Utilization, and Environmental Effects,* 29**,** 329-336.
DEMIRBAŞ, A. 2000. Mechanisms of liquefaction and pyrolysis reactions of biomass. *Energy Conversion and Management,* 41**,** 633-646.
DEMIRBAS, A. & ARIN, G. 2002. An Overview of Biomass Pyrolysis. *Energy Sources,* 24**,** 471-482.
DEMIRBAS, M. F., BALAT, M. & BALAT, H. 2009. Potential contribution of biomass to the sustainable energy development. *Energy Conversion and Management,* 50**,** 1746-1760.
DI BLASI, C. 2000. Modelling the fast pyrolysis of cellulosic particles in fluid-bed reactors. *Chemical Engineering Science,* 55**,** 5999-6013.
DI BLASI, C., SIGNORELLI, G., DI RUSSO, C. & REA, G. 1999. Product Distribution from Pyrolysis of Wood and Agricultural Residues. *Industrial & Engineering Chemistry Research,* 38**,** 2216-2224.
DIEBOLD, J. P. 1999. A review of the chemical and physical mechanisms of the storage stability of fast pyrolysis bio-oils. National Renewable Energy Lab., Golden, CO (US).
DIEBOLD, J. P. & BRIDGWATER, A. V. 1997. Overview of Fast Pyrolysis of Biomass for the Production of Liquid Fuels. *In:* BRIDGWATER, A. V. & BOOCOCK, D. G. B. (eds.) *Developments in Thermochemical Biomass Conversion: Volume 1 / Volume 2.* Dordrecht: Springer Netherlands.
DING, Y., EZEKOYE, O. A., ZHANG, J., WANG, C. & LU, S. 2018. The effect of chemical reaction kinetic parameters on the bench-scale pyrolysis of lignocellulosic biomass. *Fuel,* 232**,** 147-153.
DJOKIC, M. R., DIJKMANS, T., YILDIZ, G., PRINS, W. & VAN GEEM, K. M. 2012. Quantitative analysis of crude and stabilized bio-oils by comprehensive two-dimensional gas-chromatography. *Journal of Chromatography A,* 1257**,** 131-140.

DU, J., LIU, P., LIU, Z.-H., SUN, D.-G. & TAO, C.-Y. 2010. Fast pyrolysis of biomass for bio-oil with ionic liquid and microwave irradiation. *Journal of Fuel Chemistry and Technology,* 38**,** 554-559.

DUBOIS, M., GILLES, K. A., HAMILTON, J. K., REBERS, P. T. & SMITH, F. 1956. Colorimetric method for determination of sugars and related substances. *Analytical chemistry,* 28**,** 350-356.

ELLIOTT, D. C., HART, T. R., NEUENSCHWANDER, G. G., ROTNESS, L. J. & ZACHER, A. H. 2009. Catalytic hydroprocessing of biomass fast pyrolysis bio-oil to produce hydrocarbon products. *Environmental Progress & Sustainable Energy,* 28**,** 441-449.

ELLISON, W., LAMKAOUCHI, K. & MOREAU, J.-M. 1996. Water: a dielectric reference. *Journal of Molecular Liquids,* 68**,** 171-279.

EUROPEAN UNION 2009. Directive 2009/28/EC of the European Parliament and of the Council of 23 April 2009 on the promotion of the use of energy from renewable sources and amending and subsequently repealing Directives 2001/77/EC and 2003/30/EC. *Official Journal of the European Union,* 5**,** 2009.

EVANS, R. J. & MILNE, T. A. 1987. Molecular characterization of the pyrolysis of biomass. *Energy & Fuels,* 1**,** 123-137.

FARAG, S., MUDRABOYINA, B. P., JESSOP, P. G. & CHAOUKI, J. 2016. Impact of the heating mechanism on the yield and composition of bio-oil from pyrolysis of kraft lignin. *Biomass and Bioenergy,* 95**,** 344-353.

FARDAD, D. & LADOMMATOS, N. 1999. Evaporation of hydrocarbon compounds, including gasoline and diesel fuel, on heated metal surfaces. *Proceedings of the Institution of Mechanical Engineers, Part D: Journal of Automobile Engineering,* 213**,** 625-645.

FERNANDO, S., ADHIKARI, S., CHANDRAPAL, C. & MURALI, N. 2006. Biorefineries: current status, challenges, and future direction. *Energy & Fuels,* 20**,** 1727-1737.

FIELD, C. B., CAMPBELL, J. E. & LOBELL, D. B. 2008. Biomass energy: the scale of the potential resource. *Trends in Ecology & Evolution,* 23**,** 65-72.

FINCH, C. A. 1986. The chemistry of solid wood. Edited by R. M. Rowell, ACS Advances in Chemistry Series No. 207, American Chemical Society, Washington D.C., 1984. ISBN 0-8412-0796-8. *British Polymer Journal,* 18**,** 352-352.

FREDLUND, B. 1988. A model for heat and mass transfer in timber structures during fire: a theoretical, numerical and experimental study.

FUKUSHIMA, R. S. & HATFIELD, R. D. 2001. Extraction and isolation of lignin for utilization as a standard to determine lignin concentration using the acetyl bromide spectrophotometric method. *Journal of Agricultural and Food Chemistry,* 49**,** 3133-3139.

GALGANO, A. & BLASI, C. D. 2003. Modeling Wood Degradation by the Unreacted-Core-Shrinking Approximation. *Industrial & Engineering Chemistry Research,* 42**,** 2101-2111.

GANESAPILLAI, M., MANARA, P. & ZABANIOTOU, A. 2016. Effect of microwave pretreatment on pyrolysis of crude glycerol–olive kernel alternative fuels. *Energy Conversion and Management,* 110**,** 287-295.

GARBA, M. U., MUSA, U., OLUGBENGA, A. G., MOHAMMAD, Y. S., YAHAYA, M. & IBRAHIM, A. A. 2018. Catalytic upgrading of bio-oil from bagasse: Thermogravimetric analysis and fixed bed pyrolysis. *Beni-Suef University Journal of Basic and Applied Sciences,* 7**,** 776-781.

GARCIA-PEREZ, M., WANG, S., SHEN, J., RHODES, M., LEE, W. J. & LI, C.-Z. 2008a. Effects of Temperature on the Formation of Lignin-Derived Oligomers during the Fast Pyrolysis of Mallee Woody Biomass. *Energy & Fuels,* 22**,** 2022-2032.

GARCIA-PEREZ, M., WANG, X. S., SHEN, J., RHODES, M. J., TIAN, F., LEE, W.-J., WU, H. & LI, C.-Z. 2008b. Fast Pyrolysis of Oil Mallee Woody Biomass: Effect of Temperature on the Yield and Quality of Pyrolysis Products. *Industrial & Engineering Chemistry Research,* 47**,** 1846-1854.

GARLAPALLI, R. K., WIRTH, B. & REZA, M. T. 2016. Pyrolysis of hydrochar from digestate: Effect of hydrothermal carbonization and pyrolysis temperatures on pyrochar formation. *Bioresource Technology,* 220**,** 168-174.

GE, H., GUO, W., SHEN, L., SONG, T. & XIAO, J. 2016. Biomass gasification using chemical looping in a 25 kWth reactor with natural hematite as oxygen carrier. *Chemical Engineering Journal,* 286**,** 174-183.

GOYAL, H. B., SEAL, D. & SAXENA, R. C. 2008. Bio-fuels from thermochemical conversion of renewable resources: A review. *Renewable and Sustainable Energy Reviews,* 12**,** 504-517.

GREEN, D. W. & PERRY, R. H. 2007. *Perry's Chemical Engineers' Handbook, Eighth Edition*, McGraw-Hill Education.

GRØNLI, M. G. & MELAAEN, M. C. 2000. Mathematical Model for Wood PyrolysisComparison of Experimental Measurements with Model Predictions. *Energy & Fuels,* 14**,** 791-800.

GUO, W., LIM, C. J., BI, X., SOKHANSANJ, S. & MELIN, S. 2013. Determination of effective thermal conductivity and specific heat capacity of wood pellets. *Fuel,* 103**,** 347-355.

GUO, X., WANG, S., WANG, Q., GUO, Z. & LUO, Z. 2011. Properties of Bio-oil from Fast Pyrolysis of Rice Husk. *Chinese Journal of Chemical Engineering,* 19**,** 116-121.

GUST, S. 1997. Combustion Experiences of Flash Pyrolysis Fuel in Intermediate Size Boilers. *In:* BRIDGWATER, A. V. & BOOCOCK, D. G. B. (eds.) *Developments in Thermochemical Biomass Conversion: Volume 1 / Volume 2.* Dordrecht: Springer Netherlands.

GUTIÉRREZ, A., DEL RÍO, J. C. & MARTÍNEZ, Á. T. 2004. Chemical Analysis and Biological Removal of Wood Lipids Forming Pitch Deposits in Paper Pulp Manufacturing. *In:* WALKER, J. M., SPENCER, J. F. T. & RAGOUT DE SPENCER, A. L. (eds.) *Environmental Microbiology: Methods and Protocols.* Totowa, NJ: Humana Press.

HAELDERMANS, T., CLAESEN, J., MAGGEN, J., CARLEER, R., YPERMAN, J., ADRIAENSENS, P., SAMYN, P., VANDAMME, D., CUYPERS, A., VANREPPELEN, K. & SCHREURS, S. 2019. Microwave assisted and conventional pyrolysis of MDF – Characterization of the produced biochars. *Journal of Analytical and Applied Pyrolysis,* 138**,** 218-230.

HAGOS, F. Y., A. AZIZ, A. R. & SULAIMAN, S. A. 2015. Methane enrichment of syngas (H2/CO) in a spark-ignition direct-injection engine: Combustion, performance and emissions comparison with syngas and Compressed Natural Gas. *Energy,* 90, Part 2**,** 2006-2015.

HAN, J. H. 2013. *Innovations in Food Packaging*, Elsevier Science.

HAN, Y., GHOLIZADEH, M., TRAN, C.-C., KALIAGUINE, S., LI, C.-Z., OLARTE, M. & GARCIA-PEREZ, M. 2019. Hydrotreatment of pyrolysis bio-oil: A review. *Fuel Processing Technology,* 195**,** 106140.

HANKALIN, V., AHONEN, T. & RAIKO, R. On thermal properties of a pyrolysing wood particle. Finnish-Swedish Flame Days, 2009 Naantali, Finland. 1-20.

HANSMANN, C., GINDL, W., WIMMER, R. & TEISCHINGER, A. 2002. Permeability of wood - A review. *Wood research,* 47**,** 1-16.

HAO, N., BEN, H., YOO, C. G., ADHIKARI, S. & RAGAUSKAS, A. J. 2016. Review of NMR Characterization of Pyrolysis Oils. *Energy & Fuels,* 30**,** 6863-6880.

HAYNES, W. M. 2014. *CRC handbook of chemistry and physics*, CRC press.

HENDERSON, R. K., JIMÉNEZ-GONZÁLEZ, C., CONSTABLE, D. J., ALSTON, S. R., INGLIS, G. G., FISHER, G., SHERWOOD, J., BINKS, S. P. & CURZONS, A. D. 2011. Expanding GSK's solvent selection guide–embedding sustainability into solvent selection starting at medicinal chemistry. *Green Chemistry,* 13**,** 854-862.

HERMIZ, N. A., HASTED, J. B. & ROSENBERG, C. 1982. Microwave dielectric losses of n-alkanes. *Journal of the Chemical Society, Faraday Transactions 2: Molecular and Chemical Physics,* 78**,** 147-161.

HESS, J., BEDNARZ, D., BAE, J. & PIERCE, J. 2011. Petroleum and health care: evaluating and managing health care's vulnerability to petroleum supply shifts. *American journal of public health,* 101**,** 1568-1579.
HOU, S.-S., HUANG, W.-C. & LIN, T.-H. 2017. Co-combustion of fast pyrolysis bio-oil derived from coffee bean residue and diesel in an oil-fired furnace. *Applied Sciences,* 7**,** 1085.
HU, X. & GHOLIZADEH, M. 2019. Biomass pyrolysis: A review of the process development and challenges from initial researches up to the commercialisation stage. *Journal of Energy Chemistry,* 39**,** 109-143.
HUANG, Y. F., CHIUEH, P. T., KUAN, W. H. & LO, S. L. 2015a. Effects of lignocellulosic composition and microwave power level on the gaseous product of microwave pyrolysis. *Energy,* 89**,** 974-981.
HUANG, Y. F., CHIUEH, P. T., SHIH, C. H., LO, S. L., SUN, L. P., ZHONG, Y. & QIU, C. S. 2015b. Microwave pyrolysis of rice straw to produce biochar as an adsorbent for CO2 capture. *Energy,* 84**,** 75-82.
HUNT, J. & GU, H. 2006. Two-dimensional finite element heat transfer model of softwood. Part 1. Effective thermal conductivity. *Wood and fiber science: journal of the Society of Wood Science and Technology,* 38**,** 592-598.
IASON, V. F., JEFFERY SIMON, L. E. E., CATARINA, B. A., MARIJN, V. D. V. & DIAFAS 2009. Biochar Application to Soils - A Critical Scientific Review of Effects on Soil Properties, Processes and Functions.
IEA 2019a. World Energy Balances 2019. France: International Energy Agency.
IEA 2019b. World Energy Investment 2019. France: International Energy Agency.
INTERNATIONAL ENERGY AGENCY 2007. Annual Report 2006. Paris, France.
ISAHAK, W. N. R. W., HISHAM, M. W. M., YARMO, M. A. & YUN HIN, T.-Y. 2012. A review on bio-oil production from biomass by using pyrolysis method. *Renewable and Sustainable Energy Reviews,* 16**,** 5910-5923.
JAHIRUL, M., RASUL, M., CHOWDHURY, A. & ASHWATH, N. 2012. Biofuels Production through Biomass Pyrolysis —A Technological Review. *Energies,* 5**,** 4952.
JENKINS, B. M., BAXTER, L. L., MILES JR, T. R. & MILES, T. R. 1998. Combustion properties of biomass. *Fuel Processing Technology,* 54**,** 17-46.
JIN, X., CHEN-YANG, N., DENG-YIN, Z., YAN-HUI, G., QI-MIN, H., YU-HONG, X. & PAUL, B. 2019. Co-pyrolysis of rice straw and water hyacinth: Characterization of products, yields and biomass interaction effect. *Biomass and Bioenergy,* 127**,** 105281.
JONES, S. B., HOLLADAY, J. E., VALKENBURG, C., STEVENS, D. J., WALTON, C. W., KINCHIN, C., ELLIOTT, D. C. & CZERNIK, S. 2009. Production of Gasoline and Diesel from Biomass via Fast Pyrolysis, Hydrotreating and Hydrocracking: A Design Case. Springfield, VA, USA: U.S. Department of Energy.
KALLIOINEN, A., VAARI, A., RÄTTÖ, M., KONN, J., SIIKA-AHO, M. & VIIKARI, L. 2003. Effects of bacterial treatments on wood extractives. *Journal of Biotechnology,* 103**,** 67-76.
KANDIYOTI, R., HEROD, A., BARTLE, K. & MORGAN, T. 2017. 1 - Fossil fuels and renewables. *In:* KANDIYOTI, R., HEROD, A., BARTLE, K. & MORGAN, T. (eds.) *Solid Fuels and Heavy Hydrocarbon Liquids (Second Edition).* Elsevier.
KANSA, E. J., PERLEE, H. E. & CHAIKEN, R. F. 1977. Mathematical model of wood pyrolysis including internal forced convection. *Combustion and Flame,* 29**,** 311-324.
KAPPE, C. O. 2004. Controlled Microwave Heating in Modern Organic Synthesis. *Angewandte Chemie International Edition,* 43**,** 6250-6284.
KAPPE, C. O., STADLER, A., DALLINGER, D. 2012. Equipment Review. *In:* RAIMUND MANNHOLD, H. K., GERD FOLKERS (ed.) *Microwaves in Organic and Medicinal Chemistry.* Weinheim, Germany: Wiley-VCH Verlag & Co. KGaA.
KHARE, P. & GOYAL, D. K. 2013. Effect of high and low rank char on soil quality and carbon sequestration. *Ecological Engineering,* 52**,** 161-166.
KILZER, F. J. & BROIDO, A. 1965. Speculations on the nature of cellulose pyrolysis. *Pyrodynamics. 2: 151-163,* 2**,** 151-163.

KIM, J.-S. 2015. Production, separation and applications of phenolic-rich bio-oil – A review. *Bioresource Technology,* 178**,** 90-98.
KIM, J.-S. & CHOI, G.-G. 2018. Chapter 11 - Pyrolysis of Lignocellulosic Biomass for Biochemical Production. *In:* BHASKAR, T., PANDEY, A., MOHAN, S. V., LEE, D.-J. & KHANAL, S. K. (eds.) *Waste Biorefinery.* Elsevier.
KIM, K. H., DAUGAARD, T. J., SMITH, R., MBA-WRIGHT, M. & BROWN, R. C. 2019. Recovery of resin acids from fast pyrolysis of pine. *Journal of Analytical and Applied Pyrolysis,* 138**,** 132-136.
KOSTAS, E. T., DURÁN-JIMÉNEZ, G., SHEPHERD, B. J., MEREDITH, W., STEVENS, L. A., WILLIAMS, O. S. A., LYE, G. J. & ROBINSON, J. P. 2019a. Microwave pyrolysis of olive pomace for bio-oil and bio-char production. *Chemical Engineering Journal***,** 123404.
KOSTAS, E. T., WHITE, D. A., DU, C. & COOK, D. J. 2016. Selection of yeast strains for bioethanol production from UK seaweeds. *Journal of applied phycology,* 28**,** 1427-1441.
KOSTAS, E. T., WILLIAMS, O. S. A., DURAN-JIMENEZ, G., TAPPER, A. J., COOPER, M., MEEHAN, R. & ROBINSON, J. P. 2019b. Microwave pyrolysis of Laminaria digitata to produce unique seaweed-derived bio-oils. *Biomass and Bioenergy,* 125**,** 41-49.
KUMAR, P., KUMAR, P., RAO, P. V. C., CHOUDARY, N. V. & SRIGANESH, G. 2017. Saw dust pyrolysis: Effect of temperature and catalysts. *Fuel,* 199**,** 339-345.
LAM, S. S., WAN MAHARI, W. A., MA, N. L., AZWAR, E., KWON, E. E., PENG, W., CHONG, C. T., LIU, Z. & PARK, Y.-K. 2019. Microwave pyrolysis valorization of used baby diaper. *Chemosphere,* 230**,** 294-302.
LEE, C. S., BINNER, E., WINKWORTH-SMITH, C., JOHN, R., GOMES, R. & ROBINSON, J. 2016. Enhancing natural product extraction and mass transfer using selective microwave heating. *Chemical Engineering Science,* 149**,** 97-103.
LEI, Z.-P., HU, Z.-Q., SHUI, H.-F., REN, S.-B., WANG, Z.-C., KANG, S.-G. & PAN, C.-X. 2015. Pyrolysis of lignin following ionic liquid pretreatment at low temperature. *Fuel Processing Technology,* 138**,** 612-615.
LESTER, E., GONG, M. & THOMPSON, A. 2007. A method for source apportionment in biomass/coal blends using thermogravimetric analysis. *Journal of Analytical and Applied Pyrolysis,* 80**,** 111-117.
LESTER, E., KINGMAN, S., DODDS, C. & PATRICK, J. 2006. The potential for rapid coke making using microwave energy. *Fuel,* 85**,** 2057-2063.
LI, T., NIU, Y., WANG, L. & LØVÅS, T. 2017. Gasification of High Heating-rate Biomass-derived Chars at Elevated Temperatures. *Energy Procedia,* 105**,** 642-647.
LIAW, S.-S., WANG, Z., NDEGWA, P., FREAR, C., HA, S., LI, C.-Z. & GARCIA-PEREZ, M. 2012. Effect of pyrolysis temperature on the yield and properties of bio-oils obtained from the auger pyrolysis of Douglas Fir wood. *Journal of Analytical and Applied Pyrolysis,* 93**,** 52-62.
LIHRA, T., CLOUTIER, A. & ZHANG, S.-Y. 2007. Longitudinal and transverse permeability of balsam fir wetwood and normal heartwood. *Wood and Fiber Science,* 32**,** 164-178.
LO, S.-L., HUANG, Y.-F., CHIUEH, P.-T. & KUAN, W.-H. 2017. Microwave Pyrolysis of Lignocellulosic Biomass. *Energy Procedia,* 105**,** 41-46.
LUNDBERG, L., TCHOFFOR, P. A., PALLARÈS, D., JOHANSSON, R., THUNMAN, H. & DAVIDSSON, K. 2016. Influence of surrounding conditions and fuel size on the gasification rate of biomass char in a fluidized bed. *Fuel Processing Technology,* 144**,** 323-333.
MA, S., ZHANG, L., ZHU, L. & ZHU, X. 2018. Preparation of multipurpose bio-oil from rice husk by pyrolysis and fractional condensation. *Journal of Analytical and Applied Pyrolysis,* 131**,** 113-119.
MACQUARRIE, D. J., CLARK, J. H. & FITZPATRICK, E. 2012. The microwave pyrolysis of biomass. *Biofuels, Bioproducts and Biorefining,* 6**,** 549-560.

MAFU, L. D., NEOMAGUS, H. W. J. P., EVERSON, R. C., OKOLO, G. N., STRYDOM, C. A. & BUNT, J. R. 2018. The carbon dioxide gasification characteristics of biomass char samples and their effect on coal gasification reactivity during co-gasification. *Bioresource Technology,* 258**,** 70-78.

MAHONEY, W. D. 2000. 3.10.2 Dielectric Constant. *In:* MAHONEY, W. D. (ed.) *Wood Engineering Handbook (2nd Edition).* Los Angeles: BNI Building News.

MARSMAN, J. H., WILDSCHUT, J., EVERS, P., DE KONING, S. & HEERES, H. J. 2008. Identification and classification of components in flash pyrolysis oil and hydrodeoxygenated oils by two-dimensional gas chromatography and time-of-flight mass spectrometry. *Journal of Chromatography A,* 1188**,** 17-25.

MEREDITH, R. J. 1998. *Engineers' Handbook of Industrial Microwave Heating*, Institution of Electrical Engineers.

METAXAS, A. C. & MEREDITH, R. J. 1983. *Industrial Microwave Heating*, P. Peregrinus.

MIRANDA, I., SOUSA, V., FERREIRA, J. & PEREIRA, H. 2017. Chemical characterization and extractives composition of heartwood and sapwood from Quercus faginea. *PLOS ONE,* 12**,** e0179268.

MOHAN, D., PITTMAN, C. U. & STEELE, P. H. 2006. Pyrolysis of Wood/Biomass for Bio-oil: A Critical Review. *Energy & Fuels,* 20**,** 848-889.

MOK, W. S. L. & ANTAL, M. J. 1983. Effects of pressure on biomass pyrolysis. II. Heats of reaction of cellulose pyrolysis. *Thermochimica Acta,* 68**,** 165-186.

MONTAZERI, M. & ECKELMAN, M. J. 2015. Life Cycle Assessment of Catechols from Lignin Depolymerization. *ACS Sustainable Chemistry & Engineering*.

MORAES, M. S. A., MIGLIORINI, M. V., DAMASCENO, F. C., GEORGES, F., ALMEIDA, S., ZINI, C. A., JACQUES, R. A. & CARAMÃO, E. B. 2012. Qualitative analysis of bio oils of agricultural residues obtained through pyrolysis using comprehensive two dimensional gas chromatography with time-of-flight mass spectrometric detector. *Journal of Analytical and Applied Pyrolysis,* 98**,** 51-64.

MORTENSEN, P. M., GRUNWALDT, J. D., JENSEN, P. A., KNUDSEN, K. G. & JENSEN, A. D. 2011. A review of catalytic upgrading of bio-oil to engine fuels. *Applied Catalysis A: General,* 407**,** 1-19.

MOTASEMI, F., AFZAL, M. T. & SALEMA, A. A. 2014. Microwave dielectric characterization of hay during pyrolysis. *Industrial Crops and Products,* 61**,** 492-498.

MOTASEMI, F., SALEMA, A. A. & AFZAL, M. T. 2015. Dielectric characterization of corn stover for microwave processing technology. *Fuel Processing Technology,* 131**,** 370-375.

MUHAMMAD, N., OMAR, W. N., MAN, Z., BUSTAM, M. A., RAFIQ, S. & UEMURA, Y. 2012. Effect of Ionic Liquid Treatment on Pyrolysis Products from Bamboo. *Industrial & Engineering Chemistry Research,* 51**,** 2280-2289.

NAIK, S., GOUD, V. V., ROUT, P. K., JACOBSON, K. & DALAI, A. K. 2010. Characterization of Canadian biomass for alternative renewable biofuel. *Renewable Energy,* 35**,** 1624-1631.

NAMAZI, A. B., GRANT ALLEN, D. & JIA, C. Q. 2015. Microwave-assisted pyrolysis and activation of pulp mill sludge. *Biomass and Bioenergy,* 73**,** 217-224.

NFPA 2000. NFPA 77 - Recommended Practice on Static Electricity. Quincy, US: National Fire Protection Association.

NIK-AZAR, M., HAJALIGOL, M. R., SOHRABI, M. & DABIR, B. 1997. Mineral matter effects in rapid pyrolysis of beech wood. *Fuel Processing Technology,* 51**,** 7-17.

OJA, V. & SUUBERG, E. M. 1999. Vapor Pressures and Enthalpies of Sublimation of d-Glucose, d-Xylose, Cellobiose, and Levoglucosan. *Journal of Chemical & Engineering Data,* 44**,** 26-29.

ONIMISI, M. 2015. *Computation of Dielectric Constant and Loss Factor of Water and Dimethylsulphoxide from 0.1 to 13 GHz*.

PARK, W. C., ATREYA, A. & BAUM, H. R. 2010. Experimental and theoretical investigation of heat and mass transfer processes during wood pyrolysis. *Combustion and Flame,* 157**,** 481-494.

PARTHASARATHY, P. & NARAYANAN, K. S. 2014. Hydrogen production from steam gasification of biomass: Influence of process parameters on hydrogen yield – A review. *Renewable Energy,* 66**,** 570-579.
PATTIYA, A. 2018. 1 - Fast pyrolysis. *In:* ROSENDAHL, L. (ed.) *Direct Thermochemical Liquefaction for Energy Applications.* Woodhead Publishing.
PATWARDHAN, P. R., BROWN, R. C. & SHANKS, B. H. 2011. Product Distribution from the Fast Pyrolysis of Hemicellulose. *ChemSusChem,* 4**,** 636-643.
PATWARDHAN, P. R., SATRIO, J. A., BROWN, R. C. & SHANKS, B. H. 2009. Product distribution from fast pyrolysis of glucose-based carbohydrates. *Journal of Analytical and Applied Pyrolysis,* 86**,** 323-330.
PECHA, B. & GARCIA-PEREZ, M. 2015. Chapter 26 - Pyrolysis of Lignocellulosic Biomass: Oil, Char, and Gas. *In:* DAHIYA, A. (ed.) *Bioenergy.* Boston: Academic Press.
PIISPANEN, R. & SARANPÄÄ, P. 2002. Neutral lipids and phospholipids in Scots pine (Pinus sylvestris) sapwood and heartwood. *Tree Physiology,* 22**,** 661-666.
PLAIS, C. & AUGIER, F. 2016. Effect of liquid viscosity on mixing times in bubble columns. *Theoretical Foundations of Chemical Engineering,* 50**,** 969-974.
PRIMAZ, C. T., SCHENA, T., LAZZARI, E., CARAMÃO, E. B. & JACQUES, R. A. 2018. Influence of the temperature in the yield and composition of the bio-oil from the pyrolysis of spent coffee grounds: Characterization by comprehensive two dimensional gas chromatography. *Fuel,* 232**,** 572-580.
PROSKURINA, S., JUNGINGER, M., HEINIMÖ, J., TEKINEL, B. & VAKKILAINEN, E. 2019. Global biomass trade for energy— Part 2: Production and trade streams of wood pellets, liquid biofuels, charcoal, industrial roundwood and emerging energy biomass. *Biofuels, Bioproducts and Biorefining,* 13**,** 371-387.
RAVEENDRAN, K., GANESH, A. & KHILAR, K. C. 1995. Influence of mineral matter on biomass pyrolysis characteristics. *Fuel,* 74**,** 1812-1822.
READER, H. C. 2006. Understanding Microwave Heating Systems: A Perspective on State-of-the-Art. *In:* WILLERT-PORADA, M. (ed.) *Advances in Microwave and Radio Frequency Processing.* Berlin, Heidelberg: Springer.
RESENDE, F. L. P. 2014. Chapter 1 - Reactor configurations and design parameters for thermochemical conversion of biomass into fuels, energy, and chemicals. *In:* SHI, F. (ed.) *Reactor and Process Design in Sustainable Energy Technology.* Amsterdam: Elsevier.
ROBINSON, J., DODDS, C., STAVRINIDES, A., KINGMAN, S., KATRIB, J., WU, Z. H., MEDRANO, J. & OVEREND, R. 2015. Microwave Pyrolysis of Biomass: Control of Process Parameters for High Pyrolysis Oil Yields and Enhanced Oil Quality. *Energy & Fuels,* 29**,** 1701-1709.
ROBINSON, J., KINGMAN, S., IRVINE, D., LICENCE, P., SMITH, A., DIMITRAKIS, G., OBERMAYER, D. & KAPPE, C. O. 2010a. Understanding microwave heating effects in single mode type cavities-theory and experiment. *Physical Chemistry Chemical Physics,* 12**,** 4750-4758.
ROBINSON, J. P., KINGMAN, S. W., BARRANCO, R., SNAPE, C. E. & AL-SAYEGH, H. 2010b. Microwave Pyrolysis of Wood Pellets. *Industrial & Engineering Chemistry Research,* 49**,** 459-463.
ROMANÍ, A., LARRAMENDI, A., YÁÑEZ, R., CANCELA, Á., SÁNCHEZ, Á., TEIXEIRA, J. A. & DOMINGUES, L. 2019. Valorization of Eucalyptus nitens bark by organosolv pretreatment for the production of advanced biofuels. *Industrial Crops and Products,* 132**,** 327-335.
ROMASHOV, L. V. & ANANIKOV, V. P. 2017. Alkynylation of Bio-Based 5-Hydroxymethylfurfural to Connect Biomass Processing with Conjugated Polymers and Furanic Pharmaceuticals. *Chemistry, an Asian journal,* 12**,** 2652-2655.
ROY, C., PAKDEL, H. & BROUILLARD, D. 1990. The role of extractives during vacuum pyrolysis of wood. *Journal of Applied Polymer Science,* 41**,** 337-348.

RUIZ, M., MARTIN, E., BLIN, J., VAN DE STEENE, L. & BROUST, F. 2017. Understanding the Secondary Reactions of Flash Pyrolysis Vapors inside a Hot Gas Filtration Unit. *Energy & Fuels,* 31**,** 13785-13795.
SAFDARI, M.-S., AMINI, E., WEISE, D. R. & FLETCHER, T. H. 2019. Heating rate and temperature effects on pyrolysis products from live wildland fuels. *Fuel,* 242**,** 295-304.
SAIT, H. H. & SALEMA, A. A. 2015. Microwave dielectric characterization of Saudi Arabian date palm biomass during pyrolysis and at industrial frequencies. *Fuel,* 161**,** 239-247.
SALEMA, A. A., ANI, F. N., MOURIS, J. & HUTCHEON, R. 2017. Microwave dielectric properties of Malaysian palm oil and agricultural industrial biomass and biochar during pyrolysis process. *Fuel Processing Technology,* 166**,** 164-173.
SATO, M. K., DE LIMA, H. V., COSTA, A. N., RODRIGUES, S., PEDROSO, A. J. S. & DE FREITAS MAIA, C. M. B. 2019. Biochar from Acai agroindustry waste: Study of pyrolysis conditions. *Waste Management,* 96**,** 158-167.
SATTAR, A., LEEKE, G. A., HORNUNG, A. & WOOD, J. 2014. Steam gasification of rapeseed, wood, sewage sludge and miscanthus biochars for the production of a hydrogen-rich syngas. *Biomass and Bioenergy,* 69**,** 276-286.
SERTH, R. W. 2007. 9 - BOILING HEAT TRANSFER. *In:* SERTH, R. W. (ed.) *Process Heat Transfer.* Oxford: Academic Press.
SERWAY, R. A. & JEWETT, J. W. 2012. *Principles of Physics: A Calculus-Based Text*, Cengage Learning.
SHARMA, S. & SHETH, P. N. 2016. Air–steam biomass gasification: Experiments, modeling and simulation. *Energy Conversion and Management,* 110**,** 307-318.
SHUKLA, N., SAHOO, D. & REMYA, N. 2019. Biochar from microwave pyrolysis of rice husk for tertiary wastewater treatment and soil nourishment. *Journal of Cleaner Production,* 235**,** 1073-1079.
SIPPULA, O., HUTTUNEN, K., HOKKINEN, J., KÄRKI, S., SUHONEN, H., KAJOLINNA, T., KORTELAINEN, M., KARHUNEN, T., JALAVA, P., USKI, O., YLI-PIRILÄ, P., HIRVONEN, M.-R. & JOKINIEMI, J. 2019. Emissions from a fast-pyrolysis bio-oil fired boiler: Comparison of health-related characteristics of emissions from bio-oil, fossil oil and wood. *Environmental Pollution,* 248**,** 888-897.
SITUMORANG, Y. A., ZHAO, Z., YOSHIDA, A., ABUDULA, A. & GUAN, G. 2020. Small-scale biomass gasification systems for power generation (<200 kW class): A review. *Renewable and Sustainable Energy Reviews,* 117**,** 109486.
SLEZAK, R., KRZYSTEK, L. & LEDAKOWICZ, S. 2019. Steam gasification of pyrolysis char from spent mushroom substrate. *Biomass and Bioenergy,* 122**,** 336-342.
SMETS, K., ADRIAENSENS, P., REGGERS, G., SCHREURS, S., CARLEER, R. & YPERMAN, J. 2011. Flash pyrolysis of rapeseed cake: Influence of temperature on the yield and the characteristics of the pyrolysis liquid. *Journal of Analytical and Applied Pyrolysis,* 90**,** 118-125.
SMITH, A. D., LESTER, E., THURECHT, K. J., EL HARFI, J., DIMITRAKIS, G., KINGMAN, S. W., ROBINSON, J. P. & IRVINE, D. J. 2010. Dielectric Properties of Free-Radical Polymerizations: Molecularly Symmetrical Initiators during Thermal Decomposition. *Industrial & Engineering Chemistry Research,* 49**,** 1703-1710.
SOLANTAUSTA, Y., NYLUND, N.-O., WESTERHOLM, M., KOLJONEN, T. & OASMAA, A. 1993. Wood-pyrolysis oil as fuel in a diesel-power plant. *Bioresource Technology,* 46**,** 177-188.
SONG, Y.-C., LI, Q.-T., LI, F.-Z., WANG, L.-S., HU, C.-C., FENG, J. & LI, W.-Y. 2019. Pathway of biomass-potassium migration in co-gasification of coal and biomass. *Fuel,* 239**,** 365-372.
SPEIGHT, J. G. 2014. Chapter 3 - Gasifier Types. *In:* SPEIGHT, J. G. (ed.) *Gasification of Unconventional Feedstocks.* Boston: Gulf Professional Publishing.
SPEIGHT, J. G. 2017. *Rules of Thumb for Petroleum Engineers*, Wiley.
STANKOVIKJ, F. & GARCIA-PEREZ, M. 2017. TG-FTIR Method for the Characterization of Bio-oils in Chemical Families. *Energy & Fuels,* 31**,** 1689-1701.

STANKOVIKJ, F., MCDONALD, A. G., HELMS, G. L. & GARCIA-PEREZ, M. 2016. Quantification of Bio-Oil Functional Groups and Evidences of the Presence of Pyrolytic Humins. *Energy & Fuels,* 30**,** 6505-6524.

STANKOVIKJ, F., MCDONALD, A. G., HELMS, G. L., OLARTE, M. V. & GARCIA-PEREZ, M. 2017. Characterization of the Water-Soluble Fraction of Woody Biomass Pyrolysis Oils. *Energy & Fuels,* 31**,** 1650-1664.

STEER, M. B. 2010. C.2 Conductors, Dielectrics, and Magnetic Materials. *In:* KAY, D. R. (ed.) *Microwave and RF Design - A Systems Approach.* Raleigh, North Carolina: SciTech Publishing.

STUERGA, D. & DELMOTTE, M. 2002. Wave-material interactions, microwave technology and equipment. *In:* LOUPY, A. (ed.) *Microwaves in organic synthesis.* Weinheim, Germany: Wiley-VCH Verlag & Co. KGaA.

SUN, W. & OTHMAN, M. Z. 2019. A selective fractionation method of lignocellulosic materials using electro-assisted organosolv pretreatment. *Bioresource Technology,* 288**,** 121421.

SUNTIVARAKORN, R., TREEDET, W., SINGBUA, P. & TEERAMAETAWAT, N. 2018. Fast pyrolysis from Napier grass for pyrolysis oil production by using circulating Fluidized Bed Reactor: Improvement of pyrolysis system and production cost. *Energy Reports,* 4**,** 565-575.

SUUBERG, E. M. & OJA, V. 1997. Vapor pressures and heats of vaporization of primary coal tars. Federal Energy Technology Center, Morgantown, WV (US).

THENGANE, S. K., GUPTA, A. & MAHAJANI, S. M. 2019. Co-gasification of high ash biomass and high ash coal in downdraft gasifier. *Bioresource Technology,* 273**,** 159-168.

THOSTENSON, E. T. & CHOU, T. W. 1999. Microwave processing: fundamentals and applications. *Composites Part A: Applied Science and Manufacturing,* 30**,** 1055-1071.

TRINH, T. N., JENSEN, P. A., SÁROSSY, Z., DAM-JOHANSEN, K., KNUDSEN, N. O., SØRENSEN, H. R. & EGSGAARD, H. 2013. Fast Pyrolysis of Lignin Using a Pyrolysis Centrifuge Reactor. *Energy & Fuels,* 27**,** 3802-3810.

TRIPATHI, M., SAHU, J. N., GANESAN, P. & DEY, T. K. 2015. Effect of temperature on dielectric properties and penetration depth of oil palm shell (OPS) and OPS char synthesized by microwave pyrolysis of OPS. *Fuel,* 153**,** 257-266.

UNDRI, A., ABOU-ZAID, M., BRIENS, C., BERRUTI, F., ROSI, L., BARTOLI, M., FREDIANI, M. & FREDIANI, P. 2015. Bio-oil from pyrolysis of wood pellets using a microwave multimode oven and different microwave absorbers. *Fuel,* 153**,** 464-482.

UNITED NATIONS 2015. Paris Agreement. Paris: United Nations.

UNITED NATIONS 2019. World Population Prospects 2019: Ten Key Findings. United Nations, Department of Economic and Social Affairs, Population Division.

VAMVUKA, D. 2011. Bio-oil, solid and gaseous biofuels from biomass pyrolysis processes—An overview. *International Journal of Energy Research,* 35**,** 835-862.

VARHEGYI, G., ANTAL, M. J., SZEKELY, T. & SZABO, P. 1989. Kinetics of the thermal decomposition of cellulose, hemicellulose, and sugarcane bagasse. *Energy & Fuels,* 3**,** 329-335.

VENDERBOSCH, R. H. & PRINS, W. 2010. Fast pyrolysis technology development. *Biofuels, Bioproducts and Biorefining,* 4**,** 178-208.

VISPUTE, T. P., ZHANG, H., SANNA, A., XIAO, R. & HUBER, G. W. 2010. Renewable Chemical Commodity Feedstocks from Integrated Catalytic Processing of Pyrolysis Oils. *Science,* 330**,** 1222.

WANG, S., WANG, Q., JIANG, X., HAN, X. & JI, H. 2013. Compositional analysis of bio-oil derived from pyrolysis of seaweed. *Energy Conversion and Management,* 68**,** 273-280.

WESTERHOF, R. J. M., BRILMAN, D. W. F., VAN SWAAIJ, W. P. M. & KERSTEN, S. R. A. 2010. Effect of Temperature in Fluidized Bed Fast Pyrolysis of Biomass: Oil Quality Assessment in Test Units. *Industrial & Engineering Chemistry Research,* 49**,** 1160-1168.

XIE, Q., BORGES, F. C., CHENG, Y., WAN, Y., LI, Y., LIN, X., LIU, Y., HUSSAIN, F., CHEN, P. & RUAN, R. 2014. Fast microwave-assisted catalytic gasification of biomass for syngas production and tar removal. *Bioresource Technology,* 156**,** 291-296.

XU, J.-K., CHEN, J.-H. & SUN, R.-C. 2015. Hydrothermal microwave valorization of eucalyptus using acidic ionic liquid as catalyst toward a green biorefinery scenario. *Bioresource technology,* 193**,** 119-127.

YUAN, X., DING, X., LENG, L., LI, H., SHAO, J., QIAN, Y., HUANG, H., CHEN, X. & ZENG, G. 2018. Applications of bio-oil-based emulsions in a DI diesel engine: The effects of bio-oil compositions on engine performance and emissions. *Energy,* 154**,** 110-118.

ZHANG, S. P., DONG, Q., ZHANG, L., XIONG, Y. Q., LIU, X. Z. & ZHU, S. G. 2015. Effects of water washing and torrefaction pretreatments on rice husk pyrolysis by microwave heating. *Bioresource Technology,* 193**,** 442-448.

ZHANG, W., SATHITSUKSANOH, N., BARONE, J. R. & RENNECKAR, S. 2016a. Enhanced enzymatic saccharification of pretreated biomass using glycerol thermal processing (GTP). *Bioresource Technology,* 199**,** 148-154.

ZHANG, X., YANG, W. & BLASIAK, W. 2012. Thermal decomposition mechanism of levoglucosan during cellulose pyrolysis. *Journal of Analytical and Applied Pyrolysis,* 96**,** 110-119.

ZHANG, Y., ZHENG, Y., YANG, M. & SONG, Y. 2016b. Effect of fuel origin on synergy during co-gasification of biomass and coal in CO2. *Bioresource Technology,* 200**,** 789-794.

ZHOU, S., GARCIA-PEREZ, M., PECHA, B., MCDONALD, A. G., KERSTEN, S. R. A. & WESTERHOF, R. J. M. 2013. Secondary Vapor Phase Reactions of Lignin-Derived Oligomers Obtained by Fast Pyrolysis of Pine Wood. *Energy & Fuels,* 27**,** 1428-1438.

ZHOU, X., LI, W., MABON, R. & BROADBELT, L. J. 2018. A mechanistic model of fast pyrolysis of hemicellulose. *Energy & Environmental Science,* 11**,** 1240-1260.

Appendix A – Sycamore specific heat capacity from differential scanning calorimetry (DSC)

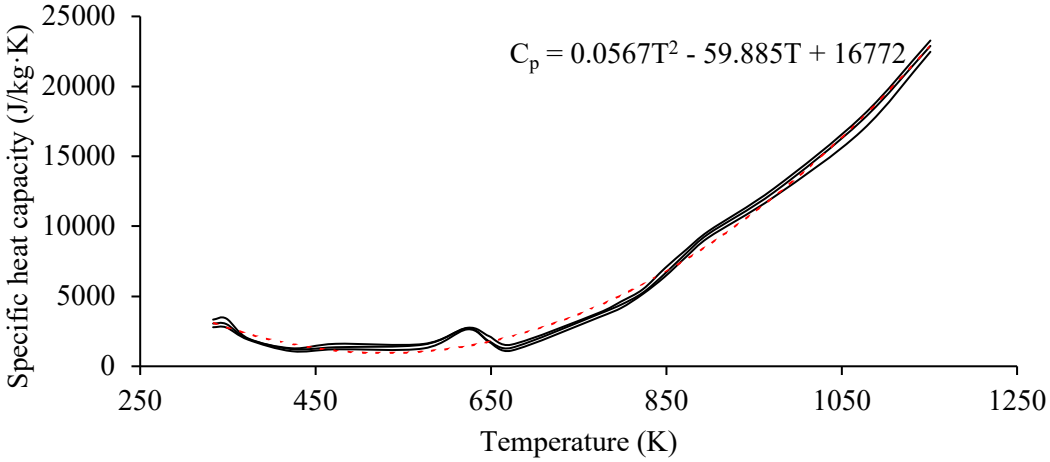


Figure A-1 – The specific heat capacity of the sycamore used within the thesis, and line of best fit equation.

Appendix B – Chapter 3 supplementary information

B.1 Additional absorbance curves

Isooctane

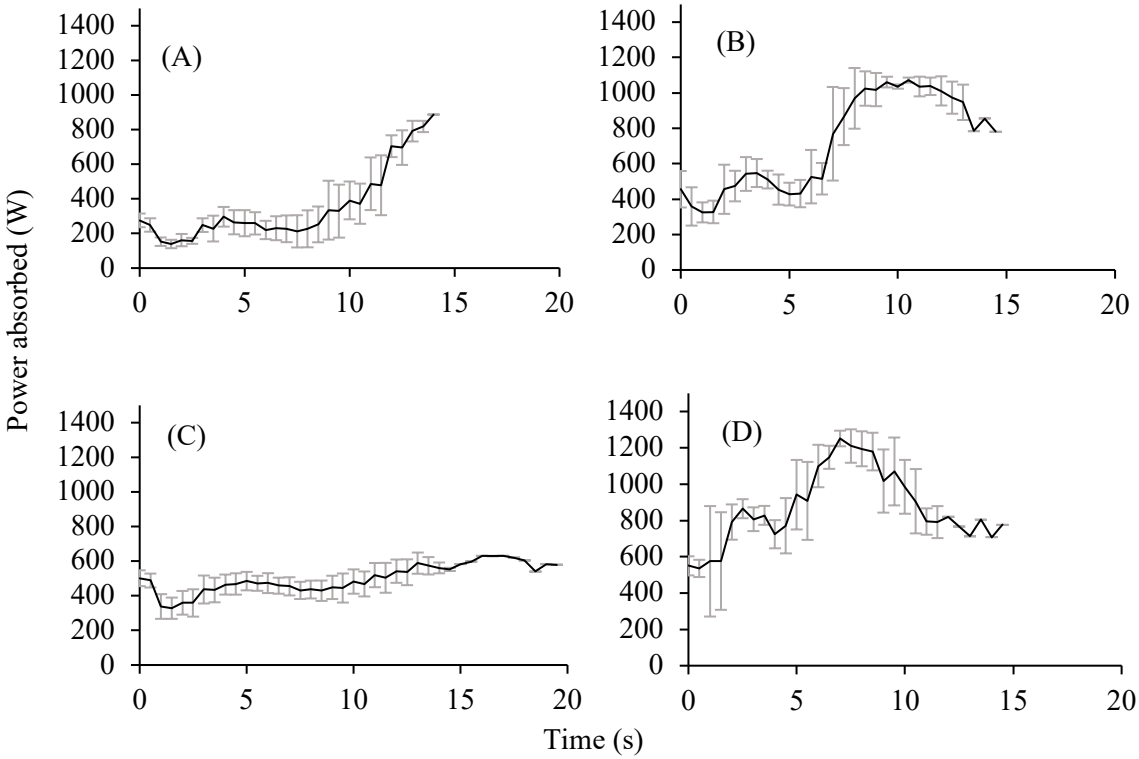


Figure B-1 - Absorbance data for isooctane based on (A) 1.00 kW, (B) 1.25 kW, (C) 1.50 kW, (D) 1.80 kW applied powers with fixed cold-matching

Kerosene

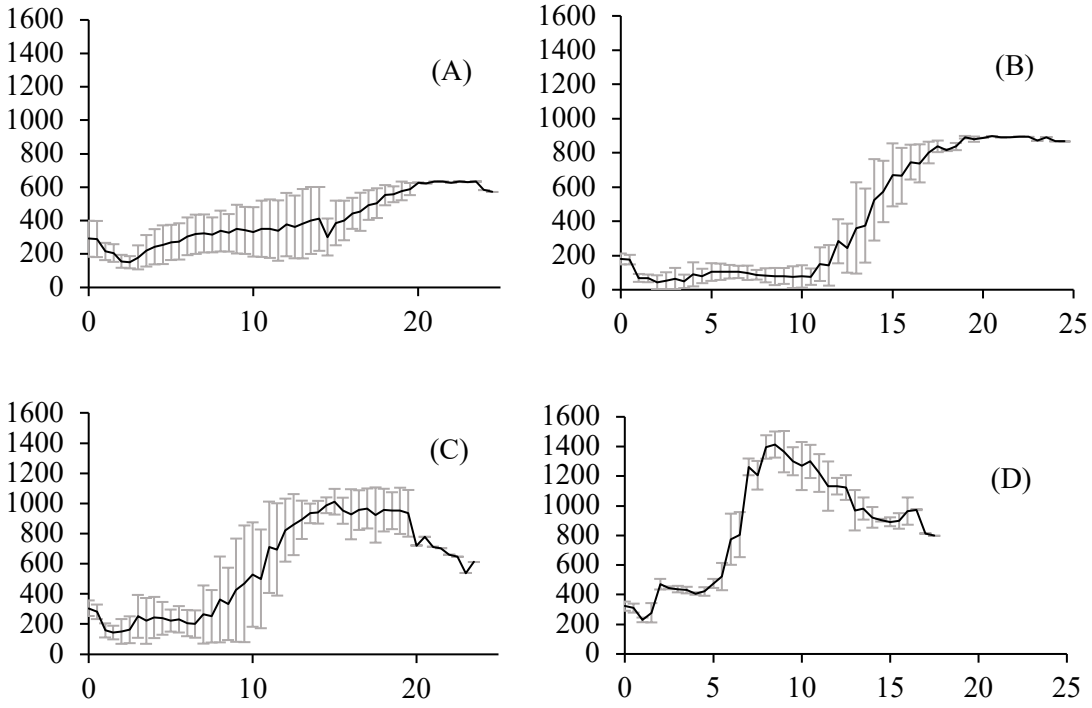


Figure B-2 - Absorbance data for kerosene based on (A) 1.00 kW, (B) 1.25 kW, (C) 1.50 kW, (D) 1.80 kW forwarded powers with fixed cold-matching

Pentane

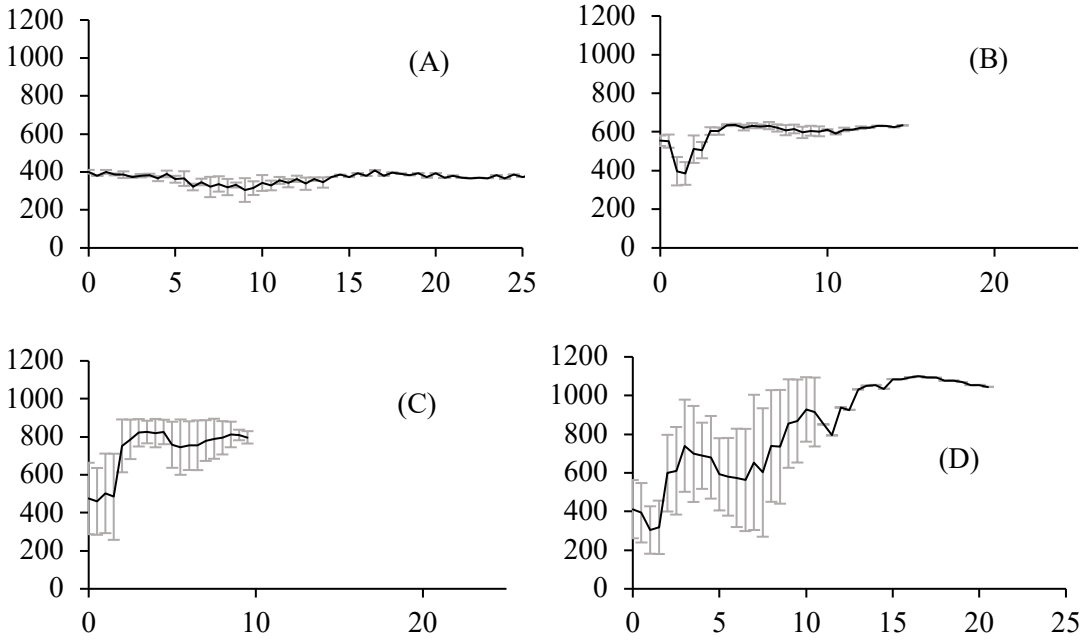


Figure B-3 - Absorbance data for pentane based on (A) 0.70 kW, (B) 1.00 kW, (C) 1.25 kW, (D) 1.50 kW forwarded powers with fixed cold-matching

Absorbance of the empty cavity

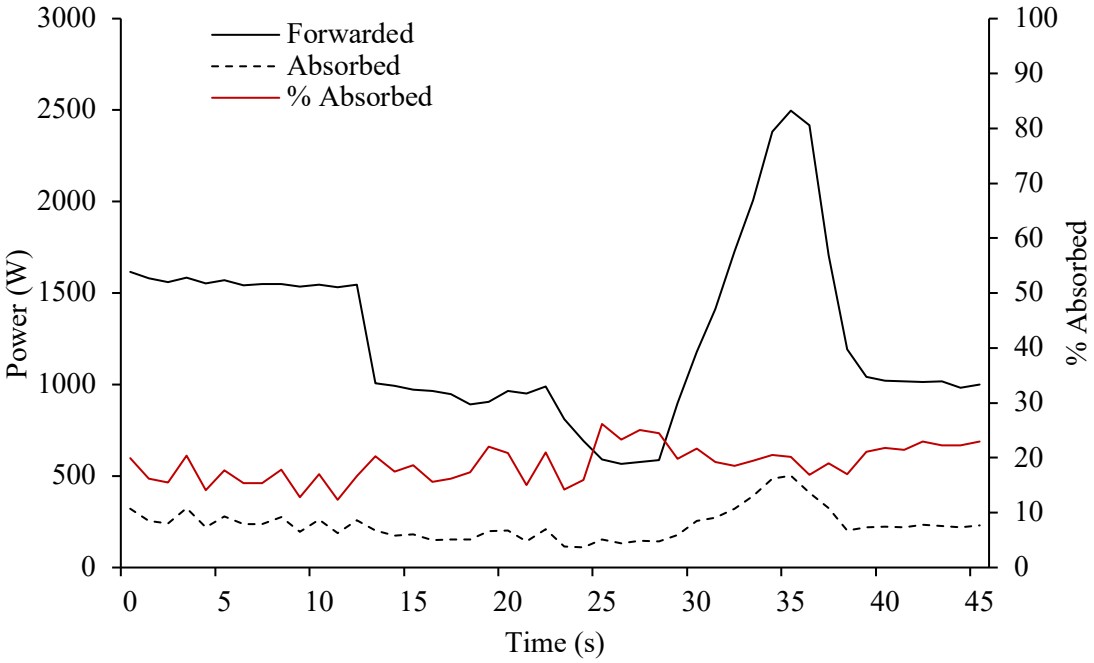


Figure B-4 - Applied power, absorbed power and percentage power absorbed for the cavity only containing the quartz tube with cyclohexane, no sycamore present

B.2 Pyrolysis oil composition

Table B-1 - Group abundance in the inerting media used, based on peak area.

Group	Peak area (%)					
	n-Hexane (aqueous)	n-Hexane (organic)	Nitrogen (1.08 kJ/g)	Nitrogen (1.89 kJ/g)	2-Propanol	Water
Aromatic	-	-	5.2	3.7	7.9	1.0
Acids and esters	18.7	5.4	0.4	0.2	-	0.6
Aldehydes	13.0	7.3	2.0	3.6	3.3	10.3
Ketones	19.2	22.8	6.6	14.5	8.8	2.8
Phenols	9.3	44.5	33.9	33.3	45.1	54.4
Alcohols	4.2	1.1	8.4	6.0	4.7	9.7
Ethers	9.7	11.3	-	-	-	-
Sugars	15.9	-	0.2	-	5.6	-
Others	4.2	0.9	23.3	3.3	13.3	16.4
Not identified	5.9	6.7	20.0	35.5	11.1	4.8

Table B-2 – Aqueous phase oil composition, *n*-hexane solvent, analysed by collaborators in Spain (hydrocarbons not considered in the final peak area calculations, considered impurities).

Time (min)	Area (%)	Name	
var	14	Acetic acid	Acids and esters
5.026	0.51	Propanedioic acid	Acids and esters
5.072	0.83	Heptane	Hydrocarbons
5.15	0.67	1,2-Ethanediol	Alcohols
5.21	0.23	Acetic acid, hydroxy-, methyl ester	Acids and esters
5.662	0.12	Cyclohexane, methyl-	Hydrocarbons
5.768	0.47	Glycerin	Alcohols
6.112	0.16	Methacrylic anhydride	Anhydrides
6.313	0.29	2,2'-Bioxirane, (R@,R@)-(.+/-.)-	Ethers
6.54	0.16	(S)-5-Hydroxymethyl-2[5H]-furanone	Ketones
6.616	5.64	2-Propanone, 1-hydroxy-	Ketones
7.012	5.02	Pentanal, 2,4-dimethyl-	Aldehydes
7.067	2.04	Dextroamphetamine	Others
8.104	0.77	Furfural	Aldehydes
8.176	1.55	2-Pentanone, 4-hydroxy-4-methyl-	Ketones
8.504	7.28	1,3-Dioxolane, 2,2,4-trimethyl-	Ethers
8.654	0.66	2-Butanone	Ketones
8.751	0.43	4-Penten-2-one, 4-methyl-	Ketones
9.51	0.74	2(3H)-Furanone, 5-ethyldihydro-	Ketones
9.713	0.22	Vinyl crotonate $$ Crotonic acid vinyl ester	Acids and esters
9.77	0.28		Non identified
9.998	1.68	2(5H)-Furanone	Ketones
10.103	0.92	Furan, 2,5-dihydro-	Others
10.203	3.04	Cyclopentanone, 2-methyl-	Ketones
10.935	0.14	Acetic acid, hexyl ester	Acids and esters
11.059	0.16		Non identified
11.133	0.24		Non identified
11.201	0.26		Non identified
11.317	0.21		Non identified
11.431	0.18	2(5H)-Furanone, 3-methyl-	Ketones
11.605	0.19		Non identified
11.789	1.17	Cyclopentane-1,2-diol	Alcohols
11.986	1.16	2-Methyliminoperhydro-1,3-oxazine	Others
12.072	0.15	Acetic acid, 1-methylethyl ester	Acids and esters
12.277	0.14	2-Cyclopenten-1-one, 2-hydroxy-3-methyl-	Ketones
12.442	0.92	1,2-Cyclopentanedione, 3-methyl-	Ketones
12.574	0.26		Non identified
12.7	0.12	1-Butene-1,4-diol, diacetate	Acids and esters
12.885	0.2	1,4-Butanediol, diacetate	Acids and esters
12.979	0.62	2-Ethyl-3-vinyloxirane	Ethers
13.185	1.85	5-Oxotetrahydrofuran-2-carboxylic acid	Acids and esters
13.705	0.18		Non identified
13.746	0.21	Methyl 2-furoate	Acids and esters
13.789	0.48	Phenol, 2-methoxy-	Phenols
14.088	0.16	1,3-Cyclohexanedione, 2-methyl-	Ketones
14.154	2.6	Pentanal	Aldehydes
14.365	0.21	Maltol	Alcohols
14.459	0.13	2-Pentenoic acid, 4-hydroxy-	Acids and esters
14.793	0.8	2H-Pyran-2-one, tetrahydro-3,6-dimethyl-	Ketones

15.192	0.32		Non identified
15.3	0.4	Glycidol $$ Oxiranemethanol	Alcohols
15.348	0.46	2,5-Furandione, dihydro-3-methyl-	Ketones
15.385	0.29		Non identified
15.554	0.15	2,3-Dihydroxybenzaldehyde	Aldehydes
15.643	0.16	3(2H)-Furanone, 4-methoxy-2,5-dimethyl-	Ketones
15.742	0.26	4H-Pyran-4-one, 3,5-dihydroxy-2-methyl	Ketones
15.846	1.64	1,2-Benzenediol	Phenols
16.018	1.35	1-Pentanol, 2,3-dimethyl-	Alcohols
16.327	0.63		Non identified
16.518	0.44	3-Hexanol, 2,5-dimethyl-	Alcohols
16.582	1.62	2-Furancarboxaldehyde, 5-(hydroxymethyl)-	Aldehydes
16.63	0.3		Non identified
16.748	0.34	2,3-Anhydro-d-galactosan	Sugars
16.822	0.27	Anhydro-d-mannosan	Sugars
17.079	0.32	Hexane, 2,3,5-trimethyl-	Hydrocarbons
17.135	0.39	1,2-Benzenediol, 3-methyl-	Phenols
17.229	0.79	1,2-Benzenediol, 3-methoxy-	Phenols
17.307	1.75	Sucrose	Sugars
17.443	0.15	Phenol, 4-ethyl-2-methoxy-	Phenols
17.645	0.36		Non identified
17.921	1.07	1,3-Dioxan-4-one, 2-(1-methylethyl)-5-methyl	Ketones
18.101	0.14	Benzaldehyde, 4-hydroxy-	Aldehydes
18.178	1.02		Non identified
18.371	0.95	Phloroglucitol	Phenols
18.64	0.16		Non identified
18.697	0.37	1,4-Benzenediol, 2-methyl-	Phenols
18.809	1.95	Phenol, 2,6-dimethoxy-	Phenols
19.012	0.26	Phenol, 3,4-dimethoxy-	Phenols
19.06	0.17	d-Glycero-d-tallo-heptose	Sugars
19.205	0.45	1,2,3-Benzenetriol	Phenols
19.399	0.35	2-Propenoic acid, 2-methyl-, pentyl ester	Acids and esters
19.569	0.43	2-Propenoic acid, 2-methyl-, hexyl ester	Acids and esters
19.658	0.16		Non identified
19.824	0.66	Vanillin	Aldehydes
19.988	0.21	Acetic acid, pentyl ester	Acids and esters
20.379	1.05	1,2,3-Trimethoxybenzene	Ethers
20.47	0.14		Non identified
20.54	0.43	Phenol, 2-methoxy-4-(1-propenyl)-	Phenols
20.717	0.46	Phenol, 2-methoxy-4-propyl-	Phenols
20.764	1.69	D-Allose	Sugars
21.227	0.37	Ethanone, 1-(4-hydroxy-3-methoxyphenyl)-	Ketones
21.288	0.27		Non identified
21.534	13.08	1,6-Anhydro-.beta.-D-glucopyranose (levoglucosan)	Sugars
21.603	0.41	Benzene, 1,2,3-trimethoxy-5-methyl-	Ethers
21.826	0.36	2-Propanone, 1-(4-hydroxy-3-methoxyphenyl)-	Ketones
22.151	0.67	.beta.-d-Ribopyranoside, methyl, 3-acetate	Sugars
22.312	1.59	3',5'-Dimethoxyacetophenone	Ketones
22.587	0.24	4-((1E)-3-Hydroxy-1-propenyl)-2-methoxyphenol	Phenols
22.71	0.12		Non identified
22.79	0.33	Phenol, 2,6-dimethoxy-4-(2-propenyl)-	Phenols
22.898	0.26	1-Butanol, 2-methyl-, acetate	Acids and esters
23.515	0.39	1-Butene, 3-methyl-3-(1-ethoxyethoxy)	Ethers

23.57	0.24	Phenol, 2,6-dimethoxy-4-(2-propenyl)-	Phenols
23.672	0.25	Methyl-(2-hydoxy-3-ethoxy-benzyl)ether	Ethers
23.719	0.11		Non identified
23.869	1.7	Benzaldehyde, 4-hydroxy-3,5-dimethoxy-	Aldehydes
24.042	0.31	4-((1E)-3-Hydroxy-1-propenyl)-2-methoxyphenol	Phenols
24.357	1.03	Phenol, 2,6-dimethoxy-4-(2-propenyl)-	Phenols
24.4	0.92		Non identified
24.866	0.98	Ethanone, 1-(4-hydroxy-3,5-dimethoxyphenyl)-	Ketones
25.061	2	4-Hydroxy-2-methoxycinnamaldehyde	Aldehydes
25.283	0.82	2,4-Hexadienedioic acid, 3,4-diethyl-, dimethyl ester	Acids and esters
26.006	0.59	Benzene, 1,2,3-trimethoxy-5-methyl-	Ethers
26.097	0.3	Ethanone, 1-(4-hydroxy-3,5-dimethoxyphenyl)-	Ketones
26.973	0.4	3,5-Dimethoxy-4-hydroxyphenethylamine	Others
27.046	0.05		Non identified
28.269	1.25	Benzoic acid, 4-(1-hydroxyethyl)-, methyl ester	Acids and esters

Table B-3 – Organic phase oil composition, *n*-hexane solvent, analysed by collaborators in Spain (hydrocarbons not considered in the final peak area calculations, considered impurities).

Time (min)	Area (%)	Name	Group
5.088	12.88	Heptane	Hydrocarbons
5.158	1.26		Non identified
5.378	0.54		Non identified
5.453	0.14	Furan, 2,5-dimethyl-	Others
5.619	0.29	Formic acid, heptyl ester	Acids and esters
5.674	3.4	Cyclohexane, methyl-	Hydrocarbons
5.759	0.3	Acetic acid, 1-methylethyl ester	Acids and esters
5.835	0.25	Cyclopentane, ethyl-	Hydrocarbons
6.054	0.16	1-Heptene, 4-methyl-	Hydrocarbons
6.209	0.25	Pentane, 2,3,3-trimethyl-	Hydrocarbons
6.326	0.3	Furan, 2-methyl-	Others
6.57	0.17	Toluene	Hydrocarbons
6.607	1.33	Butane, 2-propoxy-	Ethers
6.782	0.36	2-Butenal, 2-methyl-	Ketones
7.017	2.44	Propanoic acid, 2-oxo-, methyl ester	Acids and esters
7.174	0.13	Cyclopentanone	Ketones
7.546	0.12	Crotonic acid	Acids and esters
7.681	0.19	Furfural	Aldehydes
7.755	0.24	2(5H)-Furanone, 3-methyl-	Ketones
7.894	0.37		Non identified
8.097	5.00	Furfural	Aldehydes
8.17	2.83	2-Pentanone, 4-hydroxy-4-methyl-	Ketones
8.27	0.1	2-Propenoic acid, 2-methyl-, ethenyl ester	Acids and esters
8.32	0.09	3-Hexanone	Ketones
8.463	0.77	2-Furanmethanol	Alcohols
8.565	0.09	3-Hexanone, 2-methyl-	Ketones
8.648	0.65	2-Hexanone, 3,4-dimethyl-	Ketones
8.746	0.86	2,3-Butanedione	Ketones
8.813	0.19	Vinyl crotonate	Acids and esters
8.89	0.55	2(3H)-Furanone, 5-methyl-	Ketones
9.292	0.34	4-Cyclopentene-1,3-dione	Ketones
9.335	0.14	Furan, tetrahydro-2,5-dimethoxy-	Ethers

9.716	0.33	Methacrylic anhydride	Anhydride
9.764	0.46	2-Cyclopenten-1-one, 2-methyl-	Ketones
9.846	0.22	Ethanone, 1-(2-furanyl)-	Ketones
10	0.66	2(5H)-Furanone	Ketones
10.188	1.6	Cyclopentanone, 2-methyl-	Ketones
10.44	0.19		Non identified
10.565	0.13	3-Penten-2-one, 4-methyl-	Ketones
10.643	0.15	3-Hepten-2-one, (E)	Ketones
10.873	0.28	Heptane, 2,3,6-trimethyl-	Hydrocarbons
10.937	0.6	Acetic acid, hexyl ester	Acids and esters
11.055	0.31	2-Furancarboxaldehyde, 5-methyl-	Non identified
11.133	0.15		Non identified
11.181	0.41	2-Cyclopenten-1-one, 3-methyl-	Ketones
11.266	0.15		Non identified
11.314	0.16	Phenol	Phenols
11.433	0.23	2(5H)-Furanone, 3-methyl-	Ketones
11.527	0.19	Isooctane, (ethenyloxy)-	Ethers
11.608	0.33	2,5-Furandione, 3-methyl-	Ketones
11.782	0.09	Cyclopentane-1,2-diol	Alcohols
11.878	0.22		Non identified
11.984	0.55	2H-Pyran, 3,4-dihydro-2-methoxy-	Ethers
12.275	0.23		Non identified
12.439	1.21	1,2-Cyclopentanedione, 3-methyl-	Ketones
12.721	0.24	2-Cyclopenten-1-one, 2,3-dimethyl-	Ketones
12.806	0.11	Decane, 4-methyl-	Hydrocarbons
12.986	0.38		Non identified
13.048	0.11		Non identified
13.553	0.13		Non identified
13.655	0.28	Dodecane	Hydrocarbons
13.7	0.12		Non identified
13.793	3.21	Phenol, 2-methoxy-	Phenols
13.947	0.2		Non identified
14.086	0.19		Non identified
14.377	0.33	2-Cyclopenten-1-one, 3-ethyl-2-hydroxy-	Ketones
14.948	0.29	Phenol, 2,6-dimethyl-	Phenols
15.186	0.1		Non identified
15.48	0.1		Non identified
15.557	0.34	2,3-Dihydroxybenzaldehyde	Aldehydes
15.611	0.2	2-Methoxy-6-methylphenol $$	Phenols
15.645	0.14	Hexadecane	Hydrocarbons
15.859	3.29	Phenol, 2-methoxy-4-methyl-	Phenols
16.506	0.16		Non identified
16.637	0.29	2,6,6-Trimethyl-2-cyclohexene-1,4-dione	Ketones
17.065	0.19		Non identified
17.229	0.24	1,2-Benzenediol, 3-methoxy	Ethers
17.449	1.04	Phenol, 4-ethyl-2-methoxy-	Phenols
17.508	0.18	Hexadecane	Hydrocarbons
17.65	0.14	Ethanone, 1-(2,5-dihydroxyphenyl)-	Ketones
18.185	4.42	2-Methoxy-4-vinylphenol	Phenols
18.813	5.59	Phenol, 2,6-dimethoxy-	Phenols
18.871	1.39	Eugenol	Phenols
19.021	0.41	Phenol, 2-methoxy-4-propyl-	Phenols
19.251	0.38	Tetradecane	Hydrocarbons
19.789	0.8	Phenol, 2-methoxy-4-(1-propenyl)-	Phenols

19.825	0.43	Vanillin	Aldehydes
20.385	5.16	1,2,4-Trimethoxybenzene	Ethers
20.548	5.43	Phenol, 2-methoxy-4-(1-propenyl)-	Phenols
20.723	0.14	Phenol, 2-methoxy-4-propyl-	Phenols
20.894	0.14	Tetradecane	Hydrocarbons
21.226	0.56	Ethanone, 1-(4-hydroxy-3-methoxyphenyl)-	Ketones
21.29	0.13		Non identified
21.605	1.56	Benzene, 1,2,3-trimethoxy-5-methyl-	Ethers
21.828	0.3	2-Propanone, 1-(4-hydroxy-3-methoxyphenyl)-	Ketones
22.315	5.19	3',5'-Dimethoxyacetophenone	Ketones
22.588	0.15	4-((1E)-3-Hydroxy-1-propenyl)-2-methoxyphenol	Phenols
22.729	0.23		Non identified
22.794	1.94	Phenol, 2,6-dimethoxy-4-(2-propenyl)-	Phenols
22.883	0.34	2,4-Hexadienedioic acid, 3,4-diethyl-, dimethyl ester, (Z,Z)-	Acids and esters
23.572	1.03	Phenol, 2,6-dimethoxy-4-(2-propenyl)-	Phenols
24.363	6.7	Phenol, 2,6-dimethoxy-4-(2-propenyl)-	Phenols

Table B-4 – Pyrolysis oil composition, nitrogen inerted, 1.08 kJ/g, analysed by a collaborator in the University of Nottingham.

Area (%)	Name	Group
0.74%		Non-identified
		Non-identified
0.30%		Non-identified
3.26%	3 (dioxolan2yl)-1,1-dimethyl-2-phenylpropylhydroxylamine	Diverse Chemical groups
0.22%		Non-identified
0.79%		Non-identified
2.78%	Ethyl benzene	Aromatic
2.20%	Ethyl benzene	Aromatic
0.20%	Xylene	Aromatic
0.35%		Non-identified
5.74%	3 (dioxolan2yl)-1,1-dimethyl-2-phenylpropylhydroxylamine	Non-identified
2.10%	Furfural	Aldehyde
0.95%	Cyclopentanone	Ketone
0.58%		Non-identified
0.19%	2 propenoic acid methyl ester	Ester
0.31%		Non-identified
1.23%	2 furanmethanol	Alcohol
0.43%	Furanmethanol	Alcohol
1.02%		Non-identified
0.26%		Non-identified
0.40%		Non-identified
0.23%		Non-identified
5.02%	Dl alpha methyl glutamic acid	Diverse Chemical groups
0.89%	Cyclohexanol	Alcohol
0.82%		Non-identified
0.48%	Furanone	Ketone
0.40%	Furanone	Ketone

3.49%	Furanone	Ketone
0.12%		Non-identified
0.53%		Non-identified
0.82%	Oxazolidine 2 2 diethyl 3 methyl	Diverse Chemical groups
5.05%	2 cyclopentene1one 2 hydroxy 3 methyl	Diverse Chemical groups
1.50%	Phenol	Phenol
0.40%	Phenol	Phenol
0.58%	Phenol	Phenol
6.86%	Phenol 2 methoxy	Phenol
0.14%		Non-identified
0.24%		Non-identified
0.23%		Non-identified
0.70%		Non-identified
0.49%		Non-identified
0.63%	Cyclopentenone ethyl hydroxy	Ketone
0.77%	Methyl phenol	Phenol
0.39%	Azulene	Aromatic
0.53%		Non-identified
0.91%		Non-identified
3.06%	Phenol 2 methoxy 4 methyl	Phenol
0.57%		Non-identified
0.37%		Non-identified
1.02%	Phenol 4 ethyl 2 methoxy	Phenol
0.30%		Non-identified
0.35%		Non-identified
0.25%	1,4:3,6 dianhydro- alpha d glucopyranose	Sugars
1.02%	2 methoxy 4 vinyl phenol	Diverse Chemical groups
1.15%	Eugenol	Phenol
0.16%		Non-identified
0.65%	2 furancarboxaldehyde 4 hydroxymethyl	Diverse Chemical groups
9.72%	Phenol 2 6 dimethoxy	Phenol
0.69%	Phenol 2 methoxy 4 propyl	Phenol
2.87%	Phenol 2 methoxy 4 propyl	Phenol
3.39%	2 5 dimethoxybenzyl alcohol	Alcohol
1.57%		Non-identified
2.24%	5 tert butly pyrogallol	Alcohol
0.22%	Benzoic acid 4 hydroxy 3 methoxy methyl ester	Ester
0.88%	Ethanone 1-2 hydroxy 3 methoxyphenyl	Alcohol
1.16%	2 4 dimethoxyacetophenone	Ketone
2.86%	Phenol 2 6 dimethoxy 4 propenyl	Phenol
0.43%	Phenol 4(3hydroxy1propenyl 2 Methoxy	Phenol
0.94%	Phenol 2 6 dimethoxy 4 2-propenyl	Phenol
3.22%	Phenol 2 6 dimethoxy 4 propenyl	Phenol
0.27%	Phenol 2 6 dimethoxy 4 propenyl	Phenol
2.64%	Benzaldehyde 4 hydroxy 3 5 dimethoxy	Diverse Chemical groups
0.54%		Non-identified

0.33%		Non-identified
1.29%	Ethanone 1-4hydroxy 3 5 Dimethoxy Phenyl	Diverse Chemical groups
3.11%	2 Pentanone 1-(246trihydroxyphenyl)	Diverse Chemical groups
0.35%		Non-identified
0.63%		Non-identified
0.18%		Non-identified
2.09%	3 5 dimethoxy 4 hydroxycinnamaldehyde	Diverse Chemical groups
0.31%		Non-identified
0.19%		Non-identified

Table B-5 – Pyrolysis oil composition, nitrogen inerted, 1.89 kJ/g, analysed by a collaborator in the University of Nottingham.

Area (%)	Name	Group
0.61%		non-identified
1.35%		non-identified
0.52%		non-identified
0.27%		non-identified
2.02%		non-identified
1.02%		non-identified
0.29%		non-identified
3.15%	3 (dioxolan2yl)-1,1-dimethyl-2-phenylpropylhydroxylamine	non-identified
2.24%		non-identified
0.85%	furfural	aldehyde
0.48%		non-identified
1.10%	furanmethanol	alcohol
0.47%	furanmethanol	alcohol
0.72%		non-identified
0.08%		non-identified
0.31%		non-identified
0.26%		non-identified
0.23%		non-identified
2.81%		non-identified
0.72%		non-identified
0.63%		non-identified
0.22%	furanone	ketone
2.27%	furanone	ketone
0.30%		non-identified
1.52%	oxazolidine 2 2 diethyl 3 methyl	diverse chemical groups
2.78%	cyclopenten-1-one 2 hydroxy 3 methyl	ketone
0.56%	cyclopenten-1-one 2 hydroxy 3 methyl	ketone
0.17%		non-identified
0.23%	phenol	alcohol
0.59%	phenol	alcohol
4.92%	phenol 2 methoxy	phenol
0.30%		non-identified
0.18%		non-identified

0.30%		non-identified
0.53%		non-identified
0.42%	cyclopentenone ethyl hydroxy	ketone
0.50%	methyl phenol	phenol
0.39%		non-identified
0.31%	azulene	aromatic
0.30%		non-identified
1.20%		non-identified
3.07%	phenol 2 methoxy 4 methyl	phenol
0.55%	methoxy phenol	phenol
0.41%		non-identified
0.57%		non-identified
0.20%		non-identified
0.31%		non-identified
4.54%	2 methoxy 4 vinyl phenol	phenol
1.13%	eugenol	phenol
0.11%		non-identified
0.78%		non-identified
7.36%	phenol 2 6 dimethoxy	phenol
0.78%		non-identified
4.90%	phenol 2 methoxy 4 propyl	phenol
3.82%	2 5 dimethoxybenzyl alcohol	alcohol
1.59%		non-identified
1.70%	5 tert butylpyrogallol	phenol
0.20%	benzoic acid 4 hydroxy 3 methoxy methyl ester	ester
0.90%		non-identified
6.22%	2 4 dimethoxyacetophenone	ketone
2.54%	propanone 1 4 hydroxy 3 methoxyphenyl	ketone
0.54%		non-identified
0.95%		non-identified
5.85%	phenol 2 6 dimethoxy 4 propenyl	phenol
0.27%		non-identified
2.85%	benzaldehyde 4 hydroxy 3 5 dimethoxy	aldehyde
0.78%	anthracene	aromatic
0.47%		non-identified
1.33%		non-identified
1.36%		non-identified
1.91%	1 butanone 1 2 4 67 trihydroxy 3 methylphenyl	diverse chemical groups
1.48%		non-identified
0.37%		non-identified
0.12%		non-identified
0.78%		non-identified
0.41%		non-identified
0.28%		non-identified
0.41%		non-identified
0.45%		non-identified

2.72%	pyrene	aromatic
0.62%		non-identified

Table B-6 – Pyrolysis oil composition, 2-propanol inerted, analysed by a collaborator in the University of Nottingham.

Area (%)	Name	Group
0.68%		Non-identified
0.18%		Non-identified
0.66%		Non-identified
2.40%		Non-identified
1.92%	Toluene	Aromatic
0.86%		Non-identified
0.51%		Non-identified
0.57%	Ethyl benzene	Aromatic
	Ethyl benzene	Aromatic
	Xylene	Aromatic
		Non-identified
3.39%	Furfural	Aldehyde
1.05%	Furan 3 methyl	Diverse chemical groups
1.26%	Furan methanol	Alcohol
0.82%		Non-identified
0.35%		Non-identified
3.41%	D alpha methylglutamic acid	Diverse chemical groups
1.57%	Benzofuran	Diverse chemical groups
0.28%	Furancarboxaldehyde 5 methyl	Anhydride
1.42%	Benzene propynyl	Aromatic
3.23%	Furanone	Ketone
1.26%	Oxazolidine 2 2 diethyl 3 methyl	Diverse chemical groups
3.53%	Cyclopenten-1-one 2 hydroxy 3 methyl	Phenol
0.31%	Phenol	Phenol
1.21%	Phenol	Phenol
4.95%	Phenol 2 methoxy	Phenol
0.40%	Phenol 2 methyl	Phenol
0.16%		Non-identified
0.29%		Non-identified
0.62%		Non-identified
0.42%	Cyclopentenone ethyl hydroxy	Ketone
0.58%	Methyl phenol	Phenol
0.42%	Methyl phenol	Phenol
	Napthalene	Aromatic
0.15%	Azulene	Aromatic
0.23%		Non-identified
1.05%		Non-identified
0.39%		Non-identified

3.77%	Phenol 2 methoxy 4 methyl	Phenol
1.64%	Methoxy phenol	Phenol
0.46%		Non-identified
0.32%	Napthalene 1 methyl	Aromatic
0.84%	Phenol 4 ethyl 2 methoxy	Phenol
1.01%		Non-identified
0.28%	Phenol ethyl methoxy	Phenol
0.23%		Non-identified
0.37%	1,4:3,6 dianhydro- alpha d glucopyranose	Sugars
4.39%	2 methoxy 4 vinyl phenol	Phenol
0.77%	Eugenol	Phenol
6.74%	Phenol 2 6 dimethoxy	Phenol
0.82%	Phenol 2 methoxy 4 propyl	Phenol
1.63%	Biphenylene	Aromatic
4.42%	Phenol 2 methoxy 4 propyl	Phenol
3.57%	2 5 dimethoxy benzyl alcohol	Alcohol
0.84%	Benzaldehyde 3 hydroxy 4 methoxy	Diverse chemical groups
2.14%	5 tert butylpyrogallol	Phenol
0.34%	Ethanone 1-(4hydroxy-3-methoxyphenyl)-	Diverse chemical groups
5.35%	2 4 dimethoxyacetophenone	Ketone
2.14%	Phenol 2 6 dimethoxy 4 propenyl	Phenol
0.77%	Phenol 2 6 dimethoxy 4 propenyl	Phenol
5.41%	Levoglucosan	Sugars
5.21%	Phenol 2 6 dimethoxy 4 propenyl	Phenol
1.47%	Benzaldehyde 4 hydroxy 3 5 dimethoxy	Diverse chemical groups
0.81%	Anthracene	Aromatic
0.50%	Ethanone 1-(4hydroxy 3 5 dimethoxy phenyl)	Diverse chemical groups
0.92%	Ethanone 1-(4hydroxy 3 5 dimethoxy phenyl)	Diverse chemical groups
0.76%	3 hydroxy 1 propenyl 2 methoxy phenol	Phenol
1.98%	4 hydroxy 2 methoxycinnamaldehyde	Diverse chemical groups
0.42%		Non-identified
1.29%	Pyrene	Aromatic
0.06%		Non-identified

Table B-7 – Pyrolysis oil composition, water inerted, analysed by a collaborator in the University of Nottingham.

Area (%)	Name	Group
0.38%		Non-identified
0.09%		Non-identified
0.23%		Non-identified
6.05%	Furfural	Aldehyde
0.84%	Furfural	Aldehyde
0.75%	Furanmethanol	Alcohol
0.48%	Furan 2 ethyl 5 methyl	Non-identified
0.32%	Dl alph methylglutamic acid	Acid
0.36%		Non-identified

0.94%	2 furancarboxaldehyde 5 methyl	Aldehyde
0.89%	Furanone	Ketone
0.59%	Furanone	Ketone
1.92%	Cyclopenten-1-one 2 hydroxy 3 methyl	Alcohol
0.48%	1,3 cyclopentane dione 2 methyl	Ketone
0.31%		Non-identified
7.85%	Phenol 2 methoxy	Phenol
0.64%		Non-identified
0.26%	Cyclopentenone ethyl hydroxy	Ketone
0.25%		Non-identified
4.24%	Phenol 2 methoxy 4 methyl	Phenol
2.36%	Phenol 4 ethyl 2 methoxy	Phenol
6.05%	2 methoxy 4 vinyl phenol	Phenol
1.47%	Eugenol	Phenol
0.28%	Phenol 2 methoxyl 4 propyl	Phenol
15.13%	Phenol 2 6 dimethoxy	Phenol
0.94%	Phenol 2 methoxy 4 propenyl	Phenol
6.47%	Phenol 2 methoxy 4 propenyl	Phenol
7.38%	2 5 dimethoxy benzyl alcohol	Alcohol
1.24%	Benzaldehyde 3 hydroxy 4 methoxy	Diverse chemical groups
6.29%	5 tert butyl pyrogallol	Phenol
0.30%	Benzoic acid 4 hydroxy 3 methoxy methyl ester	Ester
0.84%	Ethanone 1-(4-hydroxy-3-methoxyphenyl)-	Ketone
2.07%	2 4 dimethoxy acetophenone	Diverse chemical groups
0.19%		Non-identified
5.72%	Phenol 2 6 dimethoxy 4 propenyl	Phenol
0.28%	Phenol 2 6 dimethoxy 4 propenyl	Phenol
0.34%	Phenol 4-(3-hydroxy-1-propenyl)-2-methoxy-	Phenol
1.08%	Phenol 2 6 dimethoxy 4 propenyl	Phenol
3.25%	Benzaldehyde 4 hydroxy 3 5 dimethoxy	Aldehyde
1.13%	Anthracene	Aromatic
0.39%	Benzoic acid 4 hydroxy 3 5 dimethoxy hydrazide	Alcohol
1.85%	Ethanone 1-4hydroxy 3 5 dimethoxyphenyl)-	Diverse chemical groups
0.39%		Non-identified
8.60%	1 butanone 1,(246 trihydroxy3 methyl phenyl)	Diverse chemical groups
0.65%		Non-identified
0.69%		Non-identified
0.17%		Non-identified
0.28%		Non-identified
3.34%	3 5 dimethoxy-4-hydroxycinnamaldehyde	Diverse chemical groups
0.55%	9-octadeceneamide	Diverse chemical groups

Appendix C – Chapter 4 supplementary information

C.1 Supplementary absorbance curves

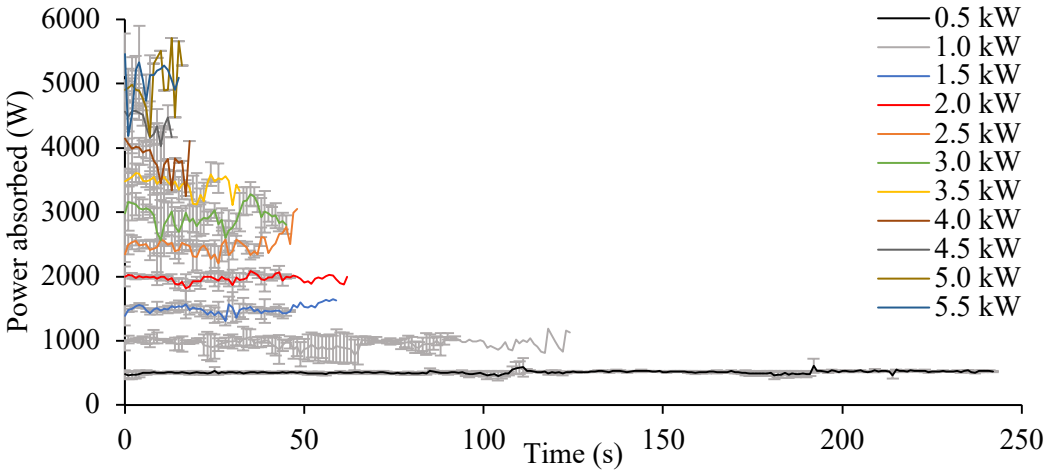


Figure C-1 – Absorbance curves for powers 0.5 – 5.5 kW applied powers in the multi-mode system, cyclohexane inerted, error bars represent the standard deviation from the mean.

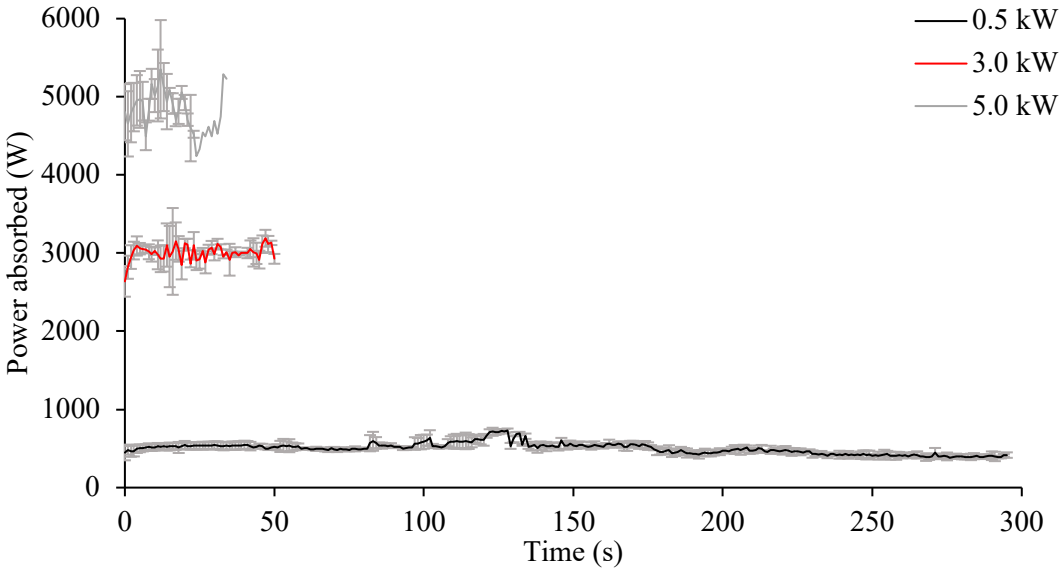


Figure C-2 – Absorbance curves for powers 0.5 – 5.0 kW applied powers in the multi-mode system, kerosene inerted, error bars represent the standard deviation from the mean.

C.2 Total pyrolysis oil yield, and oil and gas yields as a percentage of total volatiles produced.

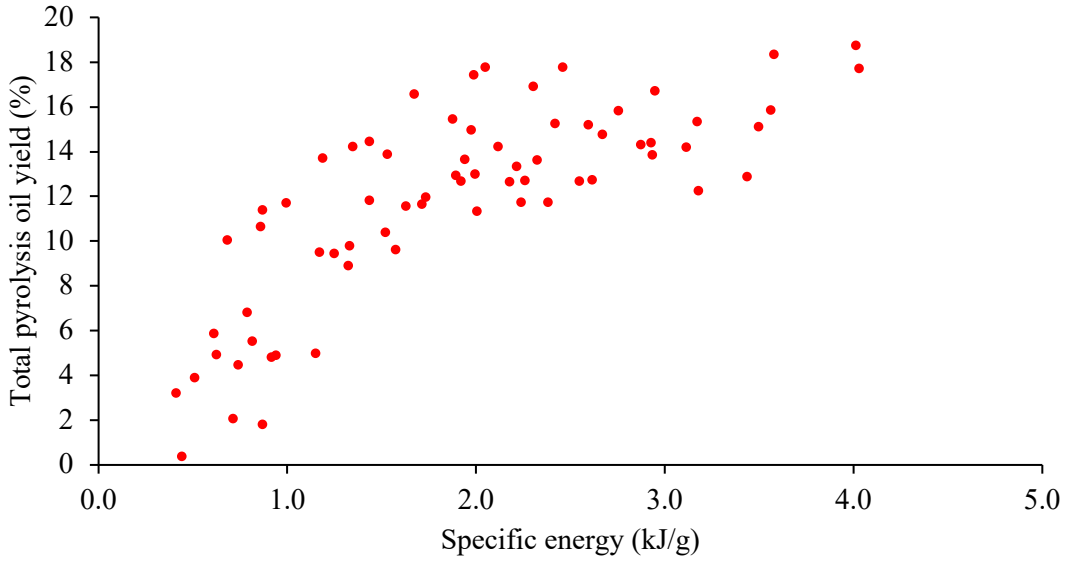


Figure C-3 – Total pyrolysis oil yields of the multimode system, using cyclohexane as an inerting liquid.

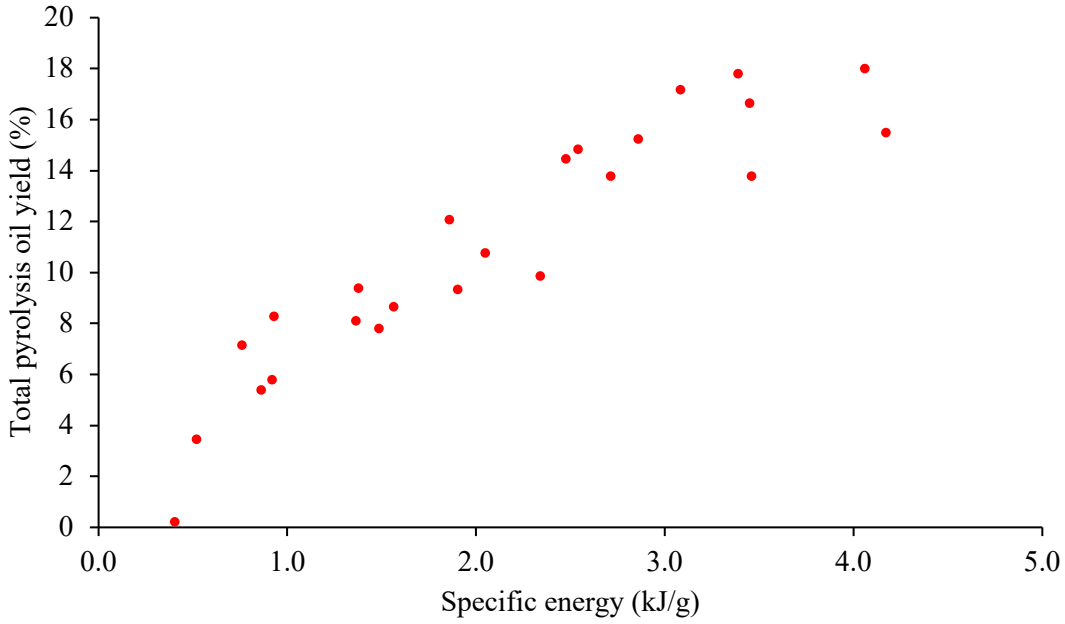


Figure C-4 – Total pyrolysis oil yields of the multimode system, using kerosene as an inerting liquid.

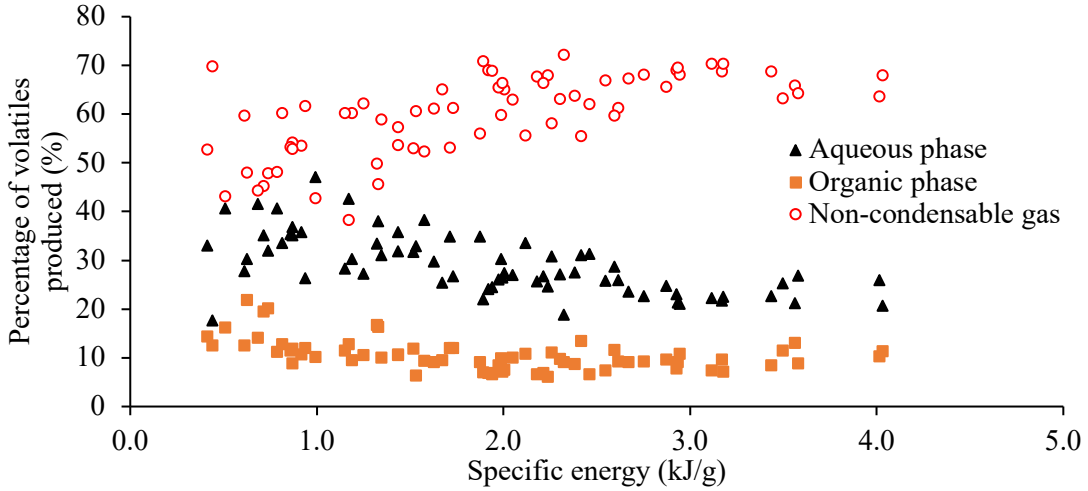


Figure C-5 – Aqueous and organic phase pyrolysis oil, and gas yields in relation to mass loss.

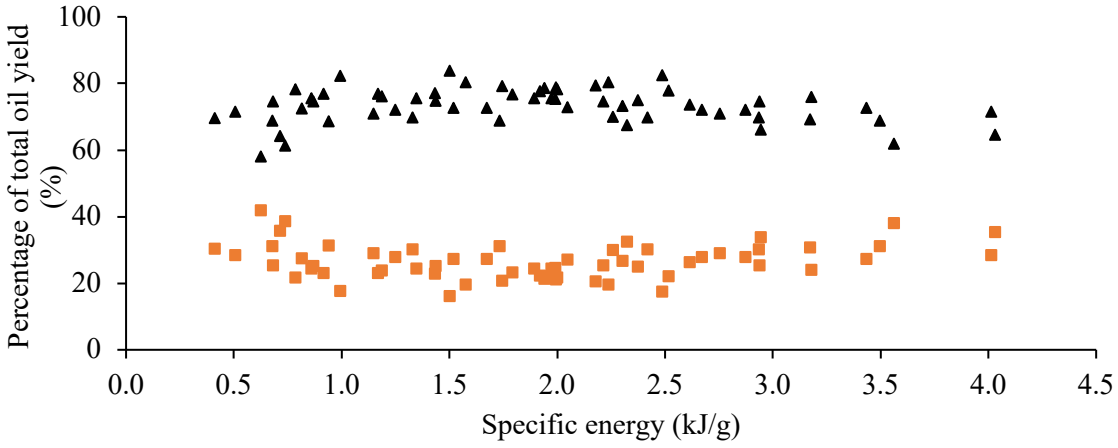


Figure C-6 – Aqueous and organic phase pyrolysis oil yields in relation to the total yield as a percentage against specific energy for the multi-mode process using cyclohexane as an inerting medium.

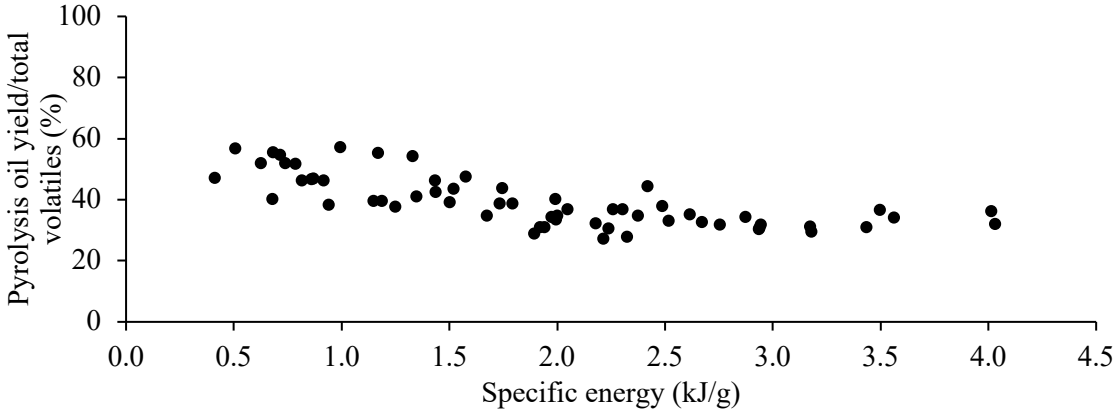


Figure C-7 – Total pyrolysis oil yield in relation to total volatiles produced as a percentage against specific energy for the multi-mode process using cyclohexane as an inerting medium.

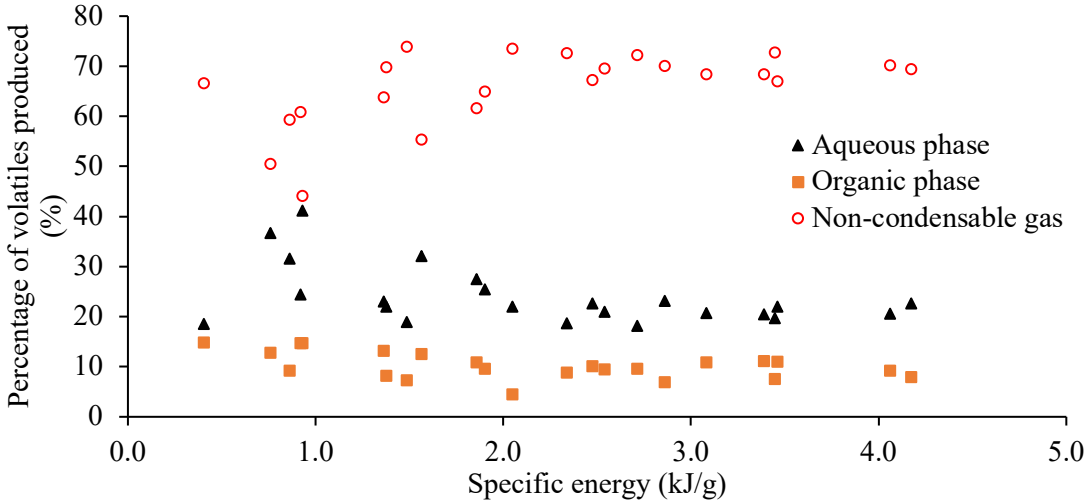


Figure C-8 – Aqueous and organic phase pyrolysis oil, and gas yields as a percentage of total volatiles produced for kerosene as an inerting liquid.

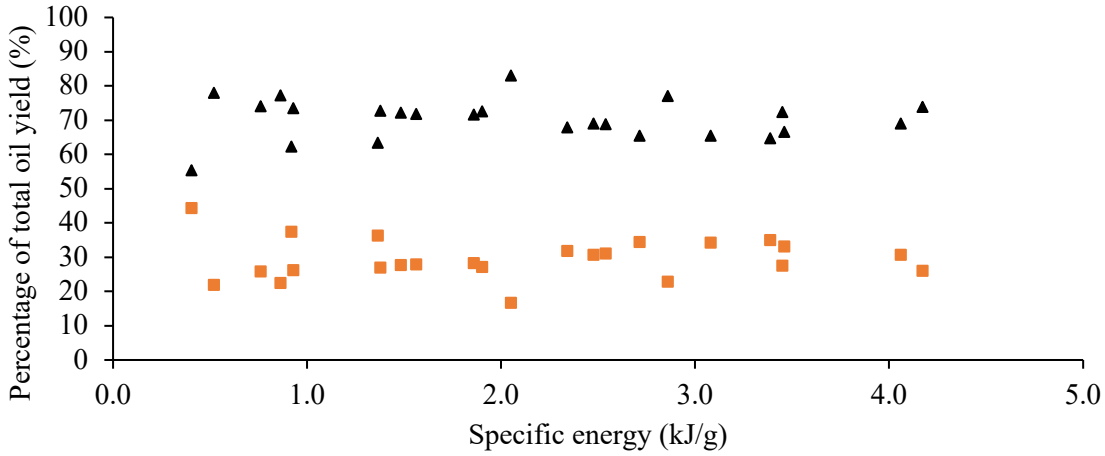


Figure C-9 – Aqueous and organic phase pyrolysis oil yields in relation to the total yield as a percentage against specific energy for the multi-mode process using kerosene as an inerting medium.

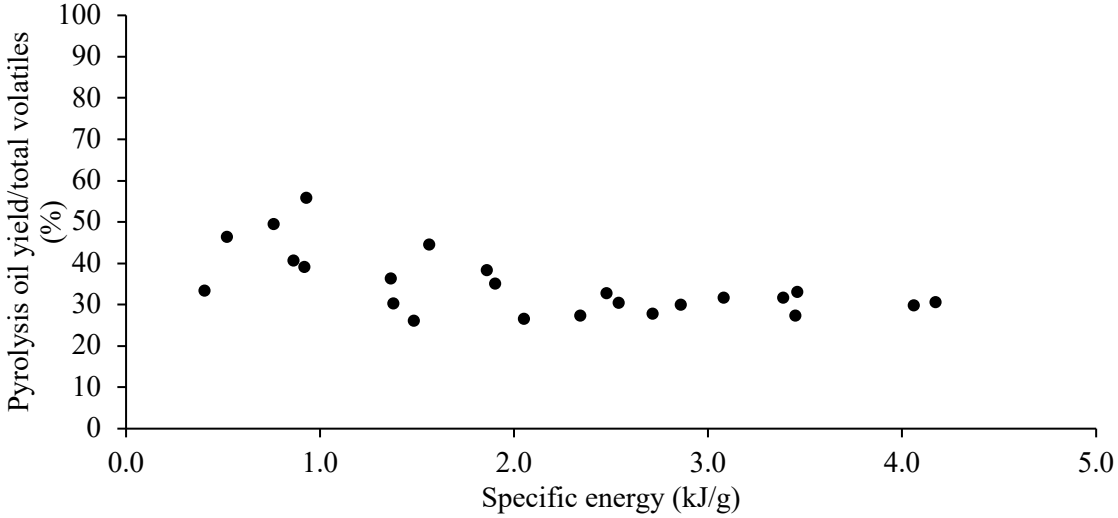


Figure C-10 – Total pyrolysis oil yield as a percentage of total volatiles produced against Specific Energy for the multi-mode process using kerosene as an inerting medium.

C.3 Pyrolysis oil composition

Table C-1 – Compound groups for the multi-mode liquid inerted microwave pyrolysis process in various inerting media, with the single-mode oils presented for comparison.

Group	Peak area (%)					
	Single-mode n-hexane (aqueous)	Single-mode n-hexane (organic)	Cyclohexane 1.33 kJ/g (Aqueous)	Cyclohexane 1.87 kJ/g (Aqueous)	Cyclohexane 1.33 kJ/g (Organic)	Cyclohexane 1.87 kJ/g (Organic)
Aromatic	0.0	0.0	1.7	0.6	0.5	13.0
Acids and esters	18.7	5.4	0.6	2.0	1.7	0.2
Aldehydes	13.0	7.3	5.4	7.9	0.3	0.2
Ketones	19.2	22.8	8.7	5.7	1.6	2.7
Phenols	9.3	44.5	12.2	10.9	52.6	47.8
Alcohols	4.2	1.1	2.9	3.9	7.9	7.8
Ethers	9.7	11.3	0.1	0.0	0.0	0.0
Sugars	15.9	0.0	21.0	20.9	0.2	0.6
Others	4.2	0.9	14.5	19.7	12.8	16.7
Not identified	5.9	6.7	32.9	28.4	22.5	10.9

Table C-2 – Aqueous phase oil composition, cyclohexane solvent, 1.33 kJ/g, analysed by a collaborator in the University of Nottingham.

Area (%)	Name		Group
0.15%			Impurity
0.88%			Non-identified
0.02%			Non-identified
0.19%			Non-identified
1.45%			Non-identified
0.18%	59 60		Non-identified
0.55%	55 74		Non-identified
0.17%	2-propenoic acid, oxiranylmethyl ester		Ester
0.77%	Ethyl benzene		Aromatic
0.61%	Ethyl benzene		Aromatic
0.37%			Non-identified
0.60%			Non-identified
0.50%	Furfural		Aldehyde
0.29%	Furfural		Aldehyde
0.22%	Furfural		Aldehyde
0.07%			Non-identified
0.88%	2-furanmethanol		Alcohol
0.14%	Furanmethanol		Alcohol
0.11%			Non-identified
0.36%			Non-identified
0.10%	Di (1-methycyclobutyl) ether		Ether
0.21%			Non-identified
1.55%	Benzofuran		Diverse chemical groups
0.68%			Non-identified
0.37%			Non-identified
0.11%	Furanone		Ketone
2.13%	2(5h) furanone		Ketone
0.76%	Oxazolidine 2 2 diethyl 3 methyl		Diverse chemical groups
1.02%	2-cyclopentene-1-one, 2 hydroxy-3-methyl		Ketone
0.20%		87	Non-identified
0.41%			Non-identified
0.30%			Non-identified
0.09%			Non-identified
0.06%			Non-identified
0.08%			Non-identified
0.05%			Non-identified
0.02%			Non-identified
0.05%			Non-identified
0.12%			Non-identified
0.08%			Non-identified
2.23%	Cyclopentenone ethyl hydroxy		Ketone
0.33%	Methyl phenol		Phenol
0.70%	Methyl phenol		Phenol

0.93%		Non-identified
0.86%		Non-identified
0.57%		Non-identified
0.49%		Non-identified
0.27%	Phenol 2 methoxy 4 methyl	Phenol
0.34%		Non-identified
0.45%	Methoxy phenol	Phenol
0.57%		Non-identified
0.21%		Non-identified
0.28%		Non-identified
0.12%		Non-identified
0.13%		Non-identified
0.22%		Non-identified
0.02%		Non-identified
0.03%		Non-identified
0.45%		Non-identified
0.07%		Non-identified
0.09%		Non-identified
0.40%		Non-identified
0.60%	Phenol ethyl methoxy	Phenol
0.13%		Non-identified
0.57%		Non-identified
0.88%		Non-identified
1.68%	1,4:3,6 dianhydro- alpha d glucopyranose	Sugars
0.28%		Non-identified
0.09%		Non-identified
0.43%	2 methoxy 4 vinyl phenol	Phenol
0.07%		Non-identified
0.05%		Non-identified
0.12%	Methoxy vinyl phenone	Ketone
0.29%		Non-identified
0.12%		Non-identified
0.30%		Non-identified
0.04%		Non-identified
1.93%	Phenol 2 6 dimethoxy 4 propenyl	Phenol
1.12%	Dihydroxypropiophenone	Ketone
2.51%	Phenol 2 6 dimethoxy	Phenol
1.86%	5-methyl-2-(2-methyl-2-tetrahydrofuryl)tetrahydrofuran	Diverse chemical groups
2.03%	Phenol 2,6 dimethoxy	Phenol
0.13%		Non-identified
0.43%		Non-identified
0.26%		Non-identified
0.38%		Non-identified
0.51%		Non-identified
0.19%		Non-identified

0.13%		Non-identified
0.49%		Non-identified
0.45%		Non-identified
0.36%		Non-identified
1.11%		Non-identified
1.04%	2 5 dimethoxy benzyl alcohol	Alcohol
1.61%	Hydroquinone	Ketone
0.23%		Non-identified
1.47%	Benzaldehyde 3 hydroxy 4 methoxy	Diverse chemical groups
0.44%		Non-identified
0.31%		Non-identified
0.74%	1,4 benzenediol, 2 methyl	Alcohol
0.31%		Non-identified
0.28%		Non-identified
0.56%	5 tert butyl pyrogallol	Phenol
0.20%		Non-identified
1.09%	5 tert butyl pyrogallol	Phenol
0.38%	Benzoic acid 4 hydroxy 3 methoxy methyl ester	Ester
0.08%		Non-identified
0.54%	Ethanone 1-(4hydroxy-3methoxyphenyl)-	Diverse chemical groups
0.13%		Non-identified
0.98%		Non-identified
0.25%		Non-identified
0.64%		Non-identified
0.81%	2 4 dimethoxy acetophenone	Diverse chemical groups
0.27%		Non-identified
0.65%	Propanone 1 4 hydroxy 3 methoxyphenyl	Diverse chemical groups
0.06%		Non-identified
0.70%	6 methoxycoumaran 7 ol 3 one	Diverse chemical groups
0.08%		Non-identified
0.05%		Non-identified
0.31%		Non-identified
0.37%		Non-identified
0.14%		Non-identified
0.11%		Non-identified
0.06%		Non-identified
0.03%		Non-identified
1.17%		Non-identified
0.33%		Non-identified
18.35%	Levoglucosan	Sugars
0.70%	Phenol 2 6 dimethoxy-4-(2propenyl)	Phenol
0.29%		Non-identified
0.16%		Non-identified
0.04%		Non-identified

0.03%	Benzaldehyde 4 hydroxy 3 5 dimethoxy	Diverse chemical groups
4.16%	Benzaldehyde 4 hydroxy 3 5 dimethoxy	Aldehyde
0.02%		Non-identified
0.80%		Non-identified
0.18%		Non-identified
0.08%		Non-identified
0.20%	Anthracene	Aromatic
0.15%		Non-identified
0.44%		Non-identified
2.80%	Ethanone 1-(4-hydroxy-3,5-dimethoxyphenyl)-	Diverse chemical groups
0.09%		Non-identified
2.65%	1-butaneone 1-(246-trihydroxy-3-methylphenyl)-	Diverse chemical groups
0.01%		Non-identified
0.34%		Non-identified
0.29%		Non-identified
0.47%		Non-identified
0.09%		Non-identified
0.37%		Non-identified
0.22%		Non-identified

Table C-3 – Aqueous phase oil composition, cyclohexane solvent, 1.87 kJ/g, analysed by a collaborator in the University of Nottingham.

Area (%)	Name	Group
0.63%		Non-identified
0.33%		Non-identified
0.91%		Non-identified
0.34%		Non-identified
0.32%		Non-identified
3.60%		Non-identified
6.15%	Furfural	Aldehyde
0.33%	Furfural	Aldehyde
1.03%	Furfural	Aldehyde
0.15%		Non-identified
0.74%		Non-identified
0.94%	2-furanmethanol	Alcohol
0.39%		Non-identified
1.00%	Dl-alpha methyl glutamic acid	Acid
1.09%	4 - pentynoic acid	Acid
0.45%		Non-identified
2.40%	2 (5h) furanone	Ketone
1.62%	Oxazolidine 2 2 diethyl 3 methyl	Diverse chemical groups
1.27%	2 cyclopentene 1 one 2 hydroxy 3 methyl	Diverse chemical groups
0.46%		Non-identified
0.22%		Non-identified
0.67%	Phenol	Phenol

0.43%		Non-identified
0.32%		Non-identified
2.04%	Cyclopentenone ethyl hydroxy	Ketone
0.94%	Methyl phenol	Phenol
0.89%		Non-identified
1.02%	Phenol 2 methoxy 4 methyl	Phenol
3.50%	Tridecane 2 2 4 10 12 12 hexamethyl 7 3 5 5 trimethylhexyl	Aliphatic
0.63%		Non-identified
0.25%		Non-identified
0.50%	Phenol ethyl methoxy	Phenol
0.45%		Non-identified
0.40%		Non-identified
1.20%	1,4:3,6 dianhydro- alpha d glucopyranose	Sugars
0.42%		Non-identified
1.91%	Eugenol	Phenol
1.27%		Non-identified
2.58%	Phenol 2 6 dimethoxy	Phenol
1.22%	1,2 benzenediol	Alcohol
0.87%	Phenol dimethoxy	Phenol
0.41%		Non-identified
1.41%		Non-identified
0.59%	2 5 dimethoxy benzyl alcohol	Alcohol
1.28%	2 5 dimethoxy benzyl alcohol	Alcohol
1.40%	Hydroquinone	Ketone
0.03%	1 2 4 trimethoxy benzene	Aromatic
1.51%	Vanillin	Phenol
0.56%	Benzaldehyde 3 hydroxy 4 methoxy	Aldehyde
0.46%		Non-identified
0.80%		Non-identified
0.41%		Non-identified
0.68%	5 tert butylpyrogallol	Phenol
0.88%		Non-identified
0.64%	Ethanone 1-(4hydroxy3methoxyphenyl)-	Diverse chemical groups
0.78%		Non-identified
1.07%		Non-identified
1.40%	2 4 dimethoxyacetophenone	Diverse chemical groups
0.18%		Non-identified
0.93%	2 4 dimethoxy acetophenone	Diverse chemical groups
0.26%		Non-identified
0.56%		Non-identified
0.29%		Non-identified
0.94%		Non-identified
20.16%	Levoglucosan	Sugars
1.54%		Non-identified
0.47%	Phenol 2 6 dimethoxy-4-(2propenyl)	Phenol
4.66%	Benzaldehyde 4 hydroxy 3 5 dimethoxy	Diverse chemical groups

0.28%		Non-identified
0.63%	Anthracene	Aromatic
0.89%		Non-identified
2.93%	Ethanone 1-(4hydroxy 3 5 dimethoxyphenyl)	Diverse chemical groups
3.53%	1- butanone 1(246 trihydroxy3methylphenyl)	Diverse chemical groups
0.42%		Non-identified
0.19%		Non-identified
1.32%		Non-identified
0.86%		Non-identified
3.14%	3 5 dimethoxy 4 hydroxycinnamaldehyde	Diverse chemical groups
1.44%		Non-identified

Table C-4 –Organic phase oil composition, cyclohexane solvent, 1.33 kJ/g, analysed by a collaborator in the University of Nottingham.

Area (%)	Name	Group
0.31%	Methyl cyclohexane	Impurity
0.24%	Cyclopentane - ethyl	Aliphatic
0.26%	Trisilane	Impurity
0.16%	Undecane -3 methylene	Aromatic
0.06%		Non-identified
0.91%	Furan tetrahydro 2 5 dimethoxy	Alcohol
0.09%		Non-identified
0.92%	Furan tetrahydro 2 5 dimethoxy	Diverse chemical groups
0.09%	Furfural	Aldehyde
0.07%	Furfural	Aldehyde
0.10%	Cyclohexylmethylsilane	Impurity
0.04%		Non-identified
0.31%		Non-identified
2.12%	2-furanmethanol	Alcohol
0.07%		Non-identified
2.17%	Furan 2 ethyl 5 methyl	Diverse chemical groups
0.84%		Non-identified
0.14%		Non-identified
0.06%	Benzofuran	Diverse chemical groups
0.33%		Non-identified
0.37%		Non-identified
0.09%	2 furancarboxaldehyde 5 methyl	Aldehyde
0.33%	Furanone	Ketone
0.28%	Furanone	Ketone
0.29%	Furanone	Ketone
0.14%		Non-identified
0.09%	Oxazolidine 2 2 diethyl 3 methyl	Diverse chemical groups
0.19%		Non-identified
0.18%		Non-identified
2.79%	Cyclopenten-1-one 2 hydroxy 3 methyl	Alcohol
0.12%		Non-identified

0.24%	1,3 cyclopentane dione 2 methyl	Ketone
0.09%		Non-identified
0.12%		Non-identified
0.12%		Non-identified
0.07%		Non-identified
7.43%	Phenol 2 methoxy	Phenol
0.10%	Phenol 2 methoxy	Phenol
0.04%		Non-identified
0.15%		Non-identified
0.68%		Non-identified
0.46%	Cyclopentenone ethyl hydroxy	Ketone
0.13%		Non-identified
0.23%	Methyl phenol	Phenol
0.32%	Methyl phenol	Phenol
0.31%	Azulene	Aromatic
0.06%		Non-identified
0.08%		Non-identified
0.07%		Non-identified
0.07%		Non-identified
0.40%		Non-identified
4.10%	Phenol 2 methoxy 4 methyl	Phenol
0.20%	Phenol 2 methoxy 4 methyl	Phenol
0.29%	Methoxymethylphenol	Phenol
0.23%		Non-identified
0.10%		Non-identified
0.04%		Non-identified
0.07%		Non-identified
0.19%		Non-identified
1.86%		Non-identified
0.01%	Phenol 4-ethyl-2-methoxy	Phenol
0.14%		Non-identified
0.11%		Non-identified
0.26%		Non-identified
0.13%		Non-identified
0.18%	1,4:3,6 dianhydro- alpha d glucopyranose	Sugars
0.20%		Non-identified
5.32%	2 methoxy 4 vinyl phenol	Phenol
0.12%	2 methoxy 4 vinyl phenol	Phenol
1.30%	Eugenol	Phenol
0.32%		Non-identified
15.11%	Eugenol	Phenol
0.11%	Phenol 2 6 dimethoxy	Phenol
0.78%		Non-identified
5.34%	Phenol 2 methoxy -4-(1-propenyl) (z)	Phenol
7.05%	Phenol 2 methoxy -4-(1-propenyl) (e)	Phenol
2.07%	2 5 dimethoxybenzyl alcohol	Alcohol

0.22%	Vanillin	Phenol
0.08%		Non-identified
5.21%	5 tert butylpyrogallol	Phenol
0.17%	tertbutylpyrogallol	Phenol
0.72%	Benzoic acid 4 hydroxy 3 methoxy methyl ester	Ester
0.96%	Benzoic acid 4 hydroxy 3 methoxy methyl ester	Ester
0.23%	Ethanone 1-(4hydroxy-3methoxyphenyl)-	Diverse chemical groups
1.52%		Non-identified
4.35%	2 4 dimethoxy acetophenone	Diverse chemical groups
0.09%		Non-identified
0.21%	6 methoxycoumaran 7 ol 3 one	Diverse chemical groups
0.11%		Non-identified
0.22%		Non-identified
0.28%		Non-identified
0.16%		Non-identified
0.08%		Non-identified
0.10%		Non-identified
0.11%		Non-identified
0.58%		Non-identified
4.46%	Benzaldehyde 4 hyroxy-3,5-dimethoxy	Non-identified
0.56%	Benzaldehyde 4 hydroxy 3 5 dimethoxy	Diverse chemical groups
0.84%		Non-identified
1.12%		Non-identified
0.04%		Non-identified
3.74%	1 butanone 1 2 4 67 trihydroxy 3 methylphenyl	Diverse chemical groups
0.44%	1-butanone 2-(246 trihydroxy-3-methylphenol)	Diverse chemical groups
0.36%		Non-identified
1.19%		Non-identified
0.20%		Non-identified
0.11%		Non-identified
0.04%		Non-identified
0.54%		Non-identified
0.06%	Pyrene	Aromatic
0.09%		Non-identified
0.49%		Non-identified
0.01%		Non-identified
0.01%		Non-identified
0.01%		Non-identified
0.03%		Non-identified
0.23%		Non-identified
0.01%		Non-identified

Table C-5 –Organic phase oil composition, cyclohexane solvent, 1.87 kJ/g, analysed by a collaborator in the University of Nottingham.

Area (%)	Name	Group
0.07%		Non-identified
0.09%	2h-1,2-oxazine 6-(4chrlorophenyl)tetrahdro2methyl	Diverse chemical groups
0.20%		Non-identified
0.11%	1 methylcyclohexa-1,3-diene	Impurity
0.03%		Non-identified
0.16%		Non-identified
0.08%	P xylene	Aromatic
0.09%	Furan, tetrahydro-2,5-dimethoxy	Diverse chemical groups
0.63%	Phenylethyne	Aromatic
0.34%	Styrene	Aromatic
0.12%	Furan tetrahydro 2 5 dimethoxy	Diverse chemical groups
0.18%	3 furaldehyde	Aldehyde
0.62%	2 hexanol 2 methyl	Alcohol
0.22%		Non-identified
0.16%		Non-identified
0.75%		Non-identified
0.12%		Non-identified
0.44%		Non-identified
0.20%	Cyclopenten-1-one 2 methyl	Diverse chemical groups
1.78%	Indene	Aromatic
0.21%	Furanone	Ketone
0.17%		Non-identified
0.13%		Non-identified
2.12%	Cyclopenten-1-one 2 hydroxy 3 methyl	Ketone
0.10%	1,3 cyclopentane dione 2 methyl	Ketone
0.93%	Phosphonic acid (p-phenol) or phenol	Diverse chemical groups
4.62%	Phenol 2 methoxy	Phenol
0.12%	Napthalene 1,2 dihydro	Aromatic
0.33%	Indene 3 methyl	Aromatic
0.70%	Phenol 2 methyl	Phenol
0.09%		Non-identified
0.32%	2-cyclopenten-1-one, 3 ethyl-2-hydroxy	Diverse chemical groups
0.29%	Cyclopentenone ethyl hydroxy	Ketone
0.91%	Phenol 3 methyl	Phenol
0.86%	Methyl phenol	Phenol
3.84%	Napthalene	Aromatic
0.08%	Azulene	Aromatic
0.17%	Dl-3,4-dehydroproline methyl ester	Diverse chemical groups
3.75%	Phenol 2 methoxy 4 methyl	Phenol
0.12%		Non-identified
0.17%		Non-identified
0.15%	Phenol 2 3 dimethyl	Phenol
0.20%		Non-identified

0.23%		Non-identified
0.72%	Napthalene 1 methyl	Aromatic
0.98%	Phenol 4 ethyl 2 methoxy	Phenol
0.11%	Napthalene 1 methyl	Aromatic
0.07%		Non-identified
0.51%	Phenol ethyl methoxy	Phenol
0.19%		Non-identified
0.28%		Non-identified
0.26%		Non-identified
0.63%	1,4:3,6 dianhydro- alpha d glucopyranose	Sugars
0.16%		Non-identified
6.63%	2 methoxy 4 vinyl phenol	Phenol
0.35%	Biphenyl	Aromatic
1.86%	Eugenol	Phenol
0.14%		Non-identified
0.11%		Non-identified
9.23%	Phenol 2 6 dimethoxy	Phenol
0.32%	1,2 benzenediol	Alcohol
0.40%		Non-identified
1.53%	Phenol 2 methoxy 4 propenyl	Phenol
1.96%	Acenaphthylene	Aromatic
7.37%	Phenol 2 methoxy 4 propenyl (isoeugenol)	Phenol
5.48%	2 5 dimethoxybenzyl alcohol	Alcohol
1.43%	Vanillin	Alcohol
2.58%	5 tert butylpyrogallol	Phenol
0.13%	tertbutylpyrogallol	Phenol
0.23%	Benzoic acid 4 hydroxy 3 methoxy methyl ester	Ester
0.12%		Non-identified
1.02%		Non-identified
0.67%	Ethanone 1-(4-hydroxy-3-methoxyphenyl)-	Diverse chemical groups
0.12%	Fluorene	Aromatic
4.84%	Dimethoxy acetophenone	Diverse chemical groups
4.14%	Phenol 2 6 dimethoxy-4-(2propenyl)-	Phenol
0.19%	Phenol 2 6 dimethoxy 4 propenyl	Phenol
0.14%		Non-identified
0.14%		Non-identified
0.16%	6 methoxycoumaran 7 ol 3 one	Diverse chemical groups
0.45%		Non-identified
0.27%		Non-identified
0.16%		Non-identified
1.84%	Phenol 2,6 dimethoxy-4-propenyl	Phenol
4.07%	Benzaldehyde 4 hydroxy 3 5 dimethoxy	Diverse chemical groups
1.50%	Anthracene	Aromatic
0.24%		Non-identified
0.17%		Non-identified
0.90%	Ethanone 1-(4hydroxy-3,5-dimethoxyphenyl)-	Diverse chemical groups

3.54%	1 butanone 1-(246trihydroxy-3-methylphenyl)-	Diverse chemical groups
0.44%		Non-identified
0.22%		Non-identified
1.21%		Non-identified
0.22%		Non-identified
0.11%		Non-identified
0.09%		Non-identified
0.42%	Pyrene	Aromatic
0.66%	3 5 dimethoxy 4 hydroxycinnamaldehyde	Diverse chemical groups
0.27%	Fluoranthene	Aromatic
0.42%	Pyrene	Aromatic
0.13%		Non-identified
0.08%		Non-identified
0.05%		Non-identified
0.12%		Non-identified
0.31%		Non-identified
0.41%		Non-identified

C.4 Lignin concentration from thermogravimetric analysis correlations

It was identified in Chapter 3 and Chapter 4 that for both the liquid inerted microwave pyrolysis process, the cellulose and hemicellulose concentration of the sycamore block was reduced (<6 %) at very low specific energies (<0.5 kJ/g) and mass losses (<10 %). It was identified, however, that lignin concentrations were not significantly reduced in the single mode system across all specific energies investigated. Samples were taken from the internal section of the blocks (both single and multi-mode sycamore blocks), and blocks were milled into a powder, homogenised and analysed using TGA and the Dubois et al. (1956) assay. TGA analysis was used to find the composition of volatile matter and fixed carbon (values converted to a dry, ash free basis), and the Dubois assay was used to find the lignin concentration of the sycamore blocks. The lignin concentration in relation to the volatile matter/fixed carbon ratio (VM/FC) are presented in Figure C-11.

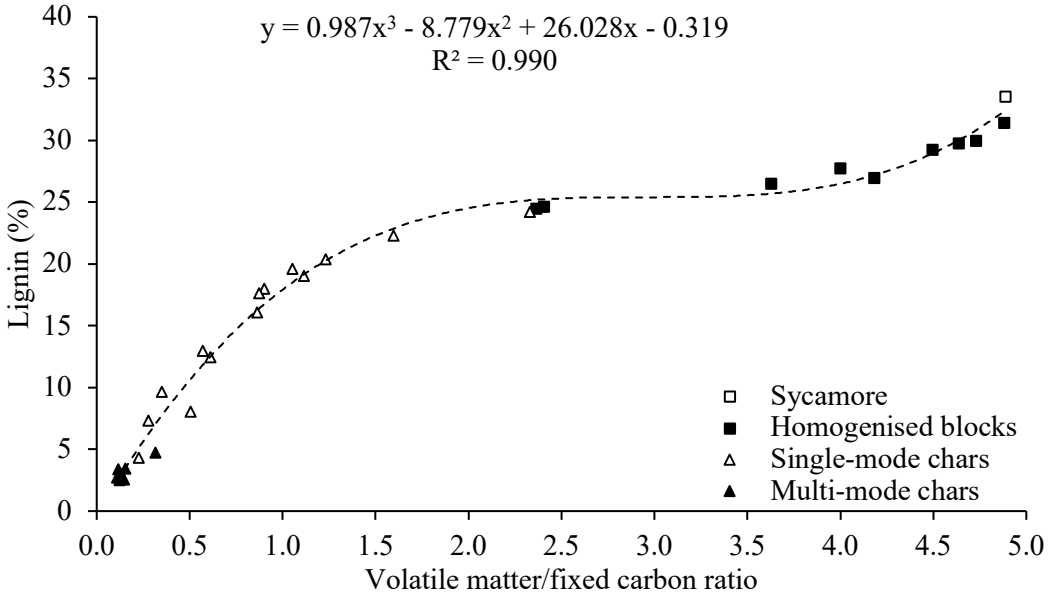


Figure C-11 – Lignin concentration of the sycamore blocks, pre and post pyrolysis, samples taken from char and homogenised blocks, against the volatile matter/fixed carbon ratio (dry, ash free basis) obtained from TGA.

It can be seen that the lignin content of the sycamore followed the volatile matter/fixed carbon ratio in a third order trend. The lignin content rose from 2.5 % to approximately 20 % from 0.0 – 1.5 VM/FC, at which point there was a plateau until around 3.5 VM/FC, where there was a small rise to around 34 % lignin content, representative of the non-pyrolysed sycamore. The VM/FC ratio was inversely proportional to the degree of pyrolysis within the process, with samples with higher fixed carbon values and lower volatile matter values being more pyrolysed. The plateau of the lignin content could explain why the lignin content of the single-mode liquid inerted microwave pyrolysis process chars were higher than the multi-mode process, as high temperatures (>450 °C) had not been reached, and so significant lignin breakdown had not been attained.

It can therefore be determined that for lignocellulosic biomass, if samples are pyrolysed at various conditions, and TGA and the lignin assay is carried out on the samples, a correlation curve can be developed. TGA is less time intensive than the lignin assay, requiring only a small amount of sample (approximately 10 mg compared to 100 mg

for the lignin assay), and requires no chemicals. This method would allow for TGA to be used to determine the lignin concentration of the sample, without the need to perform the lignin assay.

Appendix D – Chapter 5 supplementary information

D.1 Material parameters for the microwave simulations

Table D-1 – The material parameters for the microwave field simulations.

Material	Parameter	Value	Unit	Source
Sycamore	Dielectric constant, ε'	$8\times10^{-8}T^3 - 5\times10^{-5}T^2 + 0.0085T + 1.6649$		Measured
	Loss factor, ε”	$3\times10^{-8}T^3 - 2\times10^{-5}T^2 + 0.0041T + 0.0182$		Measured
	Relative permeability, μ	1		(Steer, 2010)
	Electrical conductivity, σ	1×10^{-15}	S/m	(Mahoney, 2000)
Quartz	Dielectric constant, ε'	3.9		(Church et al., 1988)
	Loss factor, ε”	0.0006		(Church et al., 1988)
	Relative permeability, μ	1		Assumed (non-polar)
	Electrical conductivity, σ	1×10^{-18}	S/m	(Serway and Jewett, 2012)
Cyclohexane	Dielectric constant, ε'	2.0		(Speight, 2017)
	Loss factor, ε”	0.001		(de la Hoz and Loupy, 2013)
	Relative permeability, μ	1		Assumed (non-polar)
	Electrical conductivity, σ	2×10^{-12}	S/m	(NFPA, 2000)
Aluminium	Relative permeability, μ	1		Assumed (non-polar)
	Electrical conductivity, σ	3.8×10^{7}	S/m	(Serway and Jewett, 2012)

D.2 Levoglucosan dielectric properties

Table D-2 – The dielectric properties of levoglucosan from 20 - 350 °C.

	Average		Standard deviation	
T(°C)	ε'	ε''	ε'	ε''
20	1.873	0.002	0.013	0.001
25	1.866	0.065	0.015	0.000
50	1.832	0.059	0.090	0.003
75	1.818	0.013	0.119	0.000
100	2.496	0.280	1.077	0.393
125	3.624	0.639	0.506	0.059
150	4.015	0.616	0.400	0.076
175	4.666	0.580	1.012	0.143
200	4.579	0.506	0.797	0.126
225	4.402	0.412	0.799	0.117
250	3.212	0.273	0.632	0.081
275	2.075	0.091	0.396	0.025
300	1.658	0.022	0.330	0.006
325	1.610	0.015	0.322	0.003
350	1.584	0.010	0.314	0.002

D.3 Parameters for volatiles generation model

Table D-3 – The parameters of the wood and volatiles for the volatiles generation model.

Parameter	Value	Source
Wood porosity	0.4	(Galgano and Blasi, 2003)
Wood permeability (m^2)	5×10^{-16}	(Di Blasi, 2000)
Volatiles dynamic viscosity (kg/m·s)	3×10^{-5}	(Kansa et al., 1977)

Table D-4 – The parameters of the wood and volatiles for the volatiles generation model, with variable porosity and permeability (ML = mass loss).

Parameter	Value	Source
Variable wood porosity	1 - 0.4(1-ML)	(Galgano and Blasi, 2003, Park et al., 2010)
Variable wood permeability (m^2)	$(1\text{-ML})5\times10^{-16} - (\text{ML})1\times10^{-13}$	(Di Blasi, 2000, Park et al., 2010)

D.4 Kinetic equations and material parameters for the pressure generation models

Table D-5 -Vaporisation kinetics of water within the sycamore structure (Ding et al., 2018).

Reaction	Water vaporisation
A_i (1/s)	5.13×10^{10}
E_i (J/mol)	88,000
Δh (kJ/kg)	2260

Table D-6 – The parameters for model 1 (Park et al., 2010).

Reaction	t	g	is	c	c2	g2
A_i (1/s)	1.08×10^{10}	4.38×10^{9}	3.75×10^{6}	1.38×10^{10}	1.00×10^{5}	4.28×10^{6}
E_i (J/mol)	148,000	152,700	111,700	161,000	108,000	108,000
Δh (kJ/kg)	80	80	80	-300	-42	-42

Table D-7 – The parameters for model 2 (Chan and Krieger, 1981, Capart et al., 2004, Varhegyi et al., 1989). [a]Initial proportion of cellulose A and B.

Reaction	A	B	1	2	*l*
A_i (1/s)	1.94×10^{15}	1.63×10^{20}	7.94×10^{16}	1.26×10^{7}	5.09×10^{5}
E_i (J/mol)	202,650	255,000	195,000	96,000	95,000
Δh (kJ/kg)	100	100	280	280	-350
Initial fraction, f_i [a]	0.837	0.163	-	-	-
Char yield, γ_i	0.087	0.087	0.56	0.46	0.335
n_i	1	0.481	-	-	-
m_i	0.481	1	-	-	-

Table D-8 – The parameters for model 3 (Ding et al., 2018). [a]The heats of pyrolysis are taken from (Park et al., 2010).

Reaction	C	H	L
A_i (1/s)	9.2×10^{9}	2.6×10^{10}	6.3×10^{7}
E_i (J/mol)	151,730	131,190	130,780
Δh (kJ/kg) [a]	100	280	350
Char yield, γ_i	0.08	0.18	0.48
n_i	0.63	2.17	2.34

Table D-9 – The parameters for model 4 (Kilzer and Broido, 1965, Park et al., 2010, Mok and Antal, 1983).

Reaction	1	2	3
A_i (1/s)	2.00×10^{10}	2.51×10^{7}	1.38×10^{10}
E_i (J/mol)	148,000	117,000	161,000
Δh (kJ/kg)	110	0	-210

Table D-10 – The material properties of the wood and volatiles produced during the pyrolysis process.

Parameter	Value/equation	Source
Wood pore size, m	$5 \times 10^{-5}(1 - \eta) + 1 \times 10^{-4}\eta$	(Grønli and Melaaen, 2000)
Wood porosity	0.4	(Galgano and Blasi, 2003)
Permeability of wood (m^2)	5×10^{-16}	(Di Blasi, 2000)
Permeability of char (m^2)	1×10^{-13}	(Di Blasi, 2000)
Volatiles dynamic viscosity (kg/m·s)	3×10^{-5}	(Kansa et al., 1977)
Molecular mass gas (kg/mol)	0.038	(Grønli and Melaaen, 2000)
Molecular mass tar (kg/mol)	0.11	(Grønli and Melaaen, 2000)
Molecular mass volatiles (kg/mol)	0.076	(Fredlund, 1988)

D.5 Preliminary investigations on processing considerations

Soaking sycamore in liquid solvent pre-pyrolysis

For efficient processing of the biomass to occur, on any scale above lab-scale, any masses or glassware used to the hold the biomass in place and stop it floating should be avoided. Any masses or extra glassware adds unnecessary complexity to the system and introduces extra potential for breakage, and even absorbing of the microwaves over the biomass itself. Sycamore that is either air or oven dried will initially float in any of the liquids investigated due to the respective densities of the sycamore and liquids. In terms of a processing context, developing a continuous microwave pyrolysis system would present issues, as the blocks initially floated pre-pyrolysis, yet sink post-pyrolysis. The

average density of the sycamore used throughout the research was 563 kg/m^3, meaning that initially, the sycamore would float on any of the liquids used. After soaking in cyclohexane, however, the soaked density of the sycamore ranged from 800-900 kg/m^3 and so would sink in the majority of liquids investigated.

Table D-11 - Densities of the liquids and samples at 25 °C

Liquid or Sample	**Density at 25 °C (kg/m^3)**
Sycamore	563
Soaked sycamore (cyclohexane)	800 - 900
n-Hexane	656
Cyclohexane	773
Kerosene	804
2-Propanol	785
Water	1000
Acetic acid	1043

The block mass immediately after pyrolysis is lower than that of the soaked biomass (approximately 200 % the value of the post-pyrolysis dried block), largely due to the loss of volatiles during pyrolysis, and the loss of liquid contained within the biomass. This new density is still larger than that of cyclohexane, however, and therefore the block is much more likely to be entrained in any moving liquid from density or boiling effects.

It was also beneficial to determine whether the soaked sycamore blocks provide superior temperature control when heating, and further increase the quality of the pyrolysis oil produced. It was also useful to investigate whether the energy was wasted on boiling the cyclohexane within the sycamore block, resulting in the block being in the same condition as pre-soaking, negating the heat-transfer benefits within the sycamore block.

Soaked blocks – bulk mass loss

Sycamore blocks of dimensions 50×50×25 mm were soaked in cyclohexane and then processed using the same method for non-soaked blocks, but without a mass to hold the block down as sinking occurs with soaked blocks. Mass losses for specific energies are presented in Figure D-1.

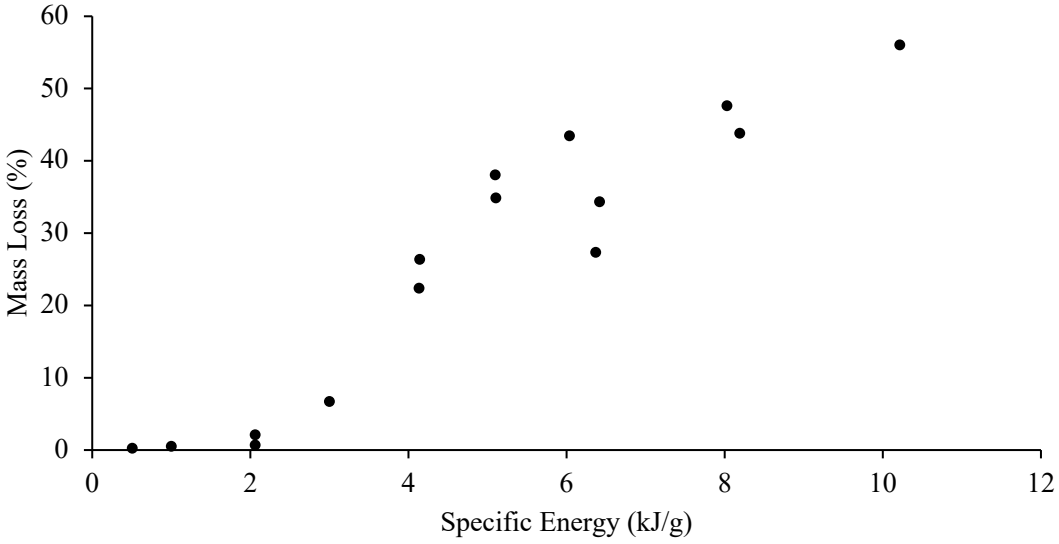


Figure D-1 - Bulk mass loss against specific energy for soaked sycamore blocks in the multimode system with 1 kW absorbed power within cyclohexane.

The mass losses of the soaked-block process followed an increasing trend with specific energies applied. There appears to be a threshold energy for pyrolysis to occur of 2.0 kJ/g, four times higher than that of the non-soaked pyrolysis process. Despite having an energy penalty for equivalent mass losses to the non-soaked blocks, there does not appear to be a mass loss penalty, as the mass losses are comparable to the non-soaked pyrolysis process.

Soaked blocks – pyrolysis oil yields

Figure D-2 shows total pyrolysis oil yields against specific energy for sycamore blocks soaked in cyclohexane, using cyclohexane as an inerting liquid.

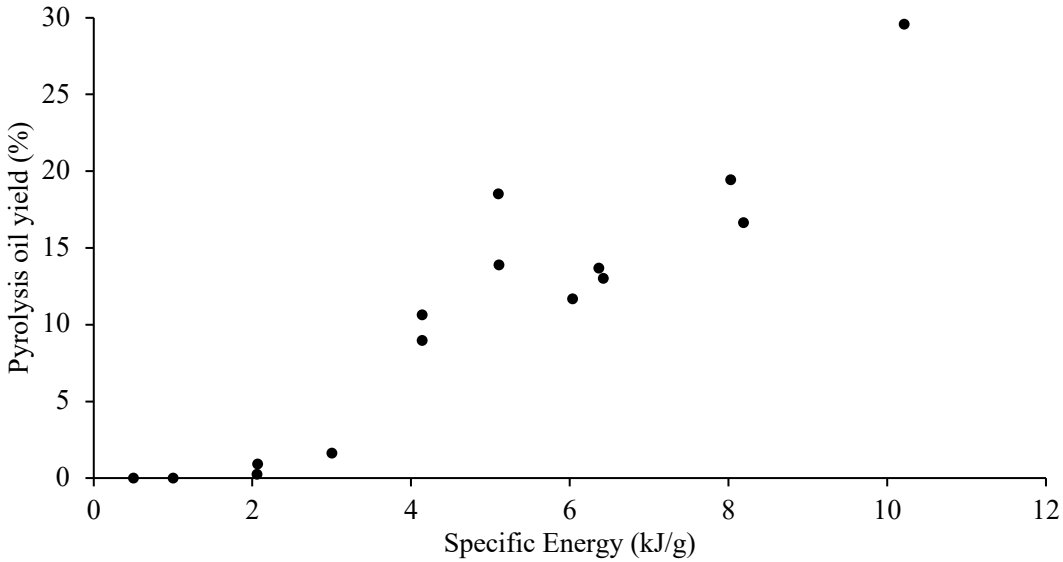


Figure D-2 – Pyrolysis oil yields against specific energy for soaked sycamore blocks in the multimode system with 1.0 kW absorbed power within cyclohexane.

The pyrolysis oil yields observed followed a similar trend to the mass losses. The maximum pyrolysis oil yield achieved was 29.6 % at 10.2 kJ/g. In comparison to the non-soaked liquid-inerted pyrolysis process, despite the energy penalty for equivalent pyrolysis oil yields, the maximum yield was much higher (29.6 % compared to 18 % in the non-soaked system).

Soaked blocks – pyrolysis oil yields in comparison to bulk-mass loss

Figure D-3 presents the pyrolysis oil yields as a ratio of the mass losses of the sycamore achieved during the liquid-inerted microwave pyrolysis process using soaked blocks.

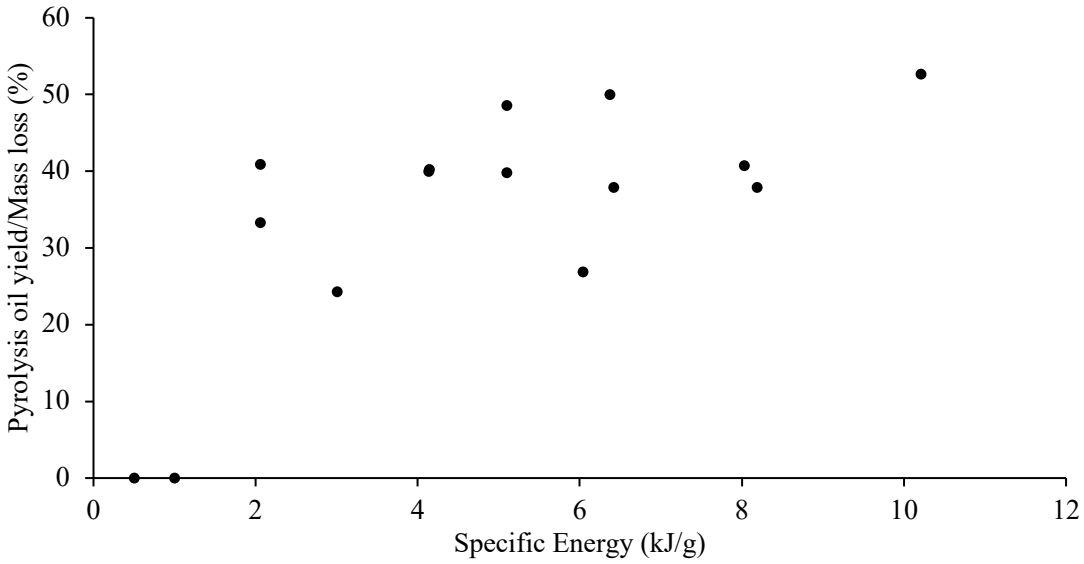


Figure D-3 – Pyrolysis oil yields compared to bulk mass loss of the sycamore blocks against specific energy for soaked biomass in the multimode system with 1 kW absorbed power

Figure D-3 shows that there is not an evident trend between the pyrolysis oil yield and mass loss when the sycamore blocks are soaked within cyclohexane. The values are centred around 40 % ±12 % for all specific energies where pyrolysis oil could be collected. This lack of trend is contrary to the non-soaked blocks, where there was a loose bell-curve shape, rising and decreasing.

Soaked blocks – conclusions

Reproducibility was greatly increased in the soaked-block system, as the increased heat transfer efficiency due to the presence of liquid within the biomass structure allowed for a slower heating rate, and less variability in microwave absorbance that is usually due to quick char formation. In other words, the pyrolysis process slowed down, allowing for more time for the dynamic impedance matching to adapt to the wood's changing dielectric properties, resulting in a more consistent absorbance of microwaves.

The specific energies required for equivalent mass losses to the non-soaked process were much higher in the soaked-block system. The increased energy requirement is largely due to the biomass structure containing liquid, as opposed to a largely internal 'dry' structure with wet exterior carried out in the non-soaked runs. The energy provided to the block then goes towards heating, and then vaporizing the liquid, creating a large inefficiency in energy requirements for pyrolysis, three times that for equivalent mass losses in the non-soaked runs. The benefit of pyrolysing a soaked block is that there is a much greater potential for temperature control; the thermal conductivity of cyclohexane (0.12 W/m·K) is greater than the air that would typically be found in the pores (0.024 W/m·K), resulting in increased heat transfer via conduction through the biomass. The specific heat capacity of cyclohexane (1.85 kJ/kg·K) is also much greater than that of air (0.74 kJ/kg·K). As specific heat capacity is directly proportional to the energy required to heat a material, it stands to reason that efficient heat transfer through the sycamore block, coupled with the latent heat of vaporization, results in a much slower heating rate of the biomass.

In terms of pyrolysis oil yields, the highest yield (29.6 %) presented some processing issues due to the long processing time and significant volatiles production. The sycamore block ruptured due to pressure and the char released contaminated the pyrolysis oil product. This contamination likely increased the pyrolysis oil mass value, and as such is likely not representative of the actual pyrolysis oil mass produced. This char contamination presents processing issues, such as the requirement for solid-liquid separation, which is not required for lower specific energies and pyrolysis oil yields.

The soaked block test was also carried out in the single-mode pyrolysis process along with the multi-mode process. The single mode system initially presented some processing issues when heating the biomass in the liquid without the presence of any

masses on a batch basis. For the cyclohexane liquid, as the sycamore was heated, this in turn heated the liquid present around the biomass within the waveguide, as the liquid heated, the density was reduced and therefore the colder, denser liquid above the waveguide section flowed down and replaced this liquid. As the sycamore density was not that much greater than that of the cyclohexane, the sample was then entrained with this rising liquid out of the waveguide, and therefore out of the microwave cavity. There was also the effect of heating the liquid within the biomass leading to a reduction in block density. When the biomass was heated, energy went towards heating the liquid within the biomass structure, and then towards vaporizing the liquid. The gas travelling through the biomass structure, paired with less liquid contained within the biomass structure lead to a lower block density, resulting in the block floating, and aiding block entrainment within the liquid.

Multiple sample pyrolysis – multi-mode

As the multi-mode reactor allowed for scale-up of the pyrolysis process, it was determined useful to investigate whether multiple sycamore blocks at the scale of the single-mode liquid-inerted pyrolysis process could be processed simultaneously. The benefit of utilising a multi-mode cavity is that it allows for a larger volume of liquid-surround and sycamore block geometry (either as a single block are multiple). As it was not possible to determine the energy applied to individual blocks, the total absorbed power was assumed to be applied evenly over the multiple blocks. Mass losses for multiple sycamore blocks placed within the multimode cavity are presented in Figure D-4.

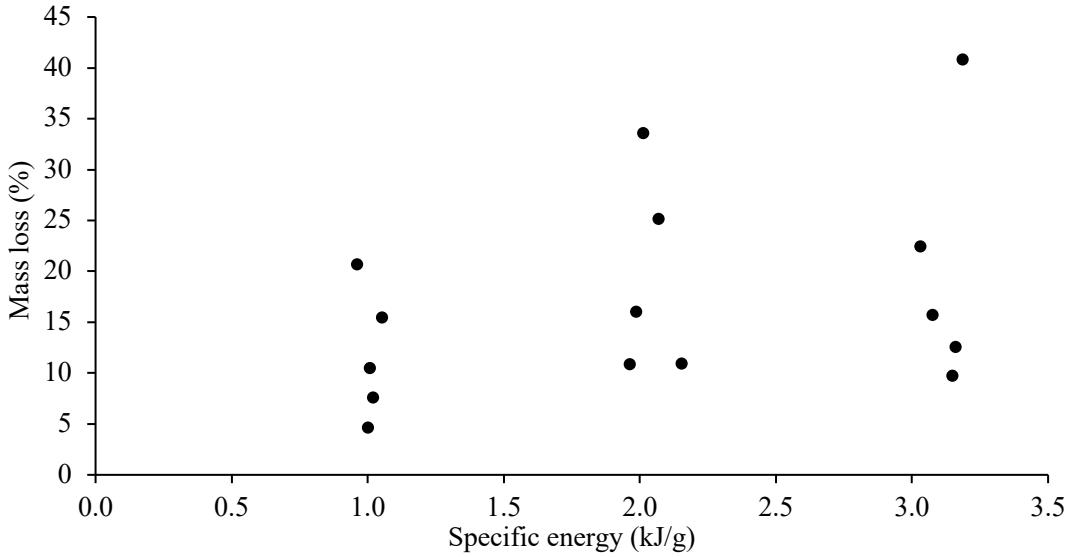


Figure D-4 - Five samples simultaneously pyrolysed at specific energies of 1.0, 2.0 and 3.0 kJ/g, and the mass losses obtained for each sample.

It can be seen from Figure D-4 that for multiple sycamore blocks within a multi-mode system pyrolysing simultaneously, the blocks did not pyrolyse equivalently. It is evident that certain blocks had pyrolysed more than others, resulting in a degree of unpredictability within the process. This processing behaviour would promote processing multiple blocks in series, one after the other, rather than in parallel in the same vessel, where processing performance could not be adequately predicted and designed for.

Compositional changes predicted by the models

Microwave pyrolysis in a liquid medium was initially determined to be carried out as it provided processing advantages in terms of larger particle sizes, volumetric heat transfer and less volatiles condensing requirements (Chapter 1, Section 1.4). It had been previously identified that the primary product production chemistry pathway was maintained with microwave pyrolysis, and as such microwave heating could be considered an alternative heating method (Robinson et al., 2015). It was identified throughout this thesis, however, that there were further processing advantages

identified such as increased temperature control within the sycamore block via pressure generation elevating the boiling point of volatiles produced.

The findings within Sections 5.3.2 - 5.3.4 were applicable to microwave pyrolysis as a whole, and were not necessarily specific to a liquid-inerted microwave pyrolysis process. The dielectric properties, temperature plateaus and internal pressures obtained within the sycamore block were likely the result of the heating rate and size of the sycamore block. The pressures and presence of volatiles within the sycamore block were determined to have the potential for slowing the heating rate of the block during the process. This slowed heating rate could have the potential to affect the selective decomposition of the lignocellulosic constituents of the sycamore block. The temperature control, for example, could explain why lignin was identified within the chars at a greater concentration for the single-mode block chars than the multi-mode block chars, possibly due to the differential in temperature plateau (450 °C as compared to 550 °C).

For the lignocellulosic models (models 2 and 3), lignin, cellulose and hemicellulose were modelled individually, therefore estimates on the composition based on specific energy applied and potential temperature plateaus could be estimated and compared to empirical values (Section 4.4.6.1). The compositional plots for both models, 1.5 kW absorbed power for a 4.5×1.5×1.5 cm block in the single mode system are presented in Figure D-5 and Figure D-6.

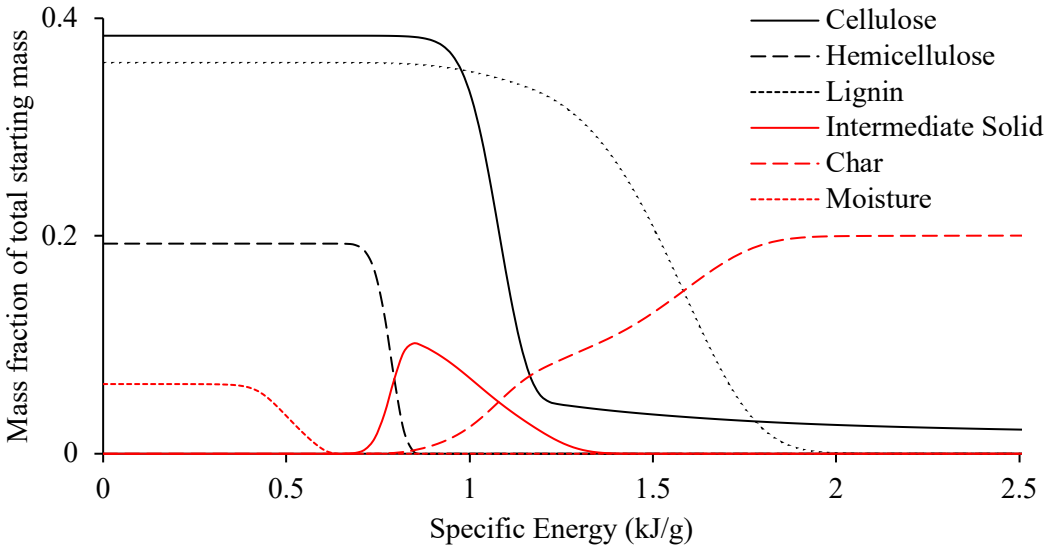


Figure D-5 – Lignocellulosic composition of the sycamore block (single-mode) for 1.5 kW applied power for model 2.

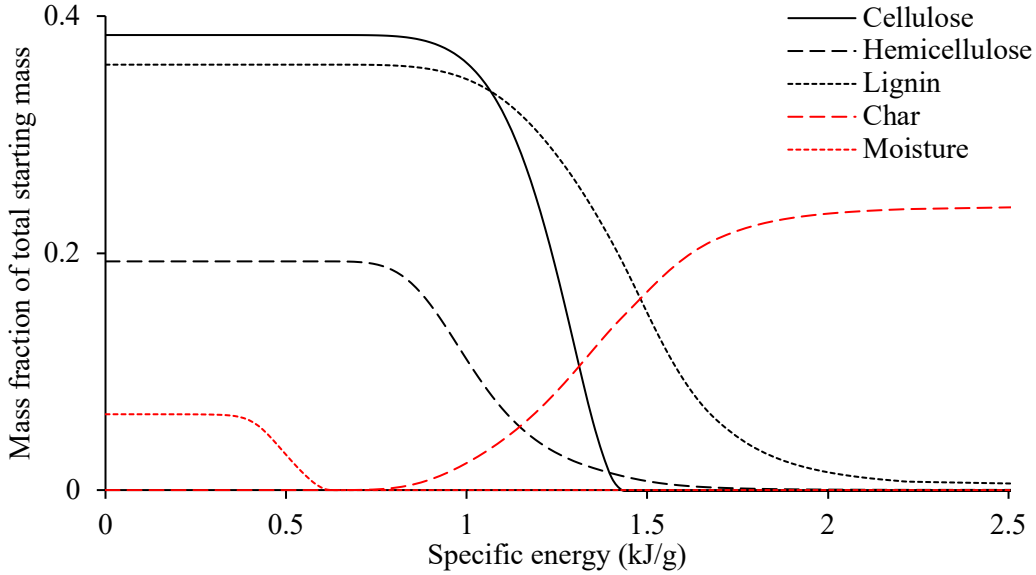


Figure D-6 – Lignocellulosic composition of the sycamore block (single-mode) for 1.5 kW applied power for model 3.

For both models 2 and 3 (Figure D-5 and Figure D-6), it would be expected that after processing and reaching 1.5 kJ/g, the cellulose and hemicellulose composition of the sycamore would have been reduced to almost zero. The slow decomposition rate of lignin across both models could explain the presence of lignin in the pyrolysed char presented in Chapter 4. Both models 2 and 3 present no mass loss until 0.5 kJ/g, coinciding with empirical data. However, unlike the empirical counterpart, mass losses

greater than the moisture content did not occur until 0.75 kJ/g, later than observed empirically by the mass loss data. It would be expected, based on the theoretical models, that in a microwave pyrolysis process, the energy range for significant mass losses to occur would be between 1.0 – 1.5 kJ/g, whereas empirically the increase in mass loss occurred from 0.5 – 1.0 kJ/g, with mass losses after 1.0 kJ/g increasing linearly. The disparity between empirical data and the theoretical models present the challenges when predicting pyrolysis behaviour based on existing kinetic data, due to the kinetic data being based on conventionally heated processes. Figure D-7 and Figure D-8 present the mass fractions of the lignocellulosic constituents of the sycamore block, compared to empirical data.

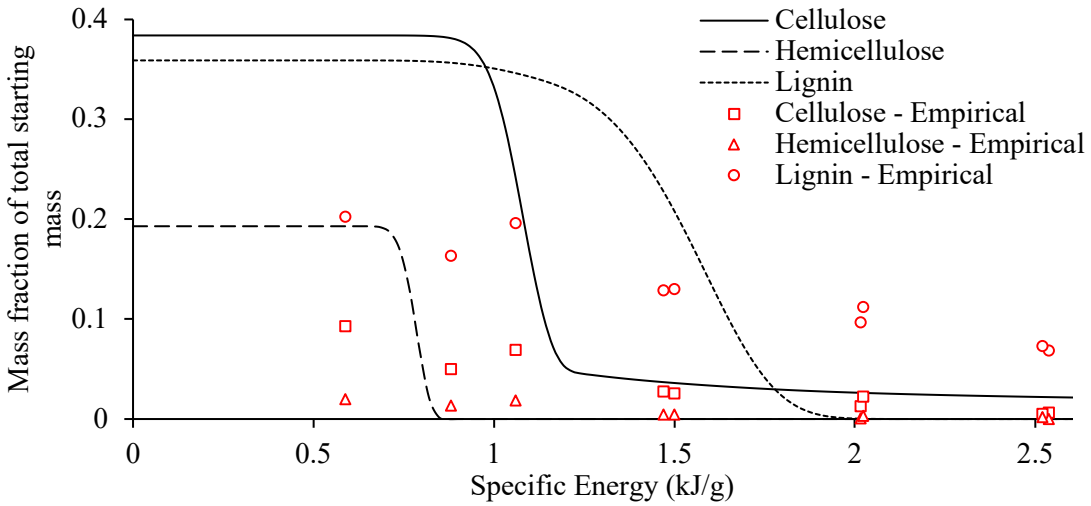


Figure D-7 - Lignocellulosic composition of the sycamore block (single-mode) for 1.5 kW applied power for model 2, with empirical mass fractions for comparison.

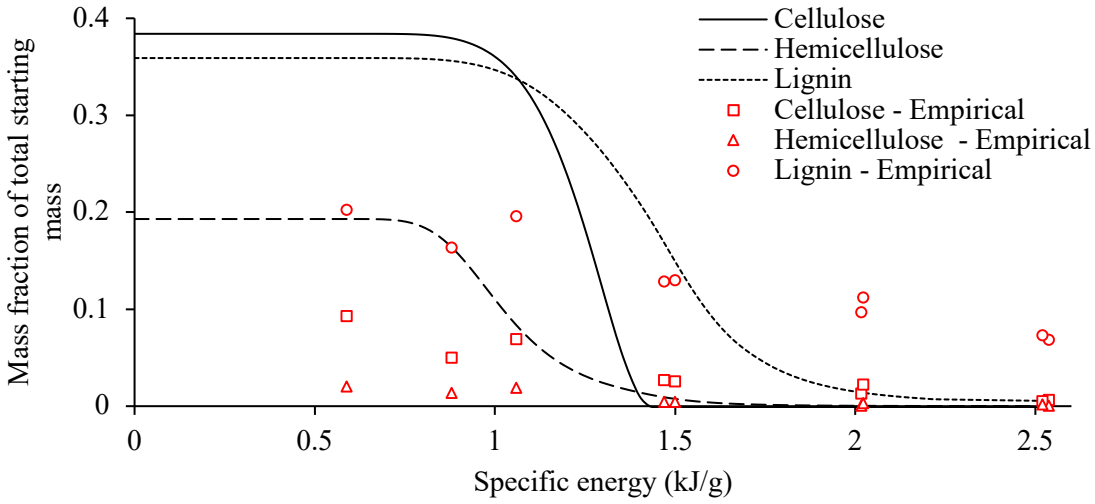


Figure D-8 - Lignocellulosic composition of the sycamore block (single-mode) for 1.5 kW applied power for model 3, with empirical mass fractions for comparison.

It is evident that when comparing the empirical data from the single-mode liquid inerted pyrolysis process and empirical compositional data, there were significant differences present. It could be identified that the onset of lignocellulosic decomposition occurred at much lower specific energies than predicted by the kinetic models. It was identified in Chapter 3 that the onset of mass loss (greater than the moisture content) was around 0.5 kJ/g. It is apparent that significant decomposition of the lignocellulosic composition occurred immediately empirically, likely due to internal temperatures >300 °C. For the models, the lignocellulosic components underwent no decomposition until the activation energy had been overcome, at which point the decrease was moderately quick. The empirical data suggested, however, there would be an initial decrease from the starting concentration between 0 – 0.5 kJ/g, at which point there would be a gradual decrease. The lower concentrations for the empirical data at low specific energies could be due to the heterogenous heating profile. As such, with the samples being taken from the most charred section of the block, temperatures would be higher than predicted for homogenous heating, and therefore there would a lower concentrations of the lignocellulosic constituents. The gradual decrease could be due to the observed

temperature plateau, coupled with the short processing time (<10 seconds for 1.5 kW applied power), resulting in little decomposition above the initial decrease.

It was identified in Chapter 3 that when processing in the single-mode liquid inerted system, the internal temperature of the sycamore plateaued at approximate 450°C. The model compositional decomposition predictions could therefore be overestimated, as higher predicted temperatures would result in a faster compositional decomposition rate. When the temperature was limited to 450 °C, as was calculated from TGA for the single-mode microwave pyrolysis system, the composition change in the sycamore structure was limited, as shown in Figure D-9 and Figure D-10.

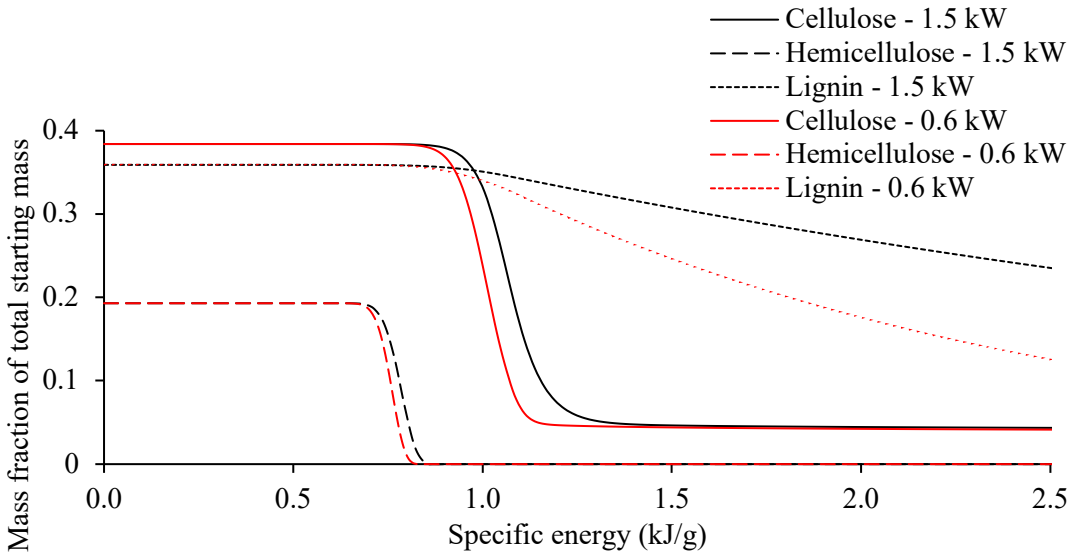


Figure D-9 - Lignocellulosic mass fraction of the sycamore block (single-mode) for 0.6 and 1.5 kW applied power for model 2, with the internal temperature limited to 450°C.

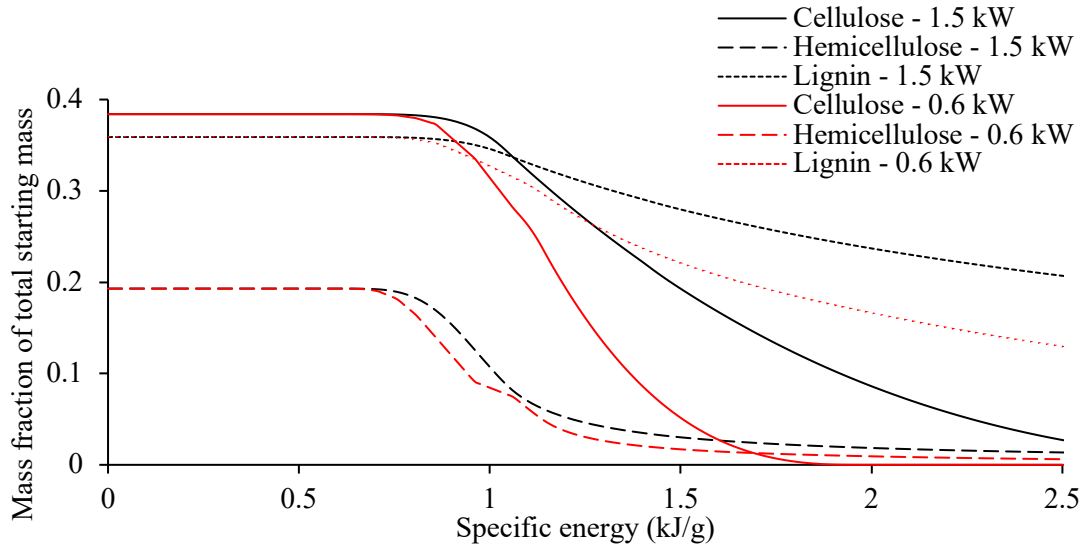


Figure D-10 - Lignocellulosic mass fraction of the sycamore block (single-mode) for 0.6 and 1.5 kW applied power for model 3, with the internal temperature limited to 450°C.

Figure D-9 and Figure D-10 show that when the peak temperature was limited to 450 °C within the sycamore block, the lignocellulosic decomposition rate is reduced when compared to a non-temperature limited process. For both models 2 and 3, lignin did not significantly decrease throughout the pyrolysis energy range. For model 3, the cellulose decomposition rate was dramatically reduced, with complete decomposition occurring at approximately 2 kJ/g for 0.6 kW absorbed power, and >2.5 kJ/g for the 1.5 kW absorbed power process. The temperature limited models further highlight the challenges with estimating the pyrolysis behaviour within a microwave pyrolysis process when using kinetics from conventionally heated processes. The temperature limited models confirmed, however, that when the process was temperature limited, the ability for selective decomposition of hemicellulose and/or cellulose could be possible and in a separate processing range to lignin decomposition.

Models 2 and 3 show that for 0.6 kW applied power, the lignocellulosic decomposition over the energy range was greater than 1.5 kW applied power, potentially due to the longer processing time allowing for greater lignin and cellulose decomposition. The

compositional breakdown, and therefore mass loss would consequently be expected to be greater for the 0.6 kW process than the 1.5 kW process shown in Section 5.3.1, which contradicts the data presented. It could therefore be possible that the surface cooling potential and heat transfer through the block to the surroundings would be more important in determining mass losses and compositional breakdown throughout the block.

From both the non-temperature limited compositional models and the 450 °C limited models, it can be determined that due to the short processing time of the pyrolysis process, selective decomposition of cellulose and hemicellulose can occur in the process, leaving a potential lignin rich solid, which was confirmed empirically by the solid assays (Figure D-7). If the microwave pyrolysis process was adequately controlled, it could potentially be possible to selectively decompose hemicellulose, leaving a cellulose and lignin rich solid. This selective decomposition could be utilised, and investigated further, to produce oils of the respective lignocellulosic component targeted (which could be on a multi-stage basis, for example removing the hemicellulose content to produce a cellulose product-rich oil).